ดีออกซิจิเนชันของน้ำมันปาล์มเพื่อผลิตน้ำมันดีเซลชีวภาพสังเคราะห์บนตัวเร่งปฏิกิริยาโลหะและโลหะซัลไฟด์ในถังปฏิกรณ์แบบทริกเคิลเบด

นายอรรถพล ศรีฟ้า

วิทยานิพนธ์นี้เป็นส่วนหนึ่งของการศึกษาตามหลักสูตรปริญญาวิศวกรรมศาสตรดุษฎีบัณฑิต
สาขาวิชาวิศวกรรมเคมี ภาควิชาวิศวกรรมเคมี
คณะวิศวกรรมศาสตร์ จุฬาลงกรณ์มหาวิทยาลัย
ปีการศึกษา 2557

DEOXYGENATION OF PALM OIL TO BIO-HYDROGENATED DIESEL OVER METAL AND METAL SULFIDE CATALYSTS IN A TRICKLE-BED REACTOR

Mr. Atthapon Srifa

A Dissertation Submitted in Partial Fulfillment of the Requirements
for the Degree of Doctor of Engineering Program in Chemical Engineering
Department of Chemical Engineering
Faculty of Engineering
Chulalongkorn University
Academic Year 2014

Thesis Title	DEOXYGENATION OF PALM OIL TO BIO-HYDROGENATED DIESEL OVER METAL AND METAL SULFIDE CATALYSTS IN A TRICKLE-BED REACTOR
By	Mr. Atthapon Srifa
Field of Study	Chemical Engineering
Thesis Advisor	Professor Suttichai Assabumrungrat, Ph.D.
Thesis Co-Advisor	Kajornsak Faungnawakij, D.Eng.

Accepted by the Faculty of Engineering, Chulalongkorn University in Partial Fulfillment of the Requirements for the Doctoral Degree

.....Dean of the Faculty of Engineering
(Professor Bundhit Eua-arporn, Ph.D.)

THESIS COMMITTEE

.....Chairman
(Associate Professor Prasert Pavasant, Ph.D.)
.....Thesis Advisor
(Professor Suttichai Assabumrungrat, Ph.D.)
.....Thesis Co-Advisor
(Kajornsak Faungnawakij, D.Eng.)
.....Examiner
(Associate Professor Artiwan Shotipruk, Ph.D.)
.....Examiner
(Associate Professor Tawatchai Charinpanitkul, D.Eng.)
.....External Examiner
(Associate Professor Navadol Laosiripojana, Ph.D.)

อรรถพล ศรีฟ้า : ดีออกซิจิเนชันของน้ำมันปาล์มเพื่อผลิตน้ำมันดีเซลชีวภาพสังเคราะห์บนตัวเร่งปฏิกิริยาโลหะและโลหะซัลไฟด์ในถังปฏิกรณ์แบบทริกเคิลเบด (DEOXYGENATION OF PALM OIL TO BIO-HYDROGENATED DIESEL OVER METAL AND METAL SULFIDE CATALYSTS IN A TRICKLE-BED REACTOR) อ.ที่ปรึกษาวิทยานิพนธ์หลัก: ศ. ดร.สุทธิชัย อัสสะบำรุงรัตน์, อ.ที่ปรึกษาวิทยานิพนธ์ร่วม: ดร.ขจรศักดิ์ เฟื่องนวกิจ, 195 หน้า.

งานวิจัยนี้ศึกษากระบวนการดีออกซิจิเนชันของน้ำมันปาล์มเพื่อผลิตน้ำมันดีเซลชีวภาพสังเคราะห์หรือที่เรียกว่ากรีนดีเซลในถังปฏิกรณ์แบบทริกเคิลเบดโดยใช้ตัวเร่งปฏิกิริยาโลหะและโลหะซัลไฟด์บนตัวรองรับแกมมาอลูมินาที่ถูกเตรียมโดยวิธีเคลือบฝัง ผลการทดลองได้ถูกแบ่งเป็น 4 ส่วน ดังนี้ ส่วนแรกการศึกษาผลกระทบของสภาวะดำเนินการ (อุณหภูมิ ความดัน ความเร็วเชิงสเปซของของเหลวของน้ำมัน และอัตราส่วนไฮโดรเจนต่อน้ำมัน) โดยใช้ตัวเร่งปฏิกิริยานิกเกิลโมลิบดีนัมซัลไฟด์ เพื่อหาสภาวะที่เหมาะสม พบว่าปฏิกิริยาไฮโดรดีออกซิจิเนชัน ดีคาร์บอนิลเลชัน และดีคาร์บอกซิเลชัน เกิดขึ้นอย่างว่องไวแบบแข่งขันกันรวมทั้งมีสภาวะที่เหมาะสมและขีดจำกัดที่แตกต่างกันในแต่ละสภาวะ ส่วนที่สองทำการศึกษาบทบาทของเร่งปฏิกิริยาโลหะโคบอลต์ นิกเกิล พาลาเดียม และแพลทินัม จากผลการตรวจสอบสมบัติพบว่าตัวปฏิกิริยาโลหะออกไซด์ที่ถูกเตรียมขึ้นถูกเปลี่ยนเป็นโลหะหลังจากการทำรีดักชันในไฮโดรเจนและมีขนาดอนุภาคและการกระจายตัวบนตัวรองรับแกมมาอลูมินาที่แตกต่างกัน การทดสอบปฏิกิริยาพบว่าประสิทธิภาพของตัวเร่งปฏิกิริยาเรียงตามลำดับคือ โคบอลต์ > พาลาเดียม > แพลทินัม > นิกเกิล ซึ่งสอดคล้องกับค่าความถี่ในการหมุนเวียน (Turnover frequency) นอกจากนี้ได้ทำการศึกษากลไกการเกิดปฏิกิริยาของโลหะทั้ง 4 ตัวผ่านสารจำลองของน้ำมันปาล์มคือกรดโอเลอีก ส่วนที่สาม การศึกษาเปรียบเทียบประสิทธิภาพ การเลือกเกิด และความเสถียรภาพของตัวเร่งปฏิกิริยาโลหะ (นิกเกิล โคบอลต์ โมลิบดีนัม นิกเกิลโมลิบดีนัม และโคบอลต์โมลิบดีนัม) และโลหะซัลไฟด์ (นิกเกิลซัลไฟด์ โคบอลต์ซัลไฟด์ โมลิบดีนัมซัลไฟด์ นิกเกิลโมลิบดีนัมซัลไฟด์ และโคบอลต์โมลิบดีนัมซัลไฟด์) พบว่า โลหะนิกเกิล โลหะโคบอล นิกเกิลโมลิบดีนัมซัลไฟด์ และโคบอลต์โมลิบดีนัมซัลไฟด์ให้ประสิทธิภาพสูงสุด โดยสามารถเลือกได้ผ่านปฏิกิริยาที่แตกต่างกันดังนี้ โลหะนิกเกิลเลือกเกิดผ่านปฏิกิริยาดีคาร์บอนิลเลชันในขณะที่นิกเกิลโมลิบดีนัมซัลไฟด์และโคบอลต์โมลิบดีนัมซัลไฟด์เลือกเกิดผ่านปฏิกิริยาไฮโดรดีออกซิจิเนชัน ส่งที่น่าสนใจอย่างมากคือ ตัวเร่งปฏิกิริยาโลหะโคบอลต์สามารถเลือกเกิดผ่านปฏิกิริยาดีคาร์บอนิลเลชันและไฮโดรดีออกซิจิเนชันได้ใกล้เคียงกัน จากการศึกษาเสถียรภาพของตัวเร่งปฏิกิริยาดังกล่าวพบว่า นิกเกิลโมลิบดีนัมซัลไฟด์จะให้ความมีเสถียรภาพสูงสุด รองลงมาเป็นโคบอลต์โมลิบดีนัมซัลไฟด์ โลหะนิกเกิล และโลหะโคบอลต์ตามลำดับ ส่วนสุดท้ายการศึกษาผลของการเสื่อมสภาพและการฟื้นคืนสภาพของตัวเร่งปฏิกิริยาโลหะนิกเกิลและโคบอลต์ พบว่าตัวเร่งปฏิกิริยาทั้งสองให้ประสิทธิภาพที่ดีและมีความเสถียรในช่วง 100 ชั่วโมงแรก หลังจากนั้นพบว่า ร้อยละผลได้ของผลิตภัณฑ์ลดลงอย่างช้าๆเมื่อใช้โลหะนิกเกิล และลดลงอย่างรวดเร็วเมื่อใช้โลหะโคบอลต์ จากผลการตรวจสอบสมบัติของตัวเร่งปฏิกิริยาหลังใช้งาน 150 ชั่วโมง พบว่า การเกาะตัวของคาร์บอนบนพื้นผิวตัวเร่งปฏิกิริยา (carbon deposition) เป็นสาเหตุหลักและการรวมกลุ่มของอนุภาคของตัวเร่งปฏิกิริยา (sintering) เป็นสาเหตุรองของการเสื่อมสภาพตัวเร่งปฏิกิริยา สิ่งที่น่าสนใจคือ หลังจากการฟื้นคืนสภาพตัวเร่งปฏิกิริยาด้วยการเผาในอากาศและการทำรีดักชันในไฮโดรเจนพบว่าประสิทธิภาพของตัวเร่งปฏิกิริยาสามารถฟื้นคืนสภาพได้อย่างสมบูรณ์

ภาควิชา วิศวกรรมเคมี	ลายมือชื่อนิสิต .....
สาขาวิชา วิศวกรรมเคมี	ลายมือชื่อ อ.ที่ปรึกษาหลัก .....
ปีการศึกษา 2557	ลายมือชื่อ อ.ที่ปรึกษาร่วม .....

5471433521 : MAJOR CHEMICAL ENGINEERING
KEYWORDS: HYDRODEOYGENATION / DEOXYGENATION / PALM OIL / METAL AND METAL SULFIDE CATALYSTS / HYDROTREATING

ATTHAPON SRIFA: DEOXYGENATION OF PALM OIL TO BIO-HYDROGENATED DIESEL OVER METAL AND METAL SULFIDE CATALYSTS IN A TRICKLE-BED REACTOR. ADVISOR: PROF. SUTTICHAI ASSABUMRUNGRAT, Ph.D., CO-ADVISOR: KAJORNSAK FAUNGNAWAKIJ, D.Eng., 195 pp.

The deoxygenation of palm oil to bio-hydrogenated diesel (BHD) or so-called green diesel over the γ-Al_2O_3-supported metal and metal sulfide catalysts prepared by impregnation method was conducted in a trickle-bed reactor. The studies were divided into 4 parts. Firstly, the effect of reaction parameters (temperature, pressure, LHSV, and H_2/oil ratio) on the deoxygenation of palm oil over $NiMoS_2$ was investigated to optimize the operating conditions. The results demonstrated that hydrodeoxygenation (HDO), decarbonylation (DCO), and decarboxylation (DCO_2) reactions actively and competitively occurred at each condition, and had different optimal and limiting conditions. Secondly, the roles of monometallic catalysts were studied. Metallic sites of the catalysts were found to be formed after pre-reduction in H_2 with differences in metal particle size and metal dispersion. These properties played important roles in the palm oil deoxygenation, resulting in the activity turnover frequency (TOF) with the order of Co > Pd > Pt > Ni. Oleic acid was used as a model compound to get the basic information on the reaction pathway. Consequently, a reaction network for the deoxygenation of palm oil was developed and discussed. Thirdly, the comparisons of the metal (Ni, Co, Mo, NiMo, and CoMo) and metal sulfide (NiS_x, CoS_x, MoS_2, $NiMoS_2$, and $CoMoS_2$) catalysts on activity, selectivity, and stability were studied. The DCO reaction was dominant over metallic Ni catalyst, whereas, the HDO was dominant when the reaction was catalyzed by $NiMoS_2$ and $CoMoS_2$ catalysts. Interestingly, the contribution of DCO was nearly comparable to that of the HDO over metallic Co catalyst. The catalytic stability of the metal sulfides was superior to that of the metal catalysts with the order of $NiMoS_2$ > $CoMoS_2$ > Ni > Co catalysts. Finally, the deactivation and regeneration behaviors of the metallic Ni and Co catalysts were examined. The catalysts exhibited the stable performance for 100 h on-stream. Nevertheless, the product yield over metallic Ni catalyst gradually decreased, whereas, the dramatic decline in product yield could be noticed over metallic Co catalyst after 150 h on-stream. The carbon deposition was found to be the main cause of the catalyst deactivation, while the metal sintering was a minor reason. The catalyst regeneration by thermal treatment in air, followed by H_2 reduction could completely restore the catalyst activity.

Department:	Chemical Engineering	Student's Signature	.....
Field of Study:	Chemical Engineering	Advisor's Signature	.....
Academic Year:	2014	Co-Advisor's Signature	.....

ACKNOWLEDGEMENTS

I would like to take this opportunity to express my sincere thankfulness to everyone contributing to the completion of my dissertation. Moreover, my appreciation extends to those who were involved in my study and research but whose names are not mentioned here.

First, I would like to express my sincere gratitude and deep appreciation to my research advisor and co-research advisor, Prof.Dr. Suttichai Assabumrungrat and Dr. Kajornsak Faungnawakij (NANOTEC, NSTDA) for all the guidance, supervision, comments, discussions and invaluable suggestions throughout this research. This work would not be accomplished without their help.

I am grateful to the National Nanotechnology Center (NANOTEC), the National Science and Technology Development Agency (NSTDA) through the Thailand Graduate Institute of Science and Technology (TGIST) for the financial support. As the most of my work was done at NANOTEC, I would like to express my special thanks to everyone at the Nanomaterials for Energy and Catalysis Laboratory (NEC) research group. They always make me enjoy my life during the study in this program.

I would like to thank committee members, Assoc. Prof. Dr. Prasert Pavasant, Assoc.Prof.Dr. Artiwan Shotipruk, Assoc.Prof.Dr. Tawatchai Charinpanitkul, and to the external examiner, Assoc.Prof.Dr. Navadol Laosiripojana from the Joint of Graduate School of Energy and Environment (JGSEE), King Mongkut's University of Technology Thonburi (KMUTT) for their helpful suggestions, comments, and corrections of this work.

Finally, my deepest appreciation goes to my parent for their unconditional love, understanding, and financial support.

CONTENTS

Page

Page

Page

Page

LIST OF TABLES

LIST OF FIGURES

CHAPTER I

INTRODUCTION

1.1 Rationale

Currently, the development of renewable fuels from biomass is an important key to future energy due to the depletion of petroleum fuels. Biomass feedstocks can be divided into three categories: carbohydrates (i.e., starch and sugar), lignocelluloses materials, and animal fats/vegetable oils composed of triglycerides and free fatty acid ranging from C_{10}-C_{20} [11]. Triglycerides have been used as an important renewable feedstocks for the production of renewable fuels because of their low degree of functionalization and simple structure compared with cellulosic biomass [12, 13]. In particular, palm oil contains primarily C_{16} and C_{18} fatty acids, making it a promising feedstock for bio-hydrogenated diesel (BHD) or green diesel and biodiesel production. There are two main catalytic reactions of triglycerides and/or organic acid using vegetable oil or animal fat for biofuel production for diesel engines: (1) a transesterification/esterification process to produce biodiesel, a mixture of esters, and (2) a catalytic deoxygenation process to produce renewable diesel, so-called bio-hydrogenated diesel or green diesel, having a similar molecular structure to that of petroleum diesel. Typically produced by transesterification of triglycerides with methanol, fatty acid methyl esters (FAMEs) or biodiesel has been used as a component in diesel blending [14]. However, some disadvantages of biodiesel compared to petroleum diesel are the C=C bonds and C=O bonds remaining in the molecules of FAMEs, e.g., low thermal and oxidation stability because of its high oxygen content, high viscosity, and low heating value [15, 16].

As a result, bio-hydrogenated diesel or green diesel, which provides better diesel properties, such as high cetane number, zero oxygen containing [17], and high thermal and oxidation stability [18], has attracted significant attention. Green diesel can be produced by the catalytic deoxygenation of triglycerides through three major

reaction pathways, including decarbonylation (DCO), decarboxylation (DCO_2), and hydrodeoxygenation (HDO) [13, 19], under reaction conditions of 350–450 °C and 5-15 MPa H_2 [20, 21]. Generally, the reaction first proceeds via hydrogenation of unsaturated triglycerides (C=C double bond) to form saturated triglycerides [22], followed by the hydrogenolysis of saturated triglycerides resulting in fatty acids and propane. Finally, the fatty acid undergoes the following reactions: (1) HDO, an exothermic reaction, to remove oxygen in the form of water and yield n-alkane with the same carbon number as the corresponding fatty acid, and (2) DCO and (3) DCO_2, endothermic reactions, to eliminate oxygen in form of CO and water or CO_2, respectively. The consequent *n*-alkane has one carbon atom loss compared to the original fatty acid [23].

The catalysts mostly used in deoxygenation of triglycerides, fatty acids, and esters are: (1) supported metalsulfide catalysts, e.g. $NiMoS_2$ [24, 25], $CoMoS_2$[26, 27], and $NiWS_2$ [28, 29]and (2) metal catalysts in reduced state, such as Ni [12, 30], Co [22, 31], Pd[5, 32], Pt[14], and Ru[33, 34]. The conventional supported metal sulfide catalysts, less expensive catalysts [35], showed high activity in deoxygenation of triglycerides and model compounds, however, sulfur leaching lead to catalyst deactivation and sulfur contamination in liquid product [31, 36, 37]. It should be noted that metal sulfide catalysts require adding the sulfiding agents e.g., CS_2 and DMDS in liquid feed to avoid catalyst deactivation during deoxygenation reactions [22, 38]. Additionally, the trace amount of water, produced from DCO and HDO reactions, would hasten the sulfur leaching and rigorously shorten the lifetime of catalysts [39]. Otherwise, the supported metal catalysts or sulfur-free catalysts in reduced form have interested great attention in deoxygenation reaction due to high reactivity at moderate temperature, no sulfur contamination in liquid product, and less H_2requirement[40]. Some metal catalysts such as Ni, Pd, and Pt are favorable in DCO and DCO_2 pathways. Since, the hydrogen consumption for deoxygenation of triglycerides/fatty acids/esters decreased in order of HDO > DCO > DCO_2 routes, thus DCO and DCO_2 routes may be more theoretically economical than HDO route [36, 41]. Several researchers have been mostly studied various metal catalysts for deoxygenation of model compounds such as palmitic acid [32, 36], stearic acid [42,

43], oleic acid [44], linoleic acid [44], methyl palmitate [30], methyl oleate [14], methyl heptanoate [31], and methyl octanoate [45]. However, only a few studies were investigated on deoxygenation of triglycerides. Supported noble metal catalysts such as Pd and Pt have attracted attention due to the high activity and selectivity in deoxygenation of triglycerides to diesel-like hydrocarbons. However, the high cost and less abundance of the precious noble metal catalysts are also limited for industrial application. Accordingly, the development of inexpensive supported metal catalysts has been a promising key in deoxygenation of triglyceride to bio-hydrogenated diesel.

The great opportunities existing in the research and development of deoxygenation catalysts are important to control the extent of hydrodeoxygenation, decarbonylation, and decarboxylation reactions, which affected to H_2 consumption and heat supply, during deoxygenation of triglycerides to bio-hydrogenated diesel. Consequently, a comprehensive understanding the influence of catalysts and reaction conditions on three main reaction pathways is crucial in the pilot scale applications.

As discussed in above mention, in order to fully understand the roles of metal and metal sulfide catalysts on their activity, selectivity, and stability, we prepared the γ-Al_2O_3-supported metallic catalysts (such as Co, Ni, Pd, Pt, Mo, NiMo, and CoMo) and γ-Al_2O_3-supported metal sulfide catalysts (e.g. NiS_x, CoS_x, MoS_2, $NiMoS_2$, and $CoMoS_2$) by incipient wetness impregnation method. The physical and chemical properties of synthesized catalysts were subsequently characterized by XRD, XANES, TPR, N_2 sorption, CO pulse chemisorption, TEM, and TPO techniques. Briefly, the phase identity and crystallinity were firstly revealed through position of X-ray diffraction (XRD) patterns. X-ray absorption near edge structure (XANES) was used to investigate the chemical state and oxidation state of the catalysts. The specific surface area and total pore volumes of synthesized catalysts were measured using N_2 sorption technique, whereas, pore size distributions were determined from the desorption branch of the isotherms using the Barrett-Joyner-Hallenda (BJH) method. The reducibility of catalysts was investigated by H_2 temperature-programmed reduction (H_2-TPR). CO pulse chemisorption experiments of catalysts were used to estimate the surface metallic atom characteristics e.g. dispersion, metal surface area, and metal particle size of synthesized catalysts. The morphology and particle size of

the catalysts were examined by transmission electron microscopy (TEM). The carbon deposited on the spent catalysts was determined by temperature-programmed oxidation (TPO). Their catalytic performances for deoxygenation of palm oil (refined palm olein type) were subsequently investigated in a custom-made continuous-flow trickle-bed reactor. In order to fully understand the deoxygenation behavior of triglycerides to bio-hydrogenated diesel (BHD), the conversion, product yield, and the contribution of HDO and DCO/DCO_2 were calculated based on mole balance corresponding to fatty acid in oil feed. The effect of important parameters including temperature, pressure, LHSV, and H_2/oil ratio was firstly investigated to determine a suitable operation conditions for deoxygenation of palm oil to bio-hydrogenated diesel. Then, activity and selectivity of γ-Al_2O_3-supported monometallic catalysts were screened and studied and a reaction network for deoxygenation of palm oil to green diesel based on model compound study with oleic acid were investigated and discussed. Thirdly, the comparisons of metal and metal sulfide catalysts on activity, selectivity, and stability were investigated. Finally, the deactivation and regeneration behaviors of the γ-Al_2O_3-supported Ni and Co catalysts were also reported and discussed.

1.2 Objectives

To use palm oil (refined palm olein type) as a local feedstock in Thailand for production of bio-hydrogenated diesel in a continuous-flow trickle-bed reactor.

To investigate the effect of reaction parameters and to find the optimal condition for deoxygenation of palm oil to bio-hydrogenated diesel i.e., reaction temperature, H_2 pressure, liquid hourly space velocity (LHSV), and H_2/oil ratio.

To study the roles of monometallic catalysts on their activity and selectivity in the hydrodeoxygenation of palm oil to green diesel and to elucidate the reaction network using the model compound study with oleic acid.

To compare the activity, selectivity, and stability of the metal and metal sulfide catalysts in the deoxygenation of palm oil to bio-hydrogenated diesel.

To study the deactivation and regeneration characteristics of the catalysts in hydrodeoxygenation of palm oil.

1.3 Scope of Works

1. Set-up and design of a continuous down-flow trickel-bed reactor under high pressure (15 MPa) in the temperature range of 300-800 ^{o}C.

2. Preparation of the γ-Al_2O_3-supported metal catalysts (including Co, Ni, Pd, Pt, Mo, NiMo, and CoMo) and γ-Al_2O_3-supported metal sulfide catalysts (including NiS_x, CoS_x, MoS_2, and $NiMoS_2$, $CoMoS_2$) by incipient wetness impregnation method.

3. Characterization of the synthesized catalysts by XRD, XANES, TPR, N_2 sorption, CO pulse chemisorption, TEM, and, TGA, TPO techniques.

4. The liquid products were analyzed offline by gas chromatography equipped with a flame ionization detector (FID) and CHNO/S analyzer. The composition of gas products were also analyzed by online gas chromatography equipped thermal conductivity detector (TCD).

5. The conversion, product yield, and the contribution of hydrodeoxygenation (HDO) and decarbonylation/decarboxylation (DCO/DCO_2) were estimated based on mole balance corresponding to fatty acid composition in oil feed in order to understand the deoxygenation behavior.

6. Performing the experiments of deoxygenation of palm oil (refined palm olein type) in a continuous fixed-bed reactor under temperature (270-420 ^{o}C), H_2 pressure of (1.5-8 MPa), liquid hourly space velocity (LHSV) (0.25-5.0 h^{-1}), and H_2/ oil ratio (250-2,000 Ncm^3/cm^3).

7. Optimizing the reaction parameters for high quality bio-hydrogenated diesel with a product yield higher than 90 % and the composition of diesel ranged-hydrocarbons (*n*-C_{15} to *n*-C_{16}) > 95 wt. %.

8. Study of the roles of monometallic catalyst in palm oil deoxygenation and elucidating the reaction mechanisms for deoxygenation of palm oil to green diesel using a model compound study with oleic acid based on the product distributions.

9. Study of a correlation between the catalyst performance (activity, selectivity, and stability) and the catalyst properties.

10. Study the deactivation and regeneration behaviors of the catalysts during palm oil hydrodeoxygenation.

1.4 Research methodology

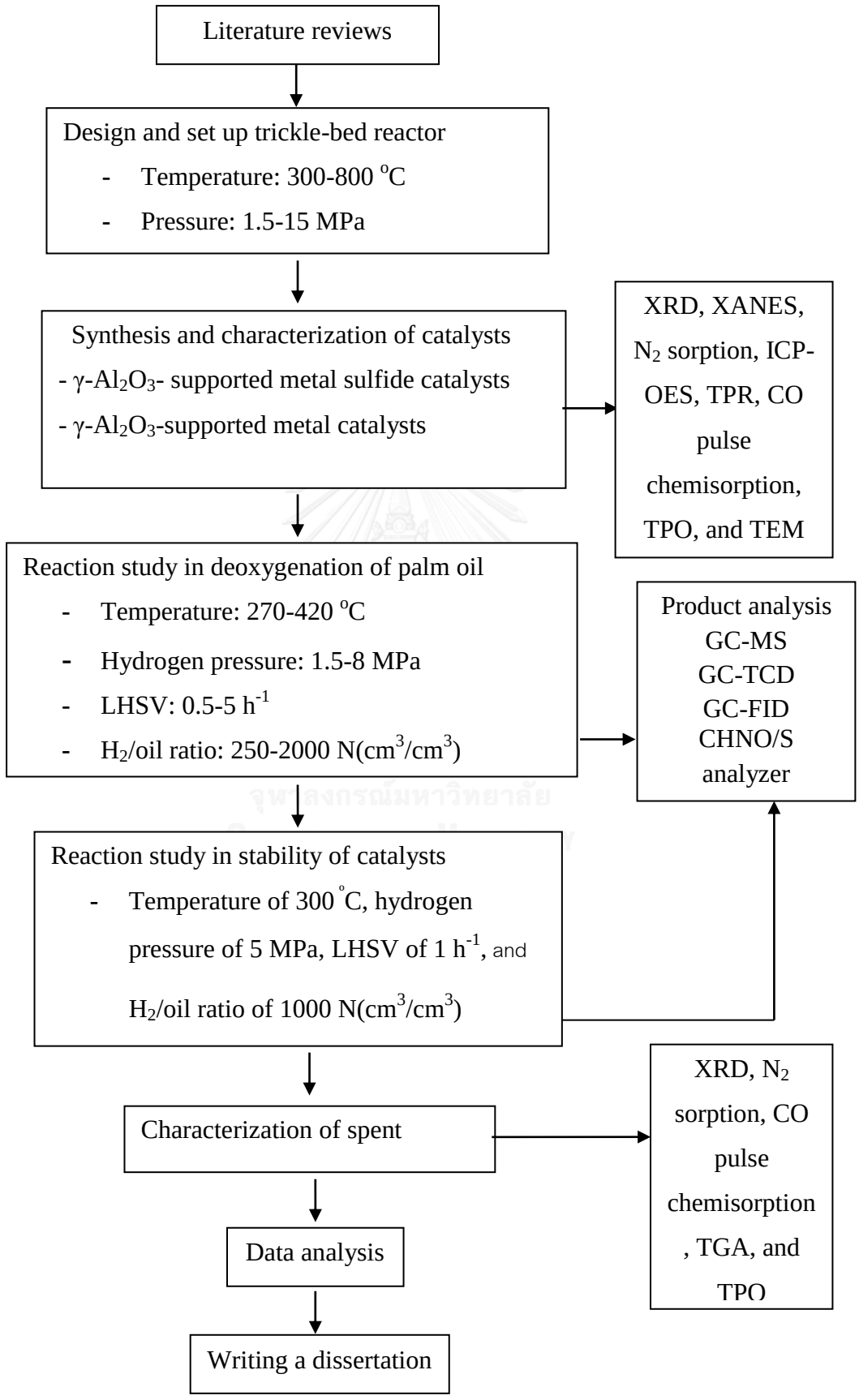

CHAPTER II

THEORY

This chapter presents a general description of the essential data for properties of triglycerides, technology for transformation of triglycerides to biofuels, deoxygenation reactions, thermodynamic data, and diesel properties.

2.1 Triglycerides

Triglycerides (vegetable oils or animal fats) are highly hydrophobic substance that are composed of 1 mole of glycerol and 3 mole of long chain fatty acid ester, are the structure of all vegetable oil and animal fats [46]. The example of an unsaturated triglyceride is represented in Figure 1. The triglycerides typically composed of C_8-C_{24} fatty acid with majority of C_{16} and C_{18} fatty acid, have been as an important renewable feedstock for production of renewable fuel because of a low degree of functionalization and a simple structure as compared with biomass [12, 19]. There are many types of vegetable oils have been considered as potential raw feedstocks for biofuel production mainly according to geography and climate. Rapeseed oils are used for biodiesel/green diesel production in Europe, corn and soybean oils are favored in the USA, while the abundant palm and coconut oils are employed in tropical countries such as Thailand, Malaysia, and Indonesia [47].

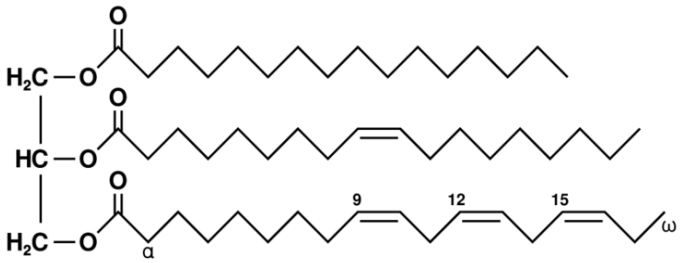

Figure 1 Example of an unsaturated triglyceride. Left part: glycerol, right part from top to bottom: fatty acids: palmitic acid, oleic acid, and linoleic acid. Chemical formula: $C_{55}H_{98}O_6$ (http://en.wikipedia.org/wiki/Triglyceride).

The properties of triglycerides depend on chain length on the fatty acid composition and degrees of unsaturation. The difference between vegetable oils and animal fats is simply one of melting point: fats are solid at room temperature (20 °C) whereas oils are liquids. Consequently, the natural fats and oils are designated as the triglyceride type in terms of saturated and unsaturated acids and isomeric forms. Saturated triglycerides have better oxidation stability and higher melting points than unsaturated triglycerides. Table 1 summarizes the nomenclature and chemical structure of fatty acids mostly found in various vegetable oils. The vegetable oil composition is commonly described by the content of fatty acids. The fatty acid compositions are regularly determined by esterification of the oil with a strong acid [1]. Furthermore, the fatty acid composition and physical properties of vegetable oil are represented in Table 2 and Table 3, respectively.

Table 1 Nomenclature and chemical structure of fatty acids mostly found in various vegetable oils [46].

Common name	Systemic name	Structure	Molecular formula
Capric acid	Decanoic acid	C10:0	$C_{10}H_{20}O_2$
Lauric acid	Dodecanoic acid	C12:0	$C_{12}H_{24}O_2$
Myristic acid	Tetradecanoeic acid	C14:0	$C_{14}H_{28}O_2$
Palmitic acid	Hexadecanoic acid	C16:0	$C_{16}H_{32}O_2$
Palmitoleic acid	9Z-Hexadecanoic acid	C16:1	$C_{16}H_{30}O_2$
Stearic acid	Octadecanoeic acid	C18:0	$C_{18}H_{36}O_2$
Oleic acid	9Z-Octadecanoeic acid	C18:1	$C_{18}H_{34}O_2$
Linoleic acid	9Z,12Z-Octadecanoeic acid	C18:2	$C_{18}H_{32}O2$
Linolnic acid	9Z,12Z-Octadecanoeic acid	C18:3	$C_{18}H_{30}O_2$
Arachidic acid	Eicosanoeic acid	C20:0	$C_{20}H_{40}O_2$
Eicosenoic acid	Docosanic acid	C22:0	$C_{22}H_{44}O_2$
Behenic acid	13Z-Docosanic acid	C22:1	$C_{22}H_{42}O_2$
Eruic acid	Tetracosanoic acid	C24:0	$C_{24}H_{48}O_2$

Table 2 Typical compositions of various vegetable oils [1].

Fatty acid	Typical composition (wt.%)				
	Jatropha	Palm	Rapeseed	Soybean	Sunflower
Capric acid	0	0	0	0	0
Lauric acid	0	0	0	0	0
Myristic acid	0	2.5	1.5	0	0
Palmitic acid	15.9	40.8	6.0	11.5	6.5
Palmitoleic acid	0.9	0	0	0	0.2
Stearic acid	6.9	3.6	3.5	4.0	5.8
Oleic acid	41.1	45.2	60	24.5	27.0
Linoleic acid	34.7	7.5	23	53.0	60
Linolenic acid	0.3	0	13	7.0	0.2
Arachidic acid	0	0	0	0	0.3
Eicosenoic acid	0.2	0	0	0	0
Behenic acid	0	0	0	0	0
Eruic acid	0	0	0	0	0
Mw	869.7	847	876.9	871.9	876.7

Table 3 Properties of various vegetable oils and petroleum diesel [46].

Properties	Vegetable oil					Petro-diesel
	Jatropha	Palm	Rapeseed	Soybean	Sunflower	
Viscosity (mm^2/s) at 40 ^oC	35.98	35.41	37.0	32.6	37.1	2.5-3.5
Density (kg/L) at 20 ^oC	0.9186	0.880	0.9115	0.9138	0.9161	0.835-0.845
ΔH (Mj/kg)	39.07	-	39.71	39.62	39.58	45.05-45.34
Cloud point (^oC)	9	-	-3.9	-3.9	7.2	-15
Pour point (^oC)	4	-	-31.7	-12.2	-15	-33
Flash point (^oC)	229	-	246	254	274	55
No ofCetane	45	-	37.6	37.9	37.1	49-52
Iodine index	-	-	120	146	143	-

2.2 Technology for transformation of triglycerides to biofuels

Triglycerides can be directly used in diesel engines, however the direct combustion causes many engine problems due to the high viscosity and low volatility of triglycerides, e.g., carbon deposits, coking on the injector, and oil ring sticking. These problems require triglycerides to be upgraded before using as biofuel. The commercial upgrading process involves of triglycerides and alcohol into fatty acid alkyl esters (FAAEs) and glycerol, which is applied in the first generation biodiesel production. Triglycerides can also be refined by cracking, pyrolysis, hydrotreating and deoxygenation processes to produce hydrocarbons as next generation biofuel [47].

2.2.1 Thermal cracking/pyrolysis of vegetable oils

The thermal cracking of vegetable oils, also known as pyrolysis of vegetable oils, to produce compounds with characteristics similar to those of petroleum fuels. The cleavage of the triglyceride molecules leads to the formation of a mixture of hydrocarbons of smaller chains and oxygenated compounds, such as alkanes, alkenes, alkadienes, aromatics, aldehydes, ketones, and carboxylic acids. Due to the complexity of the pyrolysis mechanism, several studies have proposed two distinct steps that can occur simultaneously for this type of reaction. In the first step, acid species (primarily carboxylic acids) are formed during the thermal decomposition of triglycerides from the breakdown of the C-O bonds located between the portion that corresponds to the glycerol and the rest of the molecule. This step is called primary cracking. In the second step, called secondary cracking, the species obtained in the first step undergo decomposition, which leads to the formation of organic compounds with shorter chain lengths, including saturated and/or unsaturated hydrocarbons. According to the literature, primary cracking can be explained through the mechanisms of γ-hydrogen transfer and β-elimination are represented in Figure 2 and Figure 3, respectively [46].

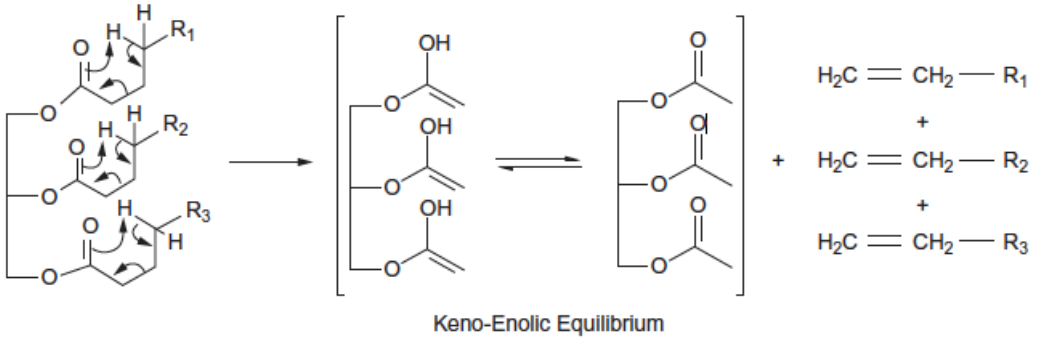

Figure 2 Mechanism for the transfer of γ-hydrogen. R_1, R_2, and R_3 represent the saturated or unsaturated carbon chains originating from the fatty acids that constitute the triglycerides.

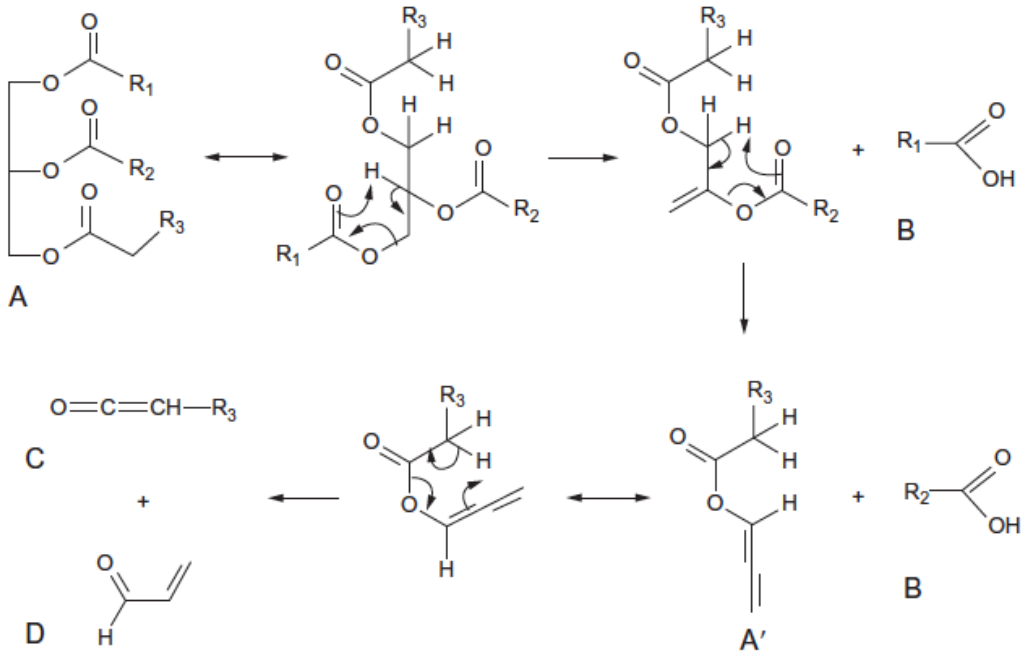

Figure 3 Mechanism of β elimination for the cracking of triglycerides. The hypothetical triglyceride molecule consists of saturated and/or unsaturated carbon chains represented by R_1, R_2, and R_3 (A). The decomposition process forms a highly unstable intermediate (A') and fatty acid (B), ketene (C), and acrolein (D) molecules.

2.2.2 Transesterification of vegetable oils

Biodiesel is an alternative biofuels derived from vegetable oils or animal fats. The most common way to produce biodiesel is the transesterification. Transesterification, also called alcoholysis defines as a chemical reaction between an ester bond of triglyceride and short-chain alcohol in the absence or presence of a catalyst to form esters and glycerol. The overall process is normally a sequence of three reversible reactions, in which triglyceride is converted stepwise to diglyceride, monoglyceride, and glycerol. A mole of ester is liberated at each step. The stoichiometric reaction requires one mole of triglyceride and three moles of alcohol to form one mole of glycerol and three moles of the respective alkyl ester. However, an excess of the alcohol is used to increase the yield of the alkyl esters and to allow its

physical separation from the glycerol formed. The complete transesterification is simplified in Figure 4a. In the presence of water, the triglyceride can be partially hydrolyzed to fatty acids and diglyceride under suitable conditions. Those fatty acids, including the free fatty acids (FFA) present in the feedstock, would be converted to the alkyl ester through an esterification reaction when water is a byproduct, as shown in Figure 4b.

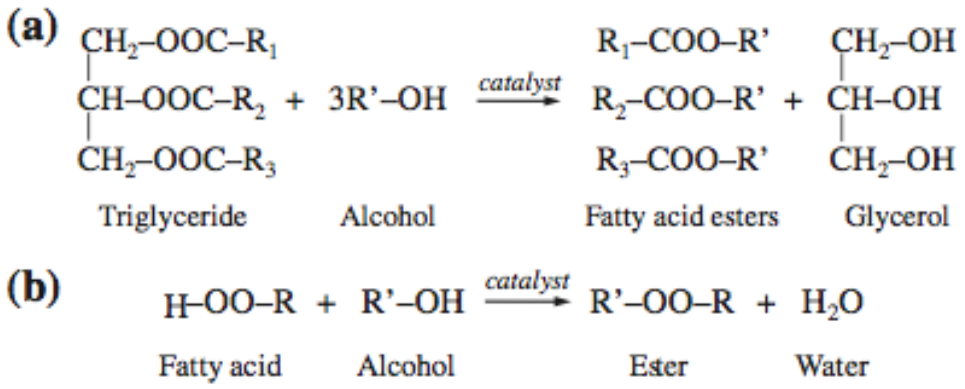

Figure 4 (a) Transesterification of triglycerides and (b) esterification of fatty acids with alcohol.R, R_1, R_2, R_3, and R' = alkyl group [19].

2.2.3 Deoxygenation of vegetable oils

There are 3 main reaction pathways for deoxygenation of triglycerides to bio-hydrogenated diesel (BHD) including decarbonylation (DCO), decarboxylation (DCO_2), and hydrodeoxygenation (HDO) [13, 48]. As demonstrated in Figure 5, the double bonds in saturated triglycerides were first hydrogenated to unsaturated triglycerides, subsequently cleaved to free fatty acids and propane. The free fatty acid, as the major oxygenated intermediates, could undergo to yield a fatty acid alcohol and subsequently hydrocarbons through three major reaction pathways. Hydrodeoxygenation (HDO), an exothermic reaction, eliminates oxygen in the form of water and yields n-alkane with same carbon number as the corresponding fatty acid. Decarbonylation (DCO), and decarboxylation (DCO_2), endothermic reactions,

lead to elimination of oxygen in form of CO and water or CO_2, respectively. The consequent n-alkane has one carbon atom loss compared to the original fatty acid [2, 49]. The other reactions (gas phase reactions), which involve this process, are methanization and water gas shift reactions. Table 4 showed the overall deoxygenation reaction of fatty acid to bio-hydrogenated diesel and thermodynamic data.

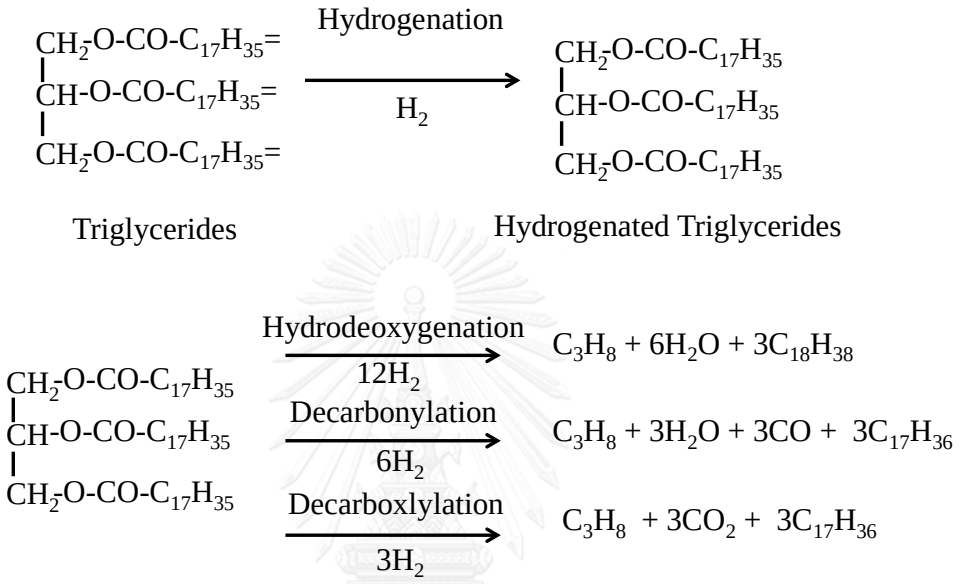

Figure 5 Reaction mechanisms for deoxygenation of triglycerides to bio-hydrogenated diesel (BHD) [19].

Table 4 Overall deoxygenation reaction of fatty acid to bio-hydrogenated diesel (BHD), other reactions, and thermodynamic data [8, 21, 39, 40, 50]

Liquid phase	Reactions	ΔG_{533} (kJ/mol)	ΔH_{533} (kJ/mol)
Hydrodeoxygenation	$R\text{-}COOH + 3H_2 \longrightarrow R\text{-}CH_3 + 2H_2O$	-88.0	-112.6
Decarbonylation	$R\text{-}COOH + H_2 \longrightarrow R\text{-}H + CO + H_2O$	-59.5	49.7
Decarboxylation	$R\text{-}COOH \longrightarrow R\text{-}H + CO_2$	-78.6	10.1
Gas phase	**Reactions**	ΔG_{533} (kJ/mol)	ΔH_{533} (kJ/mol)
Methanation	$CO + 3H_2 \longrightarrow CH_4 + H_2O$	-88.4	-215.3
Methanation	$CO_2 + 4H_2 \longrightarrow CH_4 + 2H_2O$	-69.2	-175.7
Water gas shift	$CO + H_2O \longrightarrow CO_2 + H_2$	-19.1	-39.6

2.3 Hydrodeoxygenation (HDO)

Hydrodeoxygenation (HDO) is a hydrogenolysis reaction that removes oxygenated compounds from the organic molecule in reaction with hydrogen forming water using the commercial hydrotreating catalysts. There is commonly used NiMo or CoMo supported on γ-Al_2O_3, zeolites (ZSM-5), Pd or Pt on carbon as well as alumina. The NiMo sites for hydrogenation reactions and acid catalytic sites for dehydration reactions. The summarized reactions are showed as follows in Figure 6.

The carboxylic acids as a reactant which is hydrogenated can be converted into Aldehyde and water. The aldehyde compound is enolized because α-hydrogen can be isomerized to the enol from, which is the reactive intermediate.

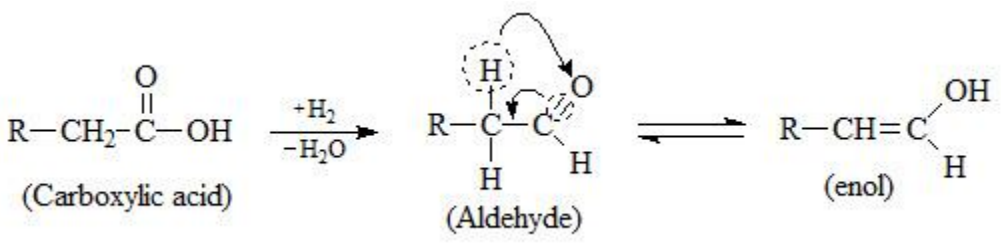

Figure 6 Reaction pathway of carboxylic acid to enol form lacking α-hydrogen cannot be isomerized to the enol form [21].

Figure 7 showed the enol form could either be hydrogenated over the catalyst at the highly reactive oxygen, at the C=C double forming alcohol or forming 1-alkene and water. The alcohol which is dehydrated can be converted into alkane and water. The alkene which is hydrogenated at C=C double can be converted to alkane [21].

When the triglycerides which have no double bond are converted by the hydrodeoxygenation route, the products for this mechanism are water, propane and three normal alkanes of the full length of fatty acid chains as represented in Figure 8. By this reaction, one mole of triglyceride reacts with 12 moles of hydrogen. The products are forms one mole of propane, six moles of water, and three moles of normal alkanes of the full length of fatty acid [21, 51].

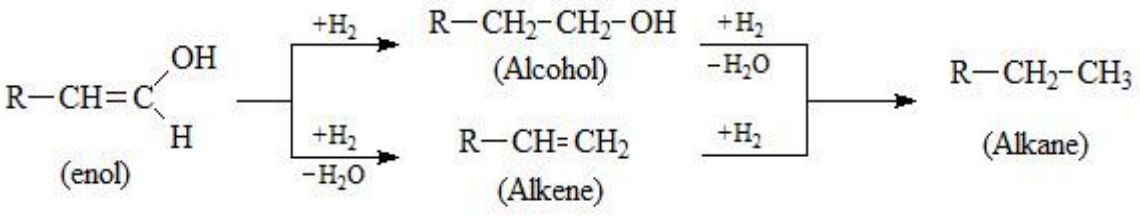

Figure 7 Reaction pathway of enol from to alkane.

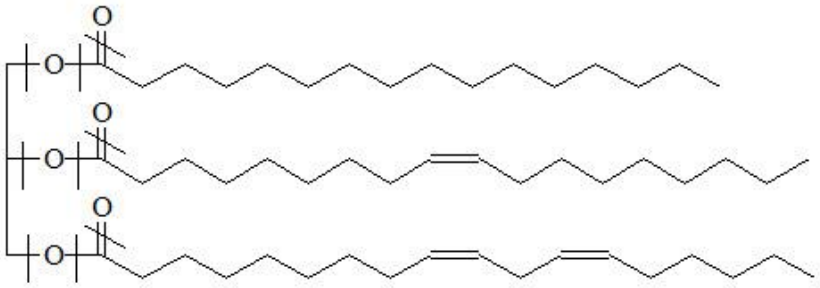

Figure 8 Mechanism of the hydrodeoxygenation reaction pathway for the removal of triglyceride oxygen.

2.4 Decarboxylation (DCO_2)

The decarboxylation is a chemical reaction which releases carbon dioxide (CO_2). Generally, decarboxylation refers to a reaction of carboxylic acids, removing a carbon atom from a carbon chain and no hydrogen required to convert a carboxylic acid group to an alkane.

When the triglycerides which have no double bond are converted by the decarboxylation route, the products of this mechanism are carbon dioxide, propane and three moles of normal alkanes with carbon numbers one less than fatty acid chains in Figure 9. By this reaction, one mole of triglyceride reacts with 3 moles of hydrogen. The products are forms one mole of propane, three moles of carbon dioxide and three moles of a normal alkanes one carbon atom shorter than the full length of fatty acid [21, 51].

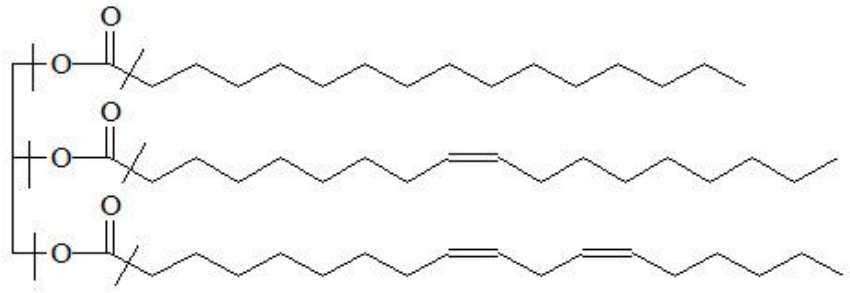

Figure 9 Mechanism of the decarboxylation reaction pathway for the removal of triglyceride oxygen.

2.5 Decarbonylation (DCO)

The decarbonylation is chemical reaction, which the carboxylic group is reacted with hydrogen for removal one or more carbonyl groups from a molecule to produce a methyl group, carbon monoxide and water. When the triglycerides which have no double bond are converted by the decarbonylation route, the products for this mechanism are carbon monoxide, water, propane and three normal alkanes with carbon numbers one less than fatty acid chains in Figure 10. By this reaction, one

mole of triglyceride reacts with 6 moles of hydrogen. The products are forms one mole of propane, three moles of carbon monoxide, three moles of water and three moles of a normal alkanes one carbon atom shorter than the full length of fatty acid [21, 51].

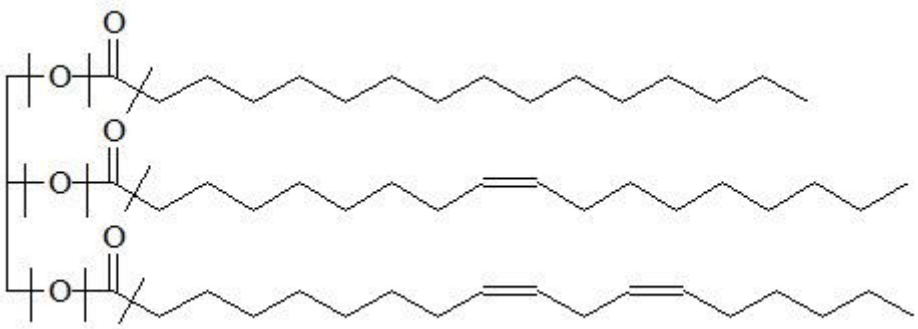

Figure 10 Mechanism of the decarbonylation reaction pathway for the removal of triglyceride oxygen.

2.6 Isomerization and cracking

The normal alkanes produced from triglyceride can undergo isomerization and cracking to produce isomerized and lighter alkanes, respectively. The normal alkanes have a high cetane number, which is a good for diesel production. If the normal alkanes are desired then the isomerization and cracking reactions should be minimized [52].

2.7 Water gas shift and methanation

The carbon monoxide and carbon dioxide are formed, there are two additional reactions. These are water gas shift and methanation. The water gas shift is a chemical reaction in which carbon dioxide reacts with hydrogen to form carbon monoxide and water vapor as shown in Eq. 2.1. The methanation is converted carbon monoxide from water gas reaction reacting with hydrogen into methane and water vapor as shown in Eq. 2.2. The both reactions are influence the hydrogen consumption and product yields [51].

$$CO_2 + H_2 \longleftrightarrow CO + H_2O \qquad (2.1)$$

$$CO + 3H_2 \longrightarrow CH_4 + H_2O \qquad (2.2)$$

2.8 Diesel product properties

After the reaction run, aqueous and organic liquid phase were physically separated and, analyzed using several gas-chromatography methods. Gas products (carbon monoxide, carbon dioxide, methane, and propane) were analyzed by gas-chromatography thermal conductivity detector (GC-TCD). Organic liquid products were analyzed by gas-chromatography with flame ionization detector (GC-FID). The physiochemical properties of the organic liquid products are shown in Table 5.

Table 5 Standard test physiochemical properties of the organic liquid products [9, 53]

Properties	Solution	Method	
		European diesel fuel standard (EN)	ASTM
Density (15°C)	aerometer	EN ISO 3675, EN ISO 12185	ASTM D-4052
Kinematical viscosity (40 °C)	Ubbelohde viscosimeter	EN ISO 3104	ASTM D-445
Fractional composition		EN ISO 3405	
Flash point	Pensky-Martens-closed cup	EN ISO2719	ASTM D-93
Cloud point			ASTM D-2500
Pour point			ASTM D-97
Corrosion			ASTM D-130
Color			ASTM D-1500
Cold filter plugging point (CFPP)		EN 116	

Table 5 Standard test physiochemical properties of the organic liquid products (Cont.)

Properties	Solution	Method	
		European diesel fuel standard (EN)	ASTM
Total acid number (TAN)	titration of the sample with KOH solution PN 85/C-04066		ASTM D-664 ASTMD974
Carbon and hydrogen			ASTM D-5291
Cetane index			ASTM D-4737
Thermal stability			ASTM D-6468
Simulated distillation			ASTM D-7213 ASTM-2887-D86
Contents of ester bonds, aromatic compounds and carboxylic groups in hydrorefined products	FTIR method		

The physiochemical properties of the organic liquid products can be comparison with European diesel fuel standard EN590, NExBTL biodiesel, GTL diesel and FAME as shown in Table 6 and cetane number in Table 7.

Table 6 The physiochemical properties standard of the organic liquid products from Hydroprocessing. [54]

Fuel properties	NExBTL biodiesel	GTL diesel	FAME	EN590/2005
density @ 15°C (kg/m^3)	775-785	770-785	≈ 885	≈ 835
viscosity @ 40°C (mm^2/s)	2.9-3.5	3.2-4.5	≈ 4.5	≈ 3.5
Cetane index	84-99	73-81	≈ 51	≈ 53
Distillation 10 vol% (°C)	260-270	≈ 260	≈ 340	≈ 200
Distillation 90 vol% (°C)	295-300	325-330	≈ 355	≈ 350
Cloud point (°C)	-5…-30	0…-25	≈ -5	≈ -5
Lower heating value (MJ/kg)	≈ 44	≈ 43	≈ 38	≈ 43
Lower heating value (MJ/litres)	≈ 34	≈ 34	≈ 34	≈ 36
Polyaromatics (wt%)	0	0	0	≈ 4
Oxygen (wt%)	0	0	≈ 11	0
Sulfur (mg/kg)	≈ 0	< 10	< 10	< 10

Table 7 Cetane number of normal and iso-paraffins. (Santana et al., 2006)

N-PARAFFINS	CN	ISO-PARAFFINS	CN
n-Butane	22	2-Methylpentane	33
n-Pentane	30	3-Methylpentane	30
n-Hexane	45	2,3-Dimethylpentane	22
n-Heptane	54	2,4-Dimethylpentane	29
n-Octane	64	2,2,4-Trimethylpentane	14
n-Nonane	72	2,2,5-Trimethylhexane	24
n-Decane	77	2,2-Dimethyloctane	59
n-Undecane	81	2,2,4,6,6-Pentamethylheptane	9
n-Dodecane	87	3-Ethyldecane	47
n-Tridecane	90	4,5-Diehtyloctane	20
n-Tetradecane	95	4-Propyldecane	39
n-Pentadecane	96	2,5-Dimethylundecane	58
n-Hexadecane	100	5-Butylnonane	53
n-Heptadecane	105	2,7-Dimethyl-4,5-diethyloctane	39
n-Octadecane	106	5-Butyldodecane	45
n-Nonadecane	110	7,8-Dimethyltetradecane	40
n-Eicosane	110	7-Butyltridecane	70
		7,8-Diethyltetradecane	67
		8-Propylpentadecane	48
		9-Methylheptadecane	66
		5,6-Dibutyldecane	30
		9,10-Dimethyloctadecane	60
		7-Hexylpentadecane	83
		2,9-Dimethyl-5,6-diisopentyldecane	48
		10,13-Dimethyldocosane	56
		9-Heptylheptadecane	88
		9,10-Dipropyloctadecane	47

CHAPTER III

LITERATURE REVIEWS

In this chapter, the literature reviews involving deoxygenation of triglycerides to bio-hydrogenated diesel (BHD) are provided. It is divided into three topics. Firstly, previous work on hydrotreating of triglycerides over supported metal sulfide catalystsis presented. Next, deoxygenation of fatty acids/triglycerides over supported metal catalysts is reviewed. Finally, advantages of bio-hydrogenated diesel (BHD) over fatty acid methyl ester/biodiesel are summarized.

3.1 Catalysts used in deoxygenation of triglycerides

Various types of catalysts have been used in deoxygenation reactions of triglycerides to hydrocarbons. Supported metal sulfide catalysts e.g. $NiMoS_2$, $CoMoS_2$, and $NiWS_2$ supported on Al_2O_3 are suggested to be catalysts for deoxygenation reaction. One of the key features of alumina support is its excellent mechanical strength. However, researches have shown the disadvantage that there are strong interactions between alumina and transition metal oxides. The interaction enables some species as precursors that are very stable and may prevent complete sulfidation, potentially decreasing the activity of the catalysts. Supported metal catalyst or sulfur-free catalysts such as Ni, Pd, Pt, Rh, and Ru supported on Al_2O_3, SiO_2, CeO_2, ZrO_2[55], and carbon, have shown quite selective propensity to formation of hydrocarbons and carbon oxides. The supported metal catalysts are favorable to decarbonlylation and decarboxylation, while hydrodeoxygenation is dominant in supported metal sulfide catalysts, except $NiWS_2$. Some metal catalysts such as Ni, Pd, and Pt strongly promoted methanation reaction, consuming large amount of hydrogen. It is essential to avoid subsequent reactions of CO_2 that consume hydrogen, such as methanization. As represented in Figure 11, the differences in the deoxygenation

pathways were observed over the supported metal catalysts (Ni, Pd) and the supported metal sulfide catalysts ($CoMoS_x$ and $NiMoS_x$). Especially, the Ni and Pd catalysts showed higher activity in decarboxylation and decarbonylation reactions (C-C bond scission), whereas the $CoMoS_x$ and $NiMoS_x$ are more favorable in hydrodeoxygenation reaction (C-O bond scission).

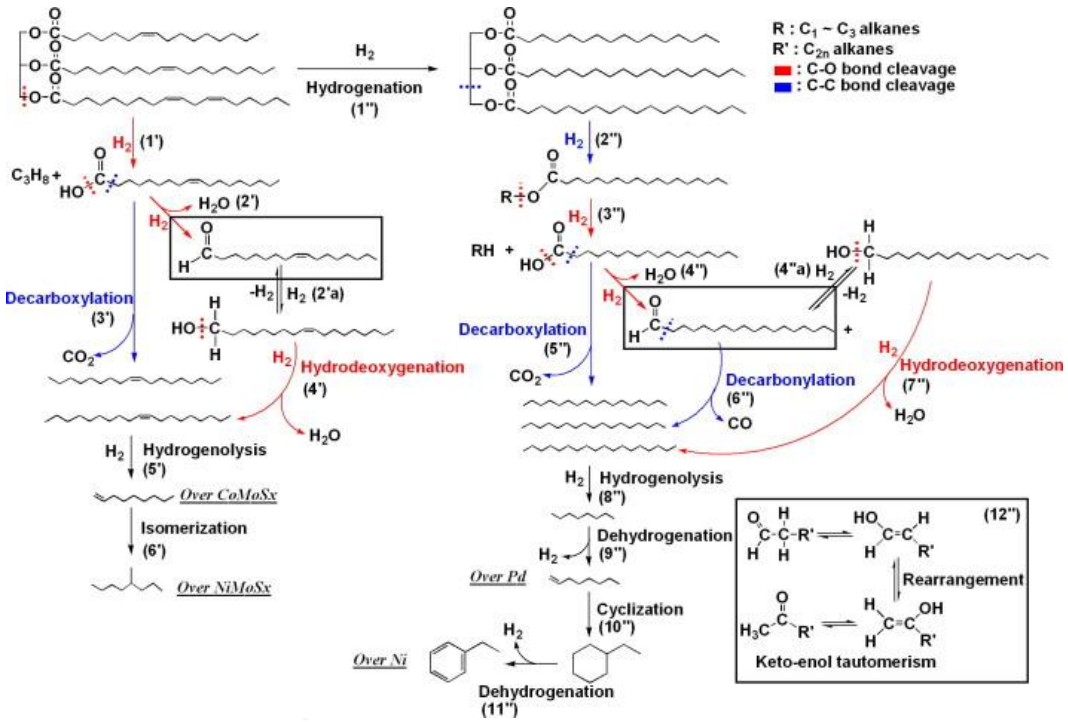

Figure 11 Reaction pathways for the catalytic deoxygenation of a triglyceride over $NiMoS_x$, $CoMoS_x$, Ni, and Pd catalysts [56].

3.2 Deoxygenation of triglycerides over supported metal sulfide catalysts

Triglycerides can be hydrotreated over convention supported metal sulfide catalysts ($NiMoS_2$, $CoMoS_2$, and $NiWS_2$) through 3 major reaction pathways including decarbonylation, decarboxylation, and hydrodeoxygenation, thus producing straight-chain alkanes ranging from *n*-C_{15} to *n*-C_{18} at 300–450 °C in the presence of

H_2 at 15–150 bar [39, 57]. Compared with thermal cracking/pyrolysis process, hydrotreating process is more selective for diesel-range hydrocarbon and yields a high conversion of triglyceride and high product yield in range of *n*-C_{15} to *n*-C_{18}corresponding to diesel fractions [39].

Kubicka, D., *et al.* studied the deoxygenation of rapeseed oil over sulfide Ni, Mo, and NiMo catalysts supported on alumina (Al_2O_3) in a fixed-bed reactor 260–280 ^{O}C, 3.5 MPa and 0.25–4 h^{-1}. They found that ability of the bimetallic NiMo catalyst in deoxygenation exhibited higher than the monometallic catalyst. Ni acts as a promoter in the NiMo sulfide catalysts during deoxygenation, whereas, NiMo sulfide catalyst yielded both hydrodeoxygenation and decarboxylation products in conversion of rapeseed oil, Ni sulfide catalyst yielded exclusively decarboxylation products and Mo sulfide catalyst almost exclusively hydrodeoxygenation products [13].

They also discussed in the reaction network of rapeseed oil to hydrocarbons, as illustrated in Figure 12. Briefly, the double bonds in triglycerides are saturated and then converted to fatty acids. The fatty acids, as main oxygenated intermediates, can be undergone to yield fatty alcohols and saturated n-alkanes with an even carbon atoms number (hydrodeoxygenation) or (ii) directly undergone hydrodecarboxylation to yield hydrocarbons [13].

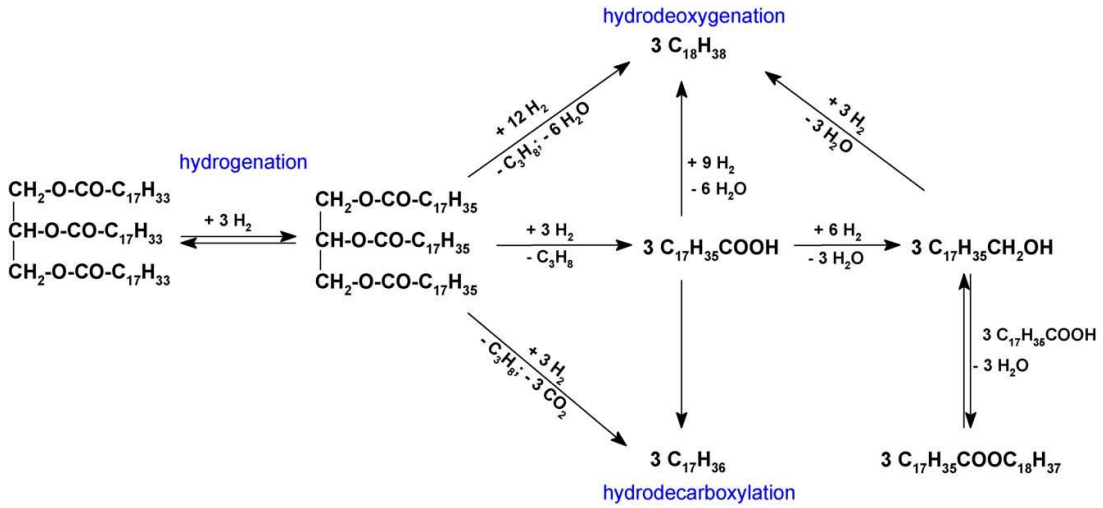

Figure 12 Proposed reaction pathway of triglycerides to hydrocarbons [13, 58].

Horáce, J., *et al.* [28] investigated the effect of promoters (Ni or Co), active phase metals (Mo or W), (NiMo, CoMo, NiW, CoW, NiCoMo, and CoNiW supported on Al_2O_3), on the activity and selectivity of catalysts in deoxygenation of rapeseed oil in a tubular reactor at 250 and 270 ^oC, and various flow rates (W/F = 0.25, 0.5, and 1 h). They found that $NiMo/Al_2O_3$ catalyst was the most active catalyst than others, whereas CoW/Al_2O_3 was the least active catalyst in deoxygenation of rapeseed oil. $CoMo/Al_2O_3$catalyst showed high selectivity for hydrodeoxygenation reaction pathway type catalysts. Additionally, the adding Co into NiMo catalyst resulted in conversion decrease.

Brillouet, S., *et al.* suggested and explained a catalytic cycle involved during the transformation of decanoic acid to hydrocarbons over sulfide metal catalysts at 340 ^oC and 4 MPa in a fixed-bed reactor, as demonstrated in Figure 13. It well knows that the active sites present the edges of the MoS_2 phase in metal sulfide catalysts is a sulfur vacancy. The first step of the proposed reaction mechanism requires the heterolytic dissociation of molecular hydrogen to a metal hydride (Mo-H) and a sulfhydryl (-SH) group [59]. Then, adsorption of carbonyl group in decanoic acid can occur on a sulfur vacancy in MoS_2 phase [60]. The next step could be a protonation of decanoic acid due to the acidity of the SH group. After elimination of water, the adsorbed carbocation could be an important intermediate. Certainly, the cationic species could be a common intermediate for the decarbonylation and the hydrodeoxygenation routes. This intermediate can undergo either a hydride addition step or an elimination step. In the first case, the direct addition of a hydride species to the cationic intermediate leading to decanal, which is the primary product formed by the hydrodeoxygenation route. In the second case, the C-C bond breaking might occur through a basic attack on the hydrogen atom in β-position with respect to the carbon atom carrying the positive charge of the cationic intermediate in decarbonylation route [61].

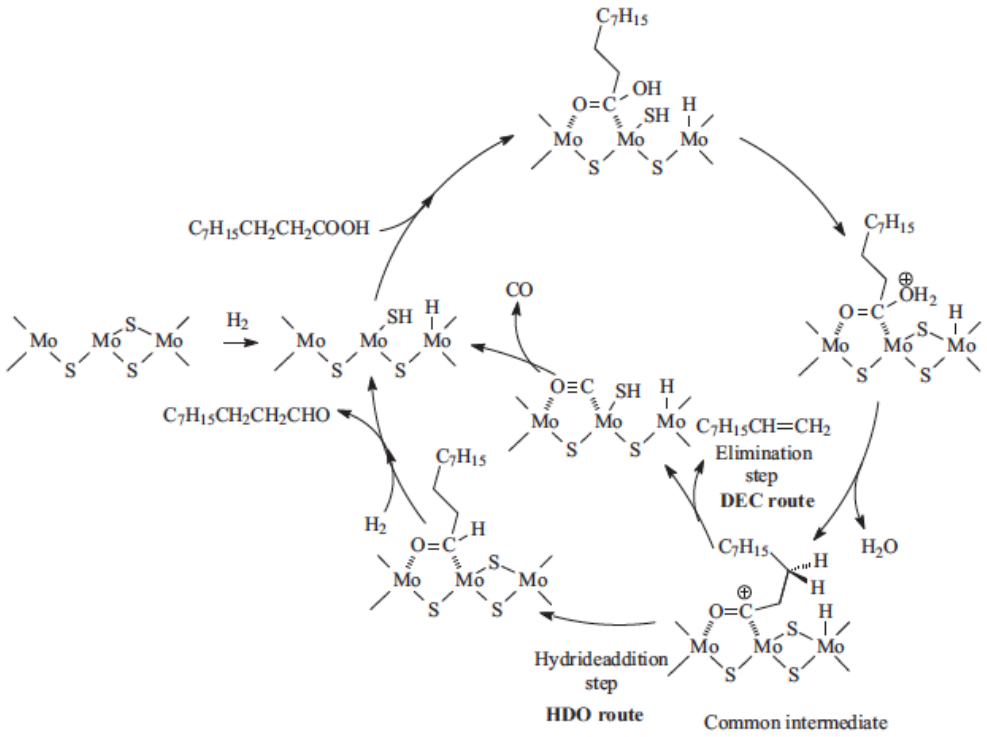

Figure 13 Proposition of a catalytic cycle involved during the deoxygenation of decanoic acid on a schematic unpromoted MoS_2 active site [61] .

Kubicka, D., *et al.* explored the effect of supports, (SiO_2, TiO_2, and Al_2O_3) , and sulfide NiMo active phase interactions for the deoxygenation of pure rapeseed oil at 260–300 ^oC, 3.5 MPa and WHSV of 2–8 h^{-1}. The results showed that the SiO_2-supported NiMo catalyst revealed smaller extent of hydrogenation reactions and a higher promotion of decarboxylation reaction, whereas, TiO_2-supported NiMo catalyst exhibited increased selectivity to hydrodeoxygenation reaction. It may be due to the larger active phase cluster size and broad pore size distribution [18].

Huber, G.W., *et al.* studied the hydrotreating of pure sunflower oil over sulfide $NiMo/Al_2O_3$ at 300- 350 °C, 5 MPa H_2, and LHSV of 5.2 h^{-1}. They found that the 100 % conversion and 70 % product yield (carbon basis) of *n*-C_{15} to *n*-C_{18} alkanes were achieved at 350 ^oC. The reaction pathways for the conversion of triglycerides to alkanes over sulfided $NiMo/Al_2O_3$ are represented in Figure 14. The hydrotreating of triglycerides mainly takes place in 3 steps (i) hydrogenation of unsaturated

triglycerides, (ii) hydrogenolysis of saturated triglycerides to fatty acids as the main oxygenated intermediates and propane, and (iii) hydrodeoxygenation, decarbonylation or decarboxylation of fatty acids to alkanes. The oxygen from fatty acids can be eliminated in form of CO (decarbonylation), CO_2 (decarboxylation), and H_2O (hydrodeoxygenation) [52].

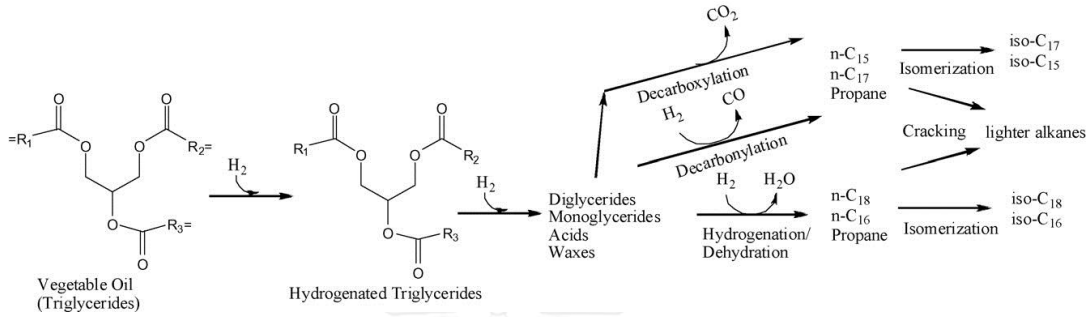

Figure 14 Reaction pathways for the conversion of triglycerides to alkanes over sulfided $NoMo/Al_2O_3$ [52].

Bezergianni *et al.* studied the catalytic hydrotreating of waste cooking oil over sulfide $NiMo/Al_2O_3$ catalyst in hydroprocessing pilot plant at temperature in the range of 330 – 398 ^oC, pressure of 8.2 MPa, LHSV of 1 h^{-1}, and H_2/Oil of 4000 scfb. The product yields, conversion, selectivity (diesel and gasoline), heteroatom removal (sulfur, nitrogen and oxygen) and saturation of double bonds were used to evaluate the effect of hydrotrating temperature. The results revealed that diesel selectivity dropped to 90% with increase temperature, whereas, the increase in temperature enhanced the gasoline selectivity. Heteroatom removal, sulfur and nitrogen, were most successfully removed in all cases (over 99.4%) while oxygen removal was more favorable by hydrotreating temperature. Moreover, the increase of temperatures favored the saturation of double bonds as indicated by the decreasing bromine index and increasing hydrogen consumption.

Furthermore, the supported metal sulfide catalysts can be deactivated during hydrotreating of triglycerides to alkanes. Since, the sulfur leaching lead to catalyst deactivation and sulfur contamination in liquid product [31, 36, 37, 41]. It should be noted that metal sulfide catalysts require adding the sulfinding agents e.g. CS_2 and DMDS in liquid feed to avoid catalyst deactivation during deoxygenation reactions [22, 38]. Additionally, the trace amount of water, produced from DCO and HDO reactions, would hasten the sulfur leaching and rigorously shorten the lifetime of catalysts [39].

As summary, various oil sources, reactor type, reaction conditions, supported metal sulfide catalysts, main production obtained during hydrotreating of vegetable oil are summarized in Table 8.

Table 8 Performance of supported metal sulfide catalysts in hydrotreating of vegetable oil [1]

Item	Catalyst	Oil	Reactor	Condition	Main product	Performance	Reference
1	Sulfided $CoMo/Al_2O_3$	Sunflower oil	Fixed-bed	T=360-380 ^oC P=6-8 MPa LHSV=1.0-1.2 h^{-1} H_2/oil ratio = 450 Nm^3/m^3	Gases C_5-C_{10} n-paraffins C_{11}-C_{19} and iso-paraffins	Conversion: 94-99.8 Yield: 63.1-71.5 wt.%	[3]
	Sulfided $NiMo/Al_2O_3$					Conversion: 81.8-97.4% Yield: 42-52.9 wt.%	
	Sulfided NiW/Al_2O_3					Conversion: 86.7-95.6% Yield: 9.4-49.3 wt.%	

Table 8 Performance of supported metal sulfide catalysts in hydrotreating of vegetable oil (Continue)

Item	Catalyst	Oil	Reactor	Condition	Main product	Performance	Reference
2	Sulfided $NiMo/Al_2O_3$-F	Sunflower oil	Fixed-bed	T=350-370 ^oC P=2-4 MPa LHSV=1.0 h^{-1} H_2/oil ratio = 500 Nm^3/m^3	n-paraffins C_{15}-C_{18}	Yield: 73.2-75.6 wt.%	[4]
3	Sulfided $CoMo/Al_2O_3$	Sunflower oil	Fixed-bed	T=380 ^oC P=4-6 MPa LHSV=1.0 h^{-1} H2/oil ratio = 500 -600 Nm^3/m^3	n-paraffins C_{15}-C_{18}	Yield: 73.7-73.9 wt.%	[7]
4	Sulfided $CoMo/Al_2O_3$	Palm oil	Fixed-bed (Pilot plant)	T=350 ^oC P=4-9 MPa LHSV=2 h^{-1} TOS=0-14 days	n-paraffins C_{15}-C_{18}	Molar yield: 100 wt.%	[9]

Table 8 Performance of supported metal sulfide catalysts in hydrotreating of vegetable oil (Continue)

Item	Catalyst	Oil	Reactor	Condition	Main product	Performance	Reference
5	Sulfided $NiMo/Al_2O_3$-SiO_2	Jatropha oil	Fixed-bed	T=350^oC P=3 MPa LHSV=2 h^{-1} H_2/oil ratio = 600 ml/ml	n-paraffins C_{15}-C_{18}	Yield: 82.4 – 88.2 wt.%	[2]
6	Sulfided NiMo/ZHM-5-Al_2O_3	Jatropha oil	Fixed-bed	T=350 ^oC P=3 MPa LHSV=2.0 h^{-1} H2/oil ratio = 600 ml/ml	n-paraffins C_{15}-C_{18}	Yield: 40.34 wt.%	[7]
7	Sulfided $NiMo/Al_2O_3$	Waste cooking oil	Fixed-bed	T= 350-390 ^oC P=1.37 MPa LHSV=0.5-2.5 h^{-1} H2/oil ratio = 1068m^3/m^3	n-paraffins C_{15}-C_{18}	Yield: 73 – 82 wt.%	[10]

3.3 Deoxygenation of fatty acids/triglycerides over supported metal catalysts

Supported metal catalysts have been reported to convert fatty acids, esters, and triglycerides into hydrocarbons through decarboxylation and decarbonlylation reactions resulting in more odd carbon number in liquid product. Furthermore, methanation and water gas shift are the main reaction in gas phase. The support metal catalysts possess several advantages over conventional sulfide catalysts [62, 63]:

(1) High reactivity at moderate temperature, achieving an energy efficient hydrodeoxygenation process.

(2) No sulfur leaching.

(3) Flexible catalyst design by tailoring the active phase and support.

Snåre et *al.* screened metal catalysts (Pd, Pt, Ru, Mo, Ni, Rh, Ir, and Os) supported on carbon, Al_2O_3, and SiO_2in deoxygenation of stearic acid to n-alkanes at 300 ^{o}C and 0.6 MPa. The catalyst screening results revealed the highest deoxygenation acitivity reaction was obtained when the reaction was catalyzed by palladium and platinum supported on activated carbons. Also, the analysis of gas product exhibited that the decarboxylation reaction was more preferable over the Pd/C catalyst, while the decarbonylation reaction showed higher activity over the Pt/C catalyst. The outcome of comparison with different metals on the equivalent supports by normalizing the results with metal content depicted that the beneficial effect of a metal in the deoxygenation reaction is in the descending order Pd> Pt > Ni > Rh > Ir > Ru > Os catalysts. The other reactions, such as hydrogenation, dehydrogenation, cyclization, ketonization, dimerization, and cracking were observed during deoxygenation of stearic acid, as represented in Figure 15 [64].

Veriansyah *et al.* investigated the effects of various supported metal catalysts on the hydroprocessing of soybean oil in a batch reactor at 400 ^{o}C and 9.2 MPa. They found that the conversion order was found to be 4.29 wt.% Pd/γ-Al_2O_3 (91.9%) > Ni/SiO_2–Al_2O_3 (60.8%) > 4.95 wt.% Pt/ γ-Al_2O_3 (50.8%) > 3.06 wt.% Ru/ γ-Al_2O_3 (39.7%) at a catalyst/oil weight ratio of 0.044. The main liquid product composition was straight chain alkanes of *n*-C_{17} and *n*-C_{15} with more than 80 wt.% over Ni and Pd catalysts [65].

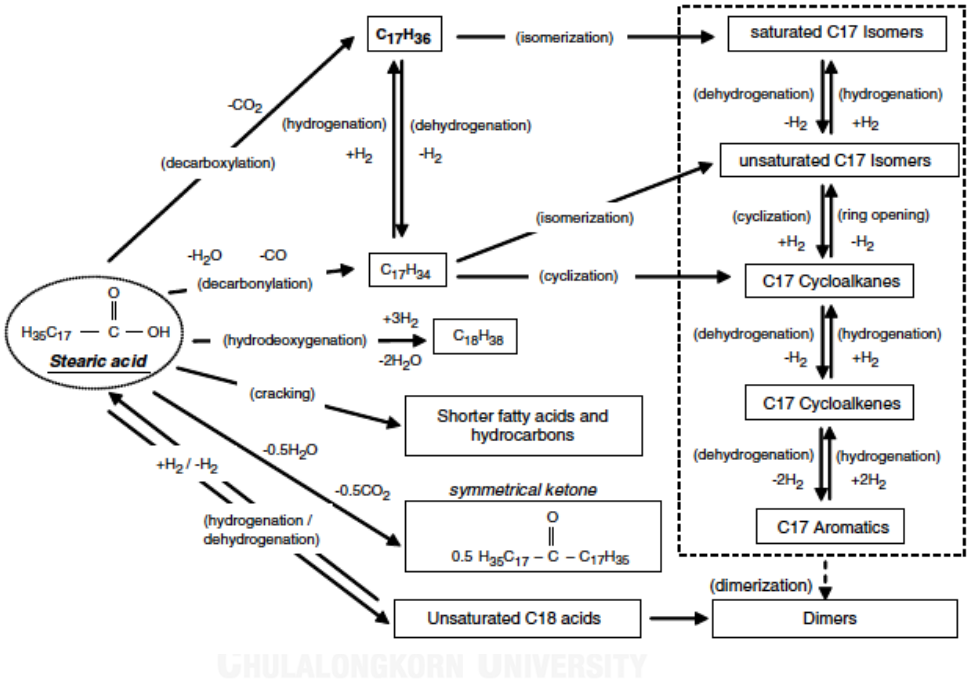

Figure 15 Proposed reaction pathways of steratic acid to hydrocarbons over various supported metal catalysts at 300 ^{o}C [64].

Duan *et al.* studied the hydrodeoxygenation of sunflower oil in an autoclaver reactor at 200-300 ^{o}C and 20 bar over Pd/Al-SBA-15 and Pd/HZSM-5 with varing Al/Si ratio. They found that the Pd/Al-SBA-15(Si/Al=300) showed a high activity as 74.4% of liquid yield and 72.9% of *n*-C15 to *n*-C18 diesel-ranged hydrocarbon at 250 °C. At a higher reaction temperature (300 °C) the strong and medium strong acid sites were in favor of C-C bond cracking to light hydrocarbons thus decreasing in diesel yield [66].

Santillan-Jimenez *et al.* explored the catalytic deoxygenation of triglycerides and fatty acids to n-alkane in a semi-batch autoclave over 20 wt.% Ni/C and 5 wt.% Pd/C catalysts. The results showed that Ni/C tended to yield lighter products in the *n*-C_{10} to *n*-C_{17} range than 5 wt. % Pd/C. Differences in the performance of these two catalysts may be attributed to the higher acidity of the Ni-based formulation, which favors the adsorption of carbonaceous species and the occurrence of cracking reactions. The effect of the gas employed (N_2, 10% H_2/N_2 or H_2) was also examined and while the presence of hydrogen resulted in improved catalytic performance, the optimum hydrogen partial pressure was found to depend on the catalyst used. For triglyceride deoxygenation, analysis of the reaction mixture at different reaction times indicates that the reaction proceeds through the decarbonylation and decarboxylation of fatty acid intermediates [43, 67].

Kumar *et al.* investigated the hydrodeoxygenation of stearic acid to hydrocarbons in a high-pressure batch reactor using *n*-dodecane as solvent over nickel metal catalysts supported on SiO_2, γ-Al_2O_3, and HZSM-5 in the temperature range of 260–290 ^{o}C. *n*-Pentadecane, *n*-hexadecane, *n*-heptadecane, *n*-octadecane, and l-octadecanol were identified as products of hydrodeoxygenation of stearic acid. The highest selectivity to *n*-heptadecane was detected when the reaction was catalyzed by Ni/γ-Al_2O_3 catalyst. A reaction mechanism of hydrodeoxygenation of stearic acid was described based on products distribution. As demonstrated in Figure 16, the hydrodeoxygenation of stearic acid mostly occurred through the reduction routes (decarbonylation and hydrodeoxygenation). First, the hydrogenolysis of stearic acid lead to formation of octadecanal and water, followed by the hydrogenation of octadecanal to octadecanol. Nevertheless, octadecanal was not found during deoxygenation of oleic acid. It should be noted to the fact that decarbonylation of octadecanal to heptadecane and CO is faster than hydrogenolysis of stearic acid to octadecanal. Accordingly, the transformation of oleic acid to hydrocarbons could proceed through two major reaction routes. In the first route, octadecanal undergoes decarbonylation to heptadecaneand carbon monoxide. On the other hand, octadecanol underwent hydrodeoxygenation to octadecane and water, as the second route. The hydrogenation, hydrogenolysis, decarbonlylation, and hydrodeoxygenation reactions

are typically occur on metallic sites of catalysts. Furthermore, No evidence to reveal that some free fatty acids could directly be converted to hydrocarbons via decarboxlylation reaction with releasing oxygen in form CO_2 [12].

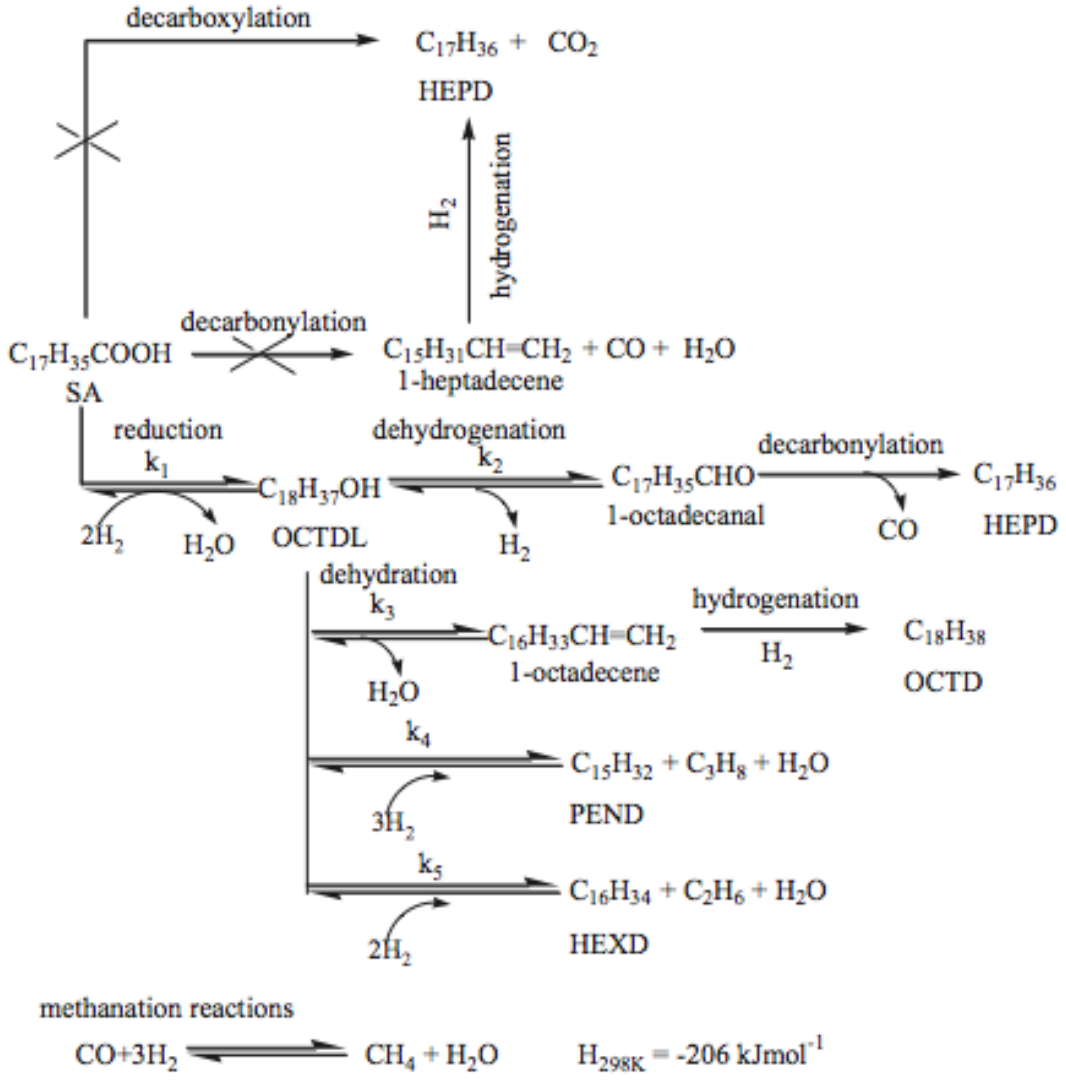

Figure 16 Reaction pathways for hydrodeoxygenation of steratic acid to hydrocarbons**.**

Apart from the supported Ni catalysts, a non-pyrophoric RANEY-type Ni catalyst was carried out in the hydroconversion of sunflower oil. The reaction was tested in the deoxygenation of octanoic acid in high-pressure fixed bed flow reactor at 280-340 °C and 21 bar of H_2. The results showed that 85% of conversion and 58% of hydrocarbon selectivity were achieved over RANEY-type Ni catalyst though the decarbonylation and decarboxylation reaction. Furthermore, Al_2O_3 supported Ni catalysts gave high active in methanation reaction and C–C bond scission, thus producing methane as by-product with high H_2 consumption. Non-pyrophoric RANEY nickel type catalyst showed higher activity than Ni/Al_2O_3 catalyst, especially in the C–C hydrogenolysis reaction [68].

Table 9 summarized the various oil sources, reactor type, reaction conditions, supported metal catalysts, the main production obtained during deoxygenation of triglycerides or fatty acids.

Table 9 Performance of supported metal catalysts in deoxygenation of triglycerides and fatty acids

Item	Catalyst	Oil	Reactor	Condition	Main product	Performance	Reference
1	1 wt.% Pd/C Sibunit	Tall oil Fatty acid	Semi-batch	T=300-325 ^{o}C P=17 bar	n-paraffins C_{17}	Conversion: 32 % (1%H_2/Ar) 59 % (100% H_2) Yield: 72 % (1%H_2/Ar) 91 % (100%H_2)	[5]
3	Pd/C	Relevant Palm oil Crude palm oil Degummed crude palm oil Palm fatty acide distillate	Batch	T=400 ^{o}C P=40 bar Reaction time=2 h	n-paraffins C_{15}-C_{18}	Yield: 51-70 wt.%	[6]
2	56 wt.% Ni/SiO_2-Al_2O_3	Soybean oil	Batch	T=300-440 ^{o}C P=25-150 bar	n-paraffins C_{17}-C_{18}	Yield: 60.48 wt.%	[8]

3.4 Advantage of deoxygenation over the transesterification

In comparison with the process to produce fatty acid methyl esters (FAME or biodiesel), the hydroprocessing of vegetable oils for production of green diesel has the following advantages. Table 10 represented the comparison of ester-based biodiesel and hydrocarbon-based green diesel.

1. The product is compatible with existing engines.
2. Flexibility with the feedstock, e.g. the content of free fatty acids in the vegetable oil does not matter.
3. Higher cetane number.
4. Higher energy density.
5. Higher oxidation stability (zero O_2 content).
6. It does not increase the emissions of NO_x.
7. It does not require water.
8. There are not byproducts that require additional treatment (e.g. glycerol).
9. The distribution of the renewable diesel does not cause additional pollution since it can be transported through the same pipelines that are currently used for distribution of petro diesel.
10. Better performance in cold weather.

Table 10 Comparison of ester-based biodiesel and hydrocarbon-based green diesel [40]

Properties	Biodiesel	Bio-hydrogenated diesel
Chemical composition	Fatty acid methyl ester	Saturated hydrocarbon
Oxygen content	10-12%	Nil
Density (g/ml)	0.888	0.78
Heating value (KJ/g)	38	45
Cloud point (^{o}C)	-5	
Sulfur content (ppm)	<1	<1
Oxidative stability	Unstable	Stable
Cetane number	50-65	70-90
Feedstock flexibility	Good quality	More feedstock flexibility
Production facility	Product require new facility	Can be produced in existing refinery
Engine modification	some changes required in existing diesel engine	No change is required

CHAPTER IV

EXPERIMENTAL

The experiment is divided into four main parts. Firstly, the preparation catalysts are provided. Second, the characterization of synthesized catalysts including XRD, XANES, N_2 sorption, CO pulse chemisorption, TPR, TPO, and TEM was performed to identify phase, physicochemical property, and morphology. Third, the deoxygenation of palm oil (refined palm olein type) in a continuous-flow fixed-bed reactor was investigated for bio-hydrogenated diesel (BHD) production. Finally, the liquid product analysis based on mole balance was calculated.

4.1 Catalyst preparations

4.1.1 Chemicals

Cobalt (II) nitrate hexahydrate [($Co(NO_3)_2.6H_2O$), purity ≥98%], nickel (II) nitrate hexahydrate [($Ni(NO_3)_2.6H_2O$), purity 99.999%], *trans*-dinitrodiamminepalladium (II) [($2NO_2.Pd.2H_3N$), purity 99.9%], and diamminedinitritoplatinum (II) [($Pt(NH_3)_2(NO_2)_2$), 3.4 wt.% solution in dilute ammonium hydroxide] were obtained from Sigma-Aldrich Chemical Co. LLC., Germany. Ammonium heptamolybdate tetrahydrate [$(NH_4)_6Mo_7O_{24}.4H_2O$), purity ≥98%] was obtained from Carlo Erba Reagent, Italy. All chemicals were used without further purification. The γ-Al_2O_3 (1.8 mm diameter, purity 99.9%) was obtained from Sasol Company, Germany.

4.1.2 Preparation of bimetallic oxide supported on γ-Al_2O_3 catalysts

The γ-Al_2O_3 support was crushed and sieved to 0.5-1.0 mm diameter. The γ-Al_2O_3 supported NiMo and CoMo catalysts were prepared by sequential impregnation. First, Mo was supported on γ-Al_2O_3 by impregnating of an aqueous

solution of ammonium heptamolybdate tetrahydrate after the sample was dried at 120 ^{o}C for 12 h to obtain Mo/γ-Al_2O_3. Then, impregnation of an aqueous solution of nickel (II) nitrate hexahydrate or cobalt (II) nitrate hexahydrate onto Mo/γ-Al_2O_3 catalyst was carried out in the similar fashion. The resultant sample was dried at 120 ^{o}C for 12 h and then calcined at 500 ^{o}C for 5 h to obtain the NiMo/γ-Al_2O_3 and NiMo/γ-Al_2O_3 catalysts with loading of Mo and Ni or Co at 14 wt.% and 3.5 wt.%, respectively.

4.1.3 Preparation of monometallic oxide supported on γ-Al_2O_3 catalysts

The γ-Al_2O_3 support was crushed and sieved to 0.5-1.0 mm diameter. The Ni, Co, Mo, Pd, and Pt supported on γ-Al_2O_3 catalysts were prepared by incipient wetness impregnation method using nickel (II) nitrate hexahydrate, cobalt (II) nitrate hexahydrate, Ammonium heptamolybdate tetrahydrate, *trans*-dinitrodiamminepalladium (II), and diamminedinitritoplatinum (II) as corresponding metal salt precursors. After impreagnation, the resultant samples were dried at 120 ^{o}C for 12 h and then calcined at 500 ^{o}C for 5 h to obtain the Ni/γ-Al_2O_3, Co/γ-Al_2O_3, Mo/γ-Al_2O_3, Pd/γ-Al_2O_3 and Pt/γ-Al_2O_3 catalysts.

4.2 Catalyst characterizations

4.2.1 X-ray diffraction (XRD)

Powder X-ray diffraction (XRD) patterns of the samples were collected on an X-ray diffractometer (D8 ADVANCE, Bruker, Ltd., Germany) using Cu Kα radiation. The measurement was operated at 40 kV and 40 mA, and in steps of 0.02^{o} s^{-1} with a step time of 0.5 s over the range of $20^{o} < 2\theta < 80^{o}$.

4.2.2 X-ray absorption near edge structure (XANES)

X-ray absorption near edge structure (XANES) technique at Ni K-edge (8333 eV) and Co K-edge (7709 eV) were acquired at the SUT-NANOTEC-SLRI XAS Beamline (BL-5.2) of the Synchrotron Light Research Institute (Public Organization), Thailand using a double Ge (2 2 0) crystal monochromator for the selection of photon energy. The data were obtained at room temperature in the transmission mode using a 13-element Ge detector. The samples were pressed into a frame covered by polyimide tape before mounting to the sample holder. The NiO, Ni foil, Co_3O_4, CoO, and Co foil were used as the reference standards for XANES analysis. The XANES spectra were analyzed through the Athena program.

4.2.3 N_2 sorption

Specific surface areas and total pore volumes were measured by a nitrogen sorption technique at –196 ^oC (Nova 2000e, Quantachrome Instruments, Germany). Prior to the measurement, the samples were degassed at 120 ^oC for 3 h. Pore size distributions of the samples were determined from the desorption branch of the isotherms using the Barrett-Joyner-Hallenda (BJH) method. The specific surface area was estimated based on the BET approach. The total pore volume was measured at a relative pressure (P/P_0) of 0.98.

4.2.4 H_2 temperature-programmed reduction (H_2-TPR)

H_2 temperature programmed reduction (H_2-TPR) was carried out using a CHEMBET-Pulsar Quantachrome Instruments in a quartz U-tube reactor with 20 mg of the sample. Prior to the experiments, the samples were pre-treated at 120 ^oC for 1 h at a He flow rate of 30 cm^3/min. The reduction was conducted in a 5 vol% H_2/Ar flow rate of 30 cm^3/min at a heating rate of 10 °C/min from 100 to 1000 ^oC. The hydrogen consumption was analyzed using a thermal conductivity detector (TCD).

4.2.5 CO pulse chemisorption experiment

CO pulse chemisorption experiments assuming a stoichiometry of 1.0 between CO and the metal atom were conducted on the same apparatus as used for H_2-TPR. A 50-mg quantity of catalyst was reduced with a 5 vol% H_2/Ar flow rate of 30 cm^3/min at 700 ^oC (Ni and Co) and at 500 ^oC (Pd and Pt) for 3 h. The pulses of CO (50 μL) were injected through the sample until CO saturation was attained.

4.2.6 Temperature-programmed oxidation (TPO)

Temperature-programmed oxidation (TPO) combined mass spectroscopy detector was used to determine the amount of coke deposited on the deactivated catalyst using the same apparatus as used for H_2-TPR experiment. Prior to TPO experiment, the samples (50 mg) were pre-treated at 400 ^oC for 1 h under He flow rate of 30 cm^3/min. The oxiation was conducted by raising the temperature from 100 ^oC to 800 ^oC at heating rate of 10 ^oC/min in 5% O_2/He flow rate of 30 cm^3/min. The product gases mainly CO_2 during TPO experiment were detected by online mass spectroscopy.

4.2.7 Inductively coupled plasma optical emission spectrometry (ICP-OES)

The metal content of the synthesized catalysts was determined using the inductively couple plasma optical emission spectrometer (ICP-OES, Jobin YVON HORIBA, ULTMA 2C). The liquid samples were pretreated with nitric acid-hydrochloric acid digestion before determing with ICP-OES.

4.2.8 Transmission electron microscopy (TEM)

The morphology and particle size of the catalysts were examined by transmission electron microscopy (TEM) (at 200 kV on an FEI TECNAI G2-20S-TWIN instrument) equipped with an energy dispersive spectrum (EDS) analysis facility.

4.3 Catalytic deoxygenation tests

4.3.1 Experimental set up

A continuous flow trickle-bed reactor was custom made of the stainless steel 316, with an internal diameter of 0.7 cm, length of 30 cm, and total volume of 12 cm^3. The effect of external mass transfer resistant in the catalysts bed was negligible under the working condition as further increasing feed flow rate (at constant LHSV) was insignificant effect the conversion and product yield (see in Figure B-1). A schematic diagram of the experimental apparatus is shown in Figure 17. It consists of a feed unit, a reactor unit and a product separation unit. The temperature was controlled by using electrical furnace with 2 positions of temperature controller. The pressure of the reactor was manually controlled by using back-pressure regulator. A HPLC pump was used to control the flow rate of feed and mass flow controller was used to control the flow rate of gas .The catalyst bed was located at the middle of the fixed-bed reactor with uniform temperature distribution.

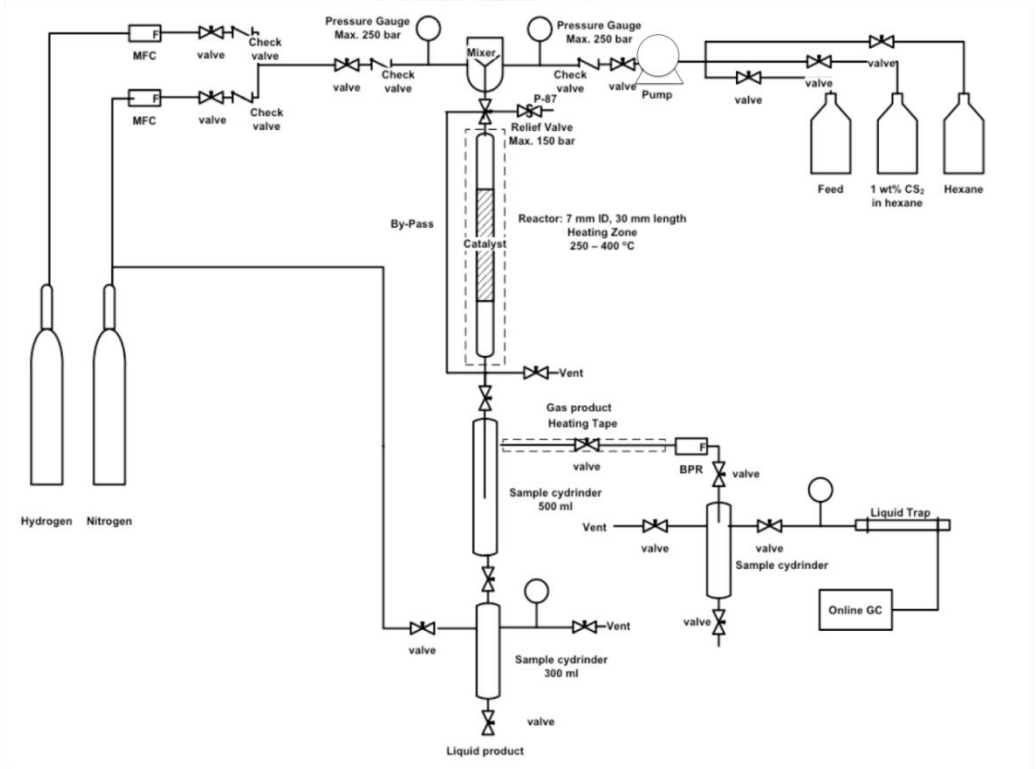

Figure 17 Schematic diagram of a continuous-flow trickle-bed reactor system.

4.3.2 Feed stock

A palm oil feedstock (refined palm olein type with free fatty acid <1 wt.%) was commercially obtained from a local market in Thailand. The fatty acid compositions of the refined palm olein (wt.%) were as follows: lauric acid (C12:0) 0.4%; myristic acid (C14:0) 0.8%; palmitic acid (C16:0) 37.4%; palmitoleic acid (C16:1) 0.2%; stearic acid (C18:0) 3.6%; oleic acid (C18:1) 45.8%; linoleic acid (C18:2) 11.1%; linolemic acid (18:3) 0.3%; arachidic acid (C20:0) 0.3%; and eicosenoic acid (C20:1) 0.1% [69].

4.3.3 Catalyst Activation

4.3.3.1 Presulphidation process

The catalysts (Ni, Co, Mo, NiMo, and CoMo) were presulfided using a mixture of 1 wt.% carbon disulfide in hexane. The presulfidation conditions were conducted in H_2 (Praxair, purity 99.99%) flow rate of 200 cm^3/min with pressure of 20 bar. The temperature was increased from 30 to 150 ^oC (10 ^oC/min) and then to a target temperature of 300 ^oC (1^oC/min), while the catalyst was held at 300 ^oC for 15.5 h.

4.3.3.2 Pre-reduction process

The Ni, Co, Mo, NiMo, and CoMo catalysts were reduced with a flow of pure H_2 (50 cm^3/min, Praxair, purity 99.99%) at 500 ^oC for 3 h. The Pd and Pt catalysts were also reduced in H_2 flow rate of 50 cm^3/min at 400 ^oC for 3 h.

4.4.4 Experimental procedure

In the reaction testing, the reactor was heated to desired temperature, and was pressurized with H_2 to desired pressure controlled by back pressure regulator. A HPLC pump was use to introduce the oil feed, while H_2 feed was controlled by mass flow controllers. After catalyst activation, the catalysts were stabilized by flowing feeds through the reactor for 24 h before actual experiments was implemented. Each reaction parameter was evaluated by the use of fresh catalysts to eliminate the effect of catalysts deactivate during the experiments. Duplicate experiment with fresh catalyst was done in some cases with less than 5% error of repeated results while triplicate experiment with same catalyst was also done for all cases with less than 5% error of repeated results. The liquid product was collected every 3-h interval time for analysis. The operating condition for deoxygenation experiments are shown in Table 11 (sections 1-4).

Table 11 Operating condition for deoxygenation experiments

Section 1: Production of bio-hydrogenated diesel by catalytic hydrotreating of palm oil over $NiMoS_2/\gamma\text{-}Al_2O_3$ catalyst: Effect of reaction parameters

Variable	Condition
Reactant	Refine palm olein type
Temperature (^oC)	270, 300, 330, 360, 390, and 420
Hydrogen pressure (MPa)	1.5, 3, 5, and 8
LHSV (h^{-1})	0.5, 1, 1.5, 2, 3, and 5
H_2 to oil ratio ($N(cm^3/cm^3)$	250, 500, 750, 1000, 1500, and 2000
Catalyst type	$NiMoS_2/\gamma\text{-}Al_2O_3$
Amount of catalyst (g)	8.5 g

Section 2: Roles of monometallic catalysts in hydrodeoxygenation of palm oil to green diesel

Variable	Condition
Reactant	Refine palm olein type and oleic acid
Temperature (^oC)	330
Hydrogen pressure (MPa)	5
LHSV (h^{-1})	1
H_2 to oil ratio ($N(cm^3/cm^3)$	1000
Catalyst type	Ni/γ-Al_2O_3, Co/γ-Al_2O_3, Pd/γ-Al_2O_3, and Pt/γ-Al_2O_3
Amount of catalyst (g)	2.8

Note that the metal catalysts with metal loadings of 2, 5, and 10 wt.% were labeled as 5CoAl, 10CoAl, 5NiAl, 10NiAl, 2PdAl, 5PdAl, 2PtAl, and 5PtAl, where the prefix numbers represent the %metal loadings.

Section 3: Hydrodeoxygenation of palm oil to bio-hydrogenated diesel over metal and metal sulfide catalysts

Variable	Condition
Reactant	Refine palm olein type
Temperature (^oC)	300
Hydrogen pressure (MPa)	5
LHSV (h^{-1})	1
H_2 to oil ratio ($N(cm^3/cm^3)$	1000
Catalyst type	Ni/γ-Al_2O_3, Co/γ-Al_2O_3, Mo/γ-Al_2O_3, NiMo/γ-Al_2O_3, CoMo/γ-Al_2O_3, NiS_x/γ-Al_2O_3, CoS_x/γ-Al_2O_3, MoS_2/γ-Al_2O_3, $NiMoS_2$/γ-Al_2O_3, and $CoMoS_2$/γ-Al_2O_3
Amount of catalyst (g)	5.5

Section 4: Deactivation and regeneration behaviors of Ni/γ-Al_2O_3 and Co/γ-Al_2O_3 catalysts during hydrodeoxygenation of palm oil

Variable	Condition
Reactant	Refine palm olein type
Temperature (^oC)	300
Hydrogen pressure (MPa)	5
LHSV (h^{-1})	1
H_2 to oil ratio ($N(cm^3/cm^3)$	1000
Catalyst type	Ni/γ-Al_2O_3 and Co/γ-Al_2O_3
Amount of catalyst (g)	5.5

4.4 Product analysis

4.4.1 Liquid product analysis

The liquid products obtained from deoxygenation of palm oil after separation of water phase were analyzed offline by gas chromatography equipped with capillary column (DB-1HT, 30 m × 0.32 mm × 0.1 μm) and a flame ionization detector (FID). The calibration curve of standards was used to quantify a composition of *n*-alkanes (*n*-C_8 to *n*-C_{18}) in liquid product. Briefly, 50 mg of sample was diluted with 1 ml of hexane and 1 μL of sample was injected into GC with the split ratio of 100. High injection and column temperature were used to direct analysis of triglyceride without chemical derivatization [1, 36]. The injection and detector temperatures were 340 and 370 ^oC, respectively. The temperature program was increased from 40 ^oC to 270 ^oCat a rate of 8 °C/min, and held for 11 min, followed by an increase of 15 °C/min to 370 °C, and held for 15 min.

The product mixtures obtained from deoxygenation of oleic acid, which consisted of oxygenated intermediates and *n*-alkanes, i.e., stearic acid, hexadecane, heptadcane, octadecanol, octadecyl stearate, and stearyloleate, were first identified by gas chromatography-mass spectrometry (5975C mass spectrometer detector, Agilent Technologies). Then, the composition of oxygenated product was performed using methyl heptadecanoate (Sigma-Aldrich, purity > 99 %) as an internal standard using GC equipped with a capillary column (DB-1HT, 30 m × 0.32 mm × 0.1 μm) and an FID.

The carbon, hydrogen, and oxygen contents in the liquid product were analyzed using a CHNS/O Analyzer.

4.4.2 Gas product analysis

The composition of gas products (C_3H_8, C_2H_6, CH_4, CO, CO_2, and H_2) were also analyzed by online gas chromatography with molecular sieve 5A and Porapak Q columns equipped with thermal conductivity detector (TCD) (GC-14B, Shimadzu).

4.5 Catalyst performance measurement

For in-depth analysis of the catalyst performance, the mole balance of the organic liquid products was used to determine the conversion and product yields; the mole balance was greater than 90% for all conditions. The conversion was defined as moles of reactants (triglyceride or oleic acid) converted to others (intermediates and hydrocarbon). The product yields were theoretically determined based on the mole balance of *n*-alkanes in the product corresponding to the moles of fatty acid in the oil feed. The product yield of the *n*-C_{15} to *n*-C_{18} fraction and conversion were calculated using the following equations:

$$\text{Conversion of TG (\%)} = \left(\frac{\text{mol TG in feed} - \text{mol TG in product}}{\text{mol TG in feed}} \right) \times 100 \qquad (3.1)$$

$$\text{Product yield (\%)} = \left(\frac{\text{Total mol of } n\text{–alkanes } (n\text{–C}_{15} \text{ to } n\text{–C}_{18}) \text{ in product}}{\text{Total mol of C}_{16} \text{ and C}_{18} \text{ fatty acid in feed}} \right) \times 100 \quad (3.2)$$

According to the possible gas-phase reactions involved, such as methanation and water-gas shift reactions, the relative activity of the decarbonylation and decarboxylation reactions could not be directly correlated with the amount of CO and CO_2 detected in the gas phase. Therefore, the %contributions of the hydrodeoxygenation (HDO) and decarbonylation/decarboxylation (DCO/DCO_2) reactions were also calculated based on the mole balance, using the total moles of *n*-alkanes with even numbers (HDO) or odd numbers (DCO/DCO_2) of carbon atoms in the liquid product to the moles of fatty acid in the oil feed using the following equations:

$$\text{HDO (\%)} = \left(\frac{\text{Total mol of } n\text{–alkanes } (n\text{–C}_{16} \text{ and } n\text{–C}_{18}) \text{ in product}}{\text{Total mol of C}_{16} \text{ and C}_{18} \text{ fatty acid in feed}} \right) \times 100 \quad (3.3)$$

$$\text{DCO/DCO}_2 \text{ (\%)} = \left(\frac{\text{Total mol of } n\text{–alkanes } (n\text{–C}_{15} \text{ and } n\text{–C}_{17}) \text{ in product}}{\text{Total mol of C}_{16} \text{ and C}_{18} \text{ fatty acid in feed}} \right) \times 100 \quad (3.4)$$

CHAPTER V

RESULTS AND DISCUSSIONS

This chapter provides the results and discussion in four main sections. The first section described the production of bio-hydrogenated diesel by catalytic deoxygenation of palm oil over $NiMoS_2/\gamma\text{-}Al_2O_3$ catalyst: effect of reaction parameters as shown in Section 5.1. In the second section, the roles of monometallic catalysts in deoxygenation of palm oil to green diesel are reported in Section 5.2. The third section reported the deoxygenation of palm oil to bio-hydrogenated diesel over metal and metal sulfide catalysts as shown in Section 5.3. In the last part Section 5.4, deactivation and regeneration behaviors of $Ni/\gamma\text{-}Al_2O_3$ and $Co/\gamma\text{-}Al_2O_3$ catalysts during deoxygenation of palm oil are described.

5.1 Production of bio-hydrogenated diesel by catalytic deoxygenation of palm oil over $NiMoS_2/\gamma\text{-}Al_2O_3$ catalyst: Effect of reaction parameters

5.1.1 Introduction

There are two types of catalyst mostly use in hydrotreating of triglycerides: (1) metal catalysts, such as Ni, Pd, Pt, Rh, Ru [43, 49, 68, 70] and (2) bimetallic sulfide catalysts e.g. $NiMoS_2$, $CoMoS_2$, and $NiWS_2$ supported on Al_2O_3 [3, 13, 15, 29]. The metal catalysts are favorable to DCO and DCO_2, while HDO is dominant in bimetallic sulfide catalysts, except $NiWS_2$. Some metal catalysts such as Ni, Pd, and Pt strongly promoted methanation reaction, consuming large amount of hydrogen. Moreover, using $NiMoS_2$ and $CoMoS_2$ as catalysts with good selectivity to HDO can be operated at lower temperature due to the nature of exothermic reaction. The formation of CO and CO_2 could affect product yield, catalyst deactivation, and downstream process for

recycle gas [21]. Therefore, using bimetallic sulfide catalysts as $NiMoS_2$, which was high activity [71] and selective to HDO, was very attractive for hydrotreating process.

The effects of hydrotreating parameters when using bimetallic sulfide catalysts were explored in various literatures. The results indicated the temperature, WHSV/LHSV, hydrogen pressure, and H_2/oil ratio as significant operating parameters that could alter reaction pathways in hydrotreating process [10, 72-74]. Furthermore, the relative activities of the DCO/DCO_2 and HDO reactions, as the most important key in hydrotreating process, were considered to evaluate hydrogen consumption, product yield, heat balance, and catalyst deactivation [21, 40]. However, many researchers estimated the relative activities of the DCO/DCO_2 and HDO reactions using the ratio of the amounts of n-alkanes with odd numbers of carbon atoms, to n-alkanes with even numbers of carbon atoms in the liquid product [8, 23, 75]. These estimations could not provide an actual relative contribution of HDO and DCO/DCO_2 reactions compared to mole balance analysis. Consequently, a comprehensive understanding the influence of reaction parameters on 3 major reaction pathways by using mole balance analysis is crucial.

In this work, the effect of important parameters in hydrotreating of triglyceride catalyzed by bimetallic sulfide $NiMoS_2/\gamma$-Al_2O_3 including effects of temperature (270-420 ^oC), H_2 pressure (1.5-8 MPa), liquid hourly space velocity (LHSV, 0.25-1.0 h^{-1}), and H_2/oil ratio (250-2000 N(cm^3/cm^3)), in the production of bio-hydrogenated diesel from palm oil in the trickle-bed reactor was demonstrated. Indeed, the fully understand these parameters, affected to contributions of HDO, DCO, and DCO_2 reactions, lead to obtain the optimal operating and limiting conditions.

The effects of hydrotreating temperature, hydrogen pressure, liquid hourly space velocity (LHSV), and hydrogen to oil ratio on the n-alkane composition of the liquid product are represented in Table 12. The palm oil used in this study was composed mainly of C_{16} and C_{18} fatty acids (>98.4 wt.%), thus the main composition of liquid product was n-alkane of C_{16} and C_{18} due to high selective HDO reaction of $NiMoS_2/\gamma\text{-}Al_2O_3$ catalyst. As demonstrated in Table 12, the increase in hydrotreating temperature enhances the cracking reaction, where the light hydrocarbon compositions, *n*-C_8 to *n*-C_{14}, were observed. Hydrotreating temperature and hydrogen pressure also affected to % contribution of hydrotreating product (HDO and DCO/DCO_2) for each n-alkane product, exhibited in Table 13.

5.1.2 Effect of temperature

Reaction temperature has been identified as one of dominant parameters on the catalyst deactivation and catalyst performance [29]. In this section, effect of hydrotreating temperature was conducted in the range of 270-420 ^oC with fixed operating conditions: 5 MPa of H_2 Pressure, 1.0 h^{-1} of LHSV, and 1000 Ncm^3/cm^3 of H_2/Oil ratio, and the results are shown in Figure 18. It should be first noted that the hydrotreating reaction over pure $\gamma\text{-}Al_2O_3$ resulted in 56% conversion of triglyceride without BHD product yield. The results indicated that only the saturated triglyceride scission to free fatty acids and propane occurred. Interestingly, the BHD product yield were obtained when the reaction was catalyzed by $NiMoS_2/\gamma\text{-}Al_2O_3$ catalyst, suggesting the hydrotreating activity of $NiMoS_2$ species.

Table 12 Effect of operating parameters on liquid product composition

Parameters	T (^oC)	P (MPa)	LHSV (h^{-1})	H_2/oil ratio N(cm^3/cm^3)	Liquid product composition (wt.%)					Product phase	Product color
					n-C_8-*n*-C_{14}	*n*-C_{15}	*n*-C_{16}	*n*-C_{17}	*n*-C_{18}		
T	270	5	1	1000	0.2	1.7	9.1	2.9	14.1	Solid	Yellow
	300	5	1	1000	0.8	6.3	30.3	10.7	47.7	Liquid	Clear
	330	5	1	1000	1.0	4.9	32.1	8.0	48.7	Liquid	Clear
	360	5	1	1000	2.5	3.2	33.5	4.6	44.6	Liquid	Light green
	390	5	1	1000	5.7	3.1	31.8	3.5	33.0	Liquid	Light green
	420	5	1	1000	12.8	3.8	22.3	2.8	12.7	Liquid	Green
P	300	1.5	1	1000	0.9	6.0	29.3	10.3	43.9	Liquid	Green
	300	3	1	1000	0.9	7.6	29.3	12.8	45.5	Liquid	Clear
	300	5	1	1000	0.8	6.3	30.3	10.7	47.7	Liquid	Clear
	300	8	1	1000	0.8	5.9	31.7	10.3	50.4	Liquid	Clear
LHSV	300	5	0.25	1000	0.6	3.4	34.3	6.1	54.7	Liquid	Clear
	300	5	0.5	1000	0.6	5.6	31.9	10.0	49.4	Liquid	Clear
	300	5	1	1000	0.6	6.3	30.7	10.9	47.4	Liquid	Clear
	300	5	1.5	1000	0.6	5.8	30.7	9.7	46.0	Liquid	Clear
	300	5	2	1000	0.6	5.6	31.2	9.2	46.1	Liquid	Clear
	300	5	3	1000	0.6	5.3	30.6	8.8	45.3	Liquid	Clear
	300	5	5	1000	0.6	5.3	29.9	8.8	44.5	Liquid	Clear
H_2/oil ratio	300	5	1	250	0.3	4.3	12.9	7.3	20.1	Solid	Yellow
	300	5	1	500	1.0	7.2	29.0	12.2	46.3	Liquid	Clear
	300	5	1	750	0.8	6.6	30.2	11.3	47.9	Liquid	Clear
	300	5	1	1000	0.6	6.6	30.9	11.1	48.2	Liquid	Clear
	300	5	1	1500	0.8	7.1	31.1	12.1	48.3	Liquid	Clear
	300	5	1	2000	0.8	6.0	31.9	10.1	49.4	Liquid	Clear

Table 13 Effect of hydrotreating temperature and hydrogen pressure on % contribution of each n-alkane

Parameters	T (^{o}C)	P (MPa)	HDO (%) (*n*-C_{16})	HDO (%) (*n*-C_{18})	DCO/DCO_2 (%) (*n*-C_{15})	DCO/DCO_2 (%) (*n*-C_{17})
Temperature	270	5	22.7	21.4	4.4	4.7
	300	5	74.1	71.0	16.4	17.1
	330	5	78.5	72.4	12.9	12.8
	360	5	83.3	66.4	8.1	6.9
	390	5	78.4	49.6	8.1	5.6
	240	5	51.9	17.0	9.5	4.2
Pressure	300	1.5	72.6	66.4	15.8	16.5
	300	3	72.6	68.7	19.8	20.3
	300	5	74.1	71.0	16.4	17.1
	300	8	79.1	76.4	15.6	16.5

The % contributions of HDO and DCO/DCO2 for each n-alkane (n-C15, n-C16, n-C17, and n-C18) were calculated based on mole balance using the total mole of n-alkanes with odd numbers (HDO) or even numbers (DCO/DCO2) of carbon atoms in the product

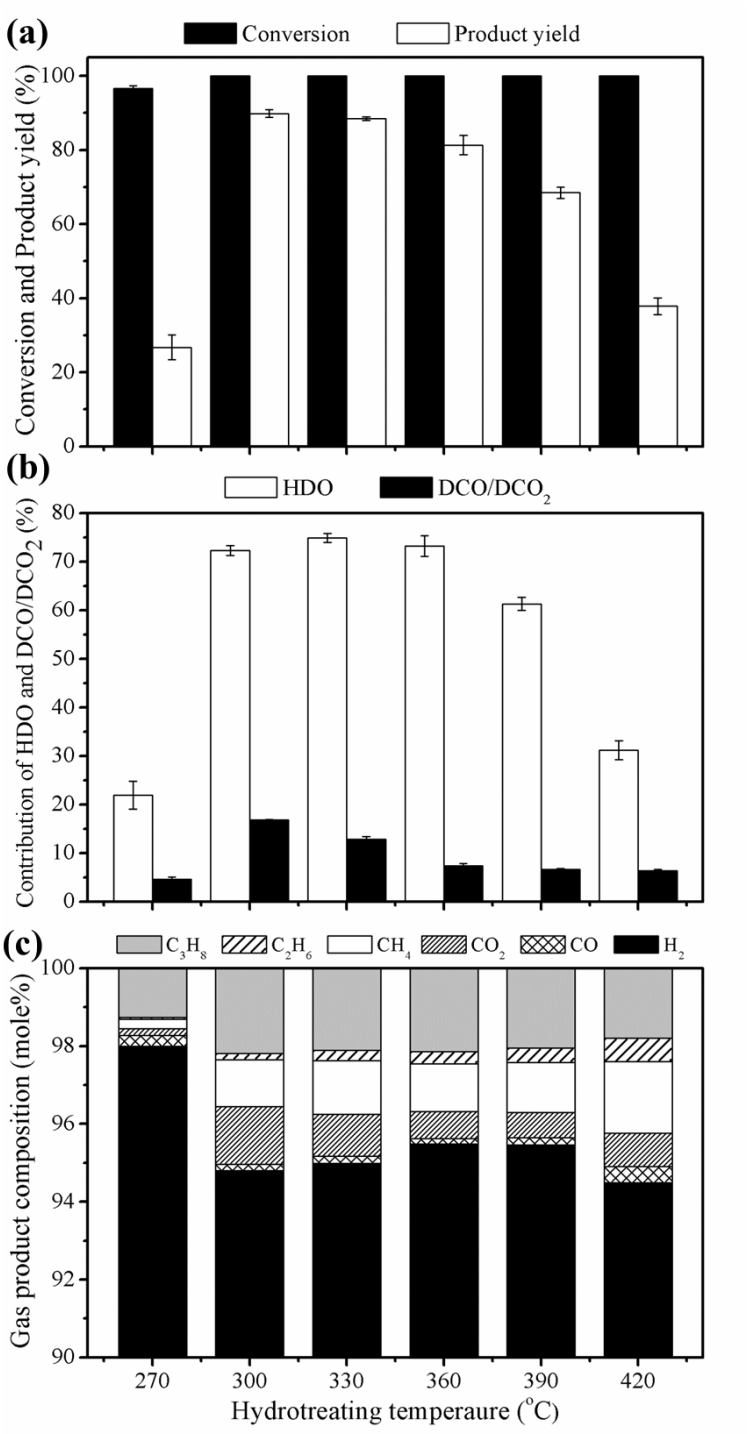

Figure 18 Effect of hydrotreating temperature on (a) conversion and product yield, (b) % contribution of HDO and DCO/DCO_2, and (c) gas product composition. All experiments were performed at a hydrotreating temperature in the range of 270-420 ^{o}C, H_2 pressure of 5 MPa, H_2/oil ratio of 1000 N(cm^3/cm^3), and LHSV of 1 h^1.

The organic liquid product obtained from hydrotreating temperature of 270 ^{o}C became solidified at room temperature and consisted of palmitic acid and stearic acid with small amount of triglyceride. Our results were consistent to those of Šimáček et al., 2009, at hydrotreating temperature lower than 310 ^{o}C, the liquid product also contained reactant and intermediates including triglyceride, free fatty acids, and n-octadecanol [76]. These results suggested that the reaction proceeded through the hydrogenation of C=C bond in unsaturated triglyceride, followed by C-O bond cleavage via hydrogenolysis of saturated triglyceride to produced free fatty acids and propane [39, 41]. As illustrated in Figure 18a, the reactants underwent to HDO, DCO, and DCO_2 reactions with product yield of 26.7% (270 ^{o}C). Based on our operating condition obtained from 330-420 ^{o}C of hydrotreating temperature, the triglyceride and fatty acids were not detected in organic liquid product, resulting in 100% conversion of triglyceride. Interestingly, as shown in Figure 18a, the product yield increased from 26.7% to 89.8% with increasing temperature from 270 to 300 ^{o}C. The results confirmed that hydrotreating temperature of 300 ^{o}C was successful to convert triglyceride to n-alkane for palm oil over $NiMoS_2$ catalyst. On the other hand, the decrease in product yield from 88.9 to 37.9% with increasing temperature from 330 to 420 ^{o}C could be related to the promotion of isomerization, cracking, and cyclization reactions because the light-hydrocarbons, iso-parafins, cycloparafins and some aromatics were found in liquid product at high reaction temperature (420 ^{o}C). The detected iso-parafins were iso-C_{15} and iso-C_{17} such as 1-methlypentadecane 1-methlypentadecane 3-methlypentadecane, and 3-methlyheptadecane, thus causing by isomerization reaction of n-C_{16} and C_{18}. However, the formation of n-alkanes possibly undergo through the thermal cracking of triglyceride rather than went through the deoxygenation reaction at higher temperature [8, 29]. Fortunately, the iso-paraffins are favorable in liquid product, thus improving the cold flow properties including cloud point and pour point.

To fully understand deoxygenation behavior at difference conditions, % contribution of HDO and DCO/DCO_2 was considered and represented in Figure 18b. The hydrodeoxygenation (HDO) is dominant through catalyzed by $NiMoS_2$ catalyst [6, 65]. The DCO/DCO_2 moderately increased from 4.6% to 16.8% with raising temperature from 270 to 300 ^oC, whereas, an increase in temperature from 270 to 330 ^oC greatly enhanced HDO from 21.9% to 74.9%. At the temperature higher than 330 ^oC, DCO/DCO_2 slightly decreased and the dramatically decrease in HDO was observed at the temperature higher than 360 ^oC due to the enhancement of cracking and isomerization reactions in good agreement with thermodynamic point of view. The exothermic HDO is unfavorable at higher temperature [49]; however, endothermic DCO and DCO_2 are not followed the trend. Therefore, it should be noted there are competitive reactions between HDO and DCO/DCO_2, occurring at each temperature.

According to the results discussed in previous section, HDO (72-75%) was a major reaction pathway, whereas DCO and DCO_2 (13-16%) were minor reaction pathways. As illustrated in Figure 19, the double bonds in saturated triglycerides were hydrogenated to unsaturated triglycerides, subsequently cleaved to free fatty acids and propane (270 ^oC). The free fatty acid, as the major oxygenated intermediates, could undergo to yield a fatty acid alcohol and subsequently hydrocarbons at temperature higher than 300 ^oC through HDO reaction, leading to elimination of water from palm oil (12-15 wt.% of total liquid product). Some free fatty acids could directly be converted to hydrocarbons via DCO and DCO_2 reactions, thus releasing oxygen in form of CO, H_2O, and CO_2, respectively. Furthermore, the cracking and isomerization reactions could proceed at temperature above 360 ^oC.

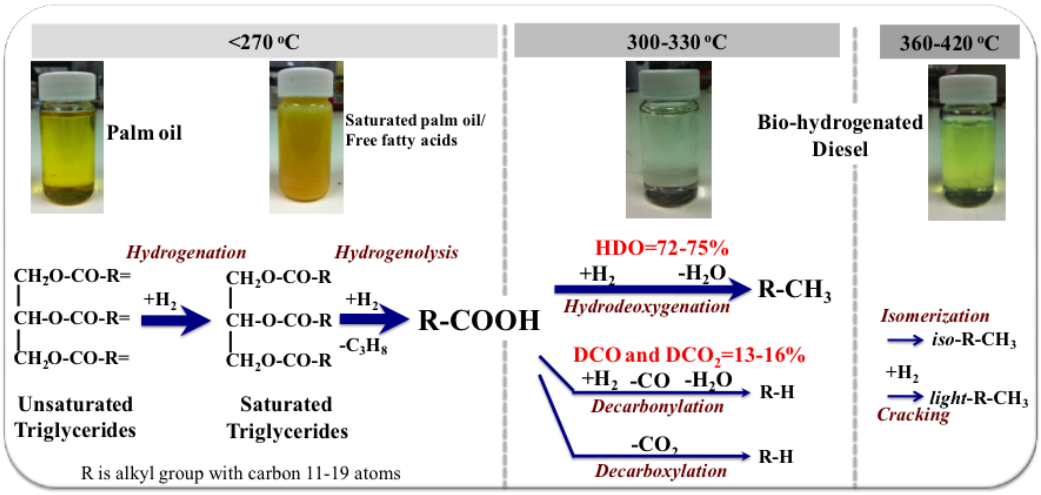

Figure 19 Proposed mechanisms for hydrotreating of palm oil catalyzed by $NiMoS_2/\gamma\text{-}Al_2O_3$ related to liquid products at different temperatures.

The activity of decarbonylation and decarboxylation reaction can be compared to amount of CO and CO_2. As we discussed in previous section, the decline in DCO/DCO_2 yield was observed at the temperature higher than 330 ^oC, thus causing in decrease of CO and CO_2 with the similar trend (Figure 18c). These results could be noted that the rate of two reactions is similar and these reactions occur with the same mechanism. By comparison amount CO and CO_2, the results showed that DCO_2 has higher activity than DCO. Moreover, the decrease in amount of CO and CO_2 could be related to methanation, exothermic reaction, between CO or CO_2 with H_2. Consequently, the higher amount of CO and CO_2 production at $_{420}$ ^oC reaction temperature was also observed. Perhaps, the slightly increase in amount of C_2H_6 between 360-420 ^oC was due to the cracking of liquid product or direct cracking of triglyceride rather than cracking of C_3H_8 to CH_4 and C_2H_6 as same as the methanation reaction. In Table 13, the results of increase in HDO of *n*-C_{16} and decrease in HDO of *n*-C_{18} suggested that the cracking of *n*-C_{18} to *n*-C_{16} and C_2H_6 would be occurred at temperature higher than 360 ^oC.

5.1.3 Effect of hydrogen pressure

Hydrogen pressure, strong effect to deoxygenation, isomerization, and cracking reactions, is an important parameter of hydrotreating reaction of triglycerides to hydrocarbons. Moreover, the H_2 consumption must be taken account of the economical evolution of operating conditions. In this experiment, hydrogen pressures were investigated in the range of 1.5-8 MPa at hydrotreating temperature of 300 ^{o}C, while the other parameters were retained as same as those discussed in Section 5.1.2, to avoid the catalyst deactivation and cracking reaction. At the pressure of 1.5 MPa, the liquid product remained small amount of palmitic acid and stearic acid, thus indicating the incomplete transformation of free fatty acids to n-alkane due to the insufficient H_2 pressure (Figure 20). Similarly to Anand & Sinha, 2012 and Kubička et al., 2009, low conversion was observed at hydrogen pressure of 2 MPa and the reduced partial pressures of hydrogen leaded hydrogen mass transfer limitations on the catalyst surface.

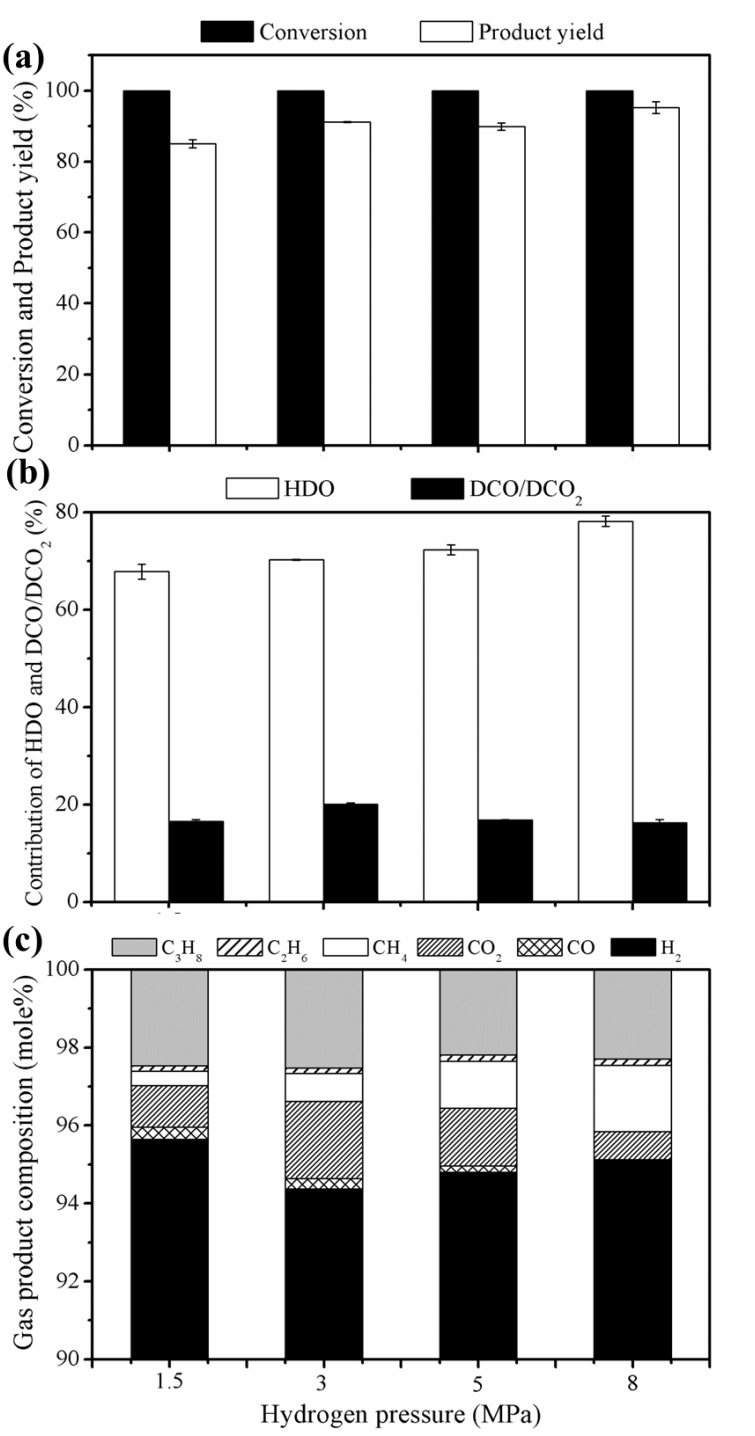

Figure 20 Effect of H_2 pressure on (a) conversion and product yield, (b) % contribution of HDO and DCO/DCO_2, and (c) gas product composition. All experiments were performed at a H_2 pressure in the range of 1.5-8 MPa, hydrotreating temperature of 300 ^oC, H_2/oil ratio of 1000 N(cm^3/cm^3), and LHSV of 1 h^1.

As shown in Figure 20a, the hydrogen pressure did not significant effect on the conversion of triglyceride (100% conversion was obtained at 1.5-8 MPa). The product yield slightly increased up to 95.2 % with increasing hydrogen pressure from 1.5 to 8 MPa. Since, the H_2 pressure is the function of adsorbed hydrogen on the surface of catalyst active sites, increase in hydrogen pressure raised the solubility of hydrogen in the vegetable oil across the catalyst surface. As presented in Figure 20b, the HDO activity enhanced from 67.8 % to 78.1% with increasing H_2 pressure from 1.5 to 8 MPa, but slightly decreased the DCO/DCO_2 from 20.1% to 16.3% when increase H_2 pressure from 3 to 8 MPa. The HDO dominated the total process under pressures because of more H_2 consumption in comparison to DCO and DCO_2 [15]. Consequently, HDO pathway was favorer than DCO/DCO_2 due to the larger amount of hydrogen at active sites. On the other hand, DCO/DCO_2 increased with decreasing hydrogen pressure as the results of lowing amount of hydrogen at the catalyst surface [13]. In proposed in various works, the fatty acids obtained from hydrogenolysis of triglyceride leads to aldehyde production with rate determining step, followed by either (1) decarboxylation of octadecanal to *n*-heptadecane and carbon monoxide or (2) hydrogenation of octadecanal to octadecanol. Subsequently, the octadecanol undergoes dehydration and hydrogenation to the *n*-octadecane (hydrodeoxygenation) [39, 41]. It should be note that increase of the H_2 pressure from 1.5 to 8 MPa led to reaction shifts from octadecanal to 1-octadecanol, followed by *n*-octadecane and decarboxlylation rate was suppressed at high H_2 pressure.

As discussed in the previous section, large amounts of CO and CO_2 were observed due to the increasing of DCO and DCO_2 reactions at low H_2 pressure of 30 bar (Figure 20c**)**. The increase in H_2 pressure led to the decreasing in composition of CO and CO_2 and increasing of CH_4 contents. Perhaps, the increase in CH_4 composition with increasing H_2 pressure was attributed to the characteristic of methanation reactions with favor at high H_2 pressure [77]. Moreover, the slightly decrease in C_3H_8 and increase in C_2H_6 would be due to the cracking of C_3H_8 to CH_4 and C_2H_6 at high H_2 pressure.

5.1.4 Effect of liquid hourly space velocity

Liquid hourly space velocity (LHSV) which, defines as the ratio of feed volume flow rate with volume of packed catalyst is used to determine the contact time between feed and catalyst. LHSV plays an important role for regulating catalyst effectiveness and catalyst life expectancy [10, 29, 72]. According to previous work, high space time (around 8-17 h^{-1}), the formation of white waxy oxygenated intermediates, mainly free fatty acids and esters are observed [26, 52, 78] and rapidly plugged the reactor. Therefore, the effect of LHSV on conversion and product yield with % contribution of HDO and DCO/DCO_2 was conducted in the wide range of LHSV (0.25 – 5 h^{-1}) with fixed the operating condition: hydrotreating temperature: 300 ^{o}C; H_2 Pressure: 5 MPa; and H_2/Oil ratio: 1,000 N(cm^3/cm^3).

As demonstrated in Figure 21a, LHSV did not significantly effect on the conversion of triglyceride; 100 % conversion was obtained at 0.25–5 h^{-1}, at hydrotreating temperature of 300 ^{o}C without wax precipitation of liquid product at higher LHSV (5 h^{-1}) and zero acid value. However, the increase in LHSV from 0.25 to 5 h^{-1} slightly dropped in the product yield from 95% to 84.3%, indicating the insufficient contact time of reactants and catalysts. Furthermore, the decrease in contact time suppressed the deoxygenation, cracking, and isomerization reactions [14]. Nevertheless, the increase in contact time (at low LHSV) would promote the cracking and isomerization reactions; thereby we demonstrated the effect of LHSV at low temperature (300 ^{o}C) to avoid this situation. The decrease in LHSV from 0.5 to 0.25 h^{-1} raised the product yield up to 95% because allowing longer contact time between reactant and catalyst in low LHSV would enhance the product yield at low hydrotreating temperature (300 ^{o}C)

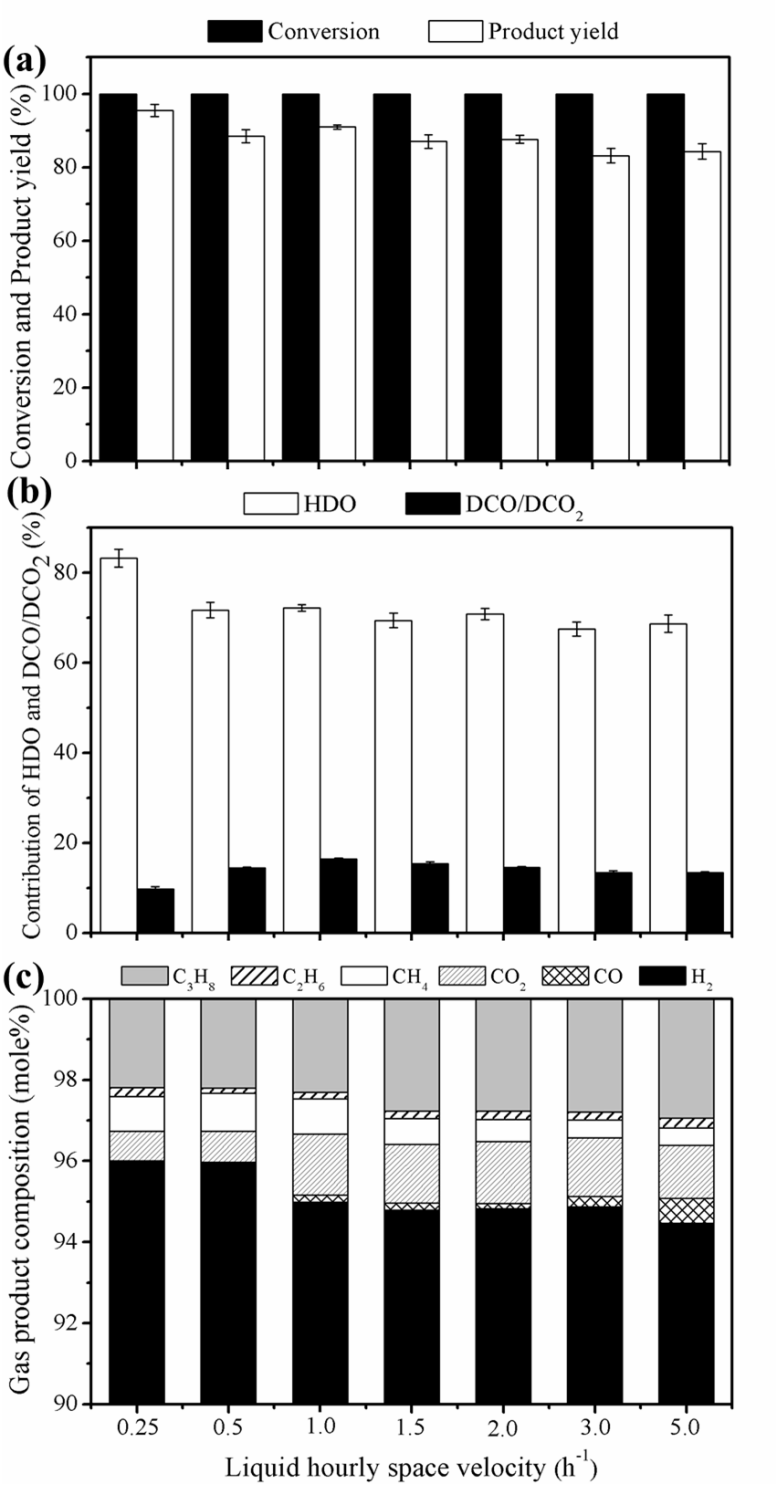

Figure 21 Effect of LHSV on (a) conversion and product yield, (b) % contribution of HDO and DCO/DCO_2, and (c) gas product composition. All experiments were performed at LHSV in the range of 0.25-5 h^1, hydrotreating temperature of 300 ^oC, H_2 pressure of 5 MPa, and H_2/oil ratio of 1000 N(cm^3/cm^3).

In Figure 21b**,** an overall similarly decline trend on % contribution of HDO from 83.1% to 68.7% was observed when increasing the LHSV from 0.25 to 5 h^{-1}. On the other hand, the increase in LHSV from 0.25 to 1 h^{-1} increased the % contribution of DCO/DCO_2 from 9.7% to 16.4%, while there is slightly decrease in % contribution of DCO/DCO_2 from 16.4% to 13.4% with increasing LHSV from 1 to 5 h^{-1}. The results can be indicated that LHSV did not significant influence on reaction pathways including HDO and DCO/DCO_2 when increase the LHSV from 1 to 5 h^{-1}. At LHSV lower than 1 h^{-1} (increase in contact time) the reactions seem to promote HDO than DCO/DCO_2. The rate of hydrogenolysis of the $(H_2)C–O$ bonds in triglyceride to fatty acid alcohols (HDO) should be slower than the cracking of the $–C(=O)–C_{17}$ bonds (DCO_2); the former reaction required higher contact time between reactant and catalyst than the later [79]. These results should be indicated that the decrease in LHSV with increase the contact time was sufficient for HDO and suppressed DCO and DCO_2 reactions at low hydrotreating temperature.

Effects of LHSV on gas product composition, illustrated in Figure 21c, suggested that LHSV had strongly influence the methanation reaction, which was favorable when decrease in LHSV i.e., higher LHSV, the more CO and CO_2 but the less CH_4 in the gas product. In addition, propane slightly increased due to cracking of propane to lighter hydrocarbon (mostly methane) was suppressed at higher LHSV.

5.1.5 Effect of hydrogen to oil ratio

The hydrogen to oil ratio, which defines to the ratio of hydrogen feed to the liquid feed, is another conventional parameter in economic feasibility and hydrotreating processes which has strong influence on hydrogenation, deoxygenation, and cracking efficiency. In this section, the effect of hydrogen to oil ratio was conducted in the range of 250-2000 Ncm^3/cm^3, while the other parameters were retained as same as those discussed in Section 5.1.4.

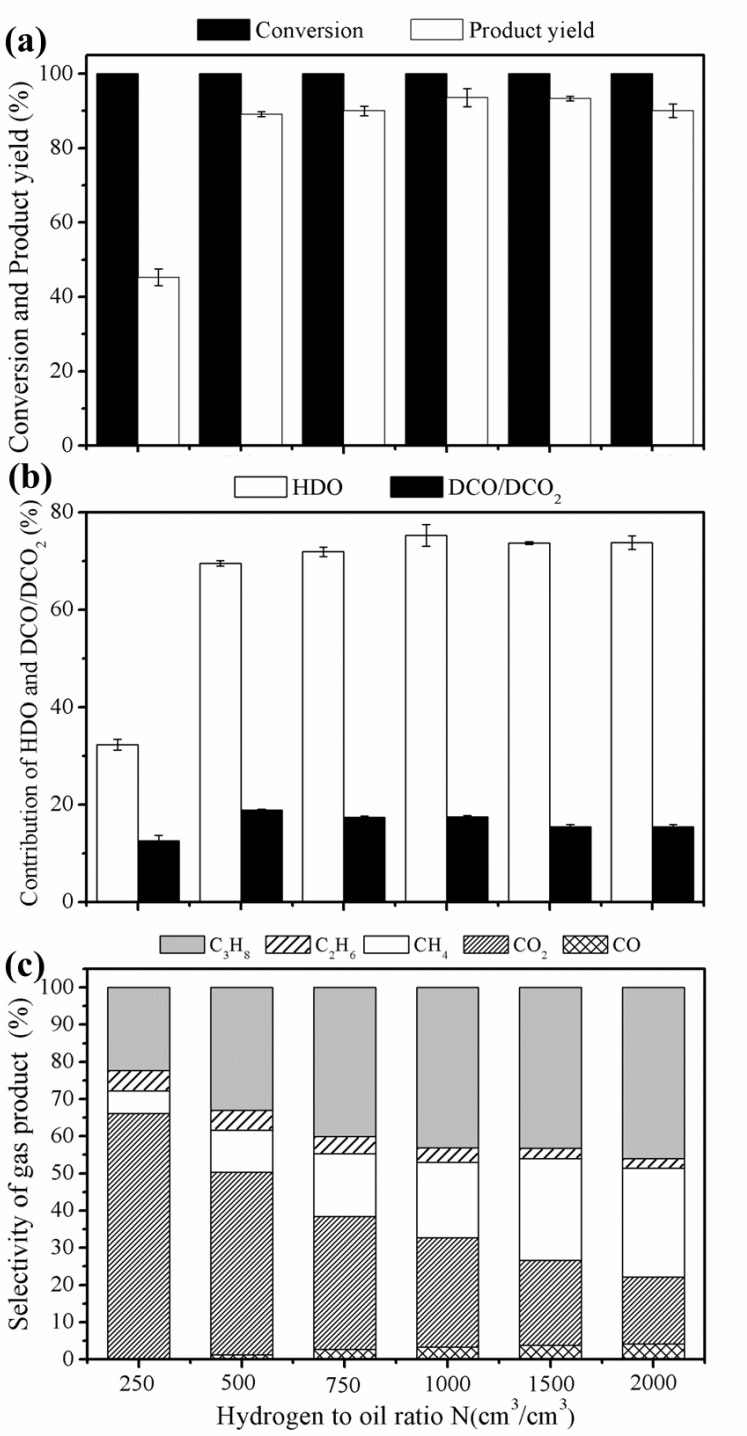

Figure 22 Effect of H_2/oil ratio on (a) conversion and product yield, (b) % contribution of HDO and DCO/DCO_2, and (c) gas product composition. All experiments were performed at H_2/oil ratio in the range of 250-2,000 N(cm^3/cm^3), hydrotreating temperature of 300 ^oC, H_2 pressure of 5 MPa, and LHSV of 1 h^1.

As illustrated in Figure 22a, the H_2/oil ratio showed small impact on the conversion; however, dramatically improvement in product yield from 45.2% up to 93.3% with the change of H_2/oil ratio from 250 to 1500 N(cm^3/cm^3) due to the improvement of deoxygenation reactions (HDO and DCO/DCO_2), Additionally, at H_2/oil ratio of 250 N(cm^3/cm^3), the product was separated into two layers at room temperature. The analysis suggested that the upper liquid phase was hydrocarbons and the bottom solid phase was fatty acids (mainly, palmitic acid and stearic acid) due to insufficient of hydrogen. However, the use of H_2 to oil ratio of 2000 N(cm^3/cm^3) reduced the product yield to 90% due to the decreasing of DCO/DCO_2 reactions (Figure 22b). The hydrogen consumption for converting 1 ml of palm oil to hydrocarbon could be estimated from fatty acid composition. We assumed that the main composition of triglyceride in palm oil is tripalmitin and triolein and assumed that the reaction was taken place through hydrodeoxygenation when using $NiMoS_2$ as catalyst. Therefore, 1 mol of tripalmitin, which contained six oxygen atoms will consume 12 mol of hydrogen to produce hexadecane, while 1 mol of triolein, which contained six oxygen atoms and 3 C=C double bonds will consume 15 mol of hydrogen to produce octadecane. By 50% of tripalmitin and 50% triolein, 1 mol of palm oil will consume 13.5 mol of hydrogen to produce hydrocarbons through hydrogenation and hydrodeoxygenation reactions. The density of palm oil was 0.903 g/ml, and the molecular weight was 838 g/mol. Finally, we obtained the conclusion that 1 ml of palm oil will consume about 325 ml of hydrogen (at standard temperature and pressure (STP)) to form hydrocarbon through hydrogenation and hydrodeoxygenation reactions. In Figure 22a, the highest production yield was obtained at H_2/oil ratio of 1000 to 1500 N(cm^3/cm^3), suggesting the hydrogen should be about 3-5 times as much as the ratio of consumed hydrogen to oil. Additionally, the larger amount of hydrogen supplied during hydrotreating process possibly retard coke deposition onto the catalyst [8] and also remove the water from the catalyst [40], thus preventing the catalysts from deactivation.

The contribution of HDO increased from 32.3% to 75.3% when increase H_2/oil ratio from 250 to 1000 N(cm^3/cm^3) and the trend was constant at H_2/oil ratio in the range 1500 to 2000 N(cm^3/cm^3) at 73.7%, represented in Figure 22b**.** On the other hand, the increase in H_2/oil ratio from 250 to 500 N(cm^3/cm^3) enhanced the contribution of DCO/DCO_2 from 12.6% to 18.9%, the increase in H_2/oil ratio up to 2000 N(cm^3/cm^3) decreased the DCO/DCO_2 to 15.5 %. We could expert similar fashion to those in the study of H_2 pressure, that the large adsorption of H_2 at catalyst active sites is enhance through the high H_2/oil ratio used via promoted overall reaction pathway. Otherwise, the trend was constant due to the saturation of adsorbed H_2 on catalyst active sites.

For CO and CO_2, the H_2/oil ratio strongly affected on the enhanced methanation reaction with high H_2/oil ratio (Figure 22c), in good agreement with Gao et al., (2012) [77]. As they analyzed the comprehensive thermodynamic of reactions occurring in the methanation of carbon oxides (CO and CO_2) using the Gibbs free energy minimization method, and found the enhancement of methanation due to the high H_2/CO and H_2/CO_2 ratio.

5.2 Roles of monometallic catalysts in deoxygenation of palm oil to green diesel

5.2.1 Introduction

The catalysts most frequently used in the deoxygenation of triglycerides, fatty acids, and esters are (1) bimetallic sulfide catalysts, e.g., $NiMoS_2$ [13, 15, 24, 61], $CoMoS_2$ [8, 26, 27, 56, 61], and $NiWS_2$ [28, 29]; (2) metal phosphide and carbide catalysts, e.g., Ni_2P [38, 80], W_2C [35], and Mo_2C [35, 81]; and (3) metal catalysts in a reduced state, such as Ni [12, 22, 30, 43, 65], Co [22, 31], Pd [5, 32, 66], Pt [14], and Ru [33, 34]. The conventional metal sulfide catalysts are less expensive catalysts [35] and show high activity in the deoxygenation of triglycerides and model compounds; however, sulfur leaching leads to catalyst deactivation and sulfur

contamination in liquid products [31, 36, 37, 41]. In addition, metal sulfide catalysts require the addition of sulfiding agents, e.g., CS_2 and DMDS, into the liquid feed to avoid catalyst deactivation during deoxygenation reactions [22, 38]. The trace amount of water produced from DCO and HDO reactions would hasten the sulfur leaching and rigorously shorten the lifetime of the catalysts [39]. The metal phosphide and carbide catalysts also revealed high activity in oxygen removal and selectivity for diesel-range alkanes. Nevertheless, the preparation process of catalysts was complicated and transformation of their catalyst active phases was mostly observed during deoxygenation reactions, resulting in a short lifetime of these catalysts [31].

Alternatively, metal catalysts and sulfur-free catalysts have attracted great attention for deoxygenation reactions due to their high reactivity at mild temperature, no sulfur contamination in liquid products, and lower H_2 requirement [40]. Some metal catalysts, such as Ni, Pd, and Pt, are favorable in the DCO and DCO_2 pathways. The hydrogen consumption for the deoxygenation of triglycerides/fatty acids/esters were in the order of HDO > DCO > DCO_2 routes; thus, the DCO and DCO_2 routes may be more theoretically economical than the HDO route [36, 41]. Several researchers have studied various metal catalysts for the deoxygenation of model compounds, such as palmitic acid [32, 36], stearic acid [12, 42-44, 67], oleic acid [44], linoleic acid [44], methyl palmitate [30], methyl oleate [14], methyl heptanoate [31], and methyl octanoate [45]. However, only a few studies investigated the deoxygenation of triglycerides, such as palm oil [43, 44], jatropha oil [14, 23], and sunflower oil [66]. In particular, Co species are good catalysts for hydrogenation/hydrogenolysis reactions [31]. However, to the best of our knowledge, the use of Co catalysts in the deoxygenation of triglycerides has never been reported in the literature. Consequently, four metal catalysts, namely Co, Ni, Pd, and Pt, are attractive for the deoxygenation of triglycerides.

In the present work, we prepared γ-Al_2O_3-supported monometallic catalysts (Co, Ni, Pd, and Pt) by the incipient wetness impregnation method. The physical and chemical properties were characterized by XRD, TPR, N_2 sorption, TEM, and CO pulse chemisorption, and their catalytic performances for the deoxygenation of palm oil were subsequently investigated in a continuous-flow trickle-bed reactor. To

understand the roles of the four monometallic catalysts on the activity and selectivity in the deoxygenation of triglycerides to hydrocarbons, the contributions of HDO and DCO/DCO_2 were estimated based on the mole balance corresponding to fatty acids in the oil feed. The obtained data could be useful for the evaluation of the hydrogen consumption and heat balance in the deoxygenation process. Moreover, the reaction network of the deoxygenation of palm oil over four supported monometallic catalysts was also discussed based on a model compound study.

Note that the metal catalysts in this section with metal loadings of 2, 5, and 10 wt.% were labeled as 5CoAl, 10CoAl, 5NiAl, 10NiAl, 2PdAl, 5PdAl, 2PtAl, and 5PtAl, where the prefix numbers represent the %metal loadings.

5.2.2 Catalyst Characterizations

The phase identity and crystallinity of the catalysts were revealed through XRD patterns (Figures 23 and 24). Three peaks at 37.5°, 46°, and 67° assigned to the γ-Al_2O_3 phase with low crystallinity [12, 82, 83] were observed for all catalysts. As represented in Figure 23a, the 5NiAl and 10NiAl catalysts exhibited diffraction peaks at 37.4°, 44°, and 63°, which correspond to NiO (111), NiO (200), and NiO (220), respectively [36], whereas the small peak at 45° could be assigned to the diffraction of $NiAl_2O_4$ [84]. On the other hand, the diffraction peaks at 31.3°, 37.7°, 59.5° and 65.4° in 10CoAl and 5CoAl were assigned to those of spinel $CoAl_2O_4$ or Co_3O_4. It is difficult to discriminate the spinel phases by XRD characteristics alone because both spinel Co_3O_4 and $CoAl_2O_4$ have a cubic spinel structure with almost identical diffraction patterns [85, 86]. As illustrated in Figure 23b, the 2PdAl and 5PdAl catalysts showed diffraction peaks at 33.7°, 55°, 61.2, and 72°, which belong to PdO [87]. The diffraction peaks at 42.3°, 47.5°, and 67.5° in 2PtAl and 5PtAl were assigned to PtO_2 [88]. The higher metal loading typically resulted in a higher intensity of the corresponding metal/metal oxide peaks. After the H_2 reduction process, the metal oxides were transformed to their corresponding metallic phases and acted as catalytic active sites in deoxygenation reactions (Figure 24).

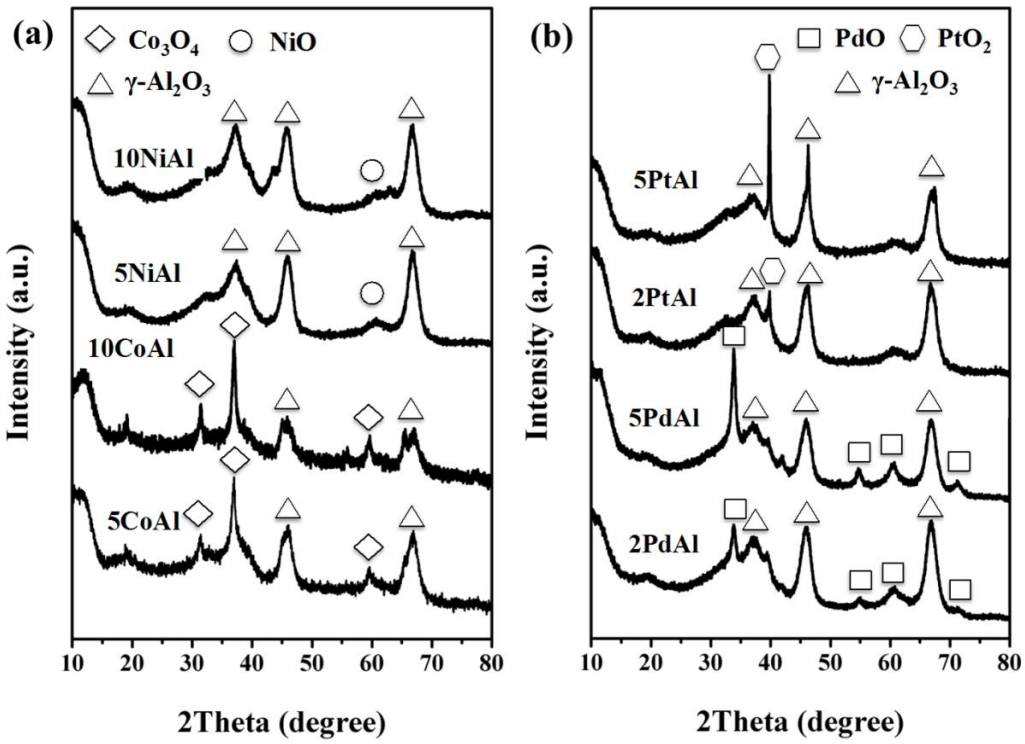

Figure 23 X-ray diffraction patterns of the (a) 5CoAl, 10CoAl, 5NiAl, and 10NiAl catalysts and (b) the 2PdAl, 5PdAl, 2PtAl and 5PtAl catalysts.

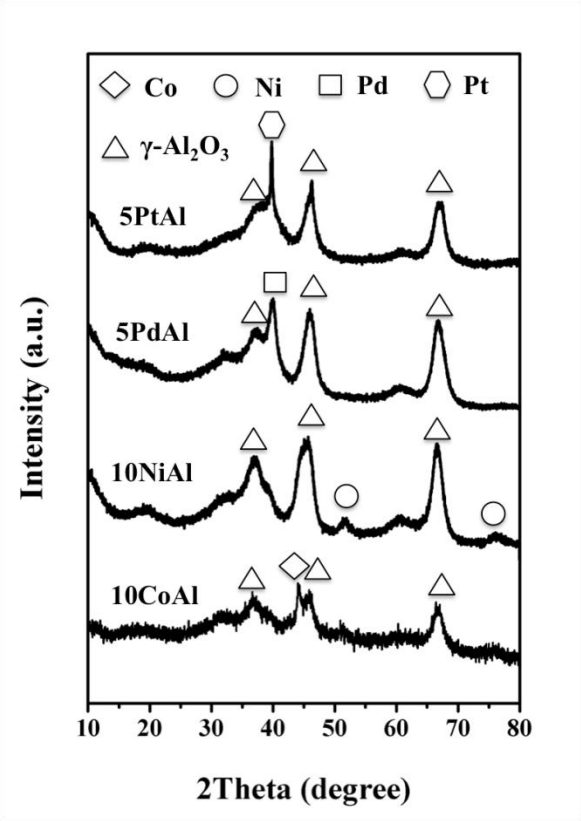

Figure 24 X-ray diffraction patterns of the reduced 10CoAl, 10NiAl, 5PdAl, and 5PtAl catalysts.

The H_2-TPR measurements were conducted to investigate the reducibility of the 10CoAl, 10NiAl, 5PdAl, and 5PtAl catalysts and to study the interaction between metal species and the γ-Al_2O_3 support in the catalysts (Figure 25**)**. The reduction profile of 10NiAl showed a broad peak composed of three contributions (~670, ~760, and ~880 ^oC), representing the presence of different nickel species. The peak at 670 ^oC was attributed to a reduction of bulk NiO species to Ni^0, occupying a weak interaction with the support. The second peak at 760 ^oC also represented NiO species, which have stronger metal and support interactions or smaller particles located inside the pores. Additionally, the reduction peak at the high temperature of 880 ^oC may be assigned to nickel aluminate phases with spinel structures ($NiAl_2O_4$) [12, 30, 84]. On the other hand, the TPR profile of 10CoAl showed a broad curve from 430 to 800 ^oC, with three different peaks at ~520, ~625, and ~750 ^oC. The transformation of Co_3O_4 to Co^0 occurred in two steps; the first peak, at 430–550 ^oC, was ascribed to the

reduction of Co_3O_4 to CoO and the second one, at 550–680 ^oC, to the subsequent reduction of CoO to Co^0. Additionally, the peak at higher temperature (750 ^oC) may be assigned to the existence of Co species with smaller crystallite sizes or stronger metal-support interactions or to the formation of a cobalt aluminate structure [22, 85]. As demonstrated in Figure 25, the reduction of 5PdAl and 5PtAl catalysts has reduction peaks at ~160 and ~260 ^oC, corresponding to the reduction of PdO and PtO_2 to metallic palladium and platinum, respectively. Likewise, both samples exhibited similar broad peaks from 400-600 ^oC (peaked at ~490 ^oC), assigned to the reduction of a more stable species interacting strongly with the support [89].

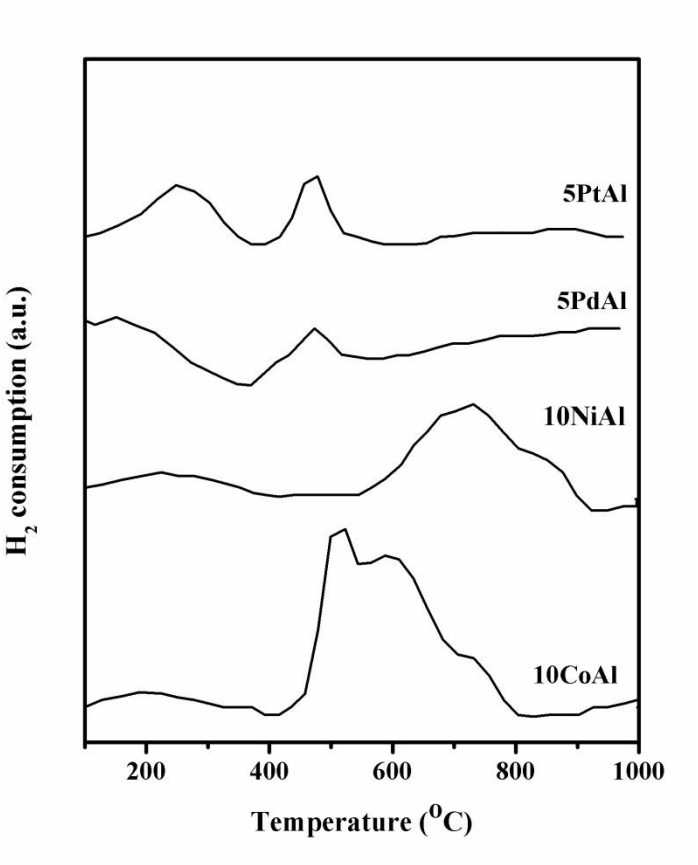

Figure 25 TPR profiles of the 10CoAl, 10NiAl, 5PdAl, and 5PtAl catalysts.

The BET specific surface area, total pore volume, and average pore diameter of bare γ-Al_2O_3 and the supported catalysts are summarized in Table 14. The surface area of γ-Al_2O_3 was 201.1 m^2/g with a total pore volume of 0.55 cm^3/g. The specific surface area and pore volume typically decreased by 2–15% after metal loading, except for 2PdAl and 2PtAl. The decrease in the specific surface area and total pore volume at higher metal loading is due to the metal converging on the γ-Al_2O_3 support and the blockage of pores by metal species. Interestingly, the observed pore sizes of all catalysts were approximately 7.5 nm and did not change significantly after metal loading in the range studied. The N_2 adsorption–desorption isotherms (not shown) of γ-Al_2O_3 and the catalysts exhibited type-IV isotherms, indicating the typical characteristics of a mesoporous structure.

Table 14 Physicochemical properties of the catalysts

Catalysts	Specific surface area[a] (m^2/g)	Pore volume[b] (cm^3/g)	Pore diameter[c] (nm)
γ-Al_2O_3	201.1	0.549	7.53
5CoAl	187.4	0.504	7.52
10CoAl	170.7	0.474	7.52
5NiAl	190.9	0.519	7.52
10NiAl	173.1	0.482	7.52
2PdAl	214.2	0.579	7.52
5PdAl	194.4	0.496	7.50
2PtAl	216.5	0.578	7.52
5PtAl	196.2	0.507	7.526

[a] BET surface area calculated from the adsorption branch of N_2 isotherm

[b] Total pore volumes calculated from the N_2 adsorption at relative pressure of 0.98

[c] Pore diameter calculated from the desorption branch using the BJH method

CO chemisorption data of monometallic catalysts supported on γ-Al_2O_3 with various metal loadings were used to estimate the surface metallic atom characteristics, namely the dispersion, metal surface area, and metal particle size of the synthesized catalysts, as summarized in Table 15. The CO uptake, which represents the number of active sites, was typically greater at higher metal loadings. The metal dispersion of the Pd and Pt catalysts increased with a decrease in the metal loading, ascribable to the aggregation of metal atoms on the γ-Al_2O_3 support. It should be noted that the metal dispersion and particle size of the Ni and Co catalysts could not be precisely estimated from the present chemisorption analysis. Some researchers have reported that Ni and Co catalysts easily form metal-aluminate phases, which are difficult to reduce [54, 55]

Table 15 CO pulse chemisorption results and metal particle size of the catalysts

Catalysts	CO uptake ($\mu mol/g_{cat}$)	Metal surface area (m^2/g_{cat})	Dispersion (%)	Metal particle size[a] (nm)	Metal particle size[b] (nm)
5CoAl	3.8	-	-	-	13.5
10CoAl	9.4	-	-	-	-
5NiAl	12.9	-	-	-	8.4
10NiAl	26.5	-	-	-	-
2PdAl	40.6	97.0	21.6	5.1	-
5PdAl	45.5	43.5	9.7	11.5	9.6
2PtAl	75.7	184.1	73.8	1.5	-
5PtAl	163.2	158.8	63.7	1.8	1.9

[a] Determined by the CO pulse chemisorption technique.

[b] Determined by the TEM images.

Figure 26 shows typical TEM images of the reduced samples at a metal loading of 5 wt.%. The TEM study revealed the difference in metal dispersion and metal particle size over four different catalysts. In the case of Co catalysts (Figure 26a), the TEM image showed a particle size of Co of approximately 13.2 nm, which was much larger than the pore size of the γ-Al_2O_3 support. The result suggested that most Co particles would be located outside the pore of the alumina. As demonstrated in Figure 26b, the Pt metal particles were homogeneously distributed on the γ-Al_2O_3 support and exhibited a narrow and small metallic particle size of approximately 1.5–2.5 nm. In the case of the Ni catalyst (Figure 26c), the TEM images revealed a broad particle size distribution of Ni particles, with significant contribution of a moderate particles size of approximately 8.4 nm. Similarly, in the case of the Pd catalyst (Figure 26d), the TEM study displayed an uneven metal particle size with a particle size of approximately 8.0–11.2 nm. The average metal particle size observed by TEM analysis was in the order Co > Pd > Ni > Pt, and the Pt catalysts exhibited the highest metal dispersion. The CO chemisorption data were in good agreement with the particle size of Pd and Pt catalysts obtained from the TEM study, as illustrated in Table 15.

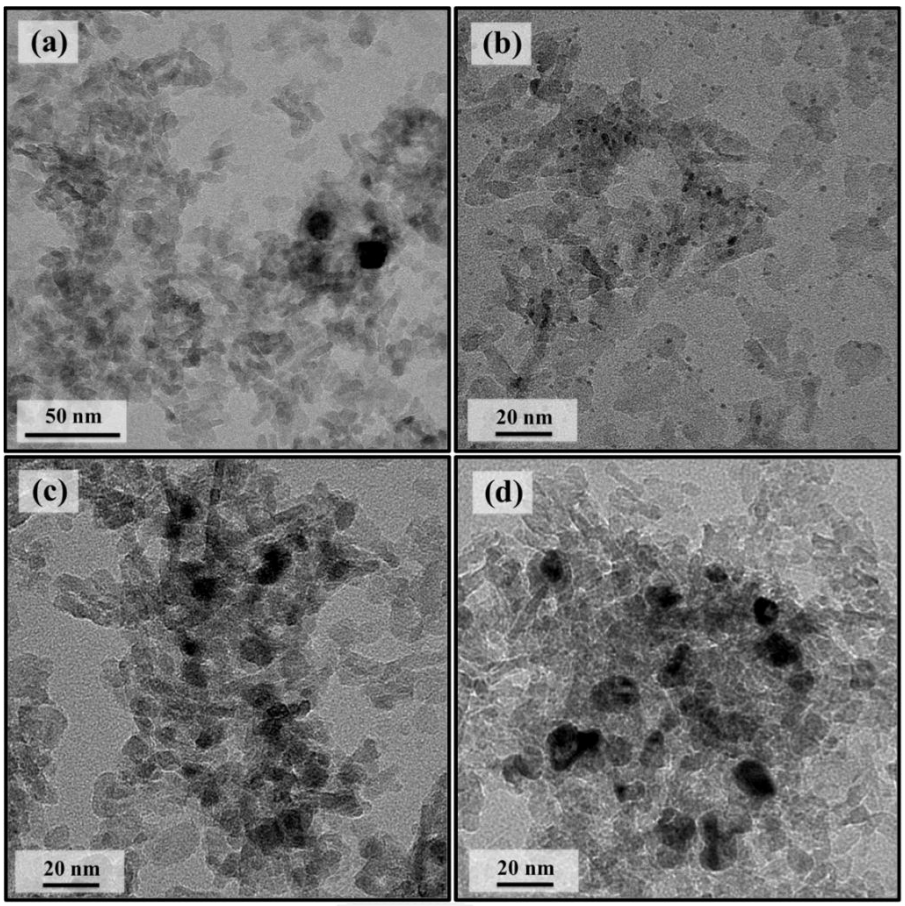

Figure 26 TEM images of the reduced (a) 5CoAl, (b) 5PtAl, (c) 5NiAl, and (d) 5PdAl catalysts.

5.2.3 Deoxygenation of refined palm olein

The deoxygenation of palm oil was conducted under the following conditions: 330 ^{o}C, 5 MPa H_2, LHSV = 1 h^{-1}, and H_2/oil ratio = 1,000 N(cm^3/cm^3) over different types of monometallic catalyst and metal loading on γ-Al_2O_3 (Figure 27). At temperatures lower than 300 ^{o}C, the liquid product had high viscosity and contained reactants and intermediates including triglycerides and free fatty acids, suggesting the incomplete deoxygenation reactions of triglycerides to *n*-alkanes. The deoxygenation reaction over pure γ-Al_2O_3 resulted in 56% conversion of triglyceride without diesel product yield. The results suggested that only saturated triglyceride scission to free fatty acids and propane occurred. It should be concluded that γ-Al_2O_3 possessed no catalytic activity in the deoxygenation of triglycerides. The product yield was achieved when the reaction was catalyzed by the metal catalysts, confirming the deoxygenation activity of the metal species.

As demonstrated in Figure 27a, the complete conversion of triglycerides was achieved for the 5NiAl, 10NiAl, 5CoAl, 10CoAl, 5PdAl, and 5PtAl catalysts, whereas it reached approximately 95% for the 2PdAl and 2PtAl catalysts. Typically, the higher metal loading in the Ni, Pd, and Pt catalysts gave improved product yields. Nonetheless, the increase in the Co loading from 5 to 10 wt.% did not significantly affect the product yield and triglyceride conversion. By comparing the catalysts at the same amount of metal loading, the deoxygenation activity in terms of product yield decreased in the order of 5CoAl (88.5%) > 5PdAl (85.2%) > 5PtAl (79.5%) > 5NiAl (69.7%).

In the presence of low metal loading (5NiAl, 2PdAl, and 2PtAl), the conversion of triglyceride was almost 100%; nevertheless, higher product yield was not achieved. The liquid product was composed of *n*-alkanes, reactants and oxygenated intermediates, including a small amount of triglycerides, free fatty acids, alcohol, and esters. These results suggested that the reaction over the low metal-loading catalysts mainly proceeded through the hydrogenation of C=C bonds in unsaturated triglycerides, followed by C-O bond cleavage via hydrogenolysis of saturated triglycerides to produce free fatty acids and propane, indicating incomplete

deoxygenation activity. Additionally, the fatty acids partially underwent HDO, DCO, and DCO_2 reactions to produce n-alkanes when the reaction was catalyzed by 5NiAl, 2PdAl, and 2PtAl, with a low product yield in the range of 30 to 60%.

To understand the deoxygenation behavior over different types of metallic catalysts, the % contributions of HDO and combined DCO and DCO_2 (DCO/DCO_2) were considered. As represented in Figure 27b, the DCO/DCO_2 was the dominant reaction when catalyzed by Ni, Pd, and Pt catalysts. These results were consistent with those of previous studies showing that DCO and/or DCO_2 was favored over HDO in the above-mentioned catalysts [8, 14, 22, 32, 42, 43, 62, 65, 67, 90]. The contributions of DCO/DCO_2 (35.4–37.8%) and HDO (45.5–52.3%) were both dominant reaction pathways over the Co catalyst, suggesting that the reactants were deoxygenated through the DCO, DCO_2, and HDO reactions. The metallic sites of the Co catalyst were responsible for all three major reaction pathways, whereas the metallic sites of Ni, Pd, and Pt strongly promoted the DCO and/or DCO_2 reactions. The palm oil used in this study was mainly composed of C_{16} and C_{18} fatty acids (>98.4 wt.%). Thus the main composition of the liquid product was *n*-alkanes of C_{15} and C_{17} due to the highly selective DCO/DCO_2 reactions over Ni, Pd, and Pt catalysts. On the contrary, *n*-C_{15}, *n*-C_{16}, *n*-C_{17}, and *n*-C_{18} were the major product composition when Co catalysts were used, as summarized in Table 16**.** The light hydrocarbon compositions (*n*-C_8 to *n*-C_{14}) observed suggested that the cracking reaction proceeded when the reaction occurred over Ni and Co catalysts. These catalysts were partially selective to C-C cleavage. In addition, the % contributions of each deoxygenation product from HDO (*n*-C_{16} and *n*-C_{18}) and DCO/DCO_2 (*n*-C_{15} and *n*-C_{17}) exhibited similar behavior over all catalysts (Table 17**)**. The chain length of the fatty acid did not significantly affect the deoxygenation behavior when the reactions catalyzed by the metallic catalysts were studied.

The effects of monometallic catalysts on the gas product composition are represented in Figure 27c. When the Ni and Co catalysts were used, CH_4 was the major gas composition (20.7 mole% for Ni catalyst, 17.5–27.1 mole% for Co catalyst) as a result of the methanation reaction between CO or CO_2 with H_2. In contrast, methanation was not strongly selective when the reaction was catalyzed by the Pd and

Pt catalysts (Figure 27c). When the reaction was catalyzed by Ni, the amount of C_3H_8 produced by the hydrogenolysis of triglycerides was lower than the others, suggesting the cracking of C_3H_8 to C_2H_6 and CH_4 during the deoxygenation reactions due to the high C-C cleavage activity of the Ni catalyst. Furthermore, the formation of the CH_4, C_2H_6, and C_3H_8 species in the gas product could be associated with the cracking reaction in the liquid phase during the deoxygenation of palm oil. The amount of CO_2 was higher than that of CO when the reaction was catalyzed by Pd and Pt catalysts. It was reported that CO is relatively easily hydrogenated to CH_4 compared to CO_2 at the same conditions [77].

The synthesized monometallic catalysts, namely 5NiAl, 5CoAl, 5PdAl, and 5PtAl, exhibited high activity for the deoxygenation of palm oil to hydrocarbons. Consequently, a reaction mechanism for the deoxygenation of palm oil was investigated via a model compound (oleic acid) study over these catalysts.

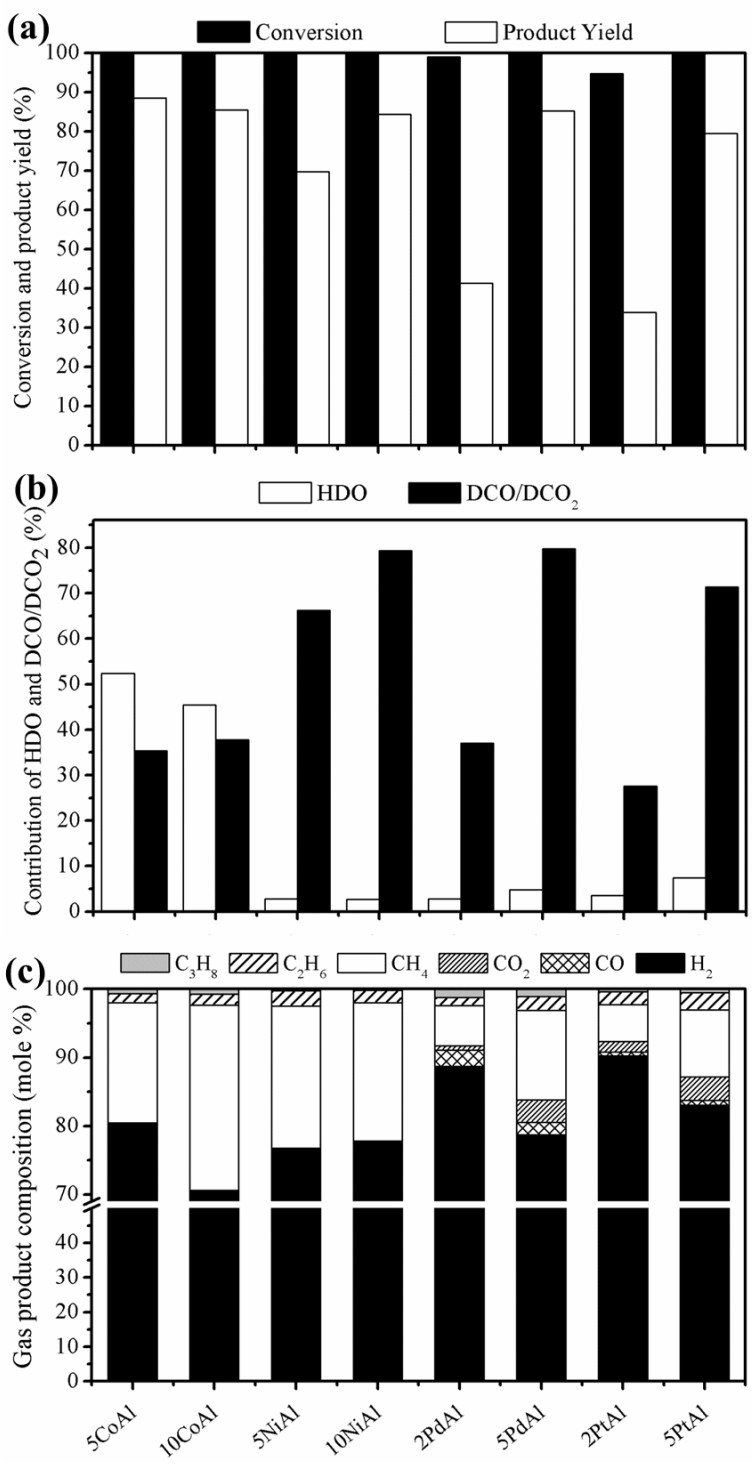

Figure 27 Effect of the monometallic catalysts at different metal loadings on (a) conversion and product yield, (b) % contribution of HDO and DCO/DCO_2, and (c) gas product composition. All experiments were performed at a temperature of 330 ^{o}C, H_2 pressure of 5 MPa, LHSV of 1 h^{-1}, and H_2/oil ratio of 1,000 N(cm^3/cm^3).

Table 16 Composition of the liquid product from palm oil deoxygenation over catalysts

Catalysts	Conversion	Liquid product (wt.%)					Liquid phase
	(%)	*n*-C_8-*n*-C_{14}	*n*-C_{15}	*n*-C_{16}	*n*-C_{17}	*n*-C_{18}	
5CoAl	100	3.5	14.8	23.2	21.9	34.4	Liquid
10CoAl	100	5.1	16.7	21.7	23.5	29.7	Liquid
5NiAl	100	0.8	25.3	1.3	40.4	1.6	Solid
10NiAl	100	1.6	33.8	1.8	54.6	1.3	Liquid
2PdAl	99	0.3	14.9	1.2	22.8	1.8	Solid
5PdAl	100	0.6	31.4	2.1	51.5	3.2	Liquid
2PtAl	95	0.2	10.4	1.3	16.3	2.3	Solid
5PtAl	100	0.7	28	3.1	46.2	5.2	Liquid

Reaction conditions: 330 ^{o}C, 5 MPa, LHSV of 1 h^{-1}, and H_2/oil ratio of 1,000 N(cm^3/cm^3)

Table 17 % contribution of HDO and DCO/DCO_2 from palm oil deoxygenation over catalysts

Catalyst	DCO/DCO_2 (%) (*n*-C_{15})	DCO/DCO_2 (%) (*n*-C_{17})	HDO (%) (*n*-C_{16})	HDO (%) (*n*-C_{18})
5CoAl	37.7	33.8	55.6	50.1
10CoAl	42.3	35.9	51.4	42.9
5NiAl	67.7	65.3	3.3	2.5
10NiAl	82.1	80.1	4.0	1.8
2PdAl	39.5	36.6	3.1	2.7
5PdAl	80.9	79.5	4.9	4.7
2PtAl	29.1	27.5	3.5	3.7
5PtAl	71.6	71.9	7.3	7.6

Reaction conditions: 330 ^oC, 5 MPa, LHSV of 1 h^{-1}, and H_2/oil ratio of 1,000 N(cm^3/cm^3).

5.2.4 Deoxygenation of oleic acid

Fatty acids are the main oxygenated intermediates in the deoxygenation of triglycerides and are produced by the hydrogenolysis of triglycerides with H_2 [8, 56]. Additionally, the formation of fatty acids is relatively fast when compared with deoxygenation reactions (HDO, DCO, and DCO_2), which are considered rate-determining steps [37, 41, 90]. C_{18} fatty acid (60.8%) was the most abundant species in the palm oil used in the experiments. Consequently, the reaction mechanisms for

the deoxygenation of palm oil were elucidated using a model compound, oleic acid, as a reactant over four different types of monometallic catalysts. The catalytic activity measurements at the same amount of metal loading (5 wt.%) were conducted at the LHSV of 2 h^{-1} with fixed operating conditions: 330 ^{o}C, 5 MPa of H_2 pressure, and 1,000 N(cm^3/cm^3) H_2/fatty acid ratio. The results are represented in Table 18. The oleic acid was almost completely converted (conversion ≈ 100%) over all catalysts. The liquid product when the reaction was catalyzed by the Ni, Pd, and Pt catalysts was solidified at room temperature and contained oxygenated intermediates, including mainly stearic acid, octadecyl stearate, and small amounts of octadecanol, indicating incomplete deoxygenation activity. The transformation of octadecanol, a secondary intermediate in the HDO pathway, to octadecane was not considered a rate-determining step. Furthermore, octadecanal, an oxygenated intermediate obtained from hydrogenation of the carboxylic group of stearic acid, was not detected during the deoxygenation of oleic acid. Therefore, the transformation of octadecanal to octadecanol ether or heptadecane via direct decarbonylation was relatively fast. Over the Co catalyst, the complete conversion of oleic acid with the highest product yield of 94.3% was achieved, indicating that the Co catalyst provided the highest catalytic activity. The deoxygenation activity in terms of product yield decreased in the order of 5CoAl (94.3%) > 5PdAl (76.1%) > 5PtAl (54.0%) > 5NiAl (26.5%), which was in line with the catalytic activity of the catalysts over palm oil. Furthermore, HDO (50%) and DCO/DCO_2 (44.3%) were the major reaction pathways over the Co catalyst, whereas DCO/DCO_2 was the dominant reaction over Ni, Pd, and Pt catalysts.

Table 18 Deoxygenation behaviors of oleic acid deoxygenation over catalysts

	Catalysts			
	5CoAl	5NiAl	5PdAl	5PtAl
Conversion (%)	100	93.0	94.6	93.6
Product yield (%)	94.3	26.5	76.1	54
Contribution (%)				
HDO	50.0	0.4	2.1	4.0
DCO+DCO_2	44.3	26.1	74.0	49.9
Gaseous product (mole %)				
CO	0	0	2.1	0.5
CO_2	0	0	1.1	1.5
CH_4	13.6	4.9	4.5	3.4
Liquid product (mole %)				
n-C_{17}	47.0	25.5	72.0	51.1
n-C_{18}	53.0	0.4	2.0	4.2
Oxygenates hydrocarbons (mole %)				
n-$C_{17}H_{33}COOH$	0	6.9	5.3	6.5
n-$C_{17}H_{35}COOH$	0	57.7	5.3	22.0
n-$C_{18}H_{37}OH$	0	0	2.0	0
n-$C_{17}H_{35}COOC_{18}H_{37}$	0	9.0	13.5	16.2
9-$C_{17}H_{33}COOC_{18}H_{37}$	0	0.5	0	0

Reaction conditions: 330 ^{o}C, 5 MPa, LHSV of 2 h^{-1}, and H_2/fatty acid ratio of 1,000 N(cm^3/cm^3).

The turnover frequencies (TOFs) at a moderate product yield of 2.5–67.7% (LHSV of 8 h^{-1}) were calculated to compare the deoxygenation activity of monometallic catalysts, which was defined as the total production rate of alkanes (*n*-C_{17} and *n*-C_{18}) per active site of catalyst using the CO uptake, as illustrated in Table 19. The highest TOF was 0.2766 s^{-1} over the Co catalyst, whereas the Pd, Pt, and Ni catalysts exhibited TOFs of 0.1320, 00271, and 0.0171 s^{-1}, respectively. The results revealed a similar order to that of the catalytic deoxygenation activity (Co > Pd > Pt > Ni). The highest TOF over the Co catalyst was associated with the significantly high rate of the deoxygenation reaction from the Co catalyst in comparison with the other catalysts, whereas the metal particle sizes of the Co, Ni, and Pd catalysts were not significantly different.

Table 19 Turnover frequency (TOF) in oleic acid deoxygenation over catalysts

Catalysts	Turnover frequency (TOF) (s^{-1})
5CoAl	0.2766
5NiAl	0.0171
5PdAl	0.1320
5PtAl	0.0271

Reaction conditions: 330 ^{o}C, 5 MPa, LHSV of 8 h^{-1}, and H_2/oil ratio of 1,000 N(cm^3/cm^3).

To investigate the possibility of reaction through an exclusive decarboxylation pathway, which does not consume H_2, the study was conducted under nitrogen pressure (5 MPa) at 330 ^{o}C over the Ni, Pd, and Pt catalysts. The decarboxylation reaction did not proceed over the Co catalyst due to the high selectivity through the HDO pathway. The results showed that the detected CO_2 was extremely low at 0.22, 0.28, and 0.32 mole% and without CO formation over the Ni, Pd, and Pt catalysts,

respectively. The deoxygenation of oleic acid over the monometallic catalysts mainly occurred through reduction routes (DCO and HDO reactions) under the present experimental conditions [12, 36]. Additionally, the hydrogen supply was also used to saturate the double bond in triglycerides/fatty acids and to prevent the catalyst deactivation by side reactions [18, 44].

The effects of the metallic catalysts on the gas product composition are also demonstrated in Table 18. The results revealed that CH_4 was the major gas product component (5–13.6 mole%), and the absence of CO and CO_2 suggested that they were completely converted to CH_4 by a methanation reaction over the Ni and Co species. These results indicated that the Ni and Co catalysts showed higher activity in the methanation reaction than the Pd and Pt catalysts, which is in good agreement with the literature [91, 92]. The results were consistent with the catalytic behavior in the deoxygenation of palm oil. Moreover, the formation of CH_4 may be due to the cracking of liquid product or direct cracking of oleic acid, accompanied by the methanation reaction. By comparing the amount of CO and CO_2, Pt catalysts produced larger amounts of CO_2 than the others, suggesting that the decarboxylation was more favorable. These results were consistent with the higher amount of CO_2 than in the experiments under nitrogen pressure.

5.2.5 Reaction network

Based on the results obtained in the previous sections, the formation of heptadecane, octadecane, stearic acid, octadecanol, and octadecyl stearate/stearyl oleate was observed during the deoxygenation of oleic acid over four monometallic catalysts (Co, Ni, Pd, and Pt). During the deoxygenation of oleic acid to *n*-alkanes, the C=C double bond in oleic acid was firstly hydrogenated to stearic acid. Subsequently, the hydrogenolysis of stearic acid, as a primary oxygenated intermediate, led to the formation of octadecanal and water and was followed by the hydrogenation of octadecanal to octadecanol. Nevertheless, octadecanal was not found during the deoxygenation of oleic acid. The decarbonylation of octadecanal to heptadecane and CO is faster than the hydrogenolysis of stearic acid to octadecanal, which is a rate-

determining step [12, 41]. Accordingly, the transformation of oleic acid to hydrocarbons could proceed through two major reaction routes. In the first route, octadecanal undergoes decarbonylation to heptadecane and carbon monoxide (C-C bond scission, major route over Ni, Pd, and Pt). On the other hand, octadecanol underwent hydrodeoxygenation to octadecane and water as the second route (C-O bond scission, major route over Co). Additionally, the formation of octadecyl stearate or stearyl oleate by the esterification of oleic acid or stearic acid and octadecanol was further converted to final products. The hydrogenation, hydrogenolysis, decarbonylation, and hydrodeoxygenation reactions typically occurred on the metallic sites of the catalysts. There was no observed evidence of the direct decarboxylation of free fatty acids to hydrocarbons with oxygen releasing in the form of CO_2.

A proposed reaction network for the deoxygenation of palm oil over four monometallic catalysts (Co, Ni, Pd, and Pt) supported on γ-Al_2O_3 is demonstrated in Figure 28. The reaction network for the deoxygenation of palm oil is similar to that of oleic acid. First, the double bonds in the saturated triglycerides were hydrogenated to unsaturated triglycerides and subsequently cleaved to free fatty acids and propane via hydrogenolysis. The free fatty acid, as the oxygenated intermediates, could react to yield a fatty acid aldehyde, alcohol, and subsequently hydrocarbons through HDO (major route over Co) and DCO (major route over Ni, Pd, and Pt) reactions, leading to the elimination of water and CO from palm oil, respectively.

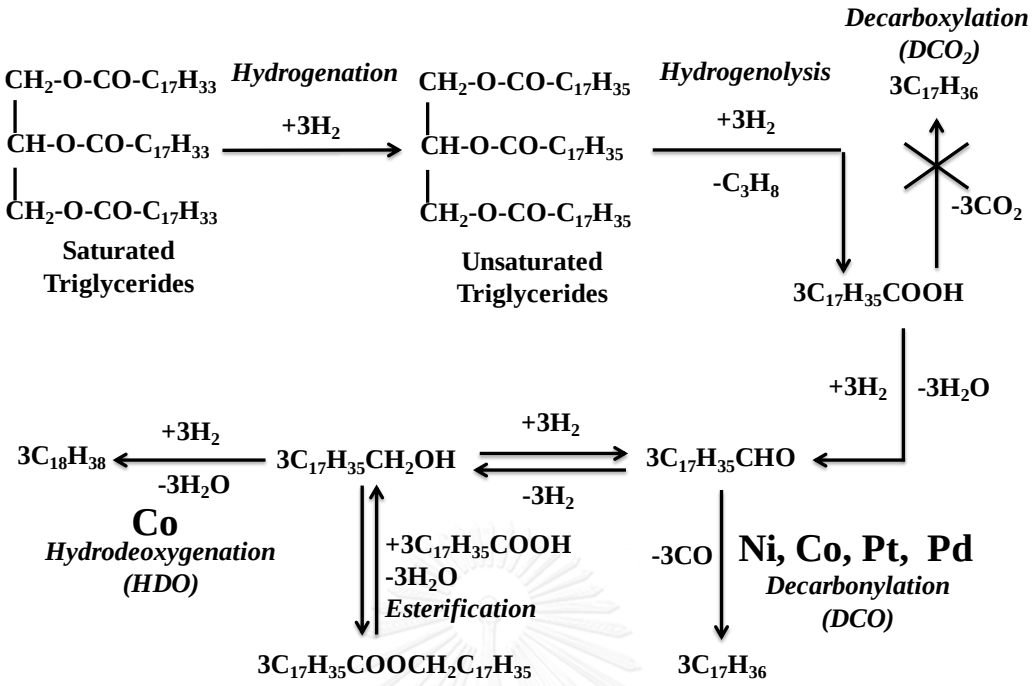

Figure 28 Proposed reaction network of palm oil deoxygenation over four supported-monometallic catalysts.

5.3 Deoxygenation of palm oil to bio-hydrogenated diesel over metal and metal sulfide catalysts

5.3.1 Introduction

In the present section, the γ-Al_2O_3-supported metal catalysts (Ni, Co, Mo, NiMo, and CoMo) and γ-Al_2O_3-supported metal sulfide catalysts (NiS_x, CoS_x, MoS_2, $NiMoS_2$, and $CoMoS_2$) were prepared by the incipient wetness impregnation method in order to understand the roles of metal and metal sulfide catalysts. Their catalytic performances for the deoxygenation of palm oil were conducted in a continuous-flow trickle-bed reactor. To understand the roles of metal and metal sulfide catalysts on the activity and selectivity in the hydrodeoxygenation of palm oil to hydrocarbons, the contributions of HDO and DCO/DCO_2 were estimated based on the mole balance

corresponding to fatty acids in the oil feed. Furthermore, the stability of metal and metal sulfide catalysts was also reported and discussed.

5.3.2 Catalysts activity investigation

The deoxygenation of palm oil was conducted and screened over γ-Al_2O_3-supported metal catalysts (Ni, Co, Mo, NiMo, and CoMo) and γ-Al_2O_3-supported metal sulfide catalysts (NiS_x, CoS_x, MoS_2, $NiMoS_2$, and $CoMoS_2$) under the following conditions: 300 ^oC, 5 MPa H_2, LHSV = 1 h^{-1}, and H_2/oil ratio = 1,000 N(cm^3/cm^3) (Figures 29-32). At temperatures lower than 300 ^oC, the liquid product had high viscosity and contained reactants and intermediates including triglycerides and free fatty acids, suggesting the incomplete deoxygenation reactions of triglycerides to *n*-alkanes [57]. The deoxygenation reaction over pure γ-Al_2O_3 resulted in 56% conversion of triglyceride without diesel product yield. The results suggested that only saturated triglyceride scission to free fatty acids and propane occurred. It should be concluded that γ-Al_2O_3 possessed no catalytic activity in the deoxygenation of triglycerides. The product yield was achieved when the reaction was catalyzed by the metal and metal sulfide catalysts, confirming the deoxygenation activity of the metal sulfide species.

As exhibited in Figures 29, the complete conversion of triglycerides was achieved for the Ni, Co, Mo, NiMo, CoMo, MoS_2, $NiMoS_2$, and $CoMoS_2$ catalysts, whereas it reached approximately 70-80 % for the NiS_x and CoS_x catalysts. It should be note that the NiS_x and CoS_x catalysts did not play the significant roles in deoxygenation reactions. It may be due to the fact that the sulfur bonding on Ni and Co species inhibited the active sites for deoxygenation of triglyceride. Although some catalysts (Mo, NiMo, and CoMo) exhibited the 100% triglyceride, the higher product yield was not achieved. The liquid product was composed of *n*-alkanes, reactants and oxygenated intermediates, including the free fatty acids (palmitic acid and stearic acid), alcohol, and esters. These results suggested that the reaction over the Mo, NiMo, CoMo catalysts in metallic phases mainly proceeded through the hydrogenation of C=C bonds in unsaturated triglycerides, followed by C-O bond cleavage via hydrogenolysis of saturated triglycerides to produce free fatty acids and

propane, indicating incomplete deoxygenation activity. By comparing the catalysts based on the deoxygenation activity in terms of product yield decreased in the order of $NiMoS_2$ (94.7%) > Co (93.2%) > Ni (92.3%) > $CoMoS_2$ (87.45%) > MoS_2 (79.8%) > NiMo (58.4%) > CoMo (19.5%) > Mo (10.2%) > NiS_x (7.2%) > CoS_x (5.5%).

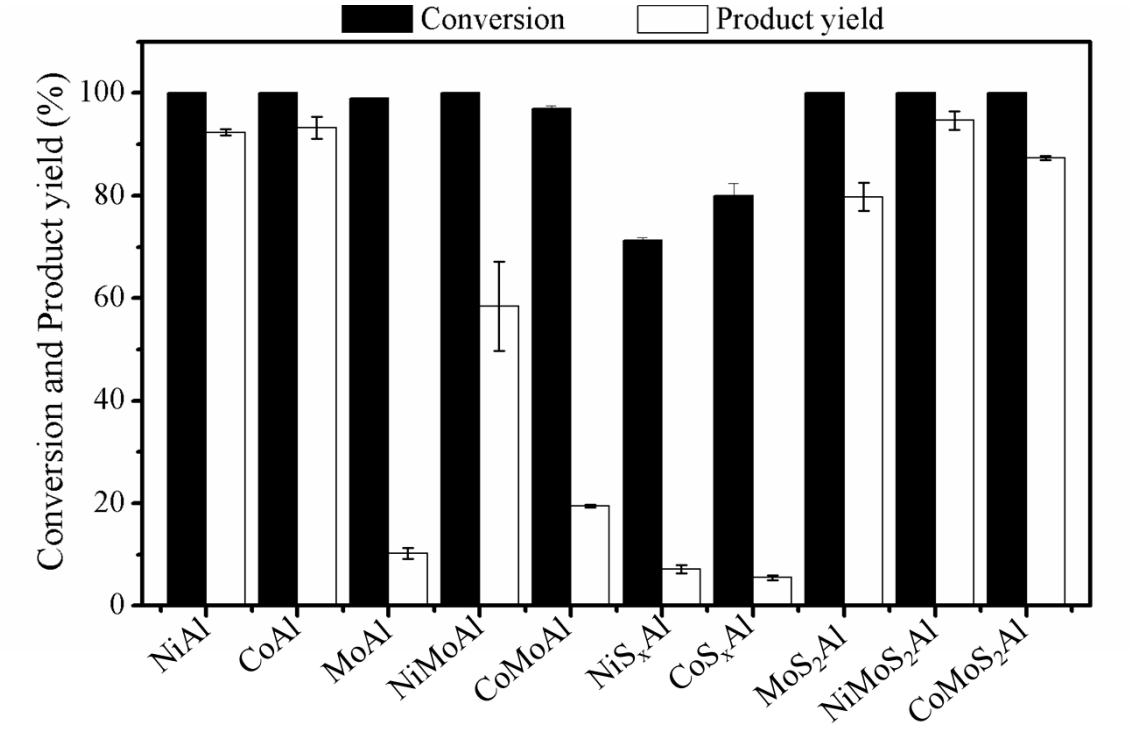

Figure 29 Effect of the metal and metal sulfide catalysts on conversion and product yield All experiments were performed at a temperature of 300 ^{o}C, H_2 pressure of 5 MPa, LHSV of 1 h^{-1}, and H_2/oil ratio of 1,000 N(cm^3/cm^3).

The Van Krevelen diagram was used to investigate the deoxygenation activity of metal and metal sulfide catalysts by analyzing the elemental contents (C, H, and O) in the liquid product (Figure 30). First, the palm oil used in hydrodeoxygenation experiment revealed the H/C (1.91) and the O/C (0.13) ratios. When metal catalysts (Ni, Co, Mo, NiMo, and CoMo) were used, shown in Figure 30a, the liquid product obtained from the Ni and Co catalysts with high product yield (>90%), exhibited the highest H/C (~2.18) and the lowest O/C (~0.04) ratios, whereas, the products obtained from metallic Mo, NiMo, and CoMo with low product yield, exhibited H/C ratios of

of (~2.10) and O/C of (~0.09) ratios. When the metal sulfide catalysts (NiS_x, CoS_x, MoS_2, $NiMoS_2$, and $CoMoS_2$) were used, shown in Figure 30b, the liquid product obtained from the MoS_2, $NiMoS_2$, and $CoMoS_2$ catalysts (product yield >90%), exhibited the highest H/C (~2.18) and the lowest O/C (~0.04) ratios, while the products obtained from Mo, NiMo, and CoMo, both exhibiting lower product yield, exhibited H/C ratios of (~2.04) and O/C ratios of (~0.13). It should be noted that the metal catalysts (Ni and Co) and metal sulfide catalysts (MoS_2, $NiMoS_2$, and $CoMoS_2$) showed the lower oxygen content in liquid product, suggesting that higher deoxygenation activity when compare to the other catalysts.

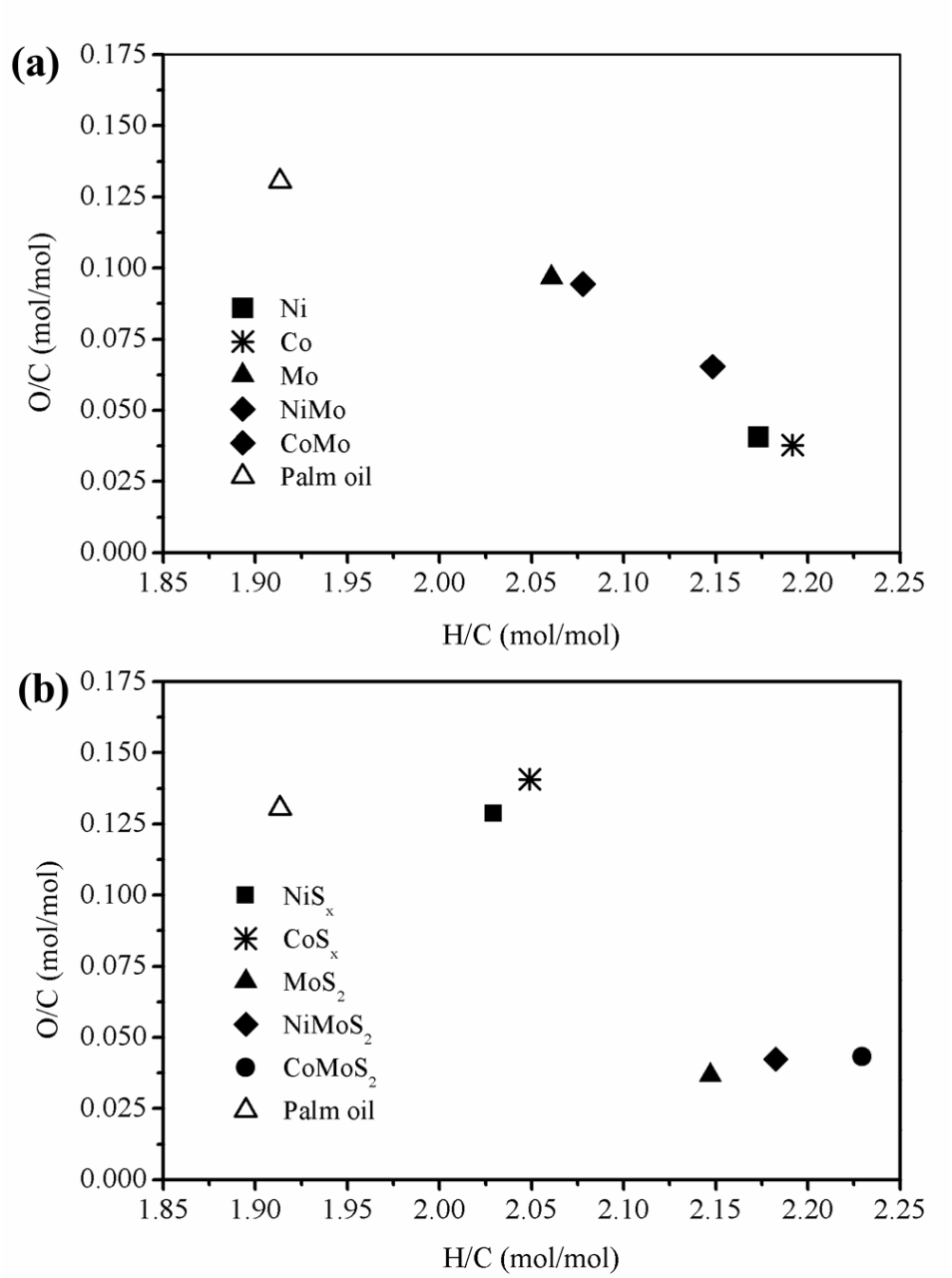

Figure 30 Van Krevelen diagram of the liquid product using (a) metal catalysts and (b) metal sulfide catalysts. All experiments were performed at a temperature of 300 ^{o}C, H_2 pressure of 5 MPa, LHSV of 1 h^{-1}, and H_2/oil ratio of 1,000 N(cm^3/cm^3).

To understand the deoxygenation behavior over γ-Al_2O_3-supported metal catalysts (Ni, Co, Mo, NiMo, and CoMo) and γ-Al_2O_3-supported metal sulfide catalysts (NiS_x, CoS_x, MoS_2, $NiMoS_2$, and $CoMoS_2$), the % contributions of HDO and combined DCO and DCO_2 (DCO/DCO_2) were considered. As represented in Figure 31, the DCO/DCO_2 (89.4%) was the dominant reaction when catalyzed by Ni catalyst. These results were consistent with those of previous studies showing that DCO and/or DCO_2 were favorer than HDO over Ni catalysts [30, 37, 41]. The HDO (>74.7%) was pre-dominant than DCO/DCO_2 when the reaction was catalyzed by MoS_2, $NiMoS_2$, and $CoMoS_2$ catalysts with consistent with those of previous work [2, 8, 11, 23, 56, 60]. Interestingly the contributions of DCO/DCO_2 (41.9%) and HDO (50.5%) were both dominant reaction pathways over the Co catalyst, suggesting that the reactants were deoxygenated through the DCO, DCO_2, and HDO reactions. Furthermore, the NiS_x and CoS_x catalysts, exhibited the lowest product yield, showed the partially selective to DCO/DCO_2, meanwhile, the Mo, NiMo, and CoMo catalysts also were selective to HDO.

Additionally, as demonstrated in Figure 29, the conversion was 100% for all molybdenum based sulfide catalysts and product yield of both promoted catalysts ($NiMoS_2$ and $CoMoS_2$) was slightly higher than that of unpromoted catalyst (MoS_2). The highest product yield (94.3%) was obtained when the reaction catalyzed by $NiMoS_2$ species. As represented in Figure 31, the contribution of DCO/DCO_2 decreased in order to $NiMoS_2$ (18.6%) > $CoMoS_2$ (8.1%) > MoS_2 (4.1%). Since the contribution of HDO of both promoted catalysts was practically equal to the contribution of HDO of unpromoted catalyst. Indeed, the adding Ni and Co strongly promoted to DCO and/or DCO_2 routes lead to increase in total product. It should be note that Ni and Co are weakening metal-sulfur bond, thus increasing the number of sulfur vacancies, as the active sites for deoxygenation of triglyceride [61].

The palm oil used in this study was mainly composed of C_{16} and C_{18} fatty acids (>98.4 wt.%). Thus the main composition of the liquid product was *n*-alkanes of C_{15} and C_{17} due to the highly selective DCO/DCO_2 reactions over Ni catalyst, whereas, the *n*-alkanes of C_{16} and C_{18} were the main composition of the liquid product due to the highly selective of HDO reaction over MoS_2, $NiMoS_2$, and $CoMoS_2$

catalysts (Table 20) On the contrary, *n*-C_{15}, *n*-C_{16}, *n*-C_{17}, and *n*-C_{18} were the major product composition when Co catalysts were used, as summarized in Table 20. The light hydrocarbon compositions (*n*-C_8 to *n*-C_{14}) observed suggested that the cracking reaction proceeded when the reaction occurred over metal and metal sulfide catalysts due to the partially selective to C-C cleavage.

Table 20 Composition of the liquid product from palm oil deoxygenation over catalysts

Catalysts	Conversion	Liquid product (wt.%)					Liquid phase
	(%)	*n*-C_8-*n*-C_{14}	*n*-C_{15}	*n*-C_{16}	*n*-C_{17}	*n*-C_{18}	
Ni	100	1.5	36.3	1.8	56.9	1.4	Liquid
Co	100	2.4	16.6	21.6	25.0	32.3	Liquid
Mo	99.1	0.0	0.4	5.3	0.2	3.4	Solid
NiMo	100	2.1	1.6	24.2	2.8	32.7	Solid
CoMo	97	0.2	0.4	9.3	0.5	7.5	Solid
NiS_x	71.3	0.0	2.6	0.0	3.7	0.0	Solid
CoS_x	80	0.0	2.6	0.0	2.4	0.0	Solid
MoS_2	100	1.1	1.7	33.2	2.7	45.4	Liquid
$NiMoS_2$	100	1.7	6.9	31.3	11.7	49.3	Liquid
$CoMoS_2$	100	1.7	3.0	34.0	5.2	50.9	Liquid

Reaction conditions: 300 ^oC, 5 MPa, LHSV of 1 h^{-1}, and H_2/oil ratio of 1,000 N(cm^3/cm^3)

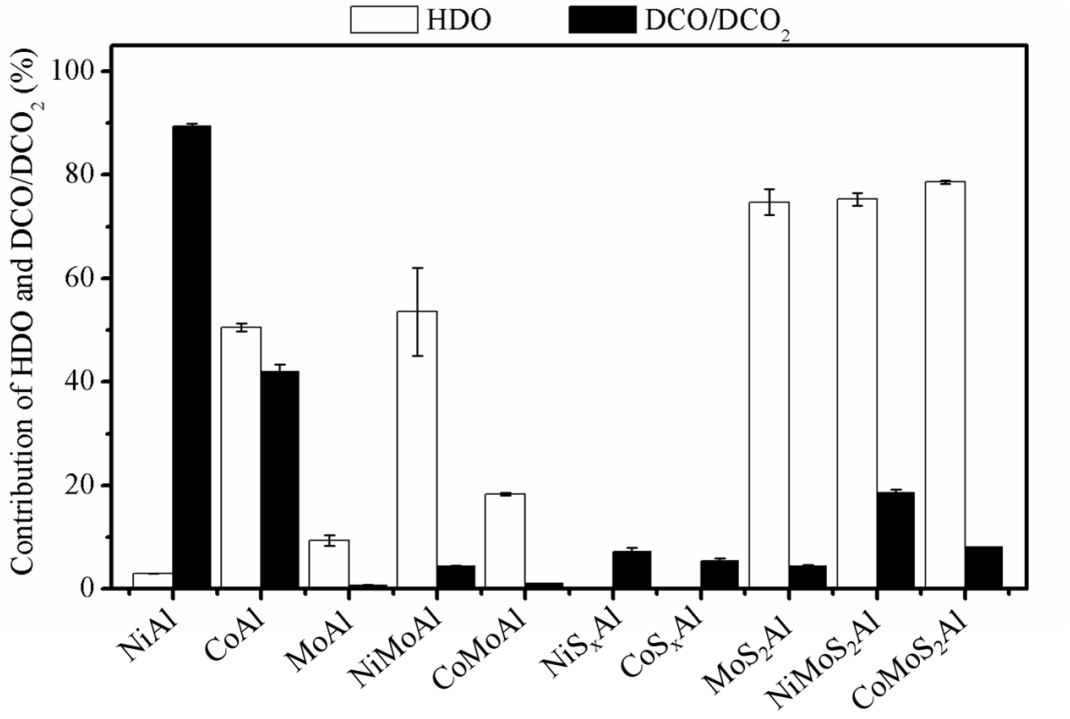

Figure 31 Effect of the metal and metal sulfide catalysts on % contribution of HDO and DCO/DCO_2. All experiments were performed at a temperature of 300 ^oC, H_2 pressure of 5 MPa, LHSV of 1 h^{-1}, and H_2/oil ratio of 1,000 N(cm^3/cm^3).

Effect of metal and metal sulfide catalyst on the gas product compositions are demonstrated in Figure 32. When the Ni and Co catalysts were used, CH_4 was a major gas composition (≈20 mole% for Ni catalyst; ≈10 mole% for Co catalyst) as a result of methanation reaction between CO or CO_2 with H_2 as well as the cracking reaction, implying that the metallic sites of Ni and Co catalysts strongly promoted methanation and cracking reactions. Furthermore, the CO and CO_2 were not detected during palm oil hydrodeoxygenation over Ni and Co catalysts. When the reaction was catalyzed by Ni, the amount of C_3H_8, produced by hydrogenolysis of triglycerides, was lower than that of Co catalyst, suggesting the highly cracking reaction of C_3H_8 to C_2H_6 and CH_4 by C-C cleavage over Ni catalyst. Besides, the formation of the CH_4, C_2H_6, and C_3H_8 species in the gas product could be associated with cracking reaction in liquid phase during the palm oil hydrodeoxygenation. Additionally, the C_3H_8 was produced in the

large amount when the Mo, NiMo, and CoMo catalysts were used. Since the product yield over the Mo, NiMo, and CoMo catalysts was lower than those of Ni and Co catalysts, the large amount of C_3H_8 indicated that the reactions was mainly taken place only the hydrogenolysis of triglycide to free fatty acid. When the MoS_2, $NiMoS_2$, and $CoMoS_2$ catalysts were used.C_3H_8, CO and CO_2 were the main gas product composition. By comparison amount of CO and CO_2, the results showed that $NiMoS_2$ and $CoMoS_2$ produced the large amount of CO and CO_2 than the unpromoted MoS_2 catalysts, indicating the adding Ni and Co strongly enhanced the DCO and DCO_2 reactions. Likewise, the NiS_x and CoS_x, exhibitng the lowest product yield, produced the CO as the a major gas product composition, suggesting that the reaction was proceed through the DCO route.

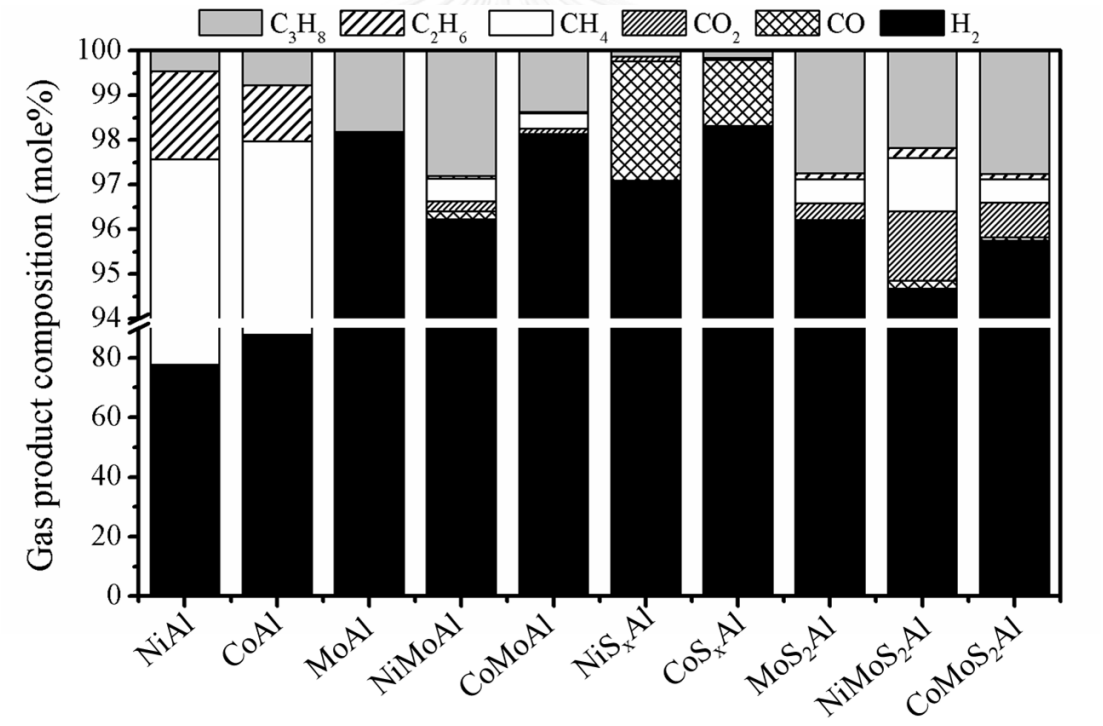

Figure 32 Effect of the metal and metal sulfide catalysts on gas product composition. All experiments were performed at a temperature of 300 ^oC, H_2 pressure of 5 MPa, LHSV of 1 h^{-1}, and H_2/oil ratio of 1,000 N(cm^3/cm^3).

5.3.3 Catalysts stability evolution

Based on the result obtained from previous section, the Ni, Co, $NiMoS_2$, $CoMoS_2$ catalysts exhibited the highest activity for the deoxygenation of palm oil to hydrocarbons. Consequently, the stability study for the deoxygenation of palm oil was investigated over these catalysts. The long-term reaction tests were performed for 150 h on-stream to study the changes in the activity performance and selectivity of metal and metal sulfide catalysts in palm oil hydrodeoxygenation (Figure 33). The reaction conditions were as follows, reaction temperature = 300 ^{o}C, H_2 pressure = 5 MPa, H_2/oil ratio = 1000 N(cm^3/cm^3), and LHSV = 1 h^{-1}. The triglyceride conversion (not shown) remained steady at ~100% throughout the 150 h reaction time during the palm oil hydrodeoxygenation.

Figure 33a shows the product yield on the catalytic performance of metal and metal sulfide catalysts as the function of reaction time. Over Ni catalyst, the product yield was generally between 85.7 – 94.4 %, with an average of 92.2±2.2%, meanwhile, over Co catalyst, the product yield was also between 83.8 – 93.8%, with an average of 88.6±3.6% at the first 100 h reaction time. Furthermore, the slightly increased product yield was observed at first 24 h reaction time was likely due to the formation of metallic Ni or Co by *in situ* reduction during operating conditions. Over $CoMoS_2$ catalyst, the product yield was mostly between 71.9 – 84.5 %, with an average of 81.7±1.82% at fist 120 h on-stream. Interesting, it could be observed that the product yield over $NiMoS_2$ was stable than the others catalysts throughout the 150 h on-stream, exhibiting the product yield between 90.8 – 94.7%, with an average of 92.6±1.5%.

As demonstrated in Figure 33a, at reaction time > 100 h, the gradually decrease in product yield from 92.2 to 75.6 % was observed over Ni catalyst, whereas, the dramatically drop in product yield from 88.6 % to ca. 56.6% could be noticed over Co catalyst. Additionally, the slightly decline in product yield from 92.2 to 75.6 % was observed over $CoMoS_2$ after 120 h on-stream. These results indicated that the Ni and Co catalysts showed a significant catalyst deactivation after 100 h reaction time, whereas the deactivation characteristic of $CoMoS_2$ catalyst was observed after 120 h on-stream. Although the triglyceride conversion remained constant throughout the

150 h reaction experiment, the changes in liquid product properties were observed at reaction time in the range of 100-150 h over the Ni, Co, and $CoMoS_2$ catalysts. After catalyst deactivation, the liquid product became a solidified at room temperature and comprised of *n*-alkanes, and oxygenated intermediates (i.e., free fatty acids, alcohol, and esters) including small amount of triglycerides. This finding indicated that the catalysts became deactivated and the reaction mainly proceeded through the hydrogenation of C=C bond in unsaturated triglyceride, followed by C-O bond cleavage via hydrogenolysis of saturated triglyceride to produced free fatty acids and propane, indicating incomplete hydrodeoxygenation activity. It should be avoided to operate at these conditions due to the strong adsorption of oxygenated intermediates on catalyst active sites, thus providing that the catalysts underwent rapid deactivation.

As discussed the previous section, the differences in deoxygenation pathways between the molybdenum based sulfide catalysts ($NiMoS_2$, $CoMoS_2$, and MoS_2) and metallic Ni and Co catalysts were distinguished from the difference between the reaction rates of C-C and C-O bond scission. As demonstrated in Figure 33b, the $NiMoS_2$ and $CoMoS_2$ catalysts was higher the C-O cleavage rate based on the higher contribution of HDO. In contrast, the considerably higher contribution of DCO/DCO_2 obtained over the Ni catalysts, indicating the dominant C-C cleavage (Figure 33b). Besides, the contribution of DCO/DCO_2 was nearly comparable to that of the contribution of HDO over Co catalyst, suggesting that the metallic sites of Co catalyst were responsible though both C-C and C-O bond scission (Figures 33b and 33c). Based on the stability test evolutions, the catalytic activity on palm oil hydrodeoxygenation was decreased in order of $NiMoS_2$ > $CoMoS_2$ > Ni > Co catalysts. It seems to be deduced that the catalysts which was highly selective to C-C bond cleavage, rapidly deactivated than the catalysts which was highly selective to C-O bond cleavage. It may be due to that fact that the C-C bond cleavage led to the higher carbon formation rate on the catalysts. As shown in Figures 33b and 33c, It should be noted that the contribution was also observed to change in similar way to that of product yield.

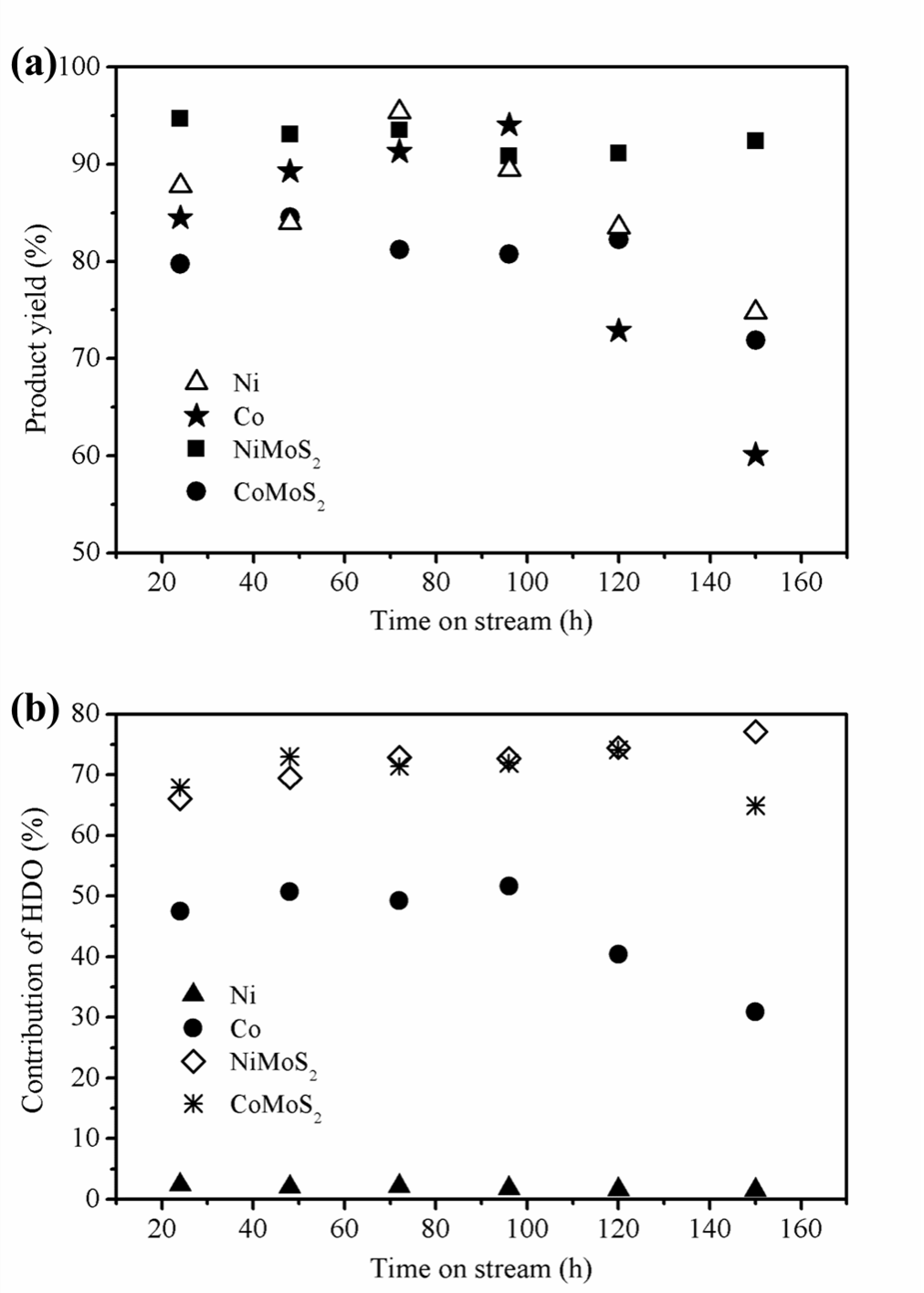
(a)
Product yield (%)
Time on stream (h)
Ni
Co
NiMoS2
CoMoS2
(b)
Contribution of HDO (%)
Time on stream (h)
Ni
Co
NiMoS2
CoMoS2

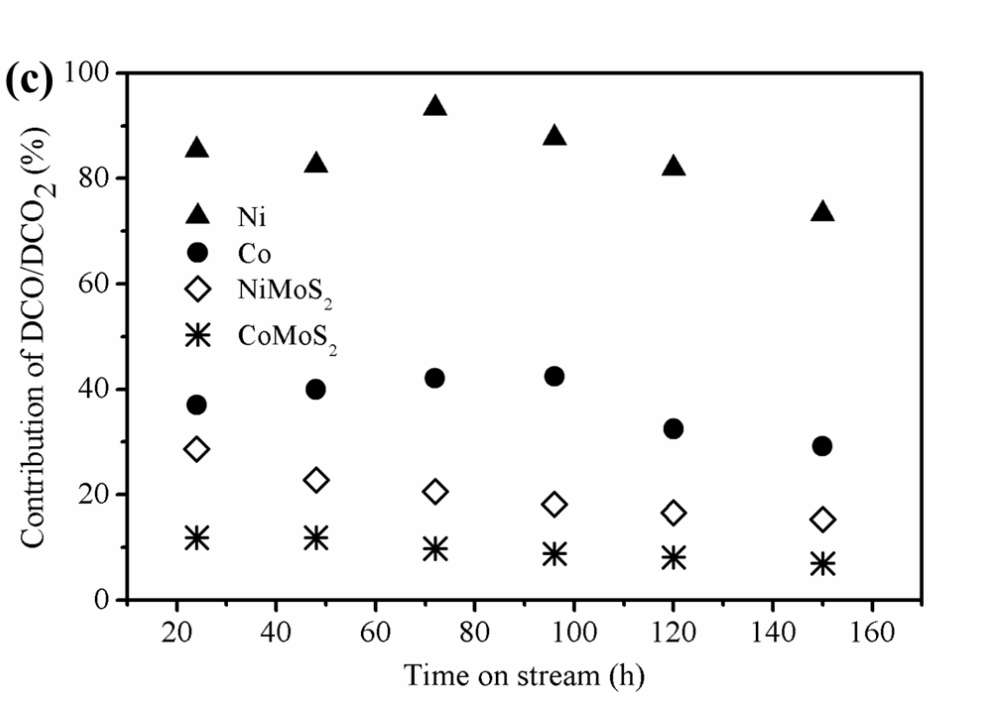

Figure 33 Time on-stream as the function of product yield (a) and contribution of HDO (b) and DCO/DCO_2 (c) with metal and metal sulfide catalysts. All experiments were performed at a temperature of 300 ^{o}C, H_2 pressure of 5 MPa, LHSV of 1 h^{-1}, and H_2/oil ratio of 1,000 N(cm^3/cm^3).

5.3.4 Characterization of deactivated catalysts

To investigate possible changes in catalyst texture, the BET specific surface area, total pore volume, and average pore diameter of bare γ-Al_2O_3, fresh and deactivated catalysts after 150 h on-stream are summarized in Table 21. The surface area of bare γ-Al_2O_3 was 201.1 m^2/g with total pore volume of 0.55 cm^3/g. The BET surface area and pore volume typically decreased approximately 10-20 % after metal loading. The decrease of specific surface area and total pore volume of the catalysts would be due to the metal converging on γ-Al_2O_3 support and blockage of pores by metal species. A significant decrease in BET surface area, pore volume, and pore diameter was observed for all catalysts after 150 h on-stream. It should be noted that the changes in physical structural properties of the deactivated catalyst were possibly caused by coke deposits on the pore channels and/or external surface of catalysts, thus leading to pore blocking. Besides, the pore blocking could be resulted in catalysts deactivation due to limiting the reactants or intermediates diffusion and the products dispersion from the catalysts active sites [75, 93].

Table 21 Physicochemical properties of the fresh and spent catalysts

Catalyst	BET surface area[a] (m^2/g)	Total pore volume[b] (cm^3/g)	Pore diameter (BJH)[c] (nm)	CO uptake[d] (umol/g)
γ-Al_2O_3	201.1	0.55	7.53	-
Fresh Ni/γ-Al_2O_3	178.1	0.45	7.52	26.5
Deactivated Ni/γ-Al_2O_3	105.1	0.24	5.44	18.7
Fresh Co/γ-Al_2O_3	181.2	0.47	7.51	9.4
Deactivated Co/γ-Al_2O_3	100.8	0.24	5.44	0
Fresh $NiMoS_2$/γ-Al_2O_3	158.1	0.34	6.33	60
Deactivated $NiMoS_2$/γ-Al_2O_3	98.7	0.25	5.43	19
Fresh $CoMoS_2$/γ-Al_2O_3	165.0	0.35	6.34	37
Deactivated $CoMoS_2$/γ-Al_2O_3	64.2	0.15	3.69	16.3

[a] BET surface area calculated from the adsorption branch of N_2 isotherm

[b] Total pore volumes calculated from the N_2 adsorption at relative pressure of 0.98

[c] Pore diameter calculated from the desorption branch using the BJH method

[d] CO uptake calculated from CO pulse chemisorption experiment

The amount of carbon deposited on deactivated catalysts was determined by temperature-programmed oxidation. The desorption curves of CO_2 measured by mass spectrometry, shown in Figure 34, indicated that the large amount of CO_2 released from the deactivated catalysts. According to the literatures, the peaks at low temperature around 300 ^{o}C correspond to more reactive amorphous carbon which adsorbed on metallic sites, meanwhile, the oxidation of crystalline or graphitic carbon occurs at temperatures above 500 ^{o}C [4, 49, 94]. The TPO profile of the deactivated Ni and Co catalysts shows a wide peak in the temperature range of 300–640 $^{\circ}$ C. It should be noted that the carbonaceous species deposited during hydrodeoxygenation could be removed above 500 ^{o}C, suggesting that the formed carbon species were both amorphous and graphitic carbons. As summarized in Table 22, the carbon deposited on the deactivated Ni, Co, $NiMoS_2$, and $CoMoS_2$ catalysts were determined as 34.88, 49.51, 10.96, and 19.95 mg/g_{cat}, respectively. It should be confirmed that the Ni and Co catalyst rapidly deactivated than the $NiMoS_2$ and $CoMoS_2$ catalysts due to the higher carbon formation rate on the catalyst surface. It may be due to the fact that that highly C-C bond cleavage led to higher carbon formation rate on catalyst surface. Thus TPO analysis indicated carbon deposited was a main cause of the catalysts deactivation.

CO uptake, which is representing a number of active sites of catalysts, was used to elucidate the losing of catalyst active sites (Table 21**)**. The CO uptake of the $NiMoS_2$ and $CoMoS_2$ catalysts were typically higher than the metallic Ni and Co catalysts. It should be confirmed that the decrease in catalysts active sites after 150 h over four difference catalysts in palm oil hydrodeoxygenation experiment was likely due to the catalyst coking.

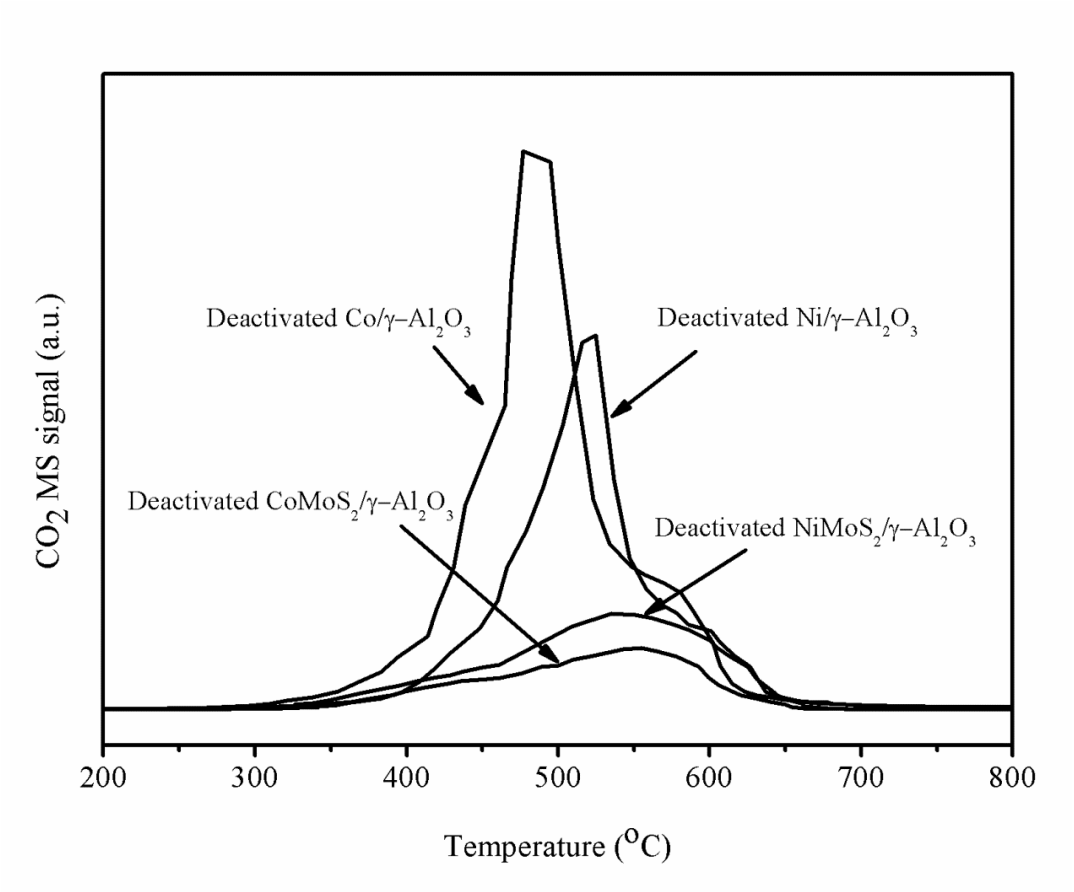

Figure 34 Temperature programmed oxidation profiles of the Ni, Co, $NiMoS_2$, and $CoMoS_2$, catalysts after 150 h on-stream.

Table 22 Total carbon deposits on spent catalysts after 150 h on-stream obtained from temperature-programmed oxidation

Catalysts	Total coke content		
	mg/g_{cat}	$mg/h.g_{cat}$	%C
Deactivated $Ni/\gamma\text{-}Al_2O_3$	34.88	0.23	3.49
Deactivated $Co/\gamma\text{-}Al_2O_3$	49.51	0.33	4.95
Deactivated $NiMoS_2/\gamma\text{-}Al_2O_3$	10.96	0.07	1.10
Deactivated $CoMoS_2/\gamma\text{-}Al_2O_3$	19.95	0.13	1.99

5.4 Deactivation and regeneration behaviors of Ni/γ-Al_2O_3 and Co/γ-Al_2O_3 catalysts during deoxygenation of palm oil

5.4.1 Introduction

The Ni- and Co-promoted molybdenum sulfide catalysts have been typically used in hydrodeoxygenation of triglycerides, fatty acids, and esters [13, 15, 65, 72, 95-97]. The conventional metal sulfide catalysts, less expensive catalysts [35], showed high activity in the deoxygenation of triglycerides and model compounds, nevertheless, sulfur leaching lead to catalyst deactivation and sulfur contamination in liquid product [31, 36, 37, 41]. It should be noted that metal sulfide catalysts require adding the sulfinding agents e.g. CS_2 and DMDS in liquid feed to avoid catalyst deactivation during deoxygenation reactions [22, 38]. Furthermore, the trace amount of water, produced from DCO and HDO reactions, would hasten the sulfur leaching and rigorously shorten the lifetime of catalysts [39].

To develop the next generation hydrodeoxygenation catalysts, metal catalysts or sulfur-free catalysts in reduced state such as Ni [12, 22, 30, 43, 65], Co [22, 31], Pd [5, 6, 32, 66], Pt [14], and Ru [33, 34] have interested great attention in deoxygenation reactions. Some metal catalysts such as Ni, Pd, and Pt are favorable in DCO and DCO_2 pathways. Since the hydrogen consumption for deoxygenation of triglycerides/fatty acids/esters decreased in order to HDO > DCO > DCO_2 routes, thus DCO and DCO_2 routes may be more theoretically economical than HDO route [36, 41]. The noble metal catalysts imply an extremely high cost in green diesel production, thus limiting in the large-scale applications [12, 22]. Accordingly the transition metal catalysts such as Ni and Co, which also display a good catalytic activity, have been employed as a great catalyst in deoxygenation process. However, only few studies have been reported on the deoxygenation of triglycerides. Peng *et al.* [41] investigated the catalytic deoxygenation of crude microalgae oil with Ni/ZrO_2 catalyst in a trickle bed reactor at 270 ^oC and 4 MPa. A 70 wt.% yield of *n*-heptadecane was obtained and the catalyst did not significant deactivate after 72 h-on stream. Kim *et al.* [8] reported the effect of temperature and pressure on the

hydrotreating of soybean oil over Ni/SiO_2-Al_2O_3 catalyst in a batch and continuous flow reactors in the range of 300-440 ^oC and 2.5 – 15 MPa. Stusentschnig and co-workers [98] hydrotreated the crude palm oil with the commercial Raney nickel catalyst at 360 ^oC and 9 MPa in a batch mode. After 5 h reaction time, 100% conversion with alkanes yield, mainly *n*-heptadecane and *n*-octadecane, between 54 and 60% was achieved. Nevertheless, to the best of our knowledge, the deactivation and regeneration in the hydrodeoxygenation reaction over metal catalysts has certainly not been reported in literature. Consequently, the understanding of deactivation and regeneration processes is important for improving and optimizing the process conditions.

In the present work, the deactivation behavior of Ni/γ-Al_2O_3 and Co/γ-Al_2O_3 catalysts in palm oil hydrodeoxygenation was studied in a continuous-flow trickle bed reactor at 300 ^oC and 5 MPa over a reaction time of 150 h. Their catalytic performances were evaluated according to the triglyceride conversion, product yield, and the contribution of HDO (hydrodeoxygenation) and DCO_x (decarbonylation and/or decarboxylation), which were estimated based on mole balance corresponding to fatty acid in oil feed. The calcined, pre-reduced, deactivated and regenerated catalysts were characterized to clarify the origin of deactivation and regeneration characteristics using a combination of techniques: temperature programmed reduction (TPR), N_2 sorption, CO pulse chemisorption, X-ray diffraction (XRD), X-ray absorption near edge structure (XANES), transmission electron microscopy (TEM) and temperature programmed oxidation (TPO). Furthermore, the regenerability of the deactivated catalysts after the long-term tests was also reported.

5.4.2 Deactivation behaviors

The long-term reaction tests were performed for 150 h on-stream to examine the changes in the activity performance and selectivity of Ni/γ-Al_2O_3 and Co/γ-Al_2O_3 catalysts in palm oil hydrodeoxygenation. The reaction conditions were as follows; reaction temperature = 300 ^oC, H_2 pressure = 5 MPa, H_2/oil ratio = 1000 N(cm^3/cm^3), and LHSV = 1 h^{-1}. Figure 35 shows triglyceride conversion and product yield on the catalytic performance of Ni/γ-Al_2O_3 and Co/γ-Al_2O_3 catalysts as the function of

reaction time. It should be noted that the hydrodeoxygenation reaction over pure γ-Al_2O_3 resulted in 56% conversion of triglyceride without liquid alkane product yield. The results suggested that only saturated triglyceride scission to free fatty acids and propane occurred. Therefore, γ-Al_2O_3 played no catalytic roles in hydrodeoxygenation of triglycerides. Interestingly, the product yield was achieved when the reaction was catalyzed by the metallic species, confirming hydrodeoxygenation activity of the metallic sites of Ni or Co species. The triglyceride conversion, shown in Figures 35a and 35b, remained steady at ~100% throughout the 150 h reaction time during the test. Over Ni catalyst, the product yield was generally between 85.7 – 94.4 %, with an average of 92.2±2.2%. Meanwhile, over Co catalyst, the product yield was also between 83.8 – 93.8%, with an average of 88.6±3.6% at the first 100 h reaction time. Furthermore, the slight increase of product yield observed at first 24-h reaction time was likely due to the formation of metallic Ni or Co by *in situ* reduction during working conditions. As demonstrated in Figure 35, at reaction time > 100 h, the decrease in product yield from 92.2 to 75.6 % was observed over Ni catalyst (Figure 35a), whereas, the dramatic drop in product yield from 88.6 % to ca. 56.6% could be noticed over Co catalyst (Figure 35b). These results indicated that the Ni and Co catalysts showed a significant catalyst deactivation over 100 h reaction time. It should be noted that the catalytic activity on palm oil hydrodeoxygenation over Ni catalyst seems to be greater than Co catalyst. Although the triglyceride conversion remained constant throughout the 150 h reaction experiment, the changes in liquid product properties were observed at reaction time in the range of 100-150 h. The liquid product became a solidified at room temperature and comprised of *n*-alkanes, and oxygenated intermediates (i.e., free fatty acids, alcohol, and esters) including small amount of triglycerides. This finding indicated that the Ni and Co metallic sites became deactivated and the reaction mainly proceeded through the hydrogenation of C=C bond in unsaturated triglyceride, followed by C-O bond cleavage via hydrogenolysis of saturated triglyceride to produced free fatty acids and propane, indicating incomplete hydrodeoxygenation activity. The actual operation should avoid at these conditions due to the strong adsorption of oxygenated intermediates on catalyst active sites, thus providing that the catalysts underwent rapid deactivation.

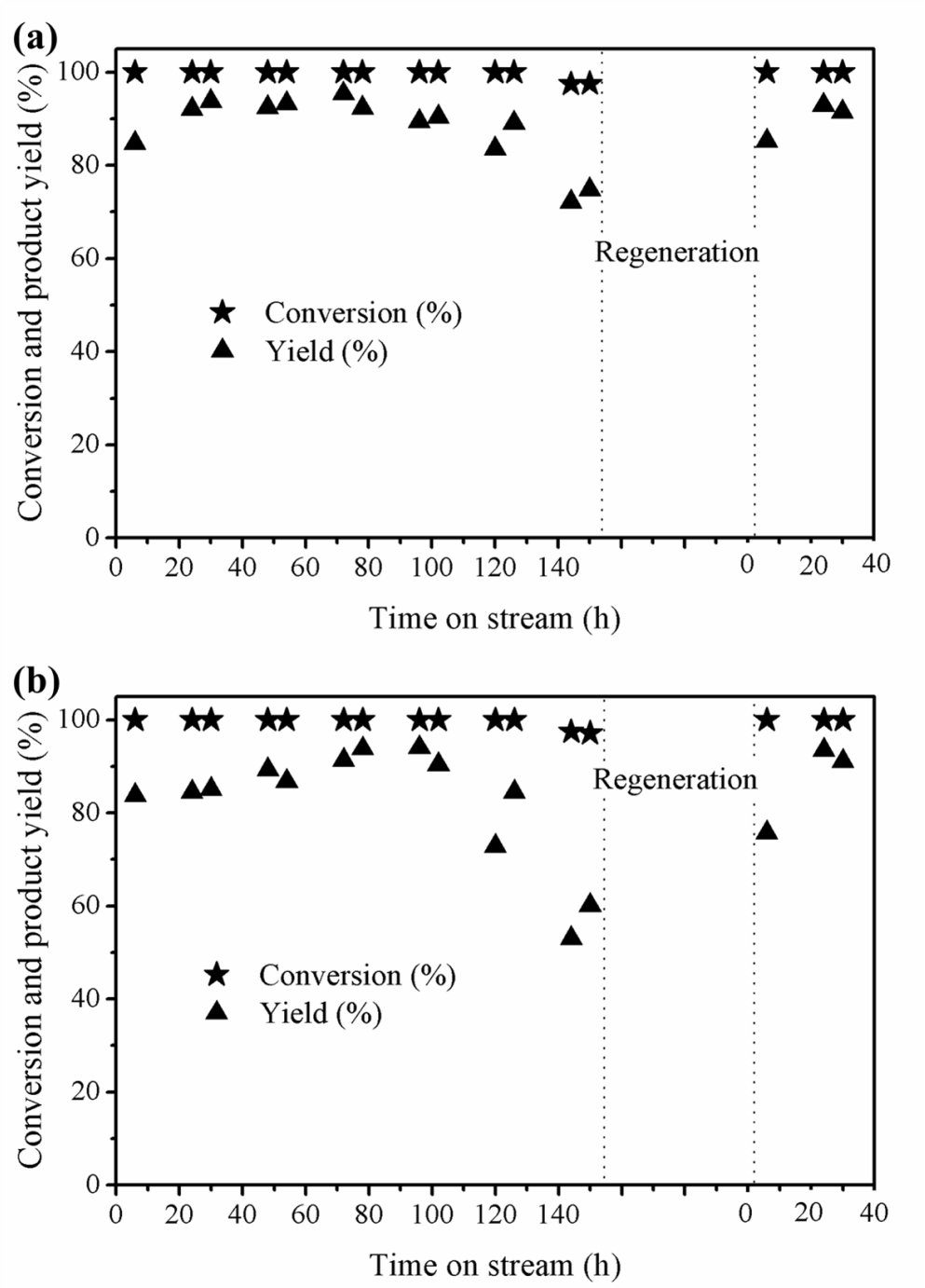

Figure 35 TG conversion and product yield with time on stream during palm oil hydrodeoxygenation on the catalytic performance and regeneration of the (a) Ni/γ-Al_2O_3 and (b) Co/γ-Al_2O_3 catalysts. Reaction conditions: 300 ^oC, 5 MPa, LHSV of 1 h^{-1}, and H_2/oil ratio of 1,000 N(cm^3/cm^3).

When the Ni was used, 100 h reaction time, DCO/DCO_2 (decarbonylation, DCO and/or decarboxylation, DCO_2 pathways) (89.2±2.4%) were a major reaction pathway, whereas, HDO, hydrodeoxygenation, (2.1±0.3%) was a minor reaction pathway (Figure 36a). Interestingly, the dominant contribution over Co catalyst, during-100 h reaction time, was from both DCO/DCO_2 (43.0±3.3%) and HDO (45.8±3.0%) pathways, suggesting that the triglycerides were deoxygenated through DCO, DCO_2, and HDO (Figure 36b). This finding indicated that the metallic sites of Co catalyst were responsible for all three major reaction pathways, whereas, metallic sites of Ni, strongly promoted DCO and/or DCO_2 reactions. The palm oil used in this study was mainly composed of C_{16} and C_{18} fatty acids (>98.4 wt.%). Thus the main composition of liquid product was *n*-alkane of C_{15} and C_{17} due to highly selective DCO and DCO_2 reactions over Ni catalyst (Figure 37a). On the contrary, *n*-C_{15}, *n*-C_{16}, *n*-C_{17}, and *n*-C_{18} were a major product composition when the Co catalysts were used (Figure 37b). Moreover, the small amount of light hydrocarbon compositions (*n*-C_8 to *n*-C_{14}) (results not shown) was observed during the hydrodeoxygenation, suggesting that the cracking reaction proceeded over Ni and Co catalysts by C-C bond cleavage. It should be noted that the contribution and liquid product composition were also observed to change in similar way to that of the product yield.

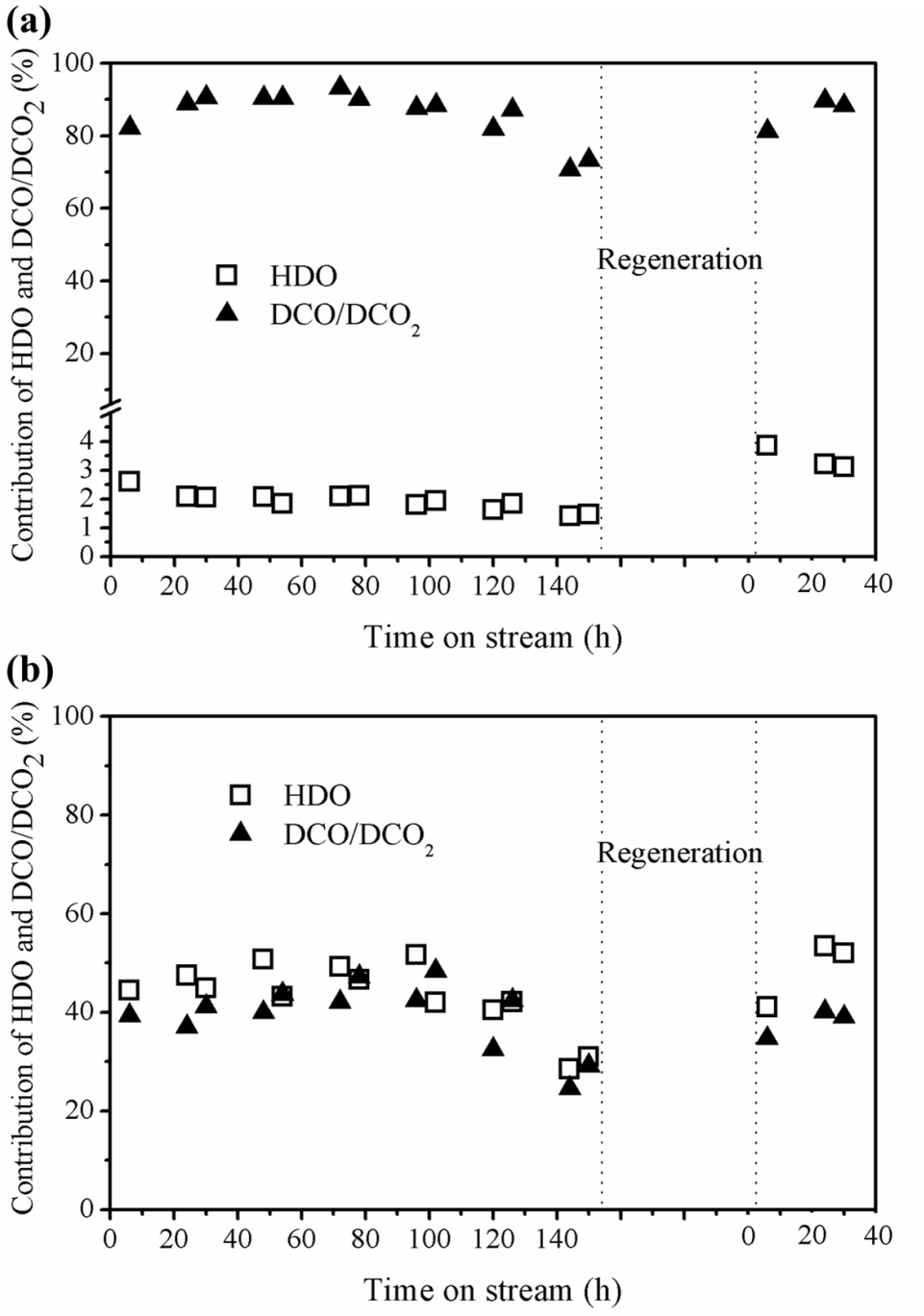

Figure 36 Contribution of HDO and DCO/DCO_2 with time on stream during palm oil hydrodeoxygenation on the catalytic performance and regeneration of the (a) $Ni/\gamma\text{-}Al_2O_3$ and (b) $Co/\gamma\text{-}Al_2O_3$ catalysts. Reaction conditions: 300 ^oC, 5 MPa, LHSV of 1 h^{-1}, and H_2/oil ratio of 1,000 N(cm^3/cm^3).

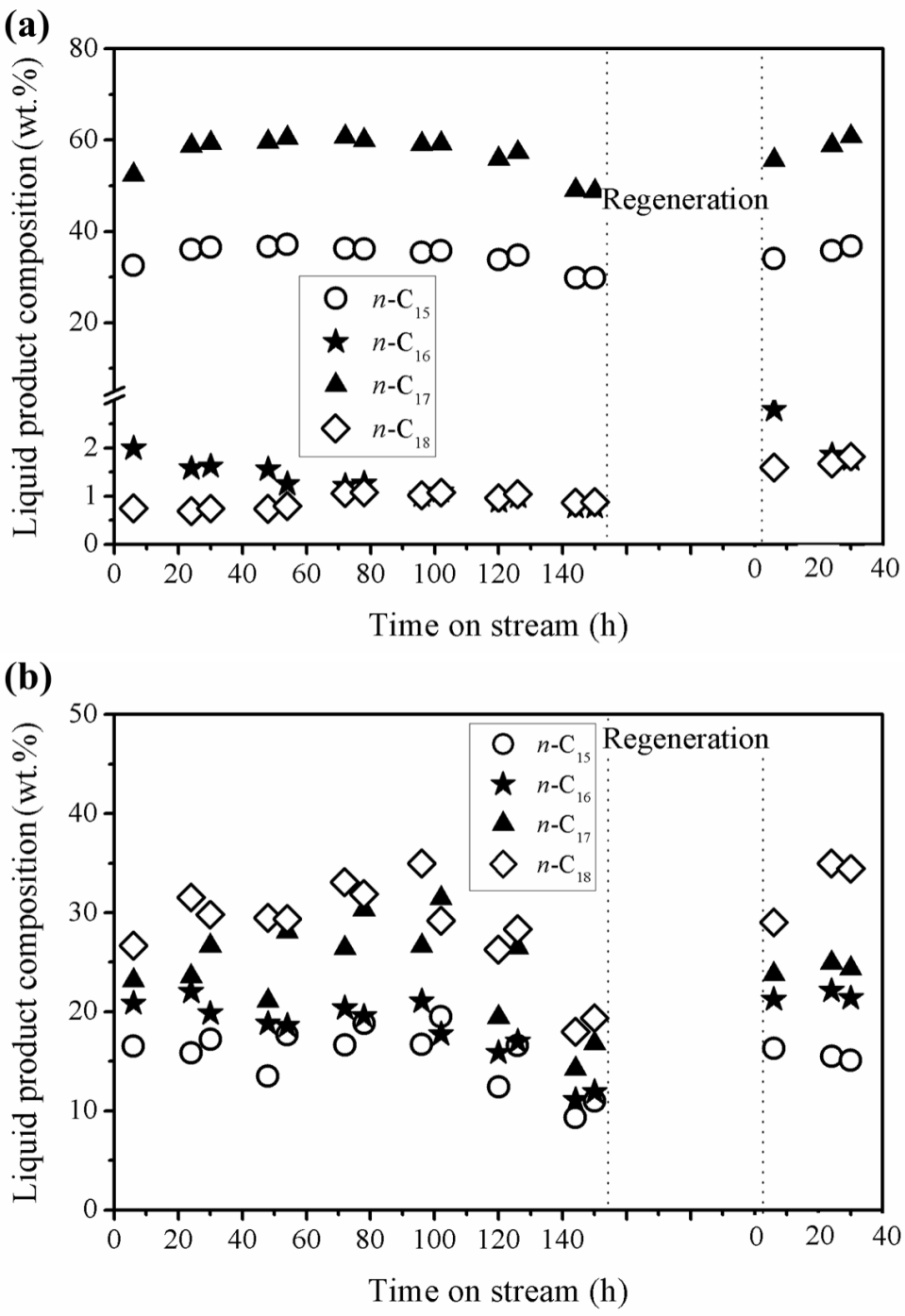

Figure 37 Liquid product composition with time on stream during palm oil hydrodeoxygenation on the catalytic performance and regeneration of the (a) Ni/γ-Al_2O_3 and (b) Co/γ-Al_2O_3 catalysts. Reaction conditions: 300 ^{o}C, 5 MPa, LHSV of 1 h^{-1}, and H_2/oil ratio of 1,000 N(cm^3/cm^3).

The gas product compositions as the function of reaction time are represented in Figure 38. When the Ni and Co catalysts were used, CH_4 was a major gas composition (≈20 mole% for Ni catalyst; ≈10 mole% for Co catalyst) as a result of methanation reaction between CO or CO_2 with H_2 as well as the cracking reaction, implying the metallic sites of Ni and Co catalysts strongly promoted methanation and cracking reactions. The CO and CO_2 were not detected during the hydrodeoxygenation. When the reaction was catalyzed by Ni, the amount of C_3H_8 (< 1 mole%), produced by hydrogenolysis of triglycerides, was lower than that of Co catalyst, suggesting the highly cracking reaction of C_3H_8 to C_2H_6 and CH_4 by C-C cleavage over Ni catalyst. Furthermore, the formation of the CH_4, C_2H_6, and C_3H_8 species in the gas product could be associated with cracking reaction in liquid phase. As can be seen in Figure 38a and 38b, the activity in the gas phase reactions (mainly methanation and cracking reactions) was not strongly be affected as the function of time on stream over Ni catalyst, nevertheless, the composition of gas product mainly CH_4, C_2H_6, and C_3H_8, slightly decreased after 80 h reaction time over Co catalyst. It should be deduced that the decay of the metallic sites of Ni catalyst showed minder effect on the gas phase reactions.

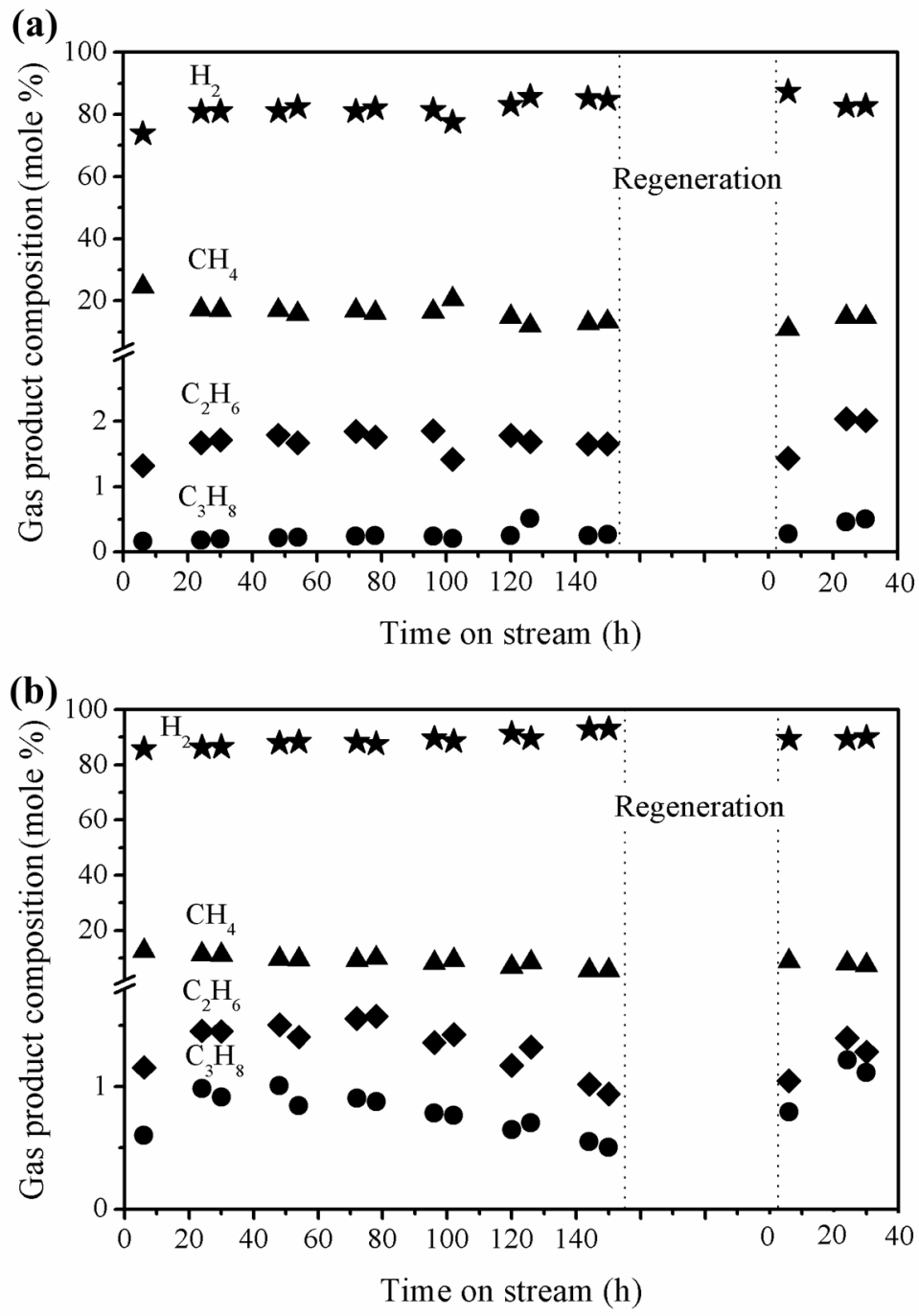

Figure 38 Gas product composition with time on stream during palm oil hydrodeoxygenation on the catalytic performance and regeneration of the (a) Ni/γ-Al_2O_3 and (b) Co/γ-Al_2O_3 catalysts. Reaction conditions: 300 ^oC, 5 MPa, LHSV of 1 h^{-1}, and H_2/oil ratio of 1,000 N(cm^3/cm^3).

5.4.3 Catalyst characterizations

In order to understand the deactivation and regeneration behaviors as well as a reason of activity decline of the Ni/γ-Al2O3 and Co/γ-Al2O3 catalysts used the hydrodeoxygenation, calcined, pre-reduced, deactivated and regenerated catalysts were characterized by temperature programmed reduction, N2 sorption, CO pulse chemisorption, X-ray diffraction, X-ray absorption near edge structure, transmission electron microscopy, and temperature programmed oxidation.

5.4.3.1 Temperature programmed reduction

The H_2-TPR experiments were conducted to investigate the reducibility of Ni/γ-Al_2O_3 and Co/γ-Al_2O_3 catalysts, as well as, to study the interaction between metal species and γ-Al_2O_3 support in the catalysts (Figure 39**)**. Firstly, the reduction peak of both pure NiO and Co_3O_4 catalysts revealed a broad peak around 450 ^oC, indicating the nature of reduction behavior of the pure metal oxide. The reduction profile of Ni/γ-Al_2O_3 showed a broad peak composed of three contributions (~670, ~760, and ~880 ^oC), representing the presence of different nickel species. The peak at 670 ^oC was attributed to reduction of bulk NiO species to Ni^0, occupying a weak interaction with the support. The second peak at 760 ^oC also represented NiO species, which have stronger metal and support interactions or smaller particles located inside the pore. Besides, the reduction peak at the high temperature of 880 ^oC could be assigned to stronger Ni and γ-Al_2O_3 interactions or nickel aluminate phases with spinel structure ($NiAl_2O_4$) [12, 30, 84]. On the other hand, the TPR profile of Co/γ-Al_2O_3 showed a broad curve from 430 to 800 ^oC with three different peaks at ~520, ~625, and ~750 ^oC. The transformation of Co_3O_4 to Co^0 occurred in two steps; the first peak, at 430–550 ^oC, was ascribed to the reduction of Co_3O_4 to CoO, and second one, at 550–680 ^oC, to the subsequent reduction of CoO to Co^0. Additionally, the peak at higher temperature (750 ^oC) may be assigned to the existence of Co species with smaller crystallite sizes or stronger metal-support interactions [22, 85]. Note that a

high reduction temperature for catalyst activation should be avoided due to the formation of large metal particle size and/or the transformation of γ-Al_2O_3 to other Al_2O_3 phases, thus providing the low activity and stability toward the reaction of catalysts. Therefore, the Ni and Co catalysts were *in situ* pre-reduced at lower temperature with pure H_2 at 500 ^oC for 3 h before catalytic hydrodeoxygenation testing.

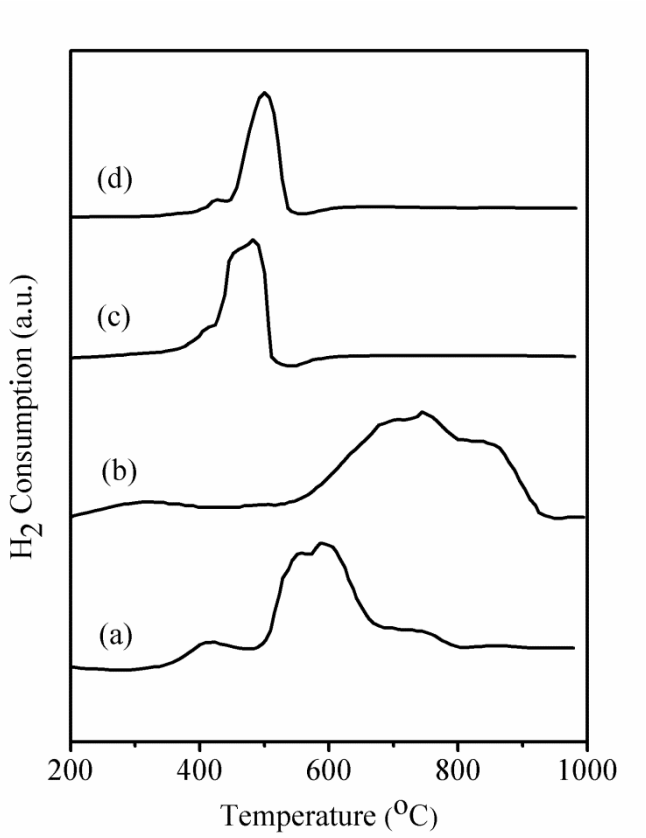

Figure 39 H_2-TPR profiles of the catalysts, (a) Ni/γ-Al_2O_3, (b) Co/γ-Al_2O_3, (c) NiO, (d) Co_3O_4.

5.4.3.2 N_2 sorption and CO pulse chemisorption data

To investigate possible changes in catalyst texture, the BET specific surface area, total pore volume, and average pore diameter of bare γ-Al_2O_3, pre-reduced, deactivated, and regenerated catalysts are summarized in Table 23. The surface area of bare γ-Al_2O_3 was 201.1 m^2/g with total pore volume of 0.55 cm^3/g. The BET surface area and pore volume typically decreased by 10 % after metal loading. The decrease of specific surface area and total pore volume of the catalysts would be due to the metal converging on γ-Al_2O_3 support and blockage of pores by metal species. Interestingly, the observed pore sizes of all catalysts were approximately 7.5 nm, and did not change significantly after metal loading in the range studied. N_2 adsorption–desorption isotherms (results not shown) of γ-Al_2O_3 and the catalysts exhibited type-IV isotherms, indicating the typical characteristic of mesoporous structure. As can be seen in Table 23, the BET surface area of pre-reduced Ni/γ-Al_2O_3 did not significantly different when compared with the calcined catalysts, whereas, the surface area of pre-reduced Co/γ-Al_2O_3 catalysts was somewhat less than that of calcined catalysts. This may be due to sintering of cobalt particles during H_2 reduction at 500 ^oC. A significant decrease in BET surface area, pore volume, and pore diameter was observed from both deactivated Ni/γ-Al_2O_3 and Co/γ-Al_2O_3 catalysts after 150 h on-stream. It should be noted that the changes in physical structural properties of the deactivated catalyst were possibly caused by carbonnaceous deposits on the pore channels and/or external surface of catalysts, thus leading to pore blocking. Besides, the pore blocking could be resulted in catalysts deactivation due to limiting the reactants or intermediates diffusion and the products dispersion from the catalysts active sites [75, 93]. However, the texture properties of the catalysts after regeneration by calcining in air at 500 ^oC for 5 h were similar to the pre-reduced catalysts, indicating that the carbon deposited on the catalyst was completely removed and the pore structure did not change under the hydrodeoxygenation experiments.

CO uptake, which is representing a number of active sites of catalysts, was used to elucidate the loss of catalyst active sites (Table 23**)**. The CO uptake of Ni/γ-Al_2O_3 was typically higher than that of Co/γ-Al_2O_3. It should be confirmed that the decrease in catalysts active sites after 150 h experiment was likely due to the coking or catalyst sintering. Furthermore, the increase in the CO uptake after regeneration may be due to the redispersion of Ni and Co species during carbon burning.

Table 23 Physicochemical properties of the calcined, pre-reduced, deactivated, and regenerated catalysts

Catalyst	Metal content[a] (wt.%)	S_{BET}[b] (m^2/g)	Total pore volume[c] (cm^3/g)	Pore diameter (BJH)[d] (nm)	CO uptake (umol/g)
γ-Al_2O_3	-	201.1	0.549	7.53	-
Calcined Ni/γ-Al_2O_3	9.42	178.1	0.454	7.51	-
Pre-reduced Ni/γ-Al_2O_3	-	177.2	0.497	7.51	26.5
Deactivated Ni/γ-Al_2O_3	-	105.1	0.236	5.44	18.7
Regenerated Ni/γ-Al_2O_3	-	178.6	0.519	7.51	32.5
Calcined Co/γ-Al_2O_3	9.05	181.2	0.470	7.51	-
Pre-reduced Co/γ-Al_2O_3	-	172.7	0.469	7.51	9.4
Deactivated Co/γ-Al_2O_3	-	100.8	0.239	5.44	0
Regenerated Co/γ-Al_2O_3	-	171.8	0.502	7.51	12.6

[a] Metal content determined by ICP-OES

[b] BET surface area calculated from the adsorption branch of N_2 isotherm

[c] Total pore volumes calculated from the N_2 adsorption at relative pressure of 0.98

[d] Pore diameter calculated from the desorption branch using the BJH method

5.4.3.3 X-ray diffraction and X-ray absorption near edge structure

The phase identity and crystallinity of the calcined, pre-reduced, deactivated, and regenerated catalysts were revealed through XRD patterns (Figures 40 and 41). Three peaks at 2θ=37.5°, 46° and 67° assigned to the γ-Al_2O_3 phase with low crystallinity were observed for all catalysts [82]. The calcined Ni/γ-Al_2O_3 catalyst (Figure 40, pattern a**)** exhibited three diffraction peaks at 2θ=37.4°, 44°, and 63° which correspond to NiO (111), NiO (200), and NiO (220), respectively, which approximately disappeared after pre-reduction in pure H_2 at 500 ^oC (Figure 40, pattern b) [36]. The diffraction peak of metallic Ni at 2θ=44.6°, 52.2°, and 76.5° could be attributed to the reflection of (111), (200), and (220) planes, respectively [99]. As represented in Figure 41, pattern a, the diffraction peaks at 2θ=31.3°, 37.7°, 59.5° and 65.4°, which were seen in calcined Co/γ-Al_2O_3 catalysts, were assigned to those of spinel Co_3O_4, meanwhile, the pre-reduced catalyst (Figure 41, pattern b) exhibited diffraction peak for CoO at 2θ=37.2° and metallic Co at 2θ=44.2° and 52.3° [29]. The XRD patterns of the catalysts after the hydrodeoxygenation reaction, shown in Figures 40, pattern c and 41, pattern c, revealed the increase in the intensity of the diffraction peak of metallic Ni and Co peaks, indicating that the crystalline size of the Ni and Co crystallites slightly increased according to the data summarized in Table 26. Since the phenomena implied that metallic Ni and Co particles start to aggregate during the 150 h hydrodeoxygenation reaction experiment. Additionally, the XRD patterns of regenerated Ni and Co by calcining in air at 500 ^oC for 5 h (Figures 40, pattern d and 41, pattern d) illustrated that the regenerated catalysts exhibit crystalline structures of NiO and Co_3O_4 for regenerated Ni and Co catalysts, respectively. Generally, in the hydrodeoxygenation reaction, water content of 10-15 wt.% was found in the liquid product. The transformation of γ-Al_2O_3 into γ-AlOOH in presence of water under hydrothermal conditions has been reported by some researchers [10, 52]. As demonstrated in the XRD patterns of catalysts after reaction, the transformation of γ-Al_2O_3 to γ-AlOOH did not occurred over 150 h on-stream. The γ-Al_2O_3 has been stabilized in presence of palm oil, alkanes, oxygenated intermediates, and water products under working conditions.

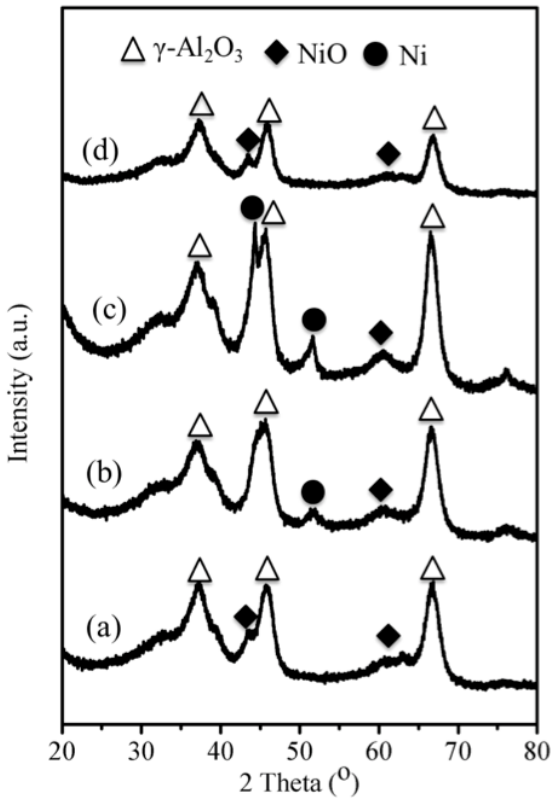

Figure 40 X-ray diffraction patterns of the (a) calcined, (b) pre-reduced, (c) deactivated, (d) regenerated of the Ni/γ-Al_2O_3 catalyst.

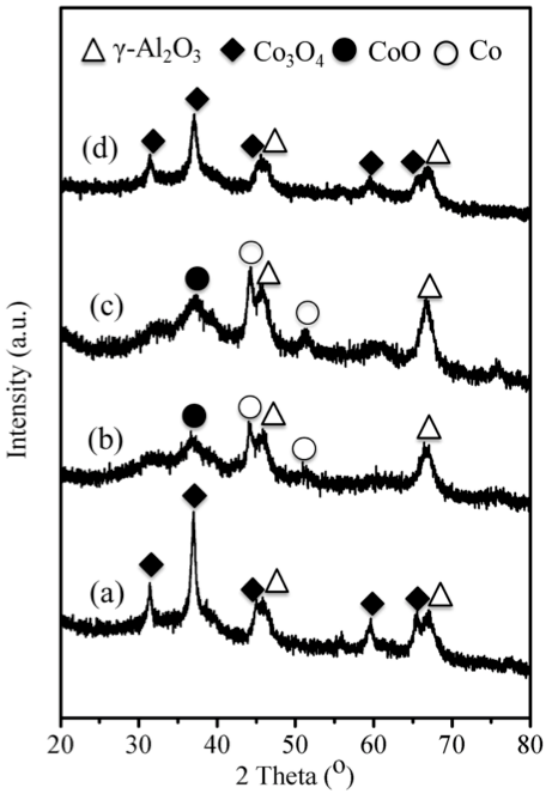

Figure 41 X-ray diffraction patterns of the (a) calcined, (b) pre-reduced, (c) deactivated, (d) regenerated of the Co/γ-Al_2O_3 catalyst.

The fist-row transition metal elements revealed well-defined site symmetry spectra in the X-ray absorption near edge structure (XANES) characteristics [78, 100]. Normalized Ni and Co K-edge XANES spectra of the calcined, pre-reduced, and deactivated Ni/γ-Al_2O_3 and Co/γ-Al_2O_3 catalysts are displayed in Figures 41 and 42, respectively. The standard edge energy was calibrated at the first inflection point in the metal foil calibration spectrum (8333.0 eV for Ni, 7709.0 eV for Co) as reported in the literatures [100, 101]. The intensity of pre-edge peak and white line was used to consider the main features, reflecting the oxidation state of the Ni and Co catalysts on γ-Al_2O_3 support. Firstly, the shape and features of the calcined Ni (Figure 41) and Co (Figure 42) catalysts were similar to the spectra of NiO and Co_3O_4 spinel, respectively, indicating that the samples were in the form of NiO and Co_3O_4 on the γ-Al_2O_3 support which was consistentwith the XRD patterns. In the case of Ni catalysts, shown in Figure 41, after pre-reduced and tested in the hydrodeoxygenation, the edge

energy of the pre-reduced and deactivated Ni catalysts shifted to that of Ni foil and the intensity of white line decreased, whereas, the pre-edge increased. This suggested that the NiO on γ-Al_2O_3 species were not completely reduced while oxides of Ni partially existed. In the case of Co catalysts (Figure 42), it is clear that the XANES data is easy to distinguish between metallic Co, CoO, and Co_3O_4 phases. After pre-reduced, the edge energy of the pre-reduced Co catalyst shifted to that of CoO, whereas, the intensity of white line decreased and the pre-edge increased when the CoO species transformed to Co metallic species were observed in the spent The transformation of Co_3O_4 to Co^0 occurred in two steps; the first step, the transition of Co_3O_4 to CoO, and second one, the reduction of CoO to Co^0, consistent with what was observed in the TPR experiments.

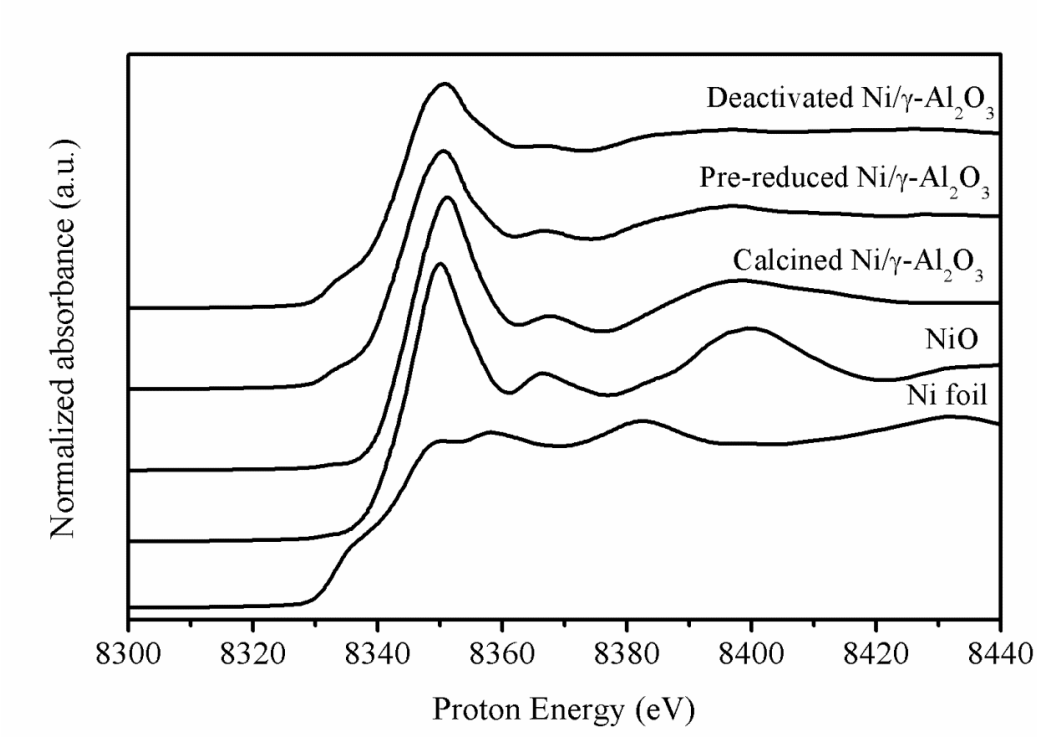

Figure 42 Normalized Ni K-edge XANES spectra of the calcined, pre-reduced, and deactivated Ni catalysts and the reference standards.

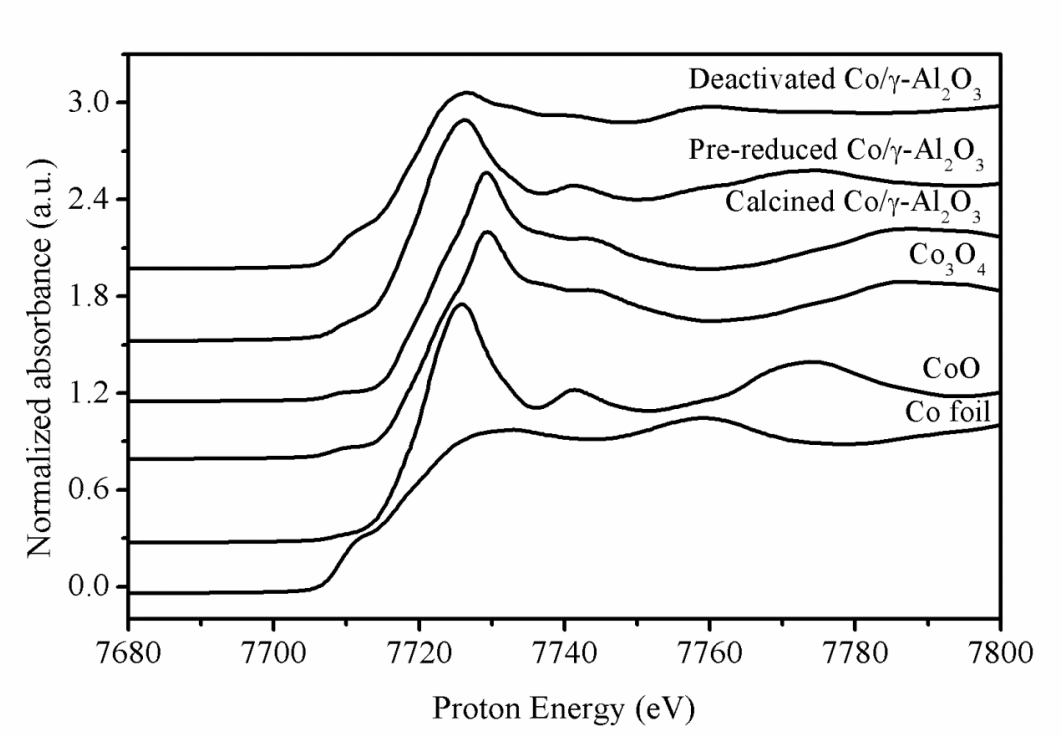

Figure 43 Normalized Ni K-edge XANES spectra of the calcined, pre-reduced, and deactivated Ni catalysts and the reference standards.

To quantify the amount of Ni and Co species in the pre-reduced, calcined and deactivated catalysts, a linear combination fit (LCF) of the XANES spectra was applied and performed using XANES data of standard materials (NiO and Ni foil for Ni; Co_3O_4, CoO, and Co foil for Co) as possible compositions. This procedure yielded the percentage of the catalyst species on the γ-Al_2O_3 support. The weight percentages are summarized in Table 24 and Table 25 for Ni and Co species, respectively. The statistical goodness-of-fit parameter with R-factor (coefficient of determination) shows that the fit is reasonably good. The LCF confirmed that the NiO and Co_3O_4 species are dominant metal phases in the calcined Ni/γ-Al_2O_3 and Co/γ-Al_2O_3 catalysts, respectively. After pre-reduced, the some NiO species were transformed to metallic Ni, whereas, the Co_3O_4 species were first transformed to CoO and further to metallic Co. It is evident form XANES data that the nickel oxide and cobalt oxide were not completely reduced to the metallic form at 500 ^oC for 3 h in presence of pure

H_2. Besides, it could be observed that the amount of metallic Ni and Co increased with increasing in the reaction time, indicating that the reduction was further occurred during the hydrotreating process.

Table 24 Results from linear combination fitting of the XANES spectra of the Ni catalysts

Catalyst	R-factor	%Composition	
		Ni	NiO
Calcined Ni/γ-Al_2O_3	0.01605	0.3	99.7
Pre-reduced Ni/γ-Al_2O_3	0.00522	31.7	68.3
Deactivated Ni/γ-Al_2O_3	0.00575	45.5	54.5

Table 25 Results from linear combination fitting of the XANES spectra of the Co catalysts

Catalyst	R-factor	%Composition		
		Co	CoO	Co_3O_4
Calcined Co/γ-Al_2O_3	0.00721	0	4.9	95.1
Pre-reduced Co/γ-Al_2O_3	0.00899	22.7	74.6	2.7
Deactivated Co/γ-Al_2O_3	0.00395	67.7	32.3	0

5.4.3.4 Transmission electron microscopy

To investigate metal particle growth or sintering affected on palm oil hydrodeoxygenation activity, typical TEM images and particle size distribution of pre-reduced, deactivated, and regenerated Ni and Co catalysts are represented in Figures 43 and 44. The TEM images of Ni catalysts (Figure 43) display an uneven metal particle size, whereas, a less clear distinction between metal and alumina was observed in TEM images of the Co catalysts (Figure 44). Nonetheless, most aggregation Co particles could be distinguished due to the darkest contrast. The Co particles were less dispersed on γ-Al_2O_3 support than the Ni particles, and most of Co particles were clustered to large particle. As summarized in Table 26, the average particle size of Ni and Co catalysts after reaction somewhat increased from 10.7 ± 2.3 to 12.7 ± 2.1 nm and from 11.8 ± 3.9 to 12.2 ± 4.9 nm, respectively. This finding indicated that the average metal particle size increased slightly after reaction, suggesting the metal sintering occurred during hydrodeoxygenation reaction. Furthermore, it should be noted that the metal particle sizes of Ni and Co were much larger than the pore size of γ-Al_2O_3, suggesting that most particles would be located outside the pore of alumina. Interestingly, the TEM images of catalysts regenerated at 500 ^oC in air for 5 h, followed by pre-reduction in H_2 at 500 ^oC for 3 h also showed that the metal particles size of Ni and Co was 12.5 ± 2.4 and 10.5 ± 3.5, respectively. It was not significantly change throughout the regeneration under thermal treatment. It should be deduced that the sintering may be not the main reason of catalyst deactivation because the reaction temperature 300 ^oC was significantly lower than the melting point of Ni and Co catalysts. The combination data of XRD and TEM analyses showed the catalyst sintering was a reason of the catalyst deactivation during palm oil hydrodeoxygenation. Note that the average metal particle size was measured from 50-100 particles to ensure a significant population variance.

Furthermore, the reduced, deactivated, and regenerated Ni and Co catalysts were also characterized by FE-SEM. As observed in the Figure 45, the morphology of the catalysts did not obviously changed after the reaction for 150 h under the present hydrodeoxygenation condition and regeneration process.

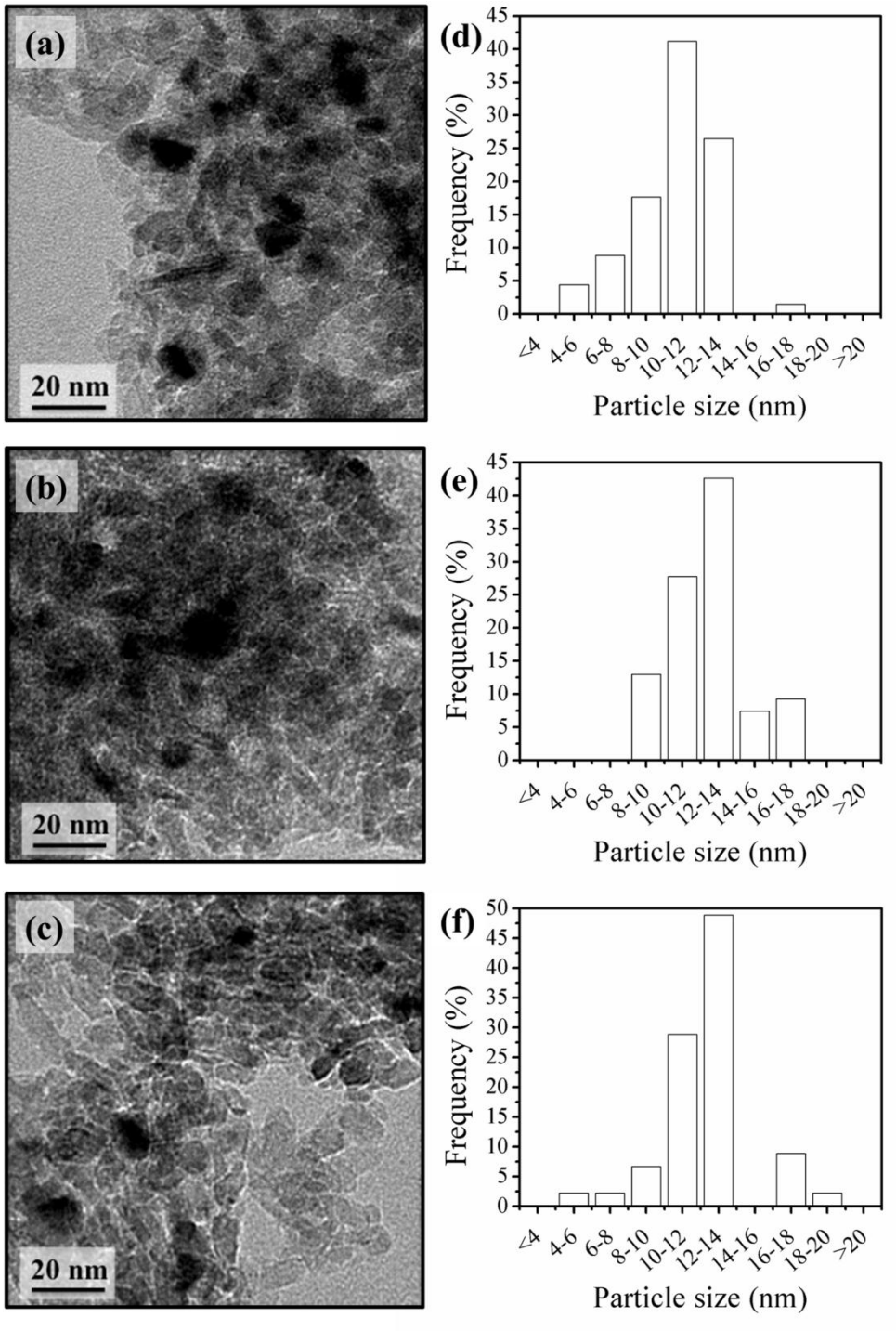

Figure 44 TEM images of the pre-reduced (a), deactivated (b), and regenerated (c) Ni/γ-Al_2O_3 and the particle size distribution of the pre-reduced (d), deactivated (e), and regenerated (f) Ni/γ-Al_2O_3.

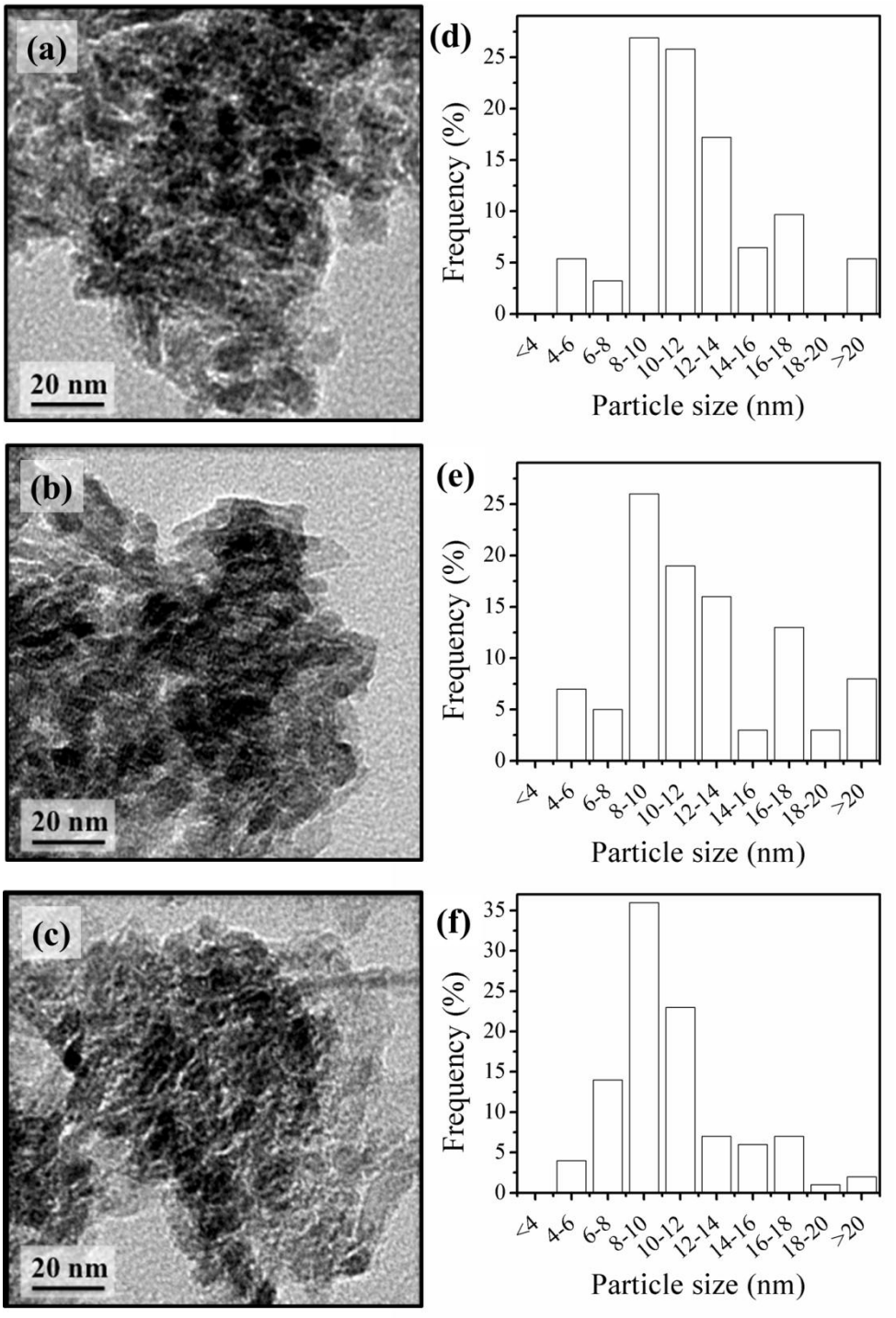

Figure 45 TEM images of the pre-reduced (a), deactivated (b), and regenerated (c) Co/γ-Al_2O_3 and the particle size distribution of the pre-reduced (d), deactivated (e), and regenerated (f) Co/γ-Al_2O_3.

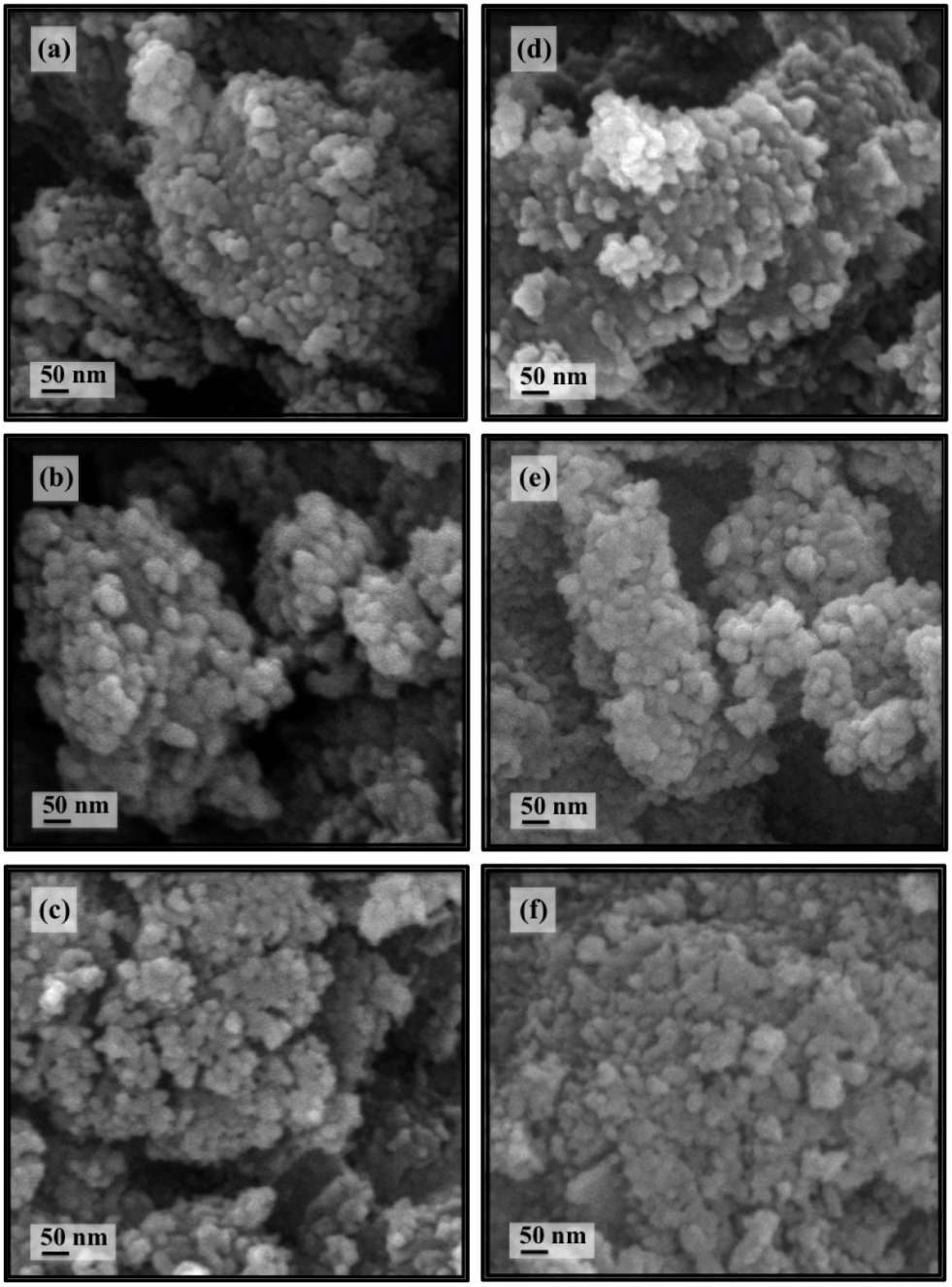

Figure 46 FE-SEM images of the pre-reduced (a), deactivated (b), and regenerated (c) Ni/γ-Al_2O_3 and the pre-reduced (d), deactivated (e), and regenerated (f) Co/γ-Al_2O_3.

Table 26 Crystalline size and metal particle size of the catalysts

Catalyst	Crystalline size[a] (nm)		Average metal particle size[b] (nm)
	Ni	Co	
Pre-reduced Ni/γ-Al_2O_3	7.68	-	10.7 (±2.3)
Deactivated Ni/γ-Al_2O_3	9.44	-	12.7 (±2.1)
Regenerated Ni/γ-Al_2O_3	-	-	12.5 (±2.4)
Pre-reduced Co/γ-Al_2O_3	-	14.56	11.8 (± 4.0)
Deactivated Co/γ-Al_2O_3	-	16.38	12.2 (± 4.9)
Regenerated Co/γ-Al_2O_3	-	-	10.5 (± 3.5)

[a] Calculated by XRD using Scherrer's equation

[b] Determined by TEM

5.4.3.5 Temperature programmed oxidation

The amount of carbon deposited on the deactivated catalysts was determined by temperature-programmed oxidation. The desorption curves of CO_2 measured by mass spectrometry, shown in Figure 44, indicated that the large amount of CO_2 released from the deactivated catalysts. According to the literatures, the peaks at low temperature around 300 ^{o}C correspond to more reactive amorphous carbon which adsorbed on the metallic sites, meanwhile, the oxidation of crystalline or graphitic carbon occurs at temperatures above 500 ^{o}C [4, 49, 94]. The TPO profile of the deactivated Ni and Co catalysts showed a wide peak in the temperature range of 300–640 $^{\circ}$ C, with peak maximum at ca. 540 ^{o}C and ca. 490 ◦C, respectively. The carbonaceous species deposited during hydrodeoxygenation could be removed above 500 ^{o}C, suggesting that the formed carbon species were both amorphous and graphitic carbons. As summarized in Table 27, the carbon content of the deactivated Ni and Co were determined as 34.88 mg/g_{cat} and 49.51 mg/g_{cat}, respectively, whereas, only trace

amounts were detected in regenerated catalysts. It should be confirmed that the Co catalyst deactivated faster than the Ni catalysts due to the higher carbon formation rate on the catalyst surface. Thus TPO analysis indicated carbon deposited was a main cause of the catalysts deactivation.

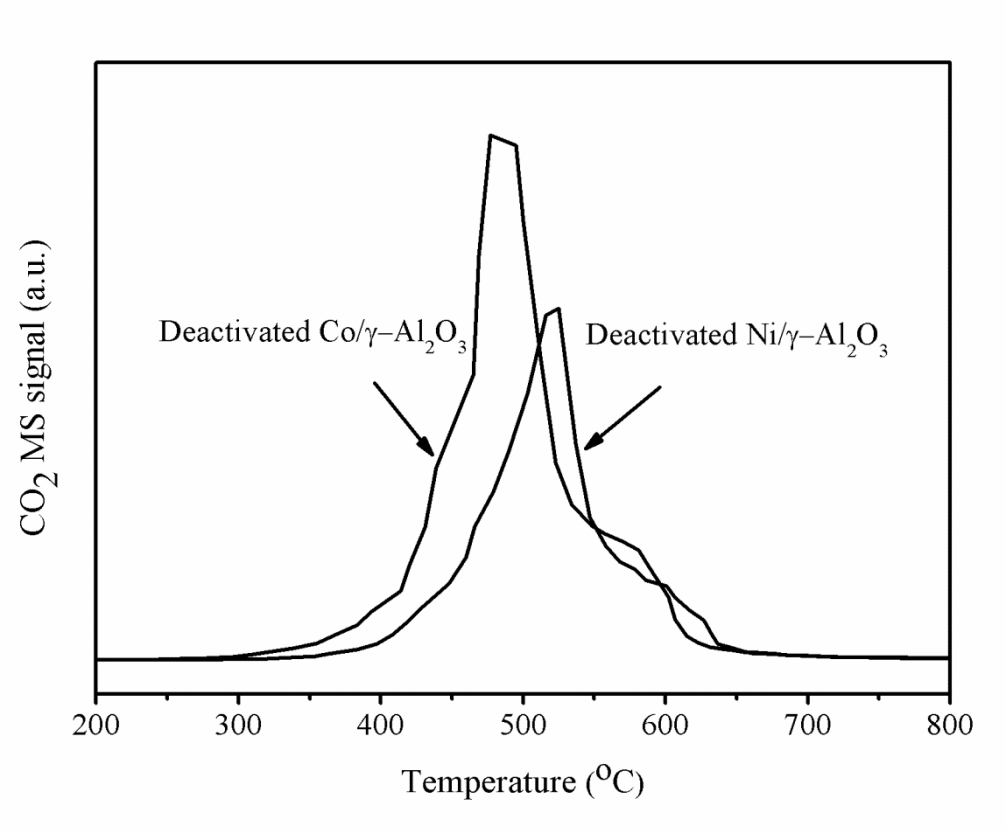

Figure 47 Temperature programmed oxidation profiles of the Ni/γ-Al_2O_3 and Co/γ-Al_2O_3 catalysts after 150 h on-stream.

Table 27 Total coke contents before and after regeneration by calcining in air at 500^{o}C for 5 h obtained from temperature programmed oxidation.

Catalysts	Carbon amount remained after the reaction (mg/g_{cat})	Carbon amount remained after the regeneration (mg/g_{cat})	Carbon amount removed after the regeneration (%)
Deactivated Ni/γ-Al_2O_3	34.88	0.02	99.94
Deactivated Co/γ-Al_2O_3	49.51	0.02	99.95

5.4.4 Regeneration behaviors

After 150 h on-stream experiments, the product yield decreased from 92.2 to ca. 75.6% over Ni catalyst and from 88.6% to ca. 56.6% over Co catalysts. As discussed above, the major reason for catalyst deactivation was caused by the formation of carbonaceous species on the catalyst and the minor reason was likely the sintering of the metal particles. At first, to find out the suitable temperature for the effective removal of the carbonaceous species, TGA (results not shown) was investigated in the range of 200-800 ^{o}C in the presence of air. The complete decomposition of carbon was observed at the temperature of 500 ^{o}C, suggesting that the appropriate regeneration temperature was 500°C. Therefore, the deactivated catalysts after 150 h on-stream were regenerated by calcining in at 500 ^{o}C for 5 h. The higher regeneration temperature should be avoided due to the formation of large metal particle size and the transformation of Ni and Co on γ-Al_2O_3 to metal aluminate phases. Since the catalysts after regeneration exhibited the crystalline structures of

metal oxide phases, implying that the pre-reduction under H_2 at 500 ^oC for 3 h was necessary. It should be deduced that the physical and chemical properties such as BET surface area, pore volume, pore diameter, and metal particles size were not significant different after the regeneration, As the results shown in Figures 35-38, the catalytic performance can be essentially restored after the regeneration, suggesting the carbon deposited on catalyst surfaces was completely removed and was the origin of the deactivation

CHAPTER VI

CONCLUSIONS AND RECOMMENDATIONS

6.1 Conclusions

The aim of this dissertation is the transformation of palm oil to bio-hydrogenated diesel or green diesel via deoxygenation reactions in a continuous-flow trickle-bed reactor with metal and sulfide catalysts. The study focuses on four main aspects; i) understanding the effect of reaction parameters (temperature, pressure, LHSV, and H_2/oil ratio), ii) monometallic catalysts screening and reaction network development, iii) catalyst performance investigation of metal and metal sulfide catalysts, and iiii) deactivation and regeneration study. It can be concluded as the following summarization.

6.1.1 Effect of reaction parameters on the deoxygenation of palm oil to bio-hydrogenated diesel over $NiMoS_2/\gamma\text{-}Al_2O_3$

The effects of important reaction parameters: temperature: 270-420 ^oC; H_2 pressure: 1.5-8 MPa; LHSV: 0.25-5.0 h^{-1}; and H_2/oil ratio: 250-2000 N(cm^3/cm^3) on the conversion, product yield, and a contribution of HDO and DCO/DCO_2 over $NiMoS_2/\gamma\text{-}Al_2O_3$ catalysts were investigated to find out the optimal hydrotreating conditions. The recommended conditions were as follows: temperature: 300 ^oC, Pressure: 3-5 MPa, LHSV: 1-2 h^{-1}, and H_2/oil ratio: 750-1000 N(cm^3/cm^3) with the product yield of 90.0% and n-alkane content >95.5%. The reaction temperature strongly affected the reaction pathways (DCO, DCO_2, HDO, cracking, and isomerization), while higher pressure promoted HDO reaction. The increase in LHSV suppressed the reactions due to the insufficient contact time. H_2/oil ratio should be

higher than 3-5 time of theoretical requirement. Furthermore, methanation reaction impacted on H_2 consumption at low temperature and high pressure.

6.1.2 Roles of monometallic catalysts in deoxygenation of palm oil to green diesel

The γ-Al_2O_3-supported monometallic catalysts (Co, Ni, Pd, and Pt) with various metal loadings (2–10 wt.%) were prepared by the incipient wetness impregnation method and were characterized by XRD, TPR, N_2 sorption, TEM, and CO pulse chemisorption. The characterization studies revealed that Co, Ni, Pd, and Pt metallic phases were formed after reduction and exhibited differences in metal particle size and metal dispersion on γ-Al_2O_3. The performance of the synthesized catalysts in green diesel production via the hydrodeoxygenation of palm oil was then investigated in a fixed-bed reactor at 330 ^{o}C, 5 MPa, LHSV of 1 h^{-1}, and H_2/oil ratio of 1,000 N(cm^3/cm^3). The results showed that the deoxygenation activity decreased in the order of product yield Co > Pd > Pt > Ni when compared at the same amount of metal loading. The TOF increased with the increase in the metal particle size. The Ni, Pd, and Pt catalysts were favorable to the DCO route, whereas DCO/DCO_2 and HDO were all dominant over the Co catalyst.

A reaction network of the deoxygenation of an oxygenated model compound, oleic acid, was investigated. Stearic acid, octadecanol, and octadecyl stearate/stearyl oleate, regarded as oxygenated intermediates, were formed during the deoxygenation of oleic acid. Based on the product distribution, the reaction network for the deoxygenation of palm oil was proposed as an initial hydrogenation of the double bond in unsaturated triglycerides to saturated triglycerides, followed by hydrogenolysis to form fatty acids and propane. Then, the free fatty acids were deoxygenated on the metallic sites of the catalyst to green diesel by DCO or HDO reactions.

6.1.3 Comparisons of γ-Al_2O_3-supported metal and metal sulfide catalysts on activity, selectivity, and stability in deoxygenation of palm oil to bio-hydrogenated diesel

The γ-Al_2O_3-supported metal catalysts (Ni, Co, Mo, NiMo, and CoMo) and γ-Al_2O_3-supported metal sulfide catalysts (NiS_x, CoS_x, MoS_2, $NiMoS_2$, and $CoMoS_2$) were prepared by the incipient wetness impregnation method. Based on the result obtained from previous sections, the Ni, Co, $NiMoS_2$, $CoMoS_2$ catalysts exhibited promising activity for the deoxygenation of palm oil to hydrocarbons. The results revealed that the DCO/DCO_2 reaction was dominant, when the reaction was catalyzed by metallic Ni catalyst, whereas, the HDO was dominant when the reaction was catalyzed by $NiMoS_2$, and $CoMoS_2$ catalysts. Interestingly, the contribution of DCO/DCO_2 was nearly comparable to that of the HDO reaction over metallic Co catalyst. Based on the stability evolution tests, the catalytic activity was decreased in order of $NiMoS_2$ > $CoMoS_2$ > Ni > Co catalysts.

6.1.4 Deactivation and regeneration characteristics of γ-Al_2O_3-supported Ni and Co catalysts during deoxygenation of palm oil

Deactivation and regeneration behaviors of the Ni/γ-Al_2O_3 and Co/γ-Al_2O_3 catalysts in palm oil hydrodeoxygenation were investigated at 300 ^oC and 5 MPa in a trickle bed reactor. The catalysts exhibited a good catalytic activity and the stable performance for 100 h on-stream. Nevertheless, the product yield over Ni catalyst gradually decreased (from 92.2 to ca. 76.2% after 150 h on-stream), whereas, the dramatic decline in product yield can be noticed over Co catalyst (from 88.6% to ca. 56.6% after 150 h on-stream). The catalysts after 150 h on-stream were subsequently characterized by N_2 sorption, CO pulse chemisorption, XRD, XANES, TEM, and TPO techniques. The physical and chemical properties of catalysts were changed significantly after the reaction tests. XRD and TEM studies revealed that the crystallinity size and metal particle size increased, suggesting the nickel and cobalt particles sintering after reaction. The XANES data by linear combination fitting confirmed the formation of nickel and cobalt metallic after pre-reduction and further

reduction *in situ* during working experiment. The carbon analysis determined by TPO implied that the carbon formation rate on cobalt catalyst was higher than that on nickel catalyst. The catalyst characterization results suggested that the carbon deposited on catalysts was the main cause of the catalyst deactivation, and the sintering of metal particles was a minor one. Interestingly, the catalyst regeneration under air at 500 ^{o}C for 5 h, followed by pre-reduction in H_2 at 500 ^{o}C for 3 h can fully re-install the catalytic performance in the palm oil hydrodeoxygenation.

6.2 Recommendations

1. Development of stable and active non-sulfide catalyst as well as decarboxylation catalysts without the use of H_2.
2. Development of one-step process of the hydroisomerization and HDO of vegetable oil into iso-paraffin with improved cold flow properties.
3. Co-processing of vegetable oils with petroleum feedstock is a promising alternative way to integrate the conventional process in existing refinery process, providing the minimal required investments and the use of large-scale facilities with high efficiencies.

REFERENCES

[1] R. Sotelo-Boyas, F. Trejo-Zarraga, F.d. Jesus Hernandez-Loyo, Hydroconversion of Triglycerides into Green Liquid Fuels, (2012).

[2] S. Gong, A. Shinozaki, E.W. Qian, Role of Support in Hydrotreatment of Jatropha Oil over Sulfided NiMo Catalysts, Industrial & Engineering Chemistry Research, 51 (2012) 13953-13960.

[3] J. Hancsók, T. Kasza, S. Kovács, P. Solymosi, A. Holló, Production of bioparaffins by the catalytic hydrogenation of natural triglycerides, Journal of Cleaner Production, 34 (2012) 76-81.

[4] S. Kovács, T. Kasza, A. Thernesz, I.W. Horváth, J. Hancsók, Fuel production by hydrotreating of triglycerides on $NiMo/Al_2O_3/F$ catalyst, Chemical Engineering Journal, 176-177 (2011) 237-243.

[5] P.i. Mäki-Arvela, B. Rozmysłowicz, S. Lestari, O. Simakova, K. Eränen, T. Salmi, D.Y. Murzin, Catalytic Deoxygenation of Tall Oil Fatty Acid over Palladium Supported on Mesoporous Carbon, Energy & Fuels, 25 (2011) 2815-2825.

[6] W. Kiatkittipong, S. Phimsen, K. Kiatkittipong, S. Wongsakulphasatch, N. Laosiripojana, S. Assabumrungrat, Diesel-like hydrocarbon production from hydroprocessing of relevant refining palm oil, Fuel Processing Technology, 116 (2013) 16-26.

[7] M. Krár, S. Kovács, D. Kalló, J. Hancsók, Fuel purpose hydrotreating of sunflower oil on $CoMo/Al_2O_3$ catalyst, Bioresource technology, 101 (2010) 9287-9293.

[8] S.K. Kim, S. Brand, H.-s. Lee, Y. Kim, J. Kim, Production of renewable diesel by hydrotreatment of soybean oil: Effect of reaction parameters, Chemical Engineering Journal, 228 (2013) 114-123.

[9] A. Guzman, J.E. Torres, L.P. Prada, M.L. Nuñez, Hydroprocessing of crude palm oil at pilot plant scale, Catalysis Today, 156 (2010) 38-43.

[10] S. Bezergianni, A. Kalogianni, Hydrocracking of used cooking oil for biofuels production, Bioresource technology, 100 (2009) 3927-3932.

[11] I.V. Deliy, E.N. Vlasova, A.L. Nuzhdin, E.Y. Gerasimov, G.A. Bukhtiyarova, Hydrodeoxygenation of methyl palmitate over sulfided Mo/Al_2O_3, $CoMo/Al_2O_3$ and $NiMo/Al_2O_3$ catalysts, RSC Advances, 4 (2014) 2242-2250.

[12] P. Kumar, S.R. Yenumala, S.K. Maity, D. Shee, Kinetics of hydrodeoxygenation of stearic acid using supported nickel catalysts: Effects of supports, Applied Catalysis A: General, 471 (2014) 28-38.

[13] D. Kubička, L. Kaluža, Deoxygenation of vegetable oils over sulfided Ni, Mo and NiMo catalysts, Applied Catalysis A: General, 372 (2010) 199-208.

[14] N. Chen, S. Gong, H. Shirai, T. Watanabe, E.W. Qian, Effects of Si/Al ratio and Pt loading on Pt/SAPO-11 catalysts in hydroconversion of Jatropha oil, Applied Catalysis A: General, 466 (2013) 105-115.

[15] Y. Liu, R. Sotelo-Boyás, K. Murata, T. Minowa, K. Sakanishi, Hydrotreatment of Vegetable Oils to Produce Bio-Hydrogenated Diesel and Liquefied Petroleum Gas Fuel over Catalysts Containing Sulfided Ni–Mo and Solid Acids, Energy & Fuels, 25 (2011) 4675-4685.

[16] C. Wang, Z. Tian, L. Wang, R. Xu, Q. Liu, W. Qu, H. Ma, B. Wang, One-step hydrotreatment of vegetable oil to produce high quality diesel-range alkanes, ChemSusChem, 5 (2012) 1974-1983.

[17] H. Zhang, H. Lin, W. Wang, Y. Zheng, P. Hu, Hydroprocessing of waste cooking oil over a dispersed nano catalyst: Kinetics study and temperature effect, Applied Catalysis B: Environmental, 150-151 (2014) 238-248.

[18] D. Kubička, J. Horáček, M. Setnička, R. Bulánek, A. Zukal, I. Kubičková, Effect of support-active phase interactions on the catalyst activity and selectivity in deoxygenation of triglycerides, Applied Catalysis B: Environmental, 145 (2014) 101-107.

[19] K. Faungnawakij, K. Suriye, Chapter 4 - Current Catalytic Processes with Hybrid Materials and Composites for Heterogeneous Catalysis, in: S.L. Suib (Ed.) New and Future Developments in Catalysis, Elsevier, Amsterdam, 2013, pp. 79-104.

[20] T.V. Choudhary, C.B. Phillips, Renewable fuels via catalytic hydrodeoxygenation, Applied Catalysis A: General, 397 (2011) 1-12.

[21] B. Donnis, R.G. Egeberg, P. Blom, K.G. Knudsen, Hydroprocessing of Bio-Oils and Oxygenates to Hydrocarbons. Understanding the Reaction Routes, Topics in Catalysis, 52 (2009) 229-240.

[22] C. Ochoa-Hernández, Y. Yang, P. Pizarro, V.A. de la Peña O'Shea, J.M. Coronado, D.P. Serrano, Hydrocarbons production through hydrotreating of methyl esters over Ni and Co supported on SBA-15 and Al-SBA-15, Catalysis Today, 210 (2013) 81-88.

[23] S. Gong, A. Shinozaki, M. Shi, E.W. Qian, Hydrotreating of Jatropha Oil over Alumina Based Catalysts, Energy & Fuels, 26 (2012) 2394-2399.

[24] D. Kubička, J. Horáček, Deactivation of HDS catalysts in deoxygenation of vegetable oils, Applied Catalysis A: General, 394 (2011) 9-17.

[25] A. Srifa, K. Faungnawakij, V. Itthibenchapong, N. Viriya-empikul, T. Charinpanitkul, S. Assabumrungrat, Production of bio-hydrogenated diesel by catalytic hydrotreating of palm oil over $NiMoS_2/\gamma$-Al_2O_3 catalyst, Bioresource technology, (2014).

[26] M. Anand, A.K. Sinha, Temperature-dependent reaction pathways for the anomalous hydrocracking of triglycerides in the presence of sulfided Co-Mo-catalyst, Bioresource technology, 126 (2012) 148-155.

[27] C. Templis, A. Vonortas, I. Sebos, N. Papayannakos, Vegetable oil effect on gasoil HDS in their catalytic co-hydroprocessing, Applied Catalysis B: Environmental, 104 (2011) 324-329.

[28] J. Horáček, Z. Tišler, V. Rubáš, D. Kubička, HDO catalysts for triglycerides conversion into pyrolysis and isomerization feedstock, Fuel, (2013).

[29] Y. Yang, Q. Wang, X. Zhang, L. Wang, G. Li, Hydrotreating of C18 fatty acids to hydrocarbons on sulphided NiW/SiO_2–Al_2O_3, Fuel Processing Technology, 116 (2013) 165-174.

[30] H. Zuo, Q. Liu, T. Wang, L. Ma, Q. Zhang, Q. Zhang, Hydrodeoxygenation of Methyl Palmitate over Supported Ni Catalysts for Diesel-like Fuel Production, Energy & Fuels, 26 (2012) 3747-3755.

[31] Q. Liu, Y. Bie, S. Qiu, Q. Zhang, J. Sainio, T. Wang, L. Ma, J. Lehtonen, Hydrogenolysis of methyl heptanoate over Co based catalysts: Mediation of support property on activity and product distribution, Applied Catalysis B: Environmental, 147 (2014) 236-245.

[32] I. Simakova, O. Simakova, P. Mäki-Arvela, A. Simakov, M. Estrada, D.Y. Murzin, Deoxygenation of palmitic and stearic acid over supported Pd catalysts: Effect of metal dispersion, Applied Catalysis A: General, 355 (2009) 100-108.

[33] L. Chen, Y. Zhu, H. Zheng, C. Zhang, Y. Li, Aqueous-phase hydrodeoxygenation of propanoic acid over the Ru/ZrO_2 and $Ru–Mo/ZrO_2$ catalysts, Applied Catalysis A: General, 411-412 (2012) 95-104.

[34] L. Chen, Y. Zhu, H. Zheng, C. Zhang, B. Zhang, Y. Li, Aqueous-phase hydrodeoxygenation of carboxylic acids to alcohols or alkanes over supported Ru catalysts, Journal of Molecular Catalysis A: Chemical, 351 (2011) 217-227.

[35] S.A.W. Hollak, R.W. Gosselink, D.S. van Es, J.H. Bitter, Comparison of Tungsten and Molybdenum Carbide Catalysts for the Hydrodeoxygenation of Oleic Acid, ACS Catalysis, 3 (2013) 2837-2844.

[36] B. Peng, C. Zhao, S. Kasakov, S. Foraita, J.A. Lercher, Manipulating catalytic pathways: deoxygenation of palmitic acid on multifunctional catalysts, Chemistry, 19 (2013) 4732-4741.

[37] B. Peng, Y. Yao, C. Zhao, J.A. Lercher, Towards quantitative conversion of microalgae oil to diesel-range alkanes with bifunctional catalysts, Angewandte Chemie, 51 (2012) 2072-2075.

[38] J. Chen, H. Shi, L. Li, K. Li, Deoxygenation of methyl laurate as a model compound to hydrocarbons on transition metal phosphide catalysts, Applied Catalysis B: Environmental, 144 (2014) 870-884.

[39] C. Zhao, T. Brück, J.A. Lercher, Catalytic deoxygenation of microalgae oil to green hydrocarbons, Green Chemistry, 15 (2013) 1720.

[40] J.K. Satyarthi, T. Chiranjeevi, D.T. Gokak, P.S. Viswanathan, An overview of catalytic conversion of vegetable oils/fats into middle distillates, Catalysis Science & Technology, 3 (2013) 70-80.

[41] B. Peng, X. Yuan, C. Zhao, J.A. Lercher, Stabilizing catalytic pathways via redundancy: selective reduction of microalgae oil to alkanes, Journal of the American Chemical Society, 134 (2012) 9400-9405.

[42] S. Lestari, P. Mäki-Arvela, K. Eränen, J. Beltramini, G.Q. Max Lu, D.Y. Murzin, Diesel-like Hydrocarbons from Catalytic Deoxygenation of Stearic Acid over Supported Pd Nanoparticles on SBA-15 Catalysts, Catalysis Letters, 134 (2009) 250-257.

[43] E. Santillan-Jimenez, T. Morgan, J. Lacny, S. Mohapatra, M. Crocker, Catalytic deoxygenation of triglycerides and fatty acids to hydrocarbons over carbon-supported nickel, Fuel, 103 (2013) 1010-1017.

[44] J.G. Immer, M.J. Kelly, H.H. Lamb, Catalytic reaction pathways in liquid-phase deoxygenation of C18 free fatty acids, Applied Catalysis A: General, 375 (2010) 134-139.

[45] M. Chiappero, P.T.M. Do, S. Crossley, L.L. Lobban, D.E. Resasco, Direct conversion of triglycerides to olefins and paraffins over noble metal supported catalysts, Fuel, 90 (2011) 1155-1165.

[46] V.T. da Silva, L.A. Sousa, Chapter 3 - Catalytic Upgrading of Fats and Vegetable Oils for the Production of Fuels, in: K.S. Triantafyllidis, A.A. Lappas, M. Stöcker (Eds.) The Role of Catalysis for the Sustainable Production of Bio-fuels and Bio-chemicals, Elsevier, Amsterdam, 2013, pp. 67-92.

[47] B. Peng, Transformation of triglycerides and fatty acids into biofuels with sulfur-free catalysts, in, TECHNISCHE UNIVERSITÄT MÜNCHEN, 2012.

[48] K. Faungnawakij, K. Suriye, Current Catalytic Processes with Hybrid Materials and Composites for Heterogeneous Catalysis, (2013) 79-104.

[49] I.K.k. Mathias Snåre, Pa1ivi Ma1ki-Arvela, Kari Era1nen, and Dmitry Yu. Murzin, Heterogeneous Catalytic Deoxygenation of Stearic Acid for Production of Biodiesel, Ind. Eng. Chem. Res., 45 (2006) 5708-5715.

[50] R.W. Gosselink, S.A. Hollak, S.W. Chang, J. van Haveren, K.P. de Jong, J.H. Bitter, D.S. van Es, Reaction Pathways for the Deoxygenation of Vegetable Oils and Related Model Compounds, ChemSusChem, (2013).

[51] J. Mikulec, J. Cvengroš, Ľ. Joríková, M. Banič, A. Kleinová, Second generation diesel fuel from renewable sources, Journal of Cleaner Production, 18 (2010) 917-926.

[52] G.W. Huber, P. O'Connor, A. Corma, Processing biomass in conventional oil refineries: Production of high quality diesel by hydrotreating vegetable oils in heavy vacuum oil mixtures, Applied Catalysis A: General, 329 (2007) 120-129.

[53] J. Walendziewski, M. Stolarski, R. Łużny, B. Klimek, Hydroprocesssing of light gas oil — rape oil mixtures, Fuel Processing Technology, 90 (2009) 686-691.

[54] C. Kongwattanakul, BIODIESEL PRODUCTION WITH HYDROPROCESSING PROCESS FROM WASTE COOKING PALM OIL OVER Ni-Mo/Al_2O_3 AND Co-Mo/Al_2O_3 CARBIDES CATALYSTS, in: Department of Chemical Engineering, Chulalongkorn University, 2010.

[55] B. Peng, X. Yuan, C. Zhao, J.A. Lercher, Stabilizing Catalytic Pathways via Redundancy: Selective Reduction of Microalgae Oil to Alkanes, Journal of the American Chemical Society, 134 (2012) 9400-9405.

[56] S.K. Kim, J.Y. Han, H.-s. Lee, T. Yum, Y. Kim, J. Kim, Production of renewable diesel via catalytic deoxygenation of natural triglycerides: Comprehensive understanding of reaction intermediates and hydrocarbons, Applied Energy, 116 (2014) 199-205.

[57] A. Srifa, K. Faungnawakij, V. Itthibenchapong, N. Viriya-empikul, T. Charinpanitkul, S. Assabumrungrat, Production of bio-hydrogenated diesel by catalytic hydrotreating of palm oil over $NiMoS_2/\gamma$-Al_2O_3 catalyst, Bioresource technology, 158 (2014) 81-90.

[58] D. Kubička, V. Tukač, Chapter Three - Hydrotreating of Triglyceride-Based Feedstocks in Refineries, in: M. Dmitry Yu (Ed.) Advances in Chemical Engineering, Academic Press, 2013, pp. 141-194.

[59] J. Mijoin, V. Thévenin, N. Garcia Aguirre, H. Yuze, J. Wang, W.Z. Li, G. Pérot, J.L. Lemberton, Thioreduction of cyclopentanone and hydrodesulfurization of dibenzothiophene over sulfided nickel or cobalt-promoted molybdenum on alumina catalysts, Applied Catalysis A: General, 180 (1999) 95-104.

[60] C. Dupont, R. Lemeur, A. Daudin, P. Raybaud, Hydrodeoxygenation pathways catalyzed by MoS_2 and NiMoS active phases: A DFT study, Journal of Catalysis, 279 (2011) 276-286.

[61] S. Brillouet, E. Baltag, S. Brunet, F. Richard, Deoxygenation of decanoic acid and its main intermediates over unpromoted and promoted sulfided catalysts, Applied Catalysis B: Environmental, 148-149 (2014) 201-211.

[62] K. Murata, Y. Liu, M. Inaba, I. Takahara, Production of Synthetic Diesel by Hydrotreatment of Jatropha Oils Using Pt−Re/H-ZSM-5 Catalyst, Energy & Fuels, 24 (2010) 2404-2409.

[63] P. Do, M. Chiappero, L. Lobban, D. Resasco, Catalytic Deoxygenation of Methyl-Octanoate and Methyl-Stearate on Pt/Al_2O_3, Catalysis Letters, 130 (2009) 9-18.

[64] M. Snåre, D.Y. Murzin, Heterogeneous Catalytic Deoxygenation of Stearic Acid for Production of Biodiesel, Industrial & Engineering Chemistry Research, 45 (2006) 6875-6875.

[65] B. Veriansyah, J.Y. Han, S.K. Kim, S.-A. Hong, Y.J. Kim, J.S. Lim, Y.-W. Shu, S.-G. Oh, J. Kim, Production of renewable diesel by hydroprocessing of soybean oil: Effect of catalysts, Fuel, 94 (2012) 578-585.

[66] J. Duan, J. Han, H. Sun, P. Chen, H. Lou, X. Zheng, Diesel-like hydrocarbons obtained by direct hydrodeoxygenation of sunflower oil over Pd/Al-SBA-15 catalysts, Catalysis Communications, 17 (2012) 76-80.

[67] E. Santillan-Jimenez, T. Morgan, J. Shoup, A.E. Harman-Ware, M. Crocker, Catalytic deoxygenation of triglycerides and fatty acids to hydrocarbons over Ni–Al layered double hydroxide, Catalysis Today, (2013).

[68] G. Onyestyák, S. Harnos, Á. Szegedi, D. Kalló, Sunflower oil to green diesel over Raney-type Ni-catalyst, Fuel, 102 (2012) 282-288.

[69] N. Viriya-empikul, P. Krasae, W. Nualpaeng, B. Yoosuk, K. Faungnawakij, Biodiesel production over Ca-based solid catalysts derived from industrial wastes, Fuel, 92 (2012) 239-244.

[70] T. Morgan, E. Santillan-Jimenez, A.E. Harman-Ware, Y. Ji, D. Grubb, M. Crocker, Catalytic deoxygenation of triglycerides to hydrocarbons over supported nickel catalysts, Chemical Engineering Journal, 189-190 (2012) 346-355.

[71] M. Toba, Y. Abe, H. Kuramochi, M. Osako, T. Mochizuki, Y. Yoshimura, Hydrodeoxygenation of waste vegetable oil over sulfide catalysts, Catalysis Today, 164 (2011) 533-537.

[72] S. Bezergianni, A. Dimitriadis, A. Kalogianni, K.G. Knudsen, Toward Hydrotreating of Waste Cooking Oil for Biodiesel Production. Effect of Pressure, H_2/Oil Ratio, aHydrotreating of waste cooking oil for biodiesel production. Part I: Effect of temperature on product yields and heteroatom removal, Bioresource technology, 101 (2010) 6651-6656.

[74] S. Bezergianni, A. Dimitriadis, T. Sfetsas, A. Kalogianni, Hydrotreating of waste cooking oil for biodiesel production. Part II: effect of temperature on hydrocarbon composition, Bioresource technology, 101 (2010) 7658-7660.

[75] J. Liu, K. Fan, W. Tian, C. Liu, L. Rong, Hydroprocessing of Jatropha oil over NiMoCe/Al2O3 catalyst, International Journal of Hydrogen Energy, 37 (2012) 17731-17737.

[76] P. Šimáček, D. Kubička, G. Šebor, M. Pospíšil, Hydroprocessed rapeseed oil as a source of hydrocarbon-based biodiesel, Fuel, 88 (2009) 456-460.

[77] J. Gao, Y. Wang, Y. Ping, D. Hu, G. Xu, F. Gu, F. Su, A thermodynamic analysis of methanation reactions of carbon oxides for the production of synthetic natural gas, RSC Advances, 2 (2012) 2358.

[78] D. Kubička, P. Šimáček, N. Žilková, Transformation of Vegetable Oils into Hydrocarbons over Mesoporous-Alumina-Supported CoMo Catalysts, Topics in Catalysis, 52 (2009) 161-168.

[79] T.M. Sankaranarayanan, M. Banu, A. Pandurangan, S. Sivasanker, Hydroprocessing of sunflower oil-gas oil blends over sulfided Ni-Mo-Al-zeolite beta composites, Bioresource technology, 102 (2011) 10717-10723.

[80] Y. Yang, J. Chen, H. Shi, Deoxygenation of Methyl Laurate as a Model Compound to Hydrocarbons on Ni_2P/SiO_2, Ni_2P/MCM-41, and Ni_2P/SBA-15 Catalysts with Different Dispersions, Energy & Fuels, 27 (2013) 3400-3409.

[81] L.A. Sousa, J.L. Zotin, V. Teixeira da Silva, Hydrotreatment of sunflower oil using supported molybdenum carbide, Applied Catalysis A: General, 449 (2012) 105-111.

[82] P. Hirunsit, K. Faungnawakij, S. Namuangruk, C. Luadthong, Catalytic behavior and surface species investigation over γ-Al_2O_3 in dimethyl ether hydrolysis, Applied Catalysis A: General, 460-461 (2013) 99-105.

[83] J. Li, Y. Chai, B. Liu, Y. Wu, X. Li, Z. Tang, Y. Liu, C. Liu, The catalytic performance of Ni_2P/Al_2O_3 catalyst in comparison with Ni/Al_2O_3 catalyst in dehydrogenation of cyclohexane, Applied Catalysis A: General, 469 (2014) 434-441.

[84] D. Hu, J. Gao, Y. Ping, L. Jia, P. Gunawan, Z. Zhong, G. Xu, F. Gu, F. Su, Enhanced Investigation of CO Methanation over Ni/Al_2O_3 Catalysts for Synthetic Natural Gas Production, Industrial & Engineering Chemistry Research, 51 (2012) 4875-4886.

[85] Z. Ferencz, K. Baán, A. Oszkó, Z. Kónya, T. Kecskés, A. Erdőhelyi, Dry reforming of CH_4 on Rh doped Co/Al_2O_3 catalysts, Catalysis Today, (2013).

[86] Y. Zhang, H. Xiong, K. Liew, J. Li, Effect of magnesia on alumina-supported cobalt Fischer–Tropsch synthesis catalysts, Journal of Molecular Catalysis A: Chemical, 237 (2005) 172-181.

[87] J. Liu, H. Wang, Y. Chen, M. Yang, Y. Wu, Effects of pretreatment atmospheres on the catalytic performance of Pd/γ-Al_2O_3 catalyst in benzene degradation, Catalysis Communications, 46 (2014) 11-16.

[88] J.G. Dickinson, P.E. Savage, Stability and activity of Pt and Ni catalysts for hydrodeoxygenation in supercritical water, Journal of Molecular Catalysis A: Chemical, (2013).

[89] S. Echeandia, B. Pawelec, V.L. Barrio, P.L. Arias, J.F. Cambra, C.V. Loricera, J.L.G. Fierro, Enhancement of phenol hydrodeoxygenation over Pd catalysts supported on mixed HY zeolite and Al_2O_3. An approach to O-removal from bio-oils, Fuel, 117 (2014) 1061-1073.

[90] R.W. Gosselink, S.A. Hollak, S.W. Chang, J. van Haveren, K.P. de Jong, J.H. Bitter, D.S. van Es, Reaction pathways for the deoxygenation of vegetable oils and related model compounds, ChemSusChem, 6 (2013) 1576-1594.

[91] Y. Yu, G. Jin, Y. Wang, X. Guo, Synthesis of natural gas from CO methanation over SiC supported Ni–Co bimetallic catalysts, Catalysis Communications, 31 (2013) 5-10.

[92] G. Zhou, T. Wu, H. Xie, X. Zheng, Effects of structure on the carbon dioxide methanation performance of Co-based catalysts, International Journal of Hydrogen Energy, 38 (2013) 10012-10018.

[93] C.H. Bartholomew, Mechanisms of catalyst deactivation, Applied Catalysis A: General, 212 (2001) 17-60.

[94] R. Sotelo-Boyás, Y. Liu, T. Minowa, Renewable Diesel Production from the Hydrotreating of Rapeseed Oil with Pt/Zeolite and $NiMo/Al_2O_3$ catalysts, Industrial & Engineering Chemistry Research, 50 (2011) 2791-2799.

[95] P. Priecel, D. Kubička, L. Čapek, Z. Bastl, P. Ryšánek, The role of Ni species in the deoxygenation of rapeseed oil over NiMo-alumina catalysts, Applied Catalysis A: General, 397 (2011) 127-137.

[96] A. Srifa, K. Faungnawakij, V. Itthibenchapong, N. Viriya-empikul, T. Charinpanitkul, S. Assabumrungrat, Production of bio-hydrogenated diesel by catalytic hydrotreating of palm oil over $NiMoS_2/\gamma\text{-}Al_2O_3$ catalyst, Bioresource technology, 158 (2014) 81-90.

[97] H. Wang, S. Yan, S.O. Salley, K.Y. Simon Ng, Support effects on hydrotreating of soybean oil over NiMo carbide catalyst, Fuel, 111 (2013) 81-87.

[98] A.F.H. Studentschnig, S. Schober, M. Mittelbach, Conversion of Crude Palm Oil into Hydrocarbons over Commercial Raney Nickel, Energy & Fuels, 27 (2013) 7480-7484.

[99] P. Bielansky, A. Weinert, C. Schönberger, A. Reichhold, Catalytic conversion of vegetable oils in a continuous FCC pilot plant, Fuel Processing Technology, 92 (2011) 2305-2311.

[100] S. Lee, G. Keskar, C. Liu, W.R. Schwartz, C.S. McEnally, J.-Y. Kim, L.D. Pfefferle, G.L. Haller, Deactivation characteristics of Ni/CeO_2-Al_2O_3 catalyst for cyclic regeneration in a portable steam reformer, Applied Catalysis B: Environmental, 111–112 (2012) 157-164.

[101] C. Wang, Q. Liu, X. Liu, L. Yan, C. Luo, L. Wang, B. Wang, Z. Tian, Influence of reaction conditions on one-step hydrotreatment of lipids in the production of iso-alkanes over Pt/SAPO-11, Chinese Journal of Catalysis, 34 (2013) 1128-1138.

[102] S. Adhikari, S. Fernando, S.R. Gwaltney, S.D. Filip To, R. Mark Bricka, P.H. Steele, A. Haryanto, A thermodynamic analysis of hydrogen production by steam reforming of glycerol, International Journal of Hydrogen Energy, 32 (2007) 2875-2880.

[103] Q. Smejkal, L. Smejkalová, D. Kubička, Thermodynamic balance in reaction system of total vegetable oil hydrogenation, Chemical Engineering Journal, 146 (2009) 155-160.

[104] K. Faungnawakij, R. Kikuchi, K. Eguchi, Thermodynamic evaluation of methanol steam reforming for hydrogen production, Journal of Power Sources, 161 (2006) 87-94.

[105] E.Y. García, M.A. Laborde, Hydrogen production by the steam reforming of ethanol: Thermodynamic analysis, International Journal of Hydrogen Energy, 16 (1991) 307-312.

[106] G. Ertl, H. Knözinger, F. Schüth, J. Weiktamp, Handbook of Heterogeneous Catalysis, in, Wiley-VCH, Weinheim, 2008.

APPENDIX

APPENDIX A

CONDITION OF GAS CHROMATROGRAPY AND CALIBRATION CURVES OF STANDARDS

The gas chromatography with flame ionization detector was used to analyze the liquid product composition (*n*-C_8 to *n*-C_{20}) and oxygenated intermediates i.e. free fatty acid, octadecanol and octadecanal. Table A-1 are shown conditions use in gas chromatography with flame ionization detector. The calibrations of standard are represented in Figures A-1 – A-10

Table A-1 Operating condition for gas chromatography equipped with flame ionization detector

Gas Chromagraphy	SHIMADZU GC-2010B
Detector	FID
Column	DB-1HT (Agilent J&W GC Columns)
- Column material	Silica
- Length	30 m
- Outer diameter	0.32 mm
- Film thickness	0.1 µm
Spilt ratio	100
Purge flow rate	4 ml/min
Carrier gas	He (99.999%)
Carrier gas flow	70 kPa
Hydrogen gas flow	60 kPa

Table A-1 Operating condition for gas chromatography equipped with flame ionization detector (cont.)

Gas Chromagraphy	SHIMADZU GC-14B
Air gas flow	50 kPa
Primary gas flow	500 kPa
Make up flow (Nitrogen)	60 kPa
Temperature limits (^{o}C)	400
Injector temperature (^{o}C)	340
Column oven temperature program	
- initial column temperature (^{o}C)	40
- ramp rate (^{o}C/min)	80
- column temperature (^{o}C)	270
-holding time (min)	11
- ramp rate (^{o}C/min)	15
- final column temperature (^{o}C)	370
- holding time (min)	15
Detector temperature (^{o}C)	370
Analysed liquids	Triglyceride, Free fatty acid, Oxygenated intermediates (i.e, octadecanol and octadecanal), and Hydrocarbon normal C_8-C_{20} alkanes

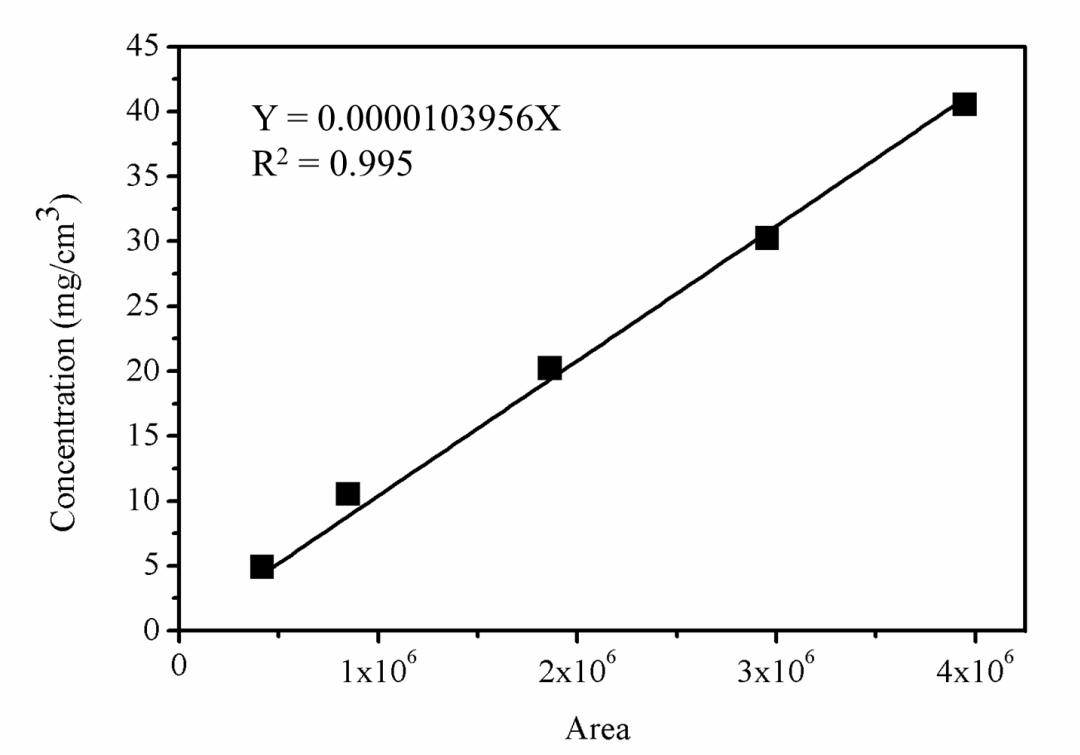

Figure A-1 Calibration curve of dodecane.

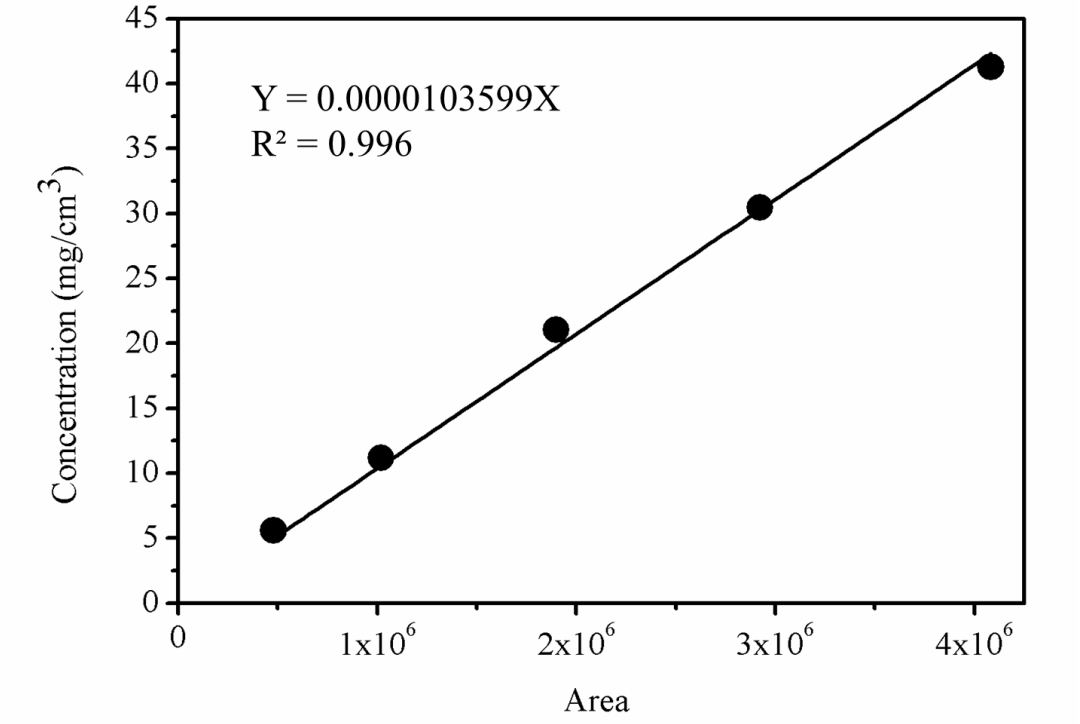

Figure A-2 Calibration curve of pentadecane.

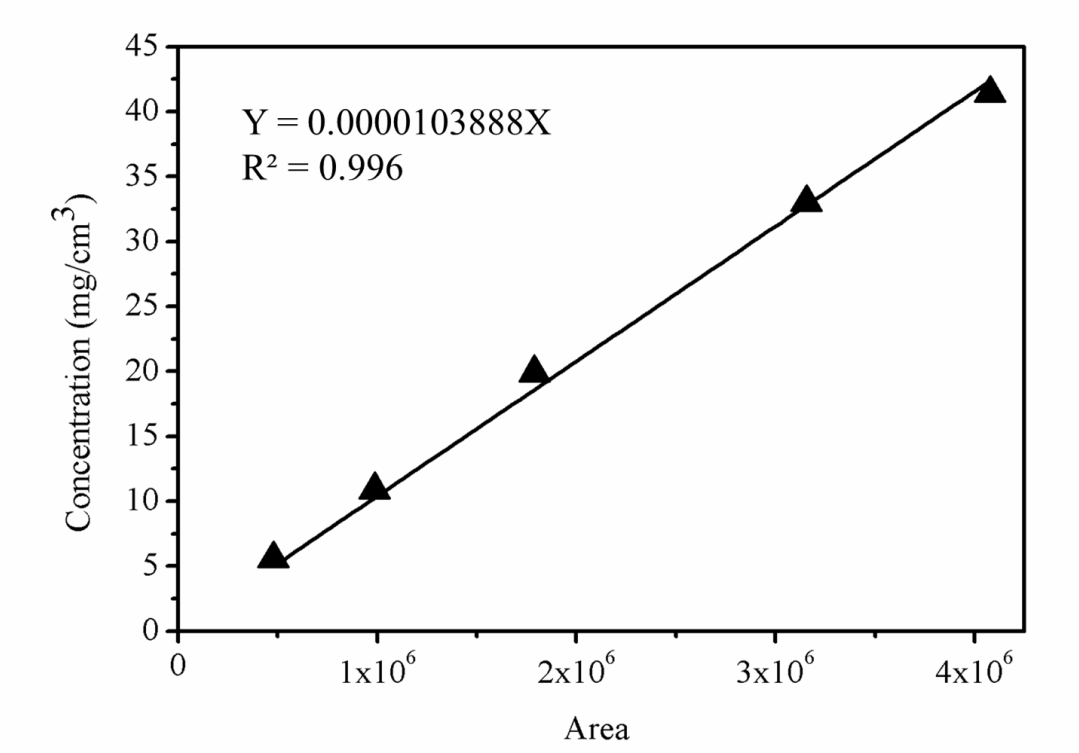

Figure A-3 Calibration curve of hexadecane.

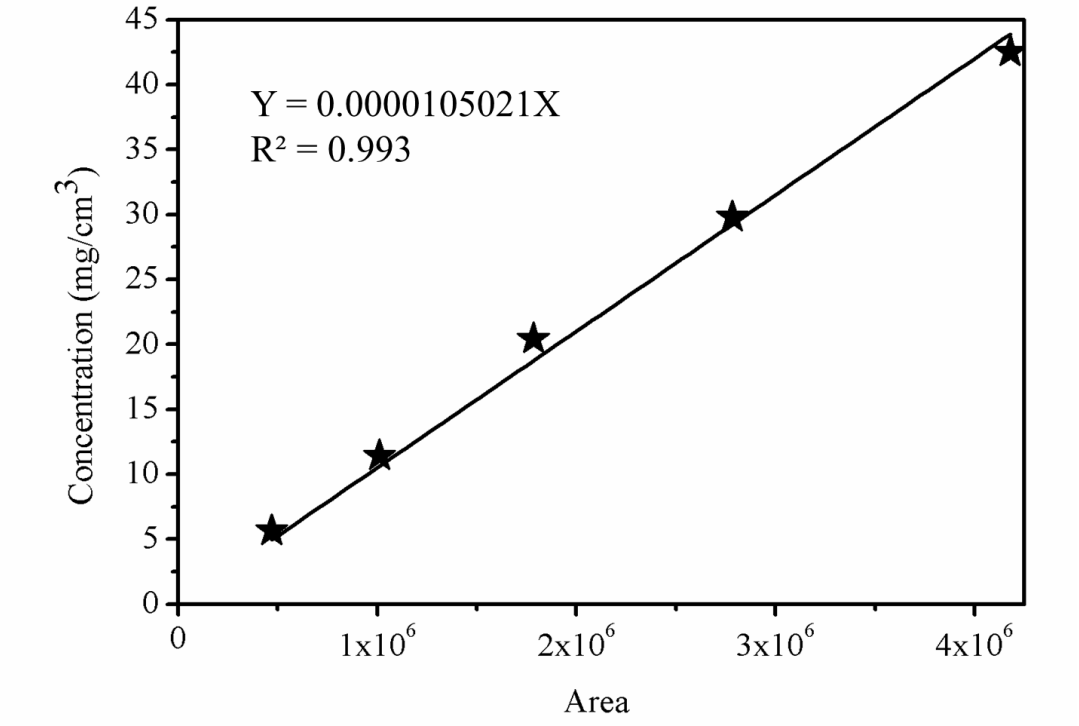

Figure A-4 Calibration curve of heptadecane.

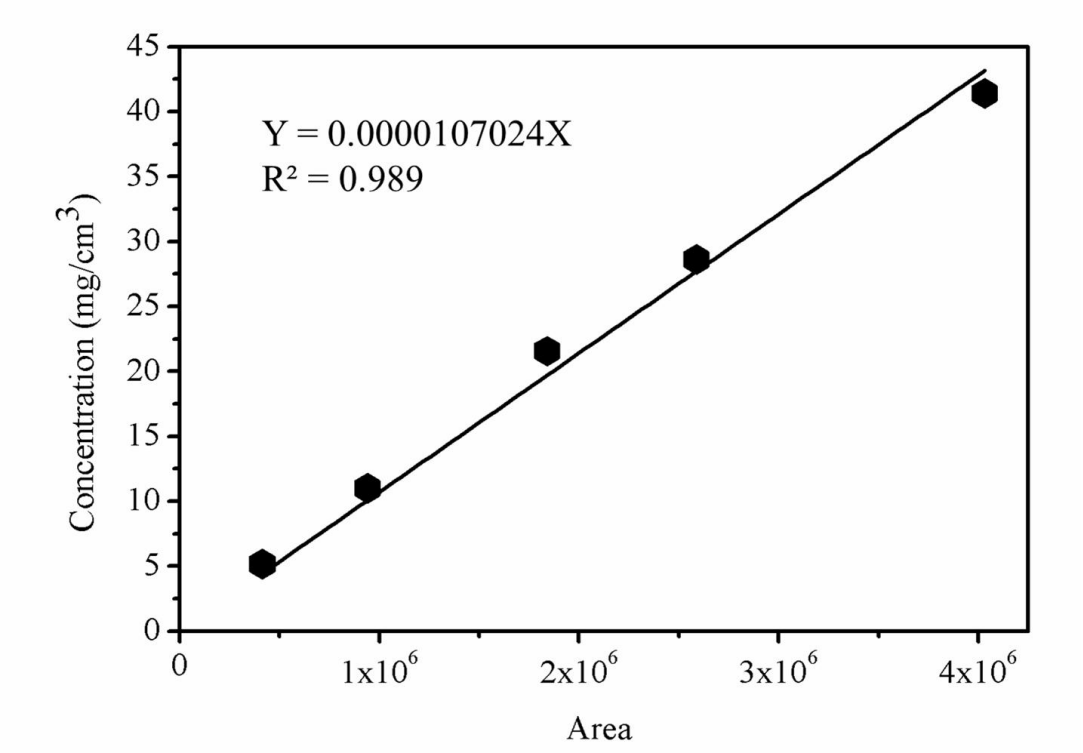

Figure A-5 Calibration curve of octadecane.

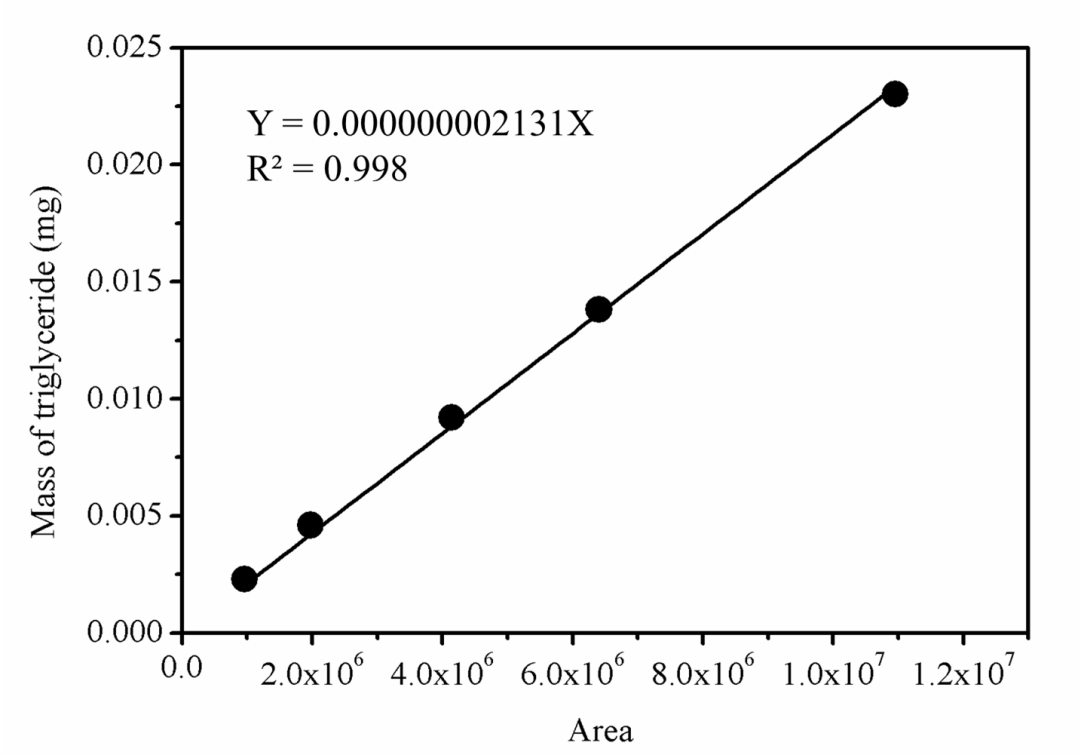

Figure A-6 Calibration curve of triglyceride.

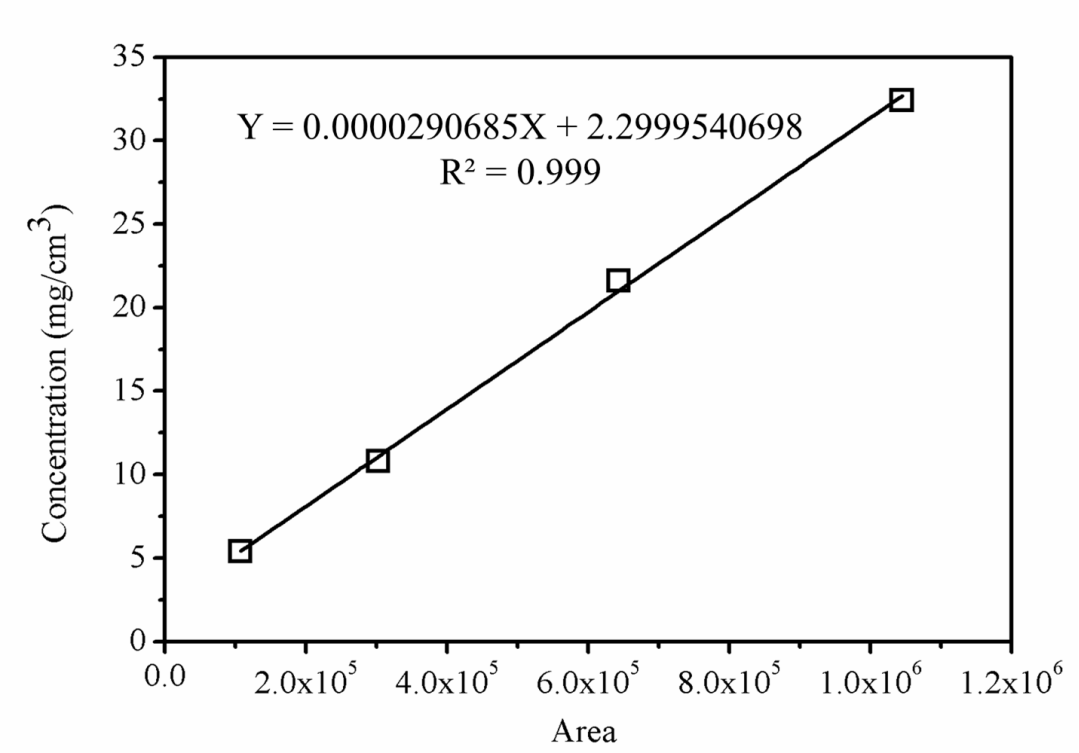

Figure A-7 Calibration curve of oleic acid.

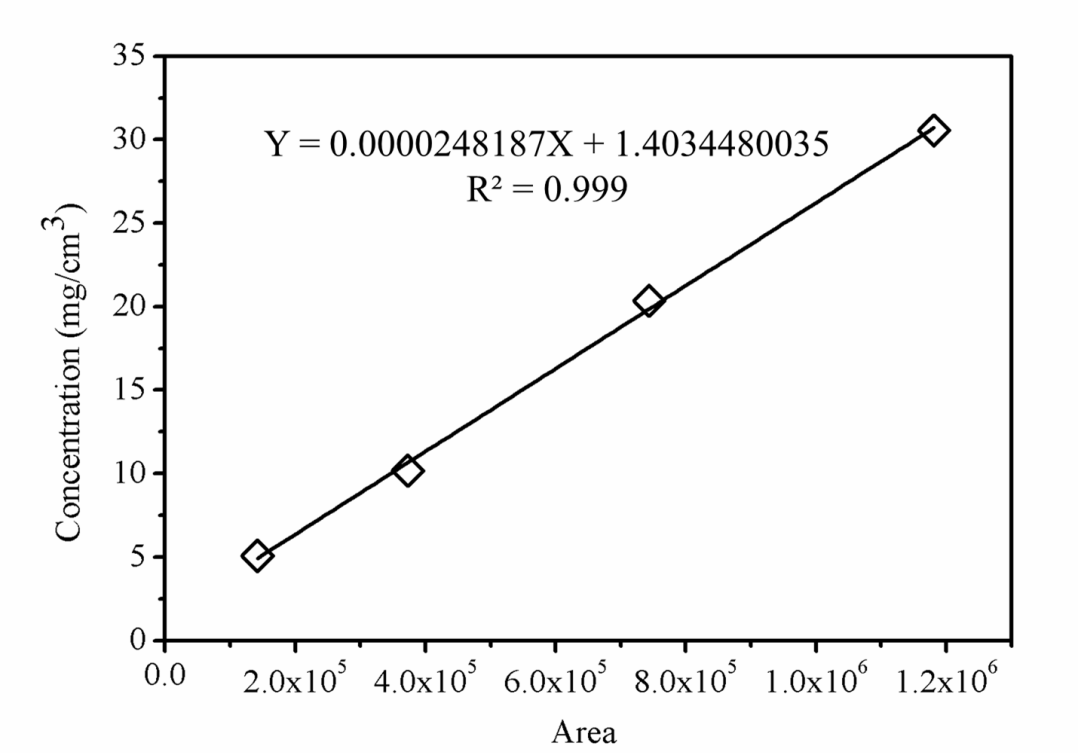

Figure A-8 Calibration curve of stearic acid.

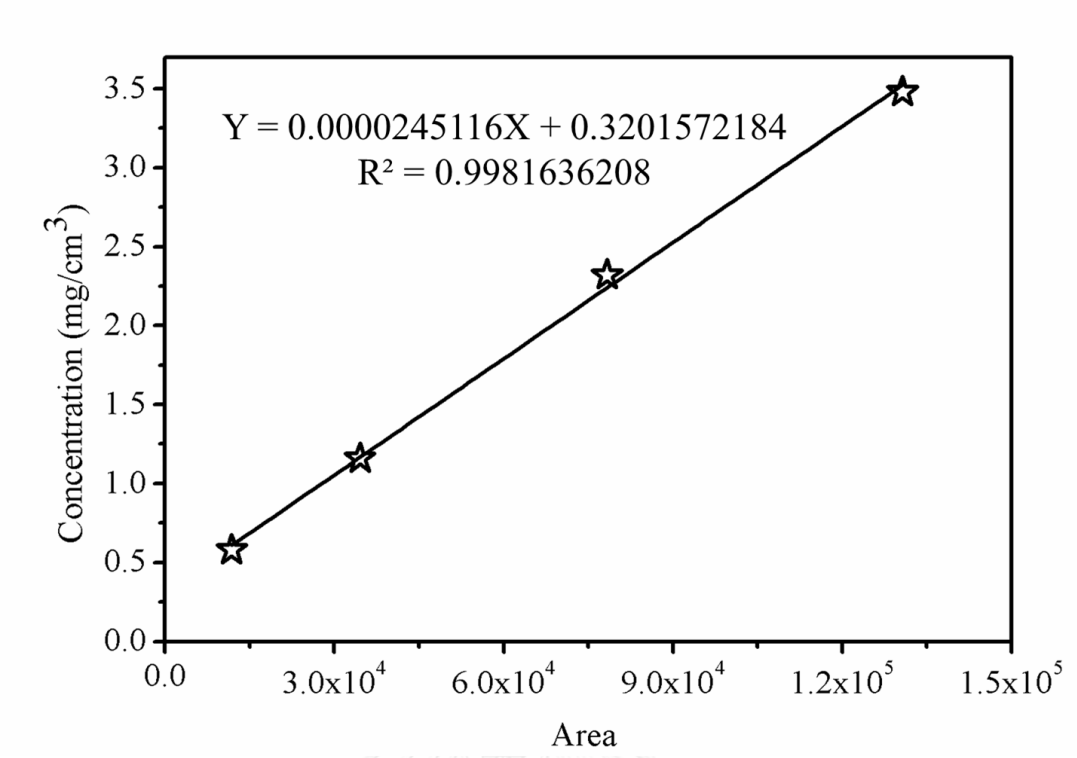

Figure A-9 Calibration curve of octadecanol.

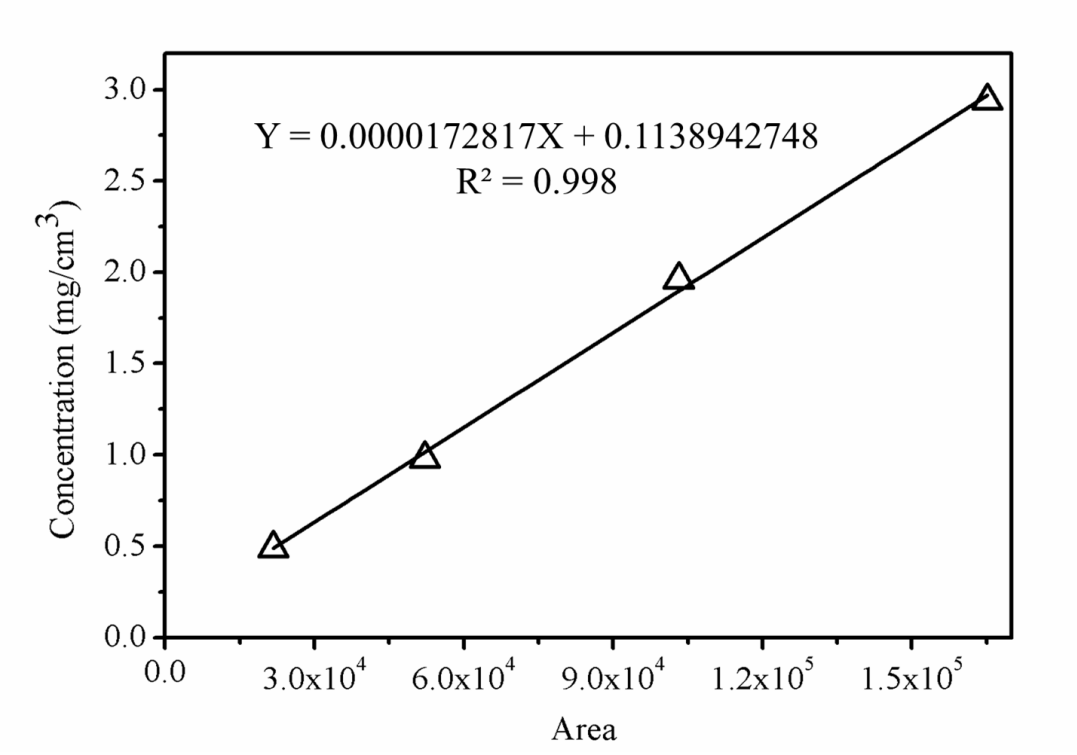

Figure A-10 Calibration curve of octadecanal.

Gas products were analyzed by gas chromatography with 2 m molecular sieve 5A and a 2 m porapak Q column equipped thermal conductivity detector (GC-14B, Shimadzu). Operating condition for gas chromatography equipped thermal conductivity detector is shown in the Table A-2. The calibration curves of carbon monoxide, carbon dioxide, methane, ethane and propane are illustrated in the following figures A-11 – A-15.

Table A-2 Operating condition for gas chromatograph equipped thermal conductivity detector

Gas Chromagraphy	SHIMADZU GC-14B	SHIMADZU GC-14B
Detector	TCD	TCD
Column	Molecular sieve 5A	Porapak Q
- Column material	Stainless steel	Stainless steel
- Length	2 m	2 m
- Outer diameter	4 mm	4 mm
- Inner diameter	3 mm	3 mm
- Mesh range	60/80	50/80
- Maximum temperature (^{o}C)	350	350
Carrier gas	He (99.995%)	He (99.995%)
Carrier gas flow	75 cm^3/min	75 cm^3/min
Column temperature		
- Initial column (^{o}C)	40	40
- Final column (^{o}C)	80	80
- ramp rate (^{o}C/min)	5	5
- Injector (^{o}C)	100	100
- Detector (^{o}C)	100	100
Current (mA)	150	150
Analysed gas	CO	CO_2, CH_4, C_2H_6, and C_3H_8

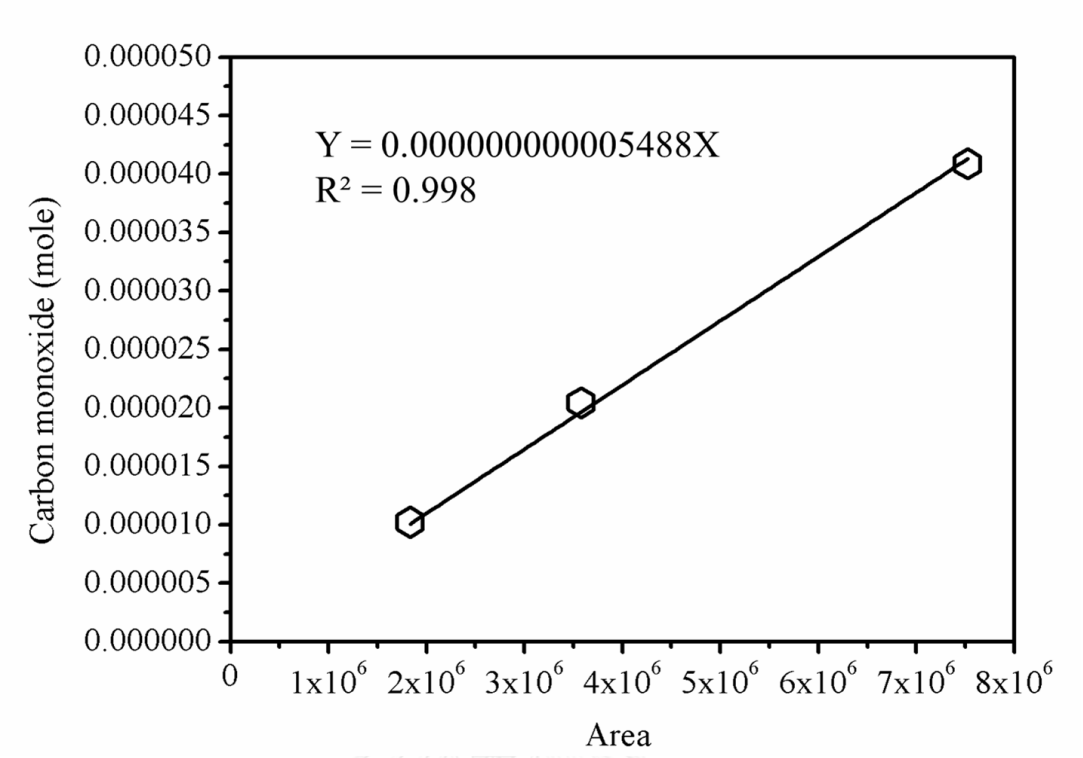

Figure A-11 Calibration curve of carbon monoxide.

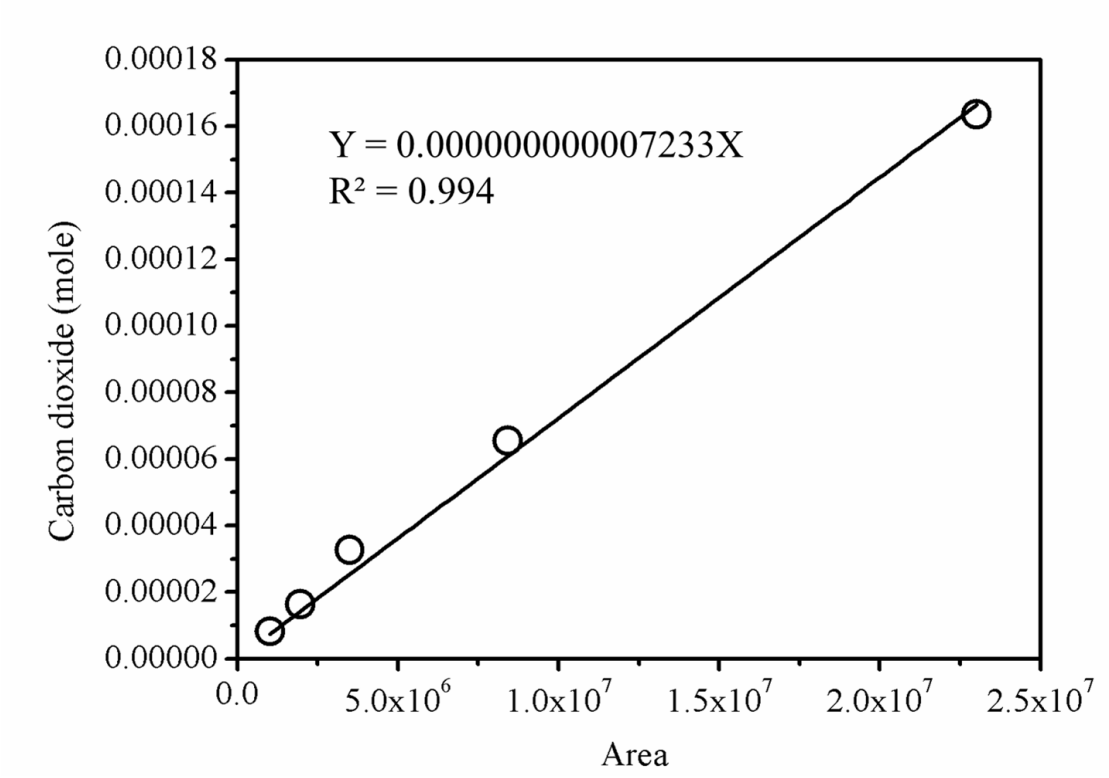

Figure A-12 Calibration curve of carbon dioxide.

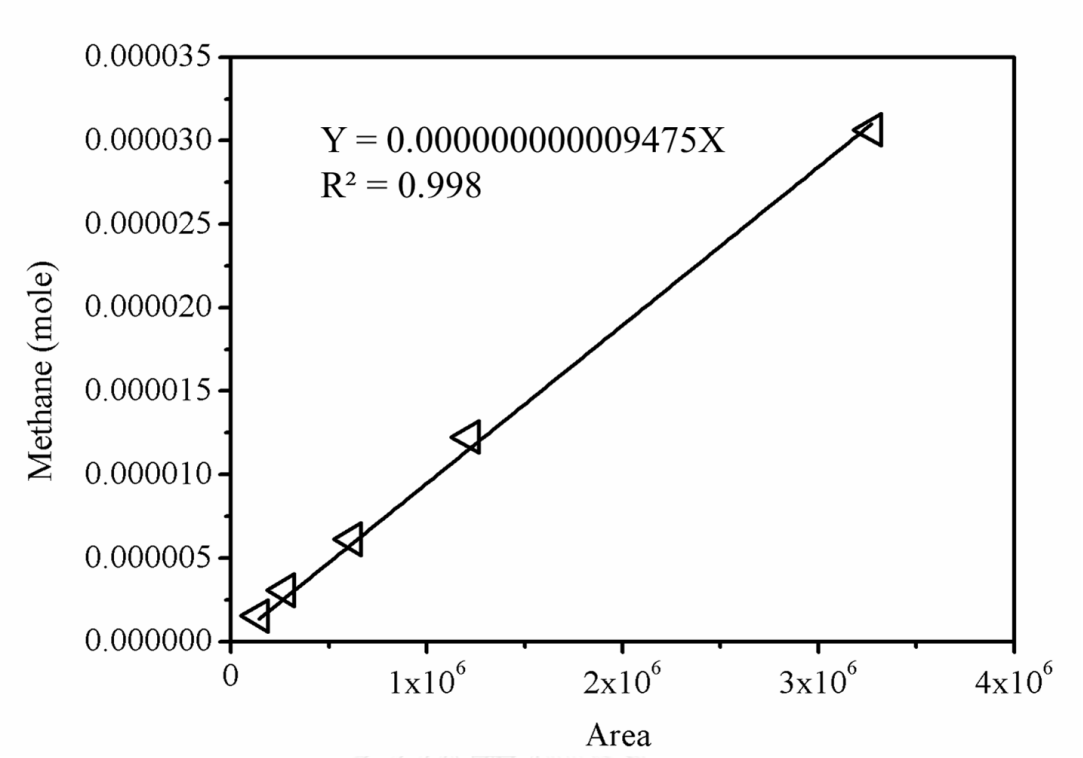

Figure A-13 Calibration curve of methane.

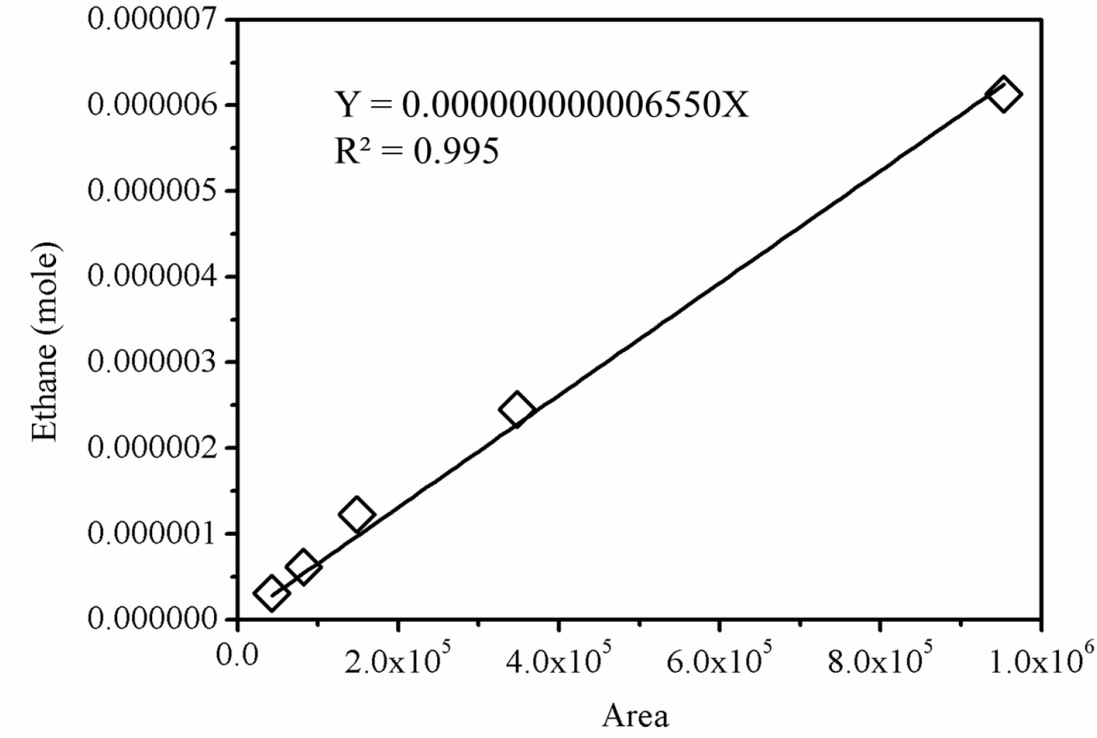

Figure A-14 Calibration curve of ethane.

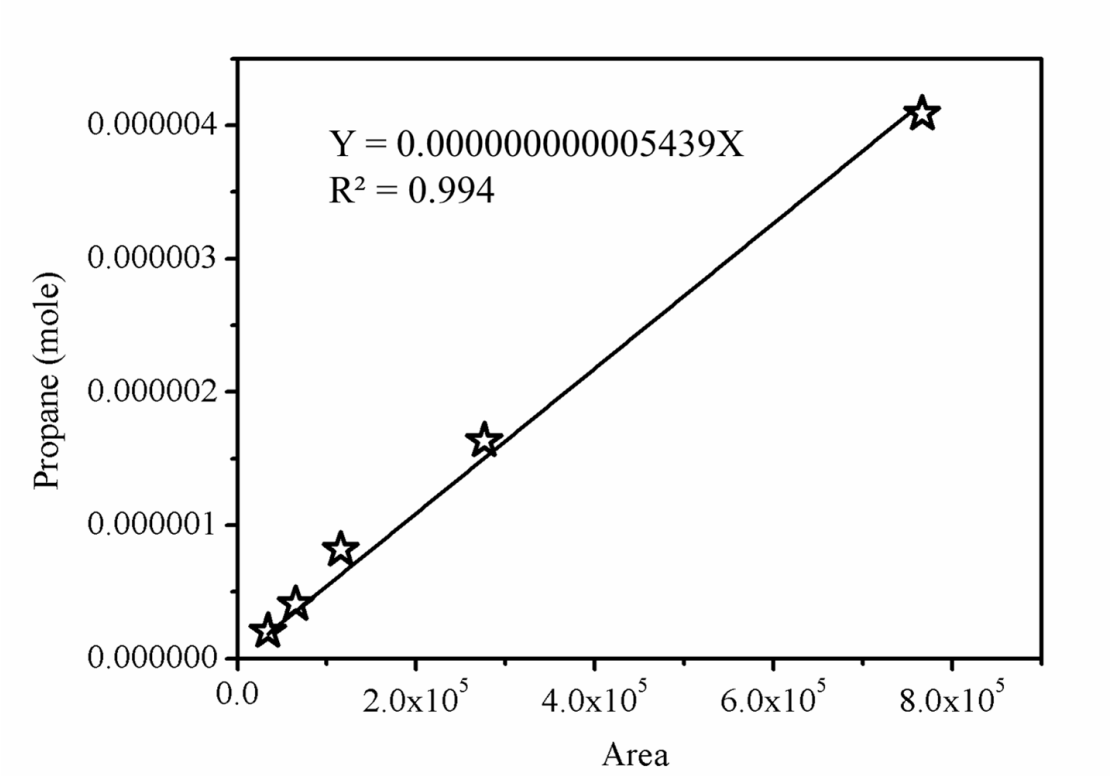

Figure A-15 Calibration curve of propane.

APPENDIX B

EXTERNAL MASS TRANSFER LIMITATION IN THE CATALYST BED

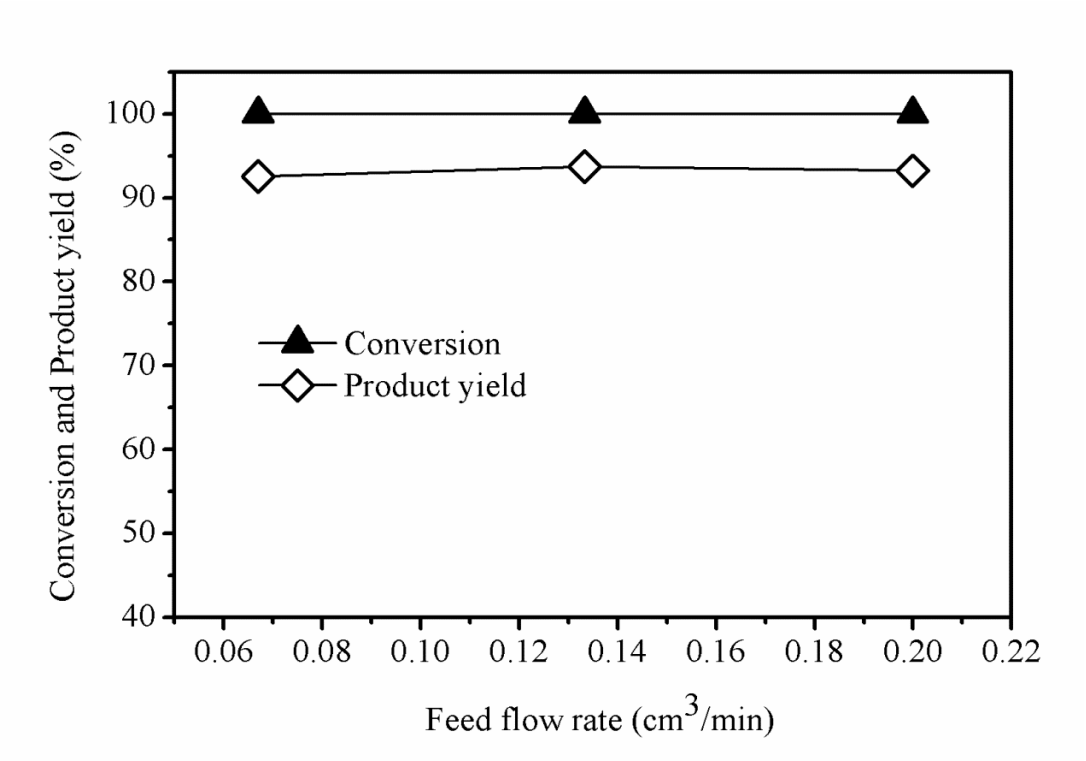

Figure B-1 Catalytic performance of $NiMoS_2/\gamma\text{-}Al_2O_3$ catalysts with different feed flow rate. Catalyst loading = 2.83 – 8.5 g. Reaction conditions: 300 ^oC, 5 MPa, LHSV of 1 h^{-1}, and H_2/oil ratio of 1,000 (Ncm^3/cm^3).

APPENDIX C

THEMODYNAMIC EVALUTION OF HYDRODEOXYGENATION OF TRIGLYCERIDES TO N-ALKANES

The composition of any reacting system is the equilibrium of the composition which can be calculated by Gibbs free energy equation [102-104]. Gibbs free energy reaction values would predict the chance for a reaction to occur by the minimization of total Gibbs free energy method. At the steady state, pressure and temperature of the system are constant, so the equations are given as follows:

$$dG = \sum_{i}^{N} \bar{\mu}_i \, \mathrm{d}n_i \tag{C-1}$$

$$G = \sum_{i}^{N} \bar{\mu}_i \, n_i \tag{C-2}$$

The total Gibbs function can be written as follows:

$$min(G^t) = \sum_{i}^{N} n_i \, G_i^{\circ} + RT \sum_{i}^{N} n_i \, ln \frac{\hat{f}_i}{f_i^0} \tag{C-3}$$

For reaction equilibrium in gas phase:

$$\hat{f}_i = \hat{\emptyset}_i y_i \, P_i \tag{C-4}$$

$$f_i^0 = P^0 \tag{C-5}$$

G_t^0 is set to zero for each chemical element in its standard state:

$$\Delta G^0 = \Delta G_{f_i}^0 \tag{C-6}$$

From the equations, *N* is the total number of components in the system; n_i is the variable that minimizes the value of Gibbs free energy. It can be solved two ways including 1) the stoichiometric thermodynamic approach which is determined by a set of stoichiometrically independent reactions, and then typically chosen arbitrarily from a set of possible reactions, and 2) A non-stoichiometric thermodynamic approach value is set up by the direct minimization of the Gibbs free energy for a given set of species [102]. The advantages of non-stoichiometric thermodynamic approach included 1) a selection of the possible set of reactions in that system is not necessary 2) no divergence occurs during the consumption, and 3) an accurate estimation of the initial equilibrium composition is not necessary [105].

$$\Delta G_{f_i}^0 = RTln\frac{\widehat{\emptyset}_i y_i P_i}{P^0} + \sum_i^N \lambda_k \alpha_{ik} = 0 \tag{C-7}$$

$$\sum_i^N n_i \left(\Delta G_{f_i}^0 + RTln\frac{\widehat{\emptyset}_i y_i P_i}{P^0} + \sum_i^N \lambda_k \alpha_{ik} \right) = 0 \tag{C-8}$$

From the constraints of elemental balances:

$$\sum_i^N n_i \alpha_{ik} = A_k \tag{C-9}$$

where α_{ik} is the number of atoms of element k in component i, A_k is the total number of atoms of element k in the reaction mixture, and *N* is the total number of elements.

Table C-1 The equilibrium chemical compositions of the hydrodeoxygenation of palm oil by Gibbs free energy minimization method using the Aspen plus, Aspen Tech™ at 300 °C and 5 MPa.

Components	Input (kmol/s)	Output (kmol/s)
TRIOLEIN	0.5	2.58E-35
TRIPALMITIN	0.5	0
H_2	10	0.000600077
$C_{15}H_{32}$	0	0.5106749
$C_{16}H_{34}$	0	0.4233229
$C_{17}H_{36}$	0	0.3019212
$C_{18}H_{38}$	0	0.2275739
C_3H_8	0	8.843395
H_2O	0	4.66775E-05
CO	0	1.615116
CO_2	0	2.192419

APPENDIX D

FATTY ACID COMPOSITION OF REFINED PALM OLEIN BY TRANSESTERIFICATION

The fatty acid composition was determined by transesterification of refined palm olein over $NaPO_4$ catalysts. Transesterification conditions were as follows; temperature = 65 ^{o}C, methanol/oil molar ratio = 18:1, and catalyst amount = 10%. The composition of methyl ester in the sample was analyzed by using gas chromatography (GC). The method used for the analysis of FAME content (wt.%) was the European Standard EN 14103.

Table D-1 Fatty acid composition of refined palm olein

Fatty acid	Composition (wt%)
Lauric acid (C12:0)	0.8
Myristic acid (C14:0)	0.0
Palmitic acid (C16:0)	36.9
Steraric acid (C18:0)	3.4
Arachidic acid (C20:0)	0.3
Saturated	41.4
Palmitoleic acid (C16:1)	0.1
Oleic acid (C18:1)	47.3
Linoleic acid (C18:2)	10.0
Linolemic acid (18:3)	0.1
Eicosenoic acid (C20:1)	0.1
Unsaturated	57.6
Total fatty acid	99.0

APPENDIX E

EXPERIMENTAL RAW DATA

Table E-1 Data of Figure 18a

Temperature (^oC)	Conversion (%)			Average	SD
	1	2	3		
270	96.49	97.09	96.07	96.58	0.72
300	100	100	100	100	0
330	100	100	100	100	0
360	100	100	100	100	0
390	100	100	100	100	0
420	100	100	100	100	0

Table E-2 Data of Figure 18a

Temperature (^oC)	Product yield (%)			Average	SD
	1	2	3		
270	23.80	29.16	24.36	26.76	3.40
300	88.75	90.75	89.99	89.83	1.01
330	88.06	88.34	88.97	88.46	0.47
360	81.53	83.78	78.61	81.31	2.59
390	68.89	69.77	66.73	68.46	1.56
420	40.42	36.24	36.90	37.85	2.25

Table E-3 Data of Figure 18b

Temperature (^oC)	HDO (%)			Average	SD
	1	2	3		
270	19.40	23.96	19.91	21.93	2.87
300	71.11	73.12	72.59	72.27	1.04
330	73.91	74.94	75.82	74.89	0.95
360	73.50	75.22	71.01	73.24	2.11
390	61.62	62.46	59.83	61.31	1.34
420	33.45	29.76	30.35	31.19	1.98

Table E-4 Data of Figure 18b

Temperature (oC)	DCO/DCO_2 (%)			Average	SD
	1	2	3		
270	4.20	4.96	4.25	4.61	0.50
300	16.92	16.88	16.66	16.82	0.14
330	13.42	12.68	12.42	12.84	0.52
360	7.36	7.87	6.95	7.40	0.46
390	6.70	6.73	6.35	6.59	0.21
420	6.64	6.18	6.24	6.35	0.25

Table E-5 Data of Figure 18c

Temperature	Gas product composition (mole %)					
(^oC)	CO	CO_2	CH_4	C_2H_6	C_3H_8	H_2
270	0.28	0.17	0.24	0.05	1.27	98.00
300	0.16	1.49	1.20	0.16	2.20	94.80
330	0.18	1.08	1.38	0.26	2.12	94.99
360	0.14	0.70	1.23	0.31	2.15	95.48
390	0.19	0.65	1.28	0.37	2.04	95.46
420	0.41	0.86	1.84	0.60	1.80	94.49

Table E-6 Data of Figure 20a

Pressure	Conversion (%)			Average	SD
(MPa)	1	2	3		
1.5	100	100	100	100	0
3	100	100	100	100	0
5	100	100	100	100	0
8	100	100	100	100	0

Table E-7 Data of Figure 20a

Pressure	Product yield (%)			Average	SD
(MPa)	1	2	3		
1.5	85.99	84.23	85.81	85.02	1.12
3	91.47	91.26	91.02	91.14	0.17
5	88.75	90.75	89.99	89.83	1.01
8	97.14	94.02	94.47	95.21	1.68

Table E-8 Data of Figure 20b

Pressure (MPa)	HDO (%)			Average	SD
	1	2	3		
1.5	67.94	66.71	68.91	67.81	1.56
3	69.76	70.23	70.35	70.29	0.09
5	71.11	73.12	72.59	72.27	1.04
8	79.30	77.20	77.97	78.16	1.06

Table E-9 Data of Figure 20b

Pressure (MPa)	DCO/DCO_2 (%)			Average	SD
	1	2	3		
1.5	17.35	16.83	16.20	16.51	0.44
3	20.96	20.28	19.92	20.10	0.26
5	16.92	16.88	16.66	16.82	0.14
8	17.04	16.04	15.73	16.27	0.68

Table E-10 Data of Figure 20c

Pressure (MPa)	Gas product composition (mole %)					
	CO	CO_2	CH_4	C_2H_6	C_3H_8	H_2
1.5	0.32	1.06	0.37	0.14	2.46	95.64
3	0.27	1.98	0.71	0.15	2.53	94.37
5	0.16	1.49	1.20	0.16	2.20	94.80
8	0.00	0.72	1.70	0.17	2.29	95.12

Table E-11 Data of Figure 21a

LHSV (h^{-1})	Conversion (%)			Average	SD
	1	2	3		
0.25	100	100	100	100	0
0.5	100	100	100	100	0
1	100	100	100	100	0
1.5	100	100	100	100	0
2	100	100	100	100	0
3	100	100	100	100	0
5	100	100	100	100	0

Table E-12 Data of Figure 21a

LHSV (h^{-1})	Product yield (%)			Average	SD
	1	2	3		
0.25	93.93	95.39	97.22	95.51	1.65
0.5	87.75	87.15	90.51	88.47	1.79
1	90.36	91.41	91.27	91.01	0.57
1.5	85.22	88.93	87.07	87.07	1.85
2	86.94	87.10	88.89	87.64	1.09
3	84.11	80.89	84.45	83.15	1.96
5	86.69	82.98	83.29	84.32	2.06

Table E-13 Data of Figure 21b

LHSV (h^{-1})	HDO (%)			Average	SD
	1	2	3		
0.25	81.15	83.45	85.11	83.24	1.99
0.5	70.77	70.59	73.64	71.67	1.71
1	71.31	72.52	72.68	72.17	0.75
1.5	67.63	70.73	69.84	69.40	1.60
2	69.80	70.45	72.19	70.81	1.23
3	68.04	65.76	68.72	67.51	1.55
5	70.86	67.59	67.50	68.65	1.91

Table E-14 Data of Figure 21b

LHSV (h^{-1})	DCO/DCO_2 (%)			Average	SD
	1	2	3		
0.25	10.30	9.41	9.53	9.75	0.48
0.5	14.65	14.25	14.47	14.46	0.20
1	16.66	16.47	16.17	16.43	0.25
1.5	15.34	15.84	14.92	15.37	0.46
2	14.83	14.34	14.35	14.51	0.28
3	13.84	12.99	13.49	13.44	0.43
5	13.53	13.19	13.58	13.43	0.21

Table E-15 Data of Figure 21c

LHSV (h^{-1})	Gas product composition (mole %)					
	CO	CO_2	CH_4	C_2H_6	C_3H_8	H_2
0.25	0.00	0.73	0.86	0.22	2.19	96.00
0.5	0.00	0.76	0.94	0.13	2.21	95.97
1	0.17	1.50	0.87	0.17	2.30	94.99
1.5	0.17	1.45	0.64	0.18	2.76	94.79
2	0.13	1.53	0.55	0.20	2.77	94.82
3	0.25	1.45	0.44	0.20	2.78	94.87
5	0.62	1.31	0.43	0.24	2.94	94.46

Table E-16 Data of Figure 22a

H_2/oil ratio N(cm^3/cm^3)	Conversion (%)			Average	SD
	1	2	3		
250	100	100	-	100	0
500	100	100	100	100	0
750	100	100	100	100	0
1000	100	100	100	100	0
1500	100	100	100	100	0
2000	100	100	100	100	0

Table E-17 Data of Figure 22a

H_2/oil ratio N(cm^3/cm^3)	Product yield (%)			Average	SD
	1	2	3		
250	46.82	43.66	-	45.24	2.24
500	89.35	89.67	88.34	89.12	0.69
750	89.54	91.44	89.06	90.01	1.26
1000	91.29	93.21	96.15	93.55	2.45
1500	94.00	92.94	93.04	93.33	0.59
2000	90.08	88.19	91.82	90.03	1.82

Table E-18 Data of Figure 22b

H_2/oil ratio N(cm^3/cm^3)	HDO (%)			Average	SD
	1	2	3		
250	33.05	31.54	-	32.30	1.07
500	69.82	69.91	68.84	69.52	0.59
750	71.45	73.04	71.28	71.92	0.97
1000	73.17	75.08	77.58	75.28	2.21
1500	73.82	73.35	73.94	73.70	0.31
2000	73.69	72.46	75.27	73.81	1.40

Table E-19 Data of Figure 22b

H_2/oil ratio $N(cm^3/cm^3)$	DCO/DCO_2 (%)			Average	SD
	1	2	3		
250	13.39	11.76	-	12.57	1.15
500	18.80	19.02	18.78	18.87	0.14
750	17.36	17.65	17.05	17.35	0.30
1000	17.37	17.37	17.79	17.51	0.24
1500	15.65	15.00	15.80	15.48	0.42
2000	15.65	15.00	15.80	15.48	0.42

Table E-20 Data of Figure 22c

H_2/oil ratio $N(cm^3/cm^3)$	Gas product composition (mole fraction)				
	CO	CO_2	CH_4	C_2H_6	C_3H_8
250	0.00	66.06	6.09	5.49	22.36
500	1.23	49.14	11.32	5.31	33.00
750	2.72	35.65	16.90	4.62	40.12
1000	3.26	29.48	20.26	3.90	43.10
1500	3.73	22.92	27.28	2.77	43.30
2000	4.09	18.08	29.23	2.62	45.98

Table E-21 Data of Figure 27

Catalysts	5NiAl	10NiAl	5CoAl	10CoAl	2PdAl	5PdAl	2PtAl	5PtAl
Conversion (%)	100	100	100	100	98.97	100	94.73	100.00
Product yield (%)	69.70	84.31	88.47	85.52	41.34	85.23	33.84	79.54
Contribution (%)								
HDO	2.84	2.65	52.35	45.49	2.79	4.78	3.56	7.46
DCO/DCO_2	66.29	79.42	35.39	37.77	37.04	79.75	27.64	71.43
Gas product composition (mole%)								
CO	0	0	0	0	2.39	1.87	0.57	0.70
CO_2	0	0.16	0	0	0.61	3.24	1.54	3.42
CH_4	20.75	20.21	17.55	27.06	5.83	13.05	5.36	9.73
C_2H_6	2.29	1.84	1.32	1.65	1.20	2.08	1.89	2.58
C_3H_8	0.23	0.14	0.69	0.70	1.25	1.06	0.40	0.49
H_2	76.74	77.65	80.44	70.59	88.72	78.70	90.23	83.07

Table E-22 Data of Figure 29

Catalysts	Conversion (%)			Average	SD
	1	2	3		
Ni	100.00	100.00	100.00	100	0.00
Co	100.00	100.00	100.00	100	0.00
Mo	99.00	99.10	-	99.05	0.07
NiMo	100.00	100.00	100.00	0.00	0.00
CoMo	97.36	97.23	96.32	96.97	0.57
NiS_x	70.95	71.94	71.13	71.34	0.53
CoS_x	81.78	80.87	77.29	79.98	2.37
MoS_2	100.00	100.00	100.00	100.00	0.00
$NiMoS_2$	100.00	100.00	100.00	100.00	0.00
$CoMoS_2$	100.00	100.00	100.00	100.00	0.00

Table E-23 Data of Figure 29

Catalysts	Product yield (%)			Average	SD
	1	2	3		
Ni	90.34	92.79	91.91	92.35	0.62
Co	91.17	91.71	94.71	93.21	2.13
Mo	11.00	9.48	-	10.24	1.07
NiMo	66.87	59.02	49.41	58.43	8.74
CoMo	19.50	19.74	19.27	19.50	0.24
NiS_x	7.95	7.29	6.36	7.20	0.80
CoS_x	5.00	5.79	5.70	5.50	0.43
MoS_2	79.13	82.78	77.46	79.79	2.72
$NiMoS_2$	93.72	95.95	93.41	94.68	1.79
$CoMoS_2$	85.18	88.22	88.72	87.37	0.35

Table E-24 Data of Figure 31

Catalysts	HDO (%)			Average	SD
	1	2	3		
Ni	3.04	3.01	2.92	2.97	0.06
Co	49.82	50.00	51.03	50.51	0.73
Mo	10.12	8.67	-	9.40	1.03
NiMo	61.74	54.14	44.80	53.56	8.48
CoMo	18.29	18.51	18.06	18.29	0.22
NiS_x	0.00	0.00	0.00	0.00	0.00
CoS_x	0.00	0.00	0.00	0.00	0.00
MoS_2	74.11	77.44	72.58	74.71	2.48
$NiMoS_2$	74.03	76.12	74.45	75.28	1.18
$CoMoS_2$	76.70	79.36	79.75	78.60	0.27

Table E-25 Data of Figure 31

Catalysts	DCO/DCO_2 (%)			Average	SD
	1	2	3		
Ni	87.31	89.78	88.99	89.38	0.56
Co	40.60	40.96	42.91	41.93	1.38
Mo	0.75	0.70	-	0.73	0.04
NiMo	4.58	4.39	4.20	4.39	0.19
CoMo	1.04	1.06	1.05	1.05	0.01
NiS_x	7.89	7.23	6.31	7.14	0.79
CoS_x	4.96	5.75	5.65	5.45	0.43
MoS_2	4.37	4.65	4.24	4.42	0.21
$NiMoS_2$	18.92	19.04	18.19	18.62	0.60
$CoMoS_2$	7.78	8.14	8.24	8.05	0.07

Table E-26 Data of Figure 32

Catalysts	Gas product composition (mole %)					
	CO	CO_2	CH_4	C_2H_6	C_3H_8	H_2
Ni	0.00	0.00	19.93	1.96	0.46	77.64
Co	0.00	0.00	10.25	1.26	0.76	87.72
Mo	0.00	0.00	0.00	0.00	1.82	98.18
NiMo	0.18	0.23	0.51	0.06	2.80	96.22
CoMo	0.00	0.12	0.35	0.03	1.37	98.13
NiS_x	2.67	0.10	0.00	0.00	0.14	97.09
CoS_x	1.47	0.04	0.00	0.00	0.18	98.32
MoS_2	0.00	0.37	0.54	0.13	2.75	96.21
$NiMoS_2$	0.17	1.55	1.20	0.22	2.18	94.68
$CoMoS_2$	0.08	0.77	0.53	0.12	2.77	95.74

Table E-26 Data of Figure 33a

Time on stream (h)	Product yield (%)			
	Ni	Co	$NiMoS_2$	$CoMoS_2$
24	87.77	84.47	94.69	79.75
48	84.00	89.26	93.07	84.53
72	95.37	91.32	93.50	81.22
96	89.46	94.03	90.82	80.74
120	83.52	72.88	91.11	82.23
150	74.76	60.11	92.39	71.91

Table E-27 Data of Figure 33b

Time on stream (h)	HDO			
	Ni	Co	$NiMoS_2$	$CoMoS_2$
24	2.37	47.47	66.07	67.89
48	2.00	50.73	69.51	73.00
72	2.10	49.24	72.92	71.41
96	1.80	51.63	72.67	71.92
120	1.62	40.41	74.48	74.10
150	1.47	30.92	77.13	64.92

Table E-28 Data of Figure 33c

Time on stream (h)	DCO/DCO_2			
	Ni	Co	$NiMoS_2$	$CoMoS_2$
24	85.40	37.00	28.62	11.86
48	82.47	39.95	22.75	11.85
72	93.27	42.08	20.58	9.81
96	87.66	42.40	18.15	8.82
120	81.91	32.47	16.63	8.13
150	73.30	29.19	15.26	6.99

Table E-29 Data of Figure 35

Time on stream (h)	Ni		Co	
	Conversion (%)	Yield (%)	Conversion (%)	Yield (%)
6	100	84.74	100	83.76
24	100	92.02	100	84.47
30	100	93.77	100	85.08
48	100	92.40	100	89.26
54	100	93.29	100	86.81
72	100	95.37	100	91.32
78	100	92.28	100	93.80
96	100	89.46	100	94.03
102	100	90.37	100	90.33
120	100	83.52	100	72.88
126	100	89.03	100	84.53
144	97.49	72.12	97.50	53.04
150	97.55	74.76	97.17	60.11
Regeneration				
6	100	85.17	100	75.77
24	100	92.89	100	93.53
30	100	91.46	100	91.06

Table E-30 Data of Figure 36

Time on stream (h)	Ni		Co	
	HDO	DCO/DCO_2	HDO	DCO/DCO_2
6	2.60	82.14	44.47	39.30
24	2.08	88.90	47.47	37.00
30	2.04	90.53	44.85	41.13
48	2.08	90.45	50.73	39.95
54	1.83	90.39	43.14	43.67
72	2.10	93.27	49.24	42.08
78	2.11	90.17	46.58	47.22
96	1.80	87.66	51.63	42.40
102	1.94	88.43	41.97	48.36
120	1.62	81.91	40.41	32.47
126	1.84	87.19	42.09	42.44
144	1.40	70.72	28.49	24.55
150	1.47	73.30	30.92	29.19
Regeneration				
6	3.85	81.32	41.07	34.70
24	3.21	89.68	53.42	40.10
30	3.11	88.35	52.01	39.04

Table E-31 Data of Figure 37

Time on stream	Ni				Co			
	Liquid product composition (wt.%)				Liquid product composition (wt.%)			
(h)	*n*-C_{15}	*n*-C_{16}	*n*-C_{17}	*n*-C_{18}	*n*-C_{15}	*n*-C_{16}	*n*-C_{17}	*n*-C_{18}
6	32.53	1.99	52.44	0.75	16.54	20.86	23.14	26.69
24	36.04	1.58	58.70	0.69	15.83	22.00	23.54	31.56
30	36.56	1.62	59.32	0.74	17.19	19.85	26.62	29.81
48	36.63	1.56	59.60	0.73	13.48	18.82	21.08	29.50
54	37.14	1.25	60.51	0.79	17.68	18.59	28.08	29.39
72	36.33	1.22	60.74	1.06	16.62	20.38	26.40	33.10
78	36.20	1.26	59.92	1.08	18.81	19.56	30.30	31.87
96	35.48	1.01	59.04	1.02	16.67	21.07	26.65	34.99
102	35.83	1.10	59.22	1.07	19.48	17.74	31.45	29.21
120	33.85	0.90	55.90	0.96	12.42	15.88	19.42	26.26
126	34.76	0.99	57.30	1.04	16.57	17.02	26.45	28.33
144	29.85	0.78	49.05	0.86	9.35	11.12	14.24	17.98
150	29.79	0.77	48.79	0.88	10.96	11.92	16.82	19.38
Regeneration								
6	34.10	2.79	55.67	1.59	16.29	21.25	23.80	29.02
24	35.76	1.86	58.88	1.68	15.50	22.12	24.90	34.98
30	36.74	1.77	60.76	1.82	15.12	21.38	24.35	34.43

Table E-32 Data of Figure 38

Time on stream (h)	Ni				Co			
	Gas product composition (mole %)				Gas product composition (mole %)			
	CH_4	C_2H_6	C_3H_8	H_2	CH_4	C_2H_6	C_3H_8	H_2
6	24.60	1.32	0.16	73.84	12.43	1.16	0.60	85.81
24	17.26	1.67	0.18	80.89	11.22	1.45	0.98	86.34
30	17.05	1.71	0.20	81.03	11.08	1.45	0.91	86.56
48	16.92	1.79	0.21	81.08	9.57	1.50	1.01	87.92
54	15.77	1.67	0.22	82.33	9.45	1.40	0.84	88.31
72	16.86	1.85	0.24	81.06	9.20	1.56	0.91	88.34
78	16.10	1.76	0.25	81.88	9.90	1.57	0.87	87.65
96	16.46	1.86	0.24	81.44	8.14	1.36	0.78	89.64
102	20.46	1.41	0.20	77.55	9.22	1.43	0.77	88.50
120	14.85	1.78	0.25	83.12	6.70	1.17	0.65	91.40
126	11.99	1.69	0.51	85.75	8.29	1.32	0.71	89.56
144	12.86	1.65	0.25	85.25	5.44	1.02	0.55	92.92
150	13.26	1.66	0.26	84.81	5.39	0.94	0.50	93.09
Regeneration								
6	10.98	1.44	0.27	87.32	8.71	1.05	0.79	89.45
24	14.90	2.04	0.46	82.61	7.96	1.40	1.22	89.43
30	14.73	2.01	0.50	82.77	7.31	1.28	1.11	90.03

APPENDIX F

THE OVERALL CARBON BALANCE OF THE HYDRODEOXYGENATION OF PALM OIL WITH METAL AND METAL SULFIDE CATALYSTS

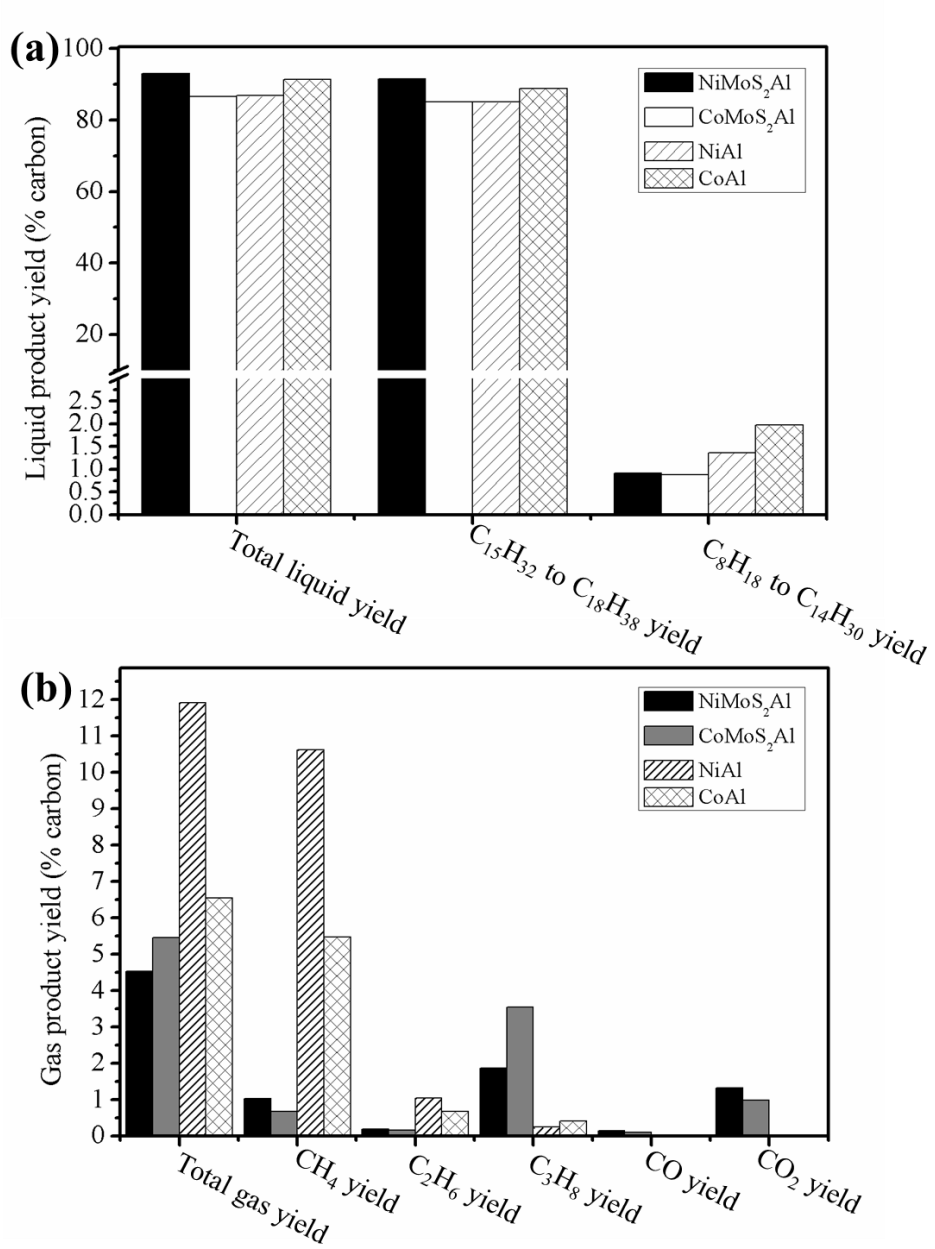

Figure F-1 The overall carbon balance of liquid (a) and gas (b) products during the hydrodeoxygenation of palm oil with metal and metal sulfide catalysts. Reaction conditions: 300 ^{o}C, 5 MPa, LHSV of 1 h^{-1}, and H_2/oil ratio of 1,000 N(cm^3/cm^3)

APPENDIX G

CALCULATION FOR CO PULSE CHEMISORPTION EXPERIMENT

Table G-1 The values of metal cross sectional area (MXSA), density (D), and molecula weaght (MW) of the metals [106].

Metal	Structure	MXSA ($Å^2$)	D (cm^3/g)	MW (g/mole)
Pd	fcc	7.93	12.02	106.42
Pt	fcc	8.07	21.45	195.08
Ni	fcc	6.51	8.91	58.69
Co	hcp	5.43	8.90	58.94

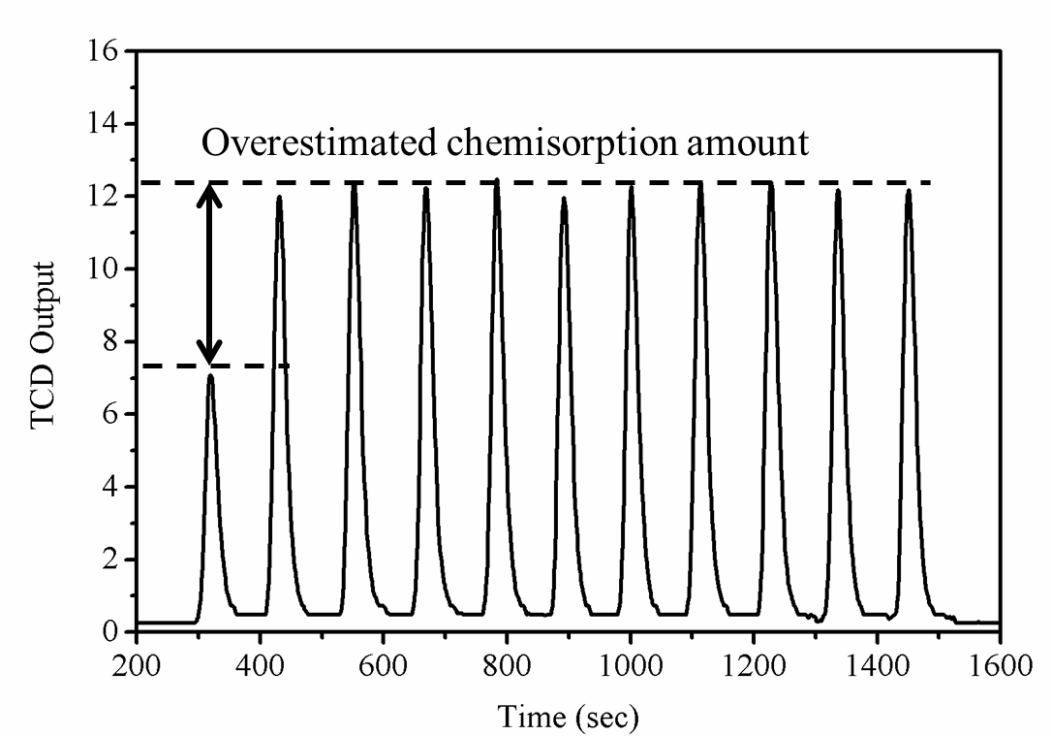

Figure G-1 Example of signal from CO pulse chemisorption experiment of the Ni/γ-Al_2O_3 catalyst.

For example, 10 wt.% Ni/ γ-Al_2O_3

1. Metal surface area (A)

$$A = V_m \times MXSA \times S \times 6.03 \times 10^{-3} \ (\frac{m^2}{g})$$

Where V_m = Gas adsorbed on active metal surface or CO uptake (umol/g)

MXSA = Metal cross sectional area ($Å^2$)

S = Metal atoms per gas molecule (metal/CO =1)

$$V_m = \frac{V_{nom} \times P \times T_{stp}}{P_{stp} \times T \times wt_{sample} \times 22.4}$$

Where V_{nom} = Total volume of CO adsorded (uL)

$$V_m = \frac{45\ uL \times 760\ mmHg \times 273.15\ K}{760\ mmHg \times 323.15\ K \times 0.047\ g \times 22.4} = 36.13\ umol/g$$

$$A = 36.13\ \frac{umol}{g} \times 6.51\ A^o \times 1 \times 6.03 \times 10^{-3} = 1.42\ (\frac{m^2}{g})$$

Metal surface per gram of metal, A_m

$$A = A \times \frac{100}{L} = 1.42\left(\frac{m^2}{g}\right) \times \frac{100}{10} = 14.20\left(\frac{m^2}{g_{metal}}\right)$$

Where L = Metal loading (wt. %)

2. Metal dispersion (%D)

$$\%D = S_f \times V_m \times \frac{MW}{\%M} \times 100\% \times 100\% \times \frac{1}{10^6}$$

Where S_f = Metal atoms per gas molecule (metal/CO =1)

MW = Molecular weight

%M = % metal loading

$$\%D = 1 \times 36.13 \frac{umol}{g} \times \frac{58.69\ g/mol}{10\%} \times 100\% \times 100\% \times \frac{1}{10^6} = 2.21\ \%$$

3. Average particles size (d)

$$d = \frac{\%M \times 100 \times f}{A \times p}$$

Where %M = % metal loading

f = Shape factor (constant = 6)

A = Metal surface area

P = Metal density (g/cm^3)

$$d = \frac{10 \times 100 \times 6}{1.42 \frac{m^2}{g} \times 8.908 \frac{g}{cm^3}} = 474.33\ A^o = 47.43\ nm$$

Note that the CO uptake can be presented in term turnover of frequency (TOF). The turnover frequencies (TOF) was defined as the total production rate of alkanes (*n*-C_{17} and *n*-C_{18}) per active site of catalyst using the CO uptake and,

$$TOF\ (S^{-1}) = \frac{Production\ rate\ (\frac{umol}{s})}{CO_{uptake}\ (\frac{umol}{g})}$$

APPENDIX H

LIST OF PUBLICATIONS

1. International Publications

1.1 **Atthapon Srifa**, Kajornsak Faungnawakij, Vorranutch Itthibenchapong, Nawin Viriya-empikul, Tawatchai Charinpanitkul, and Suttichai Assabumrungrat, Production of bio-hydrogenated diesel by catalytic hydrotreating of palm oil over $NiMoS_2/\gamma\text{-}Al_2O_3$ catalyst. ***Bioresource Technology***, 158 (2014), 81-90. (Impact factor: 5.04 (2014))

1.2 **Atthapon Srifa**, Kajornsak Faungnawakij, Vorranutch Itthibenchapong, and Suttichai Assabumrungrat, Roles of monometallic catalysts in hydrodeoxygenation of palm oil to green diesel, ***Chemical Engineering Journal***, *in press* (Impact Factor: 4.06 (2014))

2. International conferences

2.1 **A. Srifa**, K. Faungnawakij, and S. Assabumrungrat, Catalytic hydrotreating of palm oil to produce bio-hydrogenated diesel, *The 9th World Congress of Chemical Engineering incorporating 15th Asia Pacific Confederation of Chemical Engineering Congress, August 18-23, 2013, Coex, Seoul, Korea.* (Poster Presentation)

2.2 **A. Srifa**, K. Faungnawakij, and S. Assabumrungrat, Production of bio-hydrogenated diesel by catalytic deoxygenation of palm oil in a fixed-bed reactor, *TGIST scholarship progress work in The 10th NSTDA annual conference, March 31-April 3, 2014, Patumthani, Thailand.* (Oral Presentation)

2.3 **A. Srifa**, K. Faungnawakij, and S. Assabumrungrat, Hydrodeoxygenation of palm oil to bio-hydrogenated diesel over molybdenum-based sulfide catalysts, *The Grand Renewable Energy 2014 International conference and Exhibition, July 27- 1 August 1, 2014, Tokyo Big Sight, Tokyo, Japan. (Oral Presentation)*

2.4 K. Faungnawakij**, A. Srifa**, V. Itthibenchapong, and S. Assabumrungrat, Diesel-like alkanes from hydrodeoxygenation of palm oil catalyzed by metal catalysts, *The 23rd International Symposium on Chemical Reaction Engineering (ISCRE 23) and 7th Asia Pacific Chemical Reaction Engineering Symposium (APCRE 7), September 7-10, 2014, Bangkok, Thailand. (Oral Presentation)*

2.5 **A. Srifa**, K. Faungnawakij, and S. Assabumrungrat, Hydroprecessing of palm oil to green diesel over Ni/γ-Al_2O_3 and Co/γ-Al_2O_3 catalysts, *The 23rd International Symposium on Chemical Reaction Engineering (ISCRE 23) and 7th Asia Pacific Chemical Reaction Engineering Symposium (APCRE 7), September 7-10, 2014, Bangkok, Thailand. (Oral Presentation)*

VITA

Mr. Atthapon Srifa was born in April 25th, 1983, in Surat Thani, Thailand. He studied at Surat Thani 2 High School from 1999 to 2002. He received his Bachelor's Degree in Chemistry from Prince of Songkla University, Thailand in 2006. He continued studying Master's Degree in Chemical Engineering, Kasetsart University in 2006 and graduated in 2009. His thesis was entitled "Development of a proton exchange membrane fuel cell stack". During studying Master's Degree, he received a support from the granted project of the National Center of Excellence for Petroleum, Petrochemical, and Advanced Materials (NCE-PPAM). He had been studied a Doctoral degree of Chemical Engineering, Chulalongkron University since 2011, and received a full scholarship from the National Nanotechnology Center (NANOTEC), National Science and Technology Development Agency (NSTDA) through the Thailand Graduate Institute of Science and Technology (TGIST) under the mentorship of Dr. Kajornsak Faungnawakij.